

City Research Online

City St George's, University of London

Citation: Scibor-Rylski, M. T. V. (1974). Grating effect electro-optic light beam deflection and modulation. (Unpublished Doctoral thesis, The City University)

This is the accepted version of the paper.

This version of the publication may differ from the final published version. To cite this item please consult the publisher's version.

Permanent repository link: https://openaccess.city.ac.uk/id/eprint/38431/

Copyright and Reuse: Copyright and Moral Rights remain with the author(s) and/or copyright holders. Copies of full items can be used for personal research or study, educational, or not-for-profit purposes without prior permission or charge, unless otherwise indicated, provided that the authors, title and full bibliographic details are credited, a hyperlink and/or URL is given for the original metadata page and the content is not changed in any way. For full details of reuse please refer to City Research Online policy.

City Research Online: http://openaccess.city.ac.uk/ publications@citystgeorges.ac.uk

GRATING EFFECT ELECTRO-OPTIC LIGHT BEAM DEFLECTION AND MODULATION

M T V SCIBOR-RYLSKI

Thesis presented for the Degree of Doctor of Philosophy in the faculty of Engineering of the City University

1974

THE CITY UNIVERSITY LIBRARY,
ST. JOHN STREET, LONDON, E.C.1.

INDEX

ABSTRACT

1.	INTRODUCTION	2
1.1	Materials	5
1.2	Device Criteria	5
1.3	Practical Devices	7
1.4	Electro-Optic Deflectors	7
1.4.1	Prism Deflectors	7
1.4.2	The Digital Deflector	8
1.4.3	Diffraction Devices	9
1.5	Conclusions	10
2.	POTENTIAL MODULATION/DEFLECTION PROCESSES - A STUDY OF DIFFRACTION CONFIGURATIONS	11
2.1	The Controlled Grating Process	14
2.2	Dependent Sources	14
2.3	Grouped Controlled Sources	15
2.4	The Transformed Array	16
2.5	Conclusions	18
3.	REALISATION OF A PHASED ARRAY DEVICE	19
4.	PHASE CORRUGATION DEVICE	22
4.1	Introduction	22
4.2	Basic Concept of Device	22
4.3	The Electrode Field Structure	23
4.4	Solution of the Boundary Value Electrode Problem	24
4.5	Actual Boundary Conditions	26
4.6	The Anisotropic Case	28
4.7	Voltages Due to Electrodes	28
4.8	The Field Structure	30
4.9	Device Capacitance	31
4.10	Estimation of Phase Profiles	34
4.11	Induced Refractive Index Channe	35
	Effect of an Electric Field	36
	Rotational Transformation	37
	Basic Transformations	38
	Alternative Orientations	39
	First Transformation	40
	Second Transformation	41
	Combining Orientations and Fields	42

/...

INDEX continued

4.12	Field Induced Phase Profiles	42
	Comments on Device Configuration	44
	Use of ADP or an Isomorph	45
4.13	Phase Profile Programs	46
	Effects of Electrode Gap	47
	Phase Profiles for $\theta = 0$	47
4.14	Phase Profile and Misalignment	48
	The New Field Line Integral	48
	Index Ellipse in the Misaligned Case	52
4.15	Phase Change on Reflection	53
	Fresnels Equations	53
	Reflection from a Metal Surface	55
4.16	Far Field Performance	56
	The Fourier Transform Method	57
	The Incremental Amplitude Vector Summation Method	59
4.17	Device Parameters and Performance	62
	The Far Field Pattern	67
4.18	Conclusions	69
5.	SURFACE DEPOSITED DEVICES	70
5.1	Measured TIR Device Performance	70
5.1.1	Details of Constructed Devices	70
5.1.2	The Test Cell Assembly	70
5.1.3	Electrodes	70
5.1.4	Crystals	71
5.1.5	Performance Measurements	71
5.1.6	Order Intensity Characteristics	72
5.1.7	Performance Versus Incidence Angle	72
5.1.8	Performance versus Electrode Pitch	74
5.1.9	Extinction Ratios	74
5.1.10	Misalignment Performance	75
5.1.11	Far Field Patterns and Modulation	76
5.1.12	Effects of Pitch Variation	76
5.1.13	Comments on Device Handling, Alignment, and Electrical Connection	77

/...

INDEX continued

5.2	Contact Process Electroded Devices	80
5.2.1	Experimental Layout - Far Field Profiles	80
5.2.2	Time Constant Analysis	81
5.2.3	Versus Intensity	81
5.2.4	Decay Curve Study	82
5.2.5	Versus Applied Voltage	82
5.2.6	Anomalous Effects	82
5.2.7	Effects of Pitch Variation	83
5.2.8	Electrode Matching	84
5.2.9	Conclusions	85
5.3	Analysis of Sub-Electrode Layer and Mismatch Effects	86
5.3.1	Fields in the Material	86
5.3.2	Device Dynamic Measurements	87
5.3.3	Resonances	88
5.3.4	Bottom End Cut-Off	89
5.3.5	Modulation Characteristics	89
6.	THE TIR MODULATOR/DEFLECTOR AS Q-SWITCH	91
6.1.1	Device Insertion Loss	92
6.1.2	Device Response	93
6.1.3	On/Off Ratio	93
6.1.4	The CV^2 Product	94
6.1.5	Damage Levels	96
6.1.6	Phase Change on Reflection	97
6.2.1	Q-Switch - Device Construction	98
6.3.1	Device Operation	99
6.3.2	Operating Voltage	99
6.3.3	Far Field Pattern	99
6.3.4	Driving System and Operation	99
6.3.5	Insertion Loss	100
6.3.6	Q-Switching Operation	101
6.3.7	Conclusion	101
7.	OPTIMISATION OF CRYSTALS	103
8.	CRYSTAL ORIENTATION	105
9.	CUTTING AND POLISHING PROCESSES	106
9.1	Crystal Cutting	107
9.2	Polishing	107

/...

INDEX continued

10.	MASK PRODUCTION AND ELECTRODE PRODUCTION	110
10.1	Metal Deposition	111
10.2	Photographic and Etch Processes	114
11.	FURTHER WORK	116
11.1	Infra-Red Operation	116
11.2	Chromatic Considerations	117
11.3	Criteria for an Unpolarised Light Device	118
11.4	Far-Field Pattern Control	119
11.5	Uncollimated Light Operation	120
11.6	Sub-Electrode Layers	120
11.7	Use with Quadratic Material	121
11.8	Use of Thin Films	121
11.9	Q-Switching Considerations	122
11.10	Access to Transistor Action	123
11.11	Far-Field Pattern Changes	123
11.12	A Controlled Thin Film Coupler	123
11.13	Far-Field Pattern Information Content	124
ACKNOWLEDGEMENTS		125
APPENDICES:		
F1	COMPUTED PHASE PROFILES FOR THE TIR DEVICE AND THEIR FOURIER CONTENT	126
P1	FIXPAC ILLUSTRATIVE PROGRAMS	128
P2	FORTRAN PROGRAMS - DEVICE PERFORMANCE	129
REFERENCES		132
PUBLISHED PAPERS		

ABSTRACT

This work deals with an analysis of diffraction processes which may offer promise as light deflection/modulation methods. Discrete device applications are considered and two configurations found to be promising. One is a phased array with individually controlled sources followed by a transform lens and a grading mask while the other is a fine impressed phase grating form giving a Raman-Nath type farfield. Both approaches are assessed and both devices realised. The array realisation appears unpromising as yet but the phase grating approach device, constructed by employing the effect of interdigitated electrodes on an electro-optic crystal with the light beam totally internally reflected from the electrode area, proves of considerable interest. This device is assessed in a basic $LiNBO_3$ realisation and the tradeoffs of device construction identified. A typical unoptimised device at 0.63μ offers zero order extinction at ~70 volts. Q switching operation at 1.06μ by such a device is also reported using only 90 volts.

An assessment of device development prospects suggests that much work remains to be done of these TIR devices and it appears that the electro-optic discrete diffraction modulator has considerable advantages over the orthodox birefringent device and is comparable in many respects to the acousto-optic device. These advantages include low insertion loss, ease of driving, and ease of fabrication.

1. INTRODUCTION

1. INTRODUCTION

The influences that can be exerted on the passage of light through matter can fall into five categories:

1. Change of intensity (modulation)
2. Change of frequency (non-linear interaction)
3. Change of phase (phase modulation)
4. Change of direction(deflection)
5. Change of polarisation (activity, birefringence)

The functions with the greatest immediate application are the modulation and deflection of light. Potential uses include the transmission, writing, reading and display of information, Q switching and signal processing. The means employed for the control of light can be divided into three groups:

(i) Mechanical/light interactions
(ii) Piezo or acousto light interactions
(iii) Electro-optic light interactions

These overlap in the matter of response speed and overall performance. (A probable range of responses is presented in Fig. 1.1)

As criteria of modulation efficiency, we consider extinction ratio and device insertion loss and of deflection efficiency, the number of resolvable spots and the unwanted light. The latter quantity may need to be considered as a co-channel interference or as an extinction ratio concept. Both deflection and modulation may be achieved in a variety of ways. In modulation light may be dispersed or absorbed, in deflection energy may be coupled into a number of resolvable directions or into one other. Hence, further sub-divisions of modulation and deflection are needed to describe operation and usage adequately.

It is to be noted that deflectors may be considered as a sub-group of the modulator class i.e.'all deflectors are modulators, not all modulators are deflectors.' Hence, deflectors may be considered as non-absorbent modulators and the two concepts of modulation and deflection are not readily separable.

In confining interest in the high speed end of the range available, several interaction mechanisms are open to us:

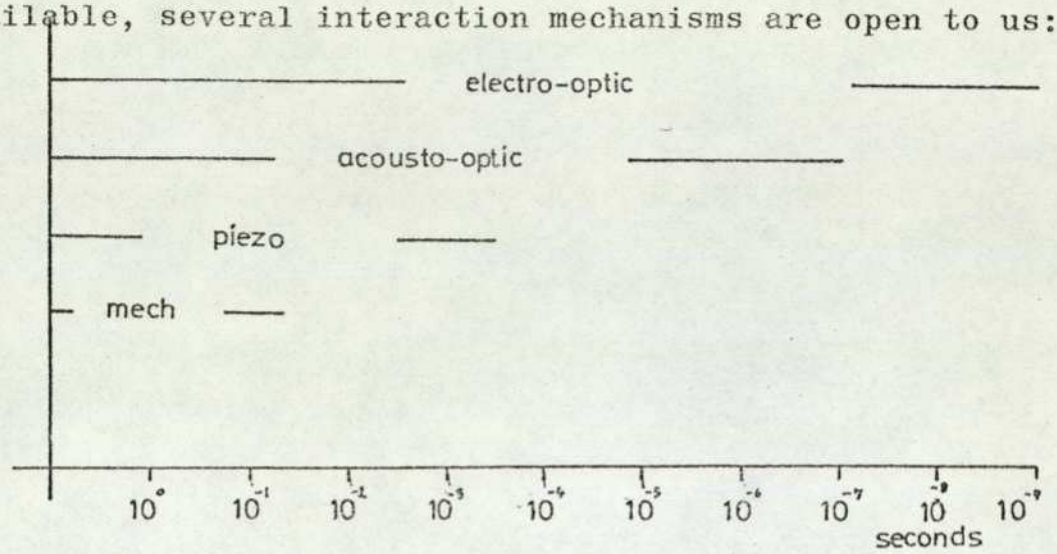


FIG 1.1 RELATIVE RESPONSE SPEEDS

a. Phase modulation

All devices employing mechanical or optical path variation form phase modulators. By a subsequent interference technique this can be turned to intensity or deflection modulation. All birefringent modulators fall into this category.

b. Refractive index variation

Light beams may be curved or reflected if refractive index changes are gradual or abrupt. Such changes may be induced by sound, heat or electro-optic means and form the basis of prism analogue deflectors and total-internal-reflection digital deflectors. Effects may be enhanced in ferroelectrics operated near the curie point.

c. Diffraction techniques

A periodic perturbation in the light beam path causes a grating effect which couples energy into one or many orders. Acousto-optic devices, operated both in Bragg and Debye Sears modes, employ such principles.

d. Band-Edge Shift

In the region of absorption cut-off of a transparent material, refractive index variations are enhanced and materials exhibiting electro-optic or Franz-Keldysh effects may be used for increased sensitivity in this region. Alternatively absorptive modulation is possible.

e. Polarisation changes

Devices that allow recombination of phase shifted orthogonally polarised waves or that exhibit Faraday rotation can be used to change polarisation. Subsequent resolvers allow these devices to be used as modulators or digital switches.

f. Nonlinear interactions

In some materials parametric combination or harmonic generation is a practical proposition. By a combination of nonlinear material properties and phasematching, harmonics may be generated in many materials. Any spectral change can constitute deflection in a dispersive medium.

The advent of the laser has provided a near perfect light source with coherence, good collimation, monochromaticity, and intensity all of a high order. This has provided ideal conditions for the development of modulators and deflectors and virtually all progress has been since 1960 and was further helped by the fact that device users systems were also largely dependent on laser light being available.

1.1. Materials

The scope of the work outlined in this thesis is confined to the electro-optic sector. State of the art performance in electro-optics is materials limited and progress must either come from the improvement (or discovery) of an emergent material or from a novel configuration offering greater sensitivity. Such an improved configuration would be further enhanced by the advent of a new material. Electro-optic modulation implies a choice from a fairly wide range of materials. The ones generally encountered are presented in Fig.1.2 and are included with their key parameters.
In general the greater the electro-optic co-efficients, the less available the material or the more temperamental its use. In spite of the (apparently) wide range in Fig. 1.2 there are relatively few of these materials freely available. Even when samples can be obtained of the more exotic materials they are small and potential usage must allow such small samples to be employed in actual devices. The conclusion is therefore, that immediate advances in device performance cannot depend on materials advances alone and must also be based on the use of novel principles which, preferably, will be further enhanced by superior materials when these become available. Long term prospects of materials improvements are reasonable if a molecular engineering approach is successfully employed and it is possible virtually to design materials to order on a molecular level.

Existing work in this direction appears to indicate dielectric rather than electro-optic improvements.

(Ref. Patent No. 1331228 Dr. M. M. Faktor).

1.2. Device Criteria

Modulators and deflectors require some criteria of quality so that the parameters to be examined will allow the tradeoffs to be indentified and a true assessment of device progress made.

TABLE OF ELECTRO-OPTIC MATERIALS

Material and formula	Ammonium Dihydrogen Phosphate (ADP) $NH_4H_2PO_4$	Potassium Dihydrogen Phosphate (KDP) KH_2PO_4	Potassium Dideuterium Phosphate (DKDP, KD*P) KD_2PO_4	Ammonium Dihydrogen Arsenate (ADA) $NH_4H_2AsO_4$	Potassium Dihydrogen Arsenate (KDA) KH_2AsO_4	Deuterated Cesium Dihydrogen Arsenate (DCDA)	Rubidium Dihydrogen Arsenate (RDA) RbH_2AsO_4	Lithium Niobate $LiNbO_3$	Lithium Tantalate $LiTaO_3$	Barium Sodium Niobate (BSN) $Ba_2NaNb_5O_{15}$	Potassium Tantalate Niobate (KTN) $KTa_{1-x}Nb_xO_3$	Strontium Barium Niobate (SBN) $Sr_{1-x}Ba_xNb_2O_6$	Barium Titanate $BaTiO_3$	Zinc Sulphide ZnS	Cuprous Chloride CuCl	Gallium Arsenide GaAs	Cadmium Telluride CdTe	Zinc Telluride ZnTe	Nitrobenzene $C_6H_5NO_2$	Barium Titanate $BaTiO_3$	Potassium Tantalate $KTaO_3$	Strontium Titanate $SrTiO_3$
Electro-optic coefficients ($\times 10^{-12}$ m/V)	r_{63}^T=-8.5 r_{41}^T=24 r_{63}^S=8.5	-10.5 8.6 8.8	26.4 8.8 24.0		r_{63}^T=10.9 r_{41}^T=12.5	r_{63}=38.7	r_{63}^T=13	r_{33}^S=30.8,22 r_{33}^T=8.6 r_{13}^T=3.4 r_{42}^T=28	r_{33}=30.3,22 r_{33}=7 r_{13}=1 r_{42}=20	@60Hz r_{33}=48 $r_{13}=r_{23}$=14 $r_{42}=r_{51}$=91	g_{11}=0.136 g_{12}=-0.038 $g_{11}-g_{12}$=0.174 g_{44}=0.147		$r_{51}-r_{42}$ (T) 1640 (S) 820	$\bar{4}3m$ r_{41}=2.1 6mm r_{33}=1.85 r_{13}=0.92	r_{41}=4.25	r_{41}=1.6	r_{41}=6.8	r_{41}=3.95	K=4.6 m/v^2 @637nm	g_{11}=0.12 g_{12}=0.01 (m^4/cm^4)	$g_{11}-g_{12}$=0.16 g_{44}=0.12	$g_{11}-g_{12}$=0.14
Spectral range (μ)	0.2 - 1	0.2 - 1	0.2 - 1.5	0.2 - 1		0.2 - 1		0.45 - 5	0.4 - 4.5	0.45 - 5	0.5 - 6	0.4 - 6		0.4 - 12	0.4 - 20	1 - 11	0.9 - 14	0.55 - 20	- 3.9			
Crystal type	$\bar{4}2m$	$\bar{4}2m$	$\bar{4}2m$	$\bar{4}2m$	$\bar{4}2m$	$\bar{4}2m$	$\bar{4}2m$	3m	3m	mm2	P4m3m for T>273°K	4mm	$m\bar{3}m$	6mm	$\bar{4}3m$	$\bar{4}3m$	$\bar{4}3m$	$\bar{4}3m$	LIQUID	m3m	m3m	m3m
Dielectric constants	ε_a^T=15 ε_a^S=14 ε_c^T=56 ε_c^S=58	ε_a^T=21 ε_a^S=21 ε_c^T=42 ε_c^S=44	ε_a^T=50 ε_a^S=48 ε_c^T=58	ε_c^T=14 ε_a^T=75 ε_c^S=13 ε_a^S=74	ε_T=21 ε_T=54 ε_S=19 ε_S=53	ε_a=64 ε_c=61	ε_T=27 ε_T=41 ε_c=24 ε_S=39	ε_a^S=44 ε_a^T=84 ε_{33}^S=29 ε_{33}^T=30	ε_a^S=45 ε_a^T=43 ε_{33}^S=51 ε_{33}^T=41	ε_3^T=42 ε_3^S=30	> 15,000		(T) 3000, 170 (S) 2000, 100	8.2	8.3	12.5 @10.6μ @d.c.	$\varepsilon \pm 11$ do ε_∞=7	10		3000 170 2000 100		
Loss tangent	$\tan\delta_o$= 7.10^{-3} $\tan\delta_e$= 6.10^{-3}	4.5.10^{-3} 7.5.10^{-3}	2.5.10^{-3} 1.0.10^{-3}	$\tan\delta_c$= 6.10^{-3} $\tan\delta_a$= 1.10^{-3}	8.0.10^{-3} 7.5.10^{-3}		$\tan\delta_3^S$= 35.10^{-2} $\tan\delta_1^S$= 3.10^{-2}	c axis < .02	<10^{-3}	≤0.006	fn of temp ~.0025 @ 10°C				1.2.10^{-3}							
Halfwave volts for a unit cube @633nm	6.14kV r_{41} 14kV r_{63}	9.1kV r_{63}	9.1kV r_{63} long 12.8kV r_{63} trans	2.63kV r_{41} 8.37kV r_{63}	6.4 kV @550nm	2.7kV		3.0kV r_{33}	2.8kV r_{33}	1.57kV r_{33}	0.347kV for 1st extinction	0.48kV r_{33}	0.48kV r_{33}		5.8kV	91kV r_{41} @ 10.6μ	44kV @10.6μ		35kV			
Availability	excellent	good	good	reasonable		reasonable	poor	excellent	reasonable	average	very poor	poor	poor	poor		good	good		good	poor	poor	poor
Comments	handling & polishing difficulties, hygroscopic	similar to ADP	similar to ADP					hard, common pyroelectric effects	higher damage threshold than $LiNbO_3$	quadratic effect material, affected by high voltages				may be photoconductive		useful at 10.6μ	useful at 10.6μ		one of several Kerr liquids	cubic	cubic	cubic
Refractive indices @6328Å	1.53 1.48	1.51 1.47	1.51 1.47	1.57 1.52 (.65μ)	1.52 (.55μ) 1.57		1.52 (.55μ) 1.56	2.29 2.20	2.180 2.176	2.22 2.32	2.287	2.26 2.32	2.36 2.42	2.35	1.968 (615nm)	3.34	2.3 cubic	2.91	1.55	2.4	2.24	2.38
Resistivity	σ_o=3.7.10^{-9} S/m	σ_o=2.5.10^{-9} σ_e=5.5.10^{-9} S/m		6.10^7 Ω-cm	>10^8 Ω-cm @ 20°C			5.10^{-8} Ω-cm @400°C	<10^{13} Ω-cm @ 20°C	1.46.10^4 Ω-cm	10^{14} Ω-cm			3.10^{13} Ω-cm		10^6 Ω-cm	10^6 Ω-cm					
Nonlinear coefficients	@1.06μ d_{36}=0.93 d_{14}=0.89	@1.06μ d_{36}=1.0 d_{14}=1.01 d_{36}=3.10^{-9} e.s.u.	@1.06μ d_{36}= 0.92 d_{14}= 0.91		@ 1.06μ d_{36}=1.06 d_{14}=1.12			d_{22}=6.3 d_{31}=11.9 @1.08μ	d_{22} = 4.3 d_{31} = 2.6 d_{33} = 40	d_{33} = 34.4 d_{31} = 29 d_{32} = 33.9 @1.06μ						d_{14}=560±140 @1.06μ				
Curie Temp °K	148	123	221	219	95		110	1210	650	560	-52 - +15°C	470	405	401	407				/	405	4	low

Modulators and deflectors need to be driven with ease. All electro-optic devices exhibit capacitance and, usually of less significance, resistance. These are voltage driven devices. Hence, one aspect of quality is low capacitance, high resistance, and a low drive voltage. A freedom from piezo resonances is also very desirable as both device operation and driving can be greatly affected and usable bandwith reduced by undue resonances. Occuring in micro-second type intervals high speed (nanosecond) device action on a one shot basis is fortunately not troubled by these effects.

In general the power dissipated is a combination of resistive and dielectric losses with the latter predominating. Resistivities are usually very high in electro-optic materials (e.g. $\sim 5 \times 10^8$ Ω- cm in Lithium Niobate) and resistive power dissipation is hence not as important as loss tangent, especially so as electro-optic systems offer the only opportunity of high frequency operation. Drive system problems are largely proportional to the CV^2 product where C is device capacitance and V the operating voltage. Linear drive system power dissipation, both peak and average, can be expressed as:-

$$P_{drive} \propto fCV^2 \qquad 1.1.$$

where f is the operating frequency.

In practical devices it is, therefore, doubly important to maintain small operating voltage ranges. This is naturally less essential in switching applications but if low switching times are combined with large voltage requirements then system design becomes difficult due to the lack of suitably fast high voltage devices. Ideally, we would wish for operating conditions of electro-optic devices to be within semiconductor technology bands and preferably at logic voltage levels.

The electro-optic interaction process, whereby the index ellipsoid is modified by the presence of an electric field, involves very little or no energy apart from that required to establish the field.

1.3. Practical Devices

Modulation and deflection in electro-optics are traditionally achieved by field induced phase modulation and refractive index change respectively. Phase modulation of significant magnitude (several wavelengths) is achieved readily and so birefringent electro-optic intensity modulation is equally readily achieved. Deflection, achieved by refractive index variations, is not so satisfactory, however, as these changes tend to be extremely small (much less than 0.1% even in the most favourable material) and do not allow useful deflection angles. The basic limiting of the number of achievable resolvable spots is the ratio of the deflection angle compared with the unavoidable beam divergence.

A beam of half divergence θ, deflected through an angle ϕ gives a number ofRayleigh Criterion resolvable spots N:

$$N = \frac{\phi}{\theta} = \frac{\phi w}{\varepsilon\lambda} \qquad \text{1.2.}$$

where w is the beam width

and $\varepsilon = 1$ for a rectangular section beam

and $\varepsilon = 1.27$ for a gaussian section beam

(Ref. Fowler & Schlafer)

Analogue deflection can convey more information than the number of resolvable spots suggests as the Rayleigh Criterion can be improved upon by detection system or beam profile changes.

1.4 Electro-optic Deflectors (Fig. 1.3)

These can be classified into three groups:

1. Prism Deflectors - These operate on the induced refractive index change principle and can also be considered as a special case of a refractive index gradient deflector. The deflection angle is readily shown to be:

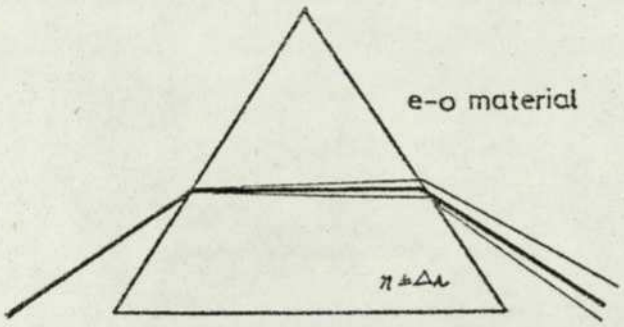


FIG. 1.3 PRISM DEFLECTOR

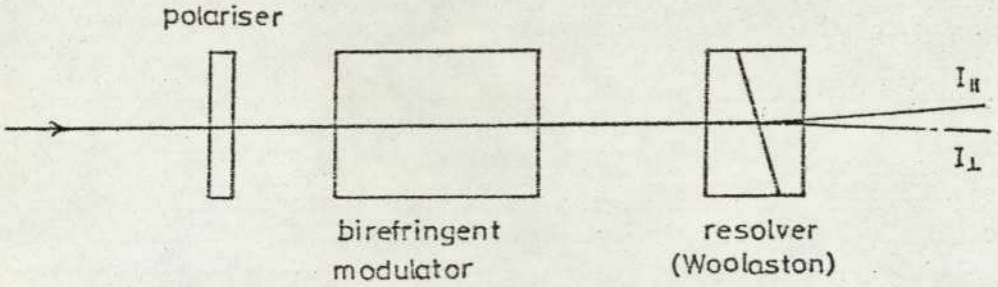


FIG. 1.4 DIGITAL DEFLECTOR

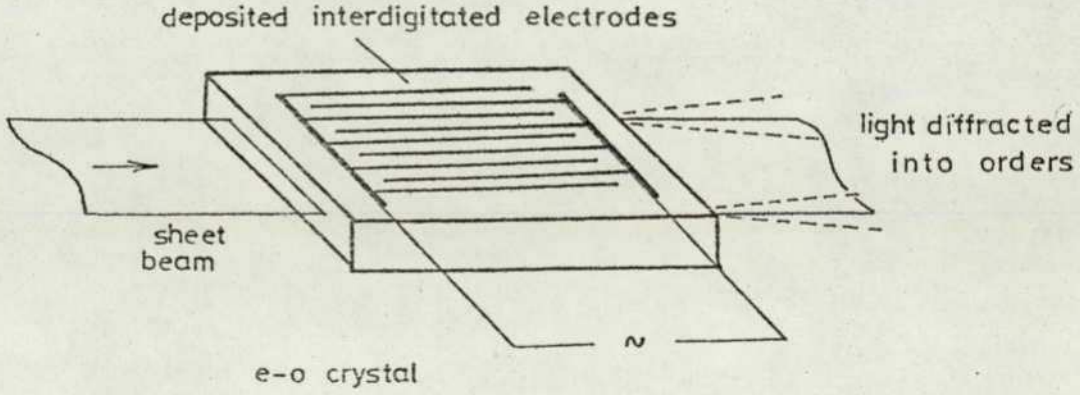


FIG. 1.5 DIFFRACTION DEVICE

$$\phi = \frac{\Delta n.x}{w} \qquad 1.3.$$

where Δn is the induced refractive index variation, and x is interaction distance and the number of resolvable spots:

$$N = \frac{\Delta n.L}{\lambda} \qquad 1.4.$$

where L is the device length and

tends to be limited by available material sizes. Operation of devices using this principle have yielded (Ref. Jones & Forno) a KTN prism which gave a deflection of 2.6^{o} at 2 kV and 10 resolvable spots. Material quality proved a problem and operation, as well as falling short of the predicted 100 spots, proved unrepeatable due to drift. An alternative approach (Ref. Kiefer) involved a multiple prism KD*P device near curie temperature and gave 200 resolvable spots at 10kV with 20% insertion loss and 120kHz operating bandwidth.

The shortcomings of these devices are the high voltages required, the poor availability and quality of materials like KTN, and the low bandwidths apparently achievable.

2. <u>The Digital Deflector (Fig. 1.4.)</u>

This is basically an electo-optic modulator configuration of polariser, birefringent or magneto-optic modulator, and deflecting analyser. Such devices form usable reading and addressing systems when cascaded. The deflecting analyser may be a Woolaston prism, or calcite prism for diverging beam direction, or a total internal reflection system which uses the polarisation sensitivity of reflection. The latter system offers large deflection angles and divergence or convergence of deflected directions as well as insensitivity

to wavelength. The cascading of N digital deflectors yields 2^N spot positions. A useful measure of performance is 'noise', i.e. light in a unaddressed direction as a percentage of light in an addressed direction. A typical system (Ref. Habegger) gave a noise of 1%, an insertion loss of 10%, and a 2kV per stage operating voltage. KD*P was used. Another reported system using $LiNBO_3$ (Ref. Mikaelyan) used iceland spar resolvers, and offered 10% insertion less, per stage, 1kV operating voltages, 100 kHz maximum frequency and a noise of 0.5%.

It may be readily seen that the common factors of this principle are excessive voltages and low operating frequency range. The latter is doubly unfortunate as electo-optic devices have speed potential as their major advantage.

3. Diffraction Devices

Thin film optical devices translate three dimensional problems basically into two dimensions. Techniques developed in thick and thin film forms, tending towards integrated optics applications, appeared to exhibit promising performanc. Prominent devices in this category were St. Ledger & Ash[1] (1968) Fig(1.5) Hammer[2] (1971), De Barros & Wilson[3] (1971), and Gia Russo & Harris[4] (1971). An interesting and unique method using a microwave generated grating was suggested by Gordon (1965):

Table 1.1.

Device	1 & 3	2	4	
Material	$LiNBO_3$	$LiNBO_3$	Nitrobenzene	
% Modulation	~100%	74	3.2	
Volts	25	800	30	at 6328 A^o
Response	<1.5 nS	<10nS		
Electrode Pitch	300μ	300μ	12.8μ	

These devices combine low, or very low, voltages with fast response and the absence of a resolver. The modulation is of Raman and Nath type with a phase corrugation being impressed on the light wavefronts and the resultant far field pattern exhibits the coupling of energy into various order directions. Devices 1 and 3 assume a zero thickness incident sheet beam while device 2 allows for finite beam thickness and device 4 operates on a guided thin film principle.

No device applications have been reported to date for this type of device although development is continuing.

This classification of electro-optic modulator/deflector classes is generalised, but all unusual device configurations (e.g. Fabry-Perot modulators, critical angle deflectors etc.) can be associated with one or other of the basic groupings.

1.5. Conclusions

From the relative performance of these three classes of device it appears that the most useful performance is suggested by the thin film devices operating on the diffraction principle. While really of use in integrated optics only, nevertheless, the conclusion is that diffraction processes offer promise whereby the required deflection or modulation effect is achieved by synthesizing wavefront phase to cause changes of virtual direction, thereby harnessing the fact that light does not travel in straight lines.

With a view to studying the prospects of diffraction processes a range of possible configurations are examined in the next section and promising systems isolated. This work therefore undertakes the analysis and construction of discrete diffraction devices.

2. POTENTIAL MODULATION/DEFLECTION PROCESSES - A STUDY OF DIFFRACTION CONFIGURATIONS

2. POTENTIAL MODULATION/DEFLECTION PROCESSES - A STUDY OF DIFFRACTION CONFIGURATIONS

In order to identify systems of promise, a range of interference configurationswas examined by modelling on a Ferranti FM1600B computer using FIXPAC and a line plotter output.
(These programs are listed in Appendix P1)

This modelling technique illustrates the operation of the fundamental diffraction phenomena which can form the basis of modulation/deflection methods.

Starting with the multiple slit diffraction grating and considering Fraunhofer diffraction initially (Fig.2.1) the far field intensity can be expressed as:-

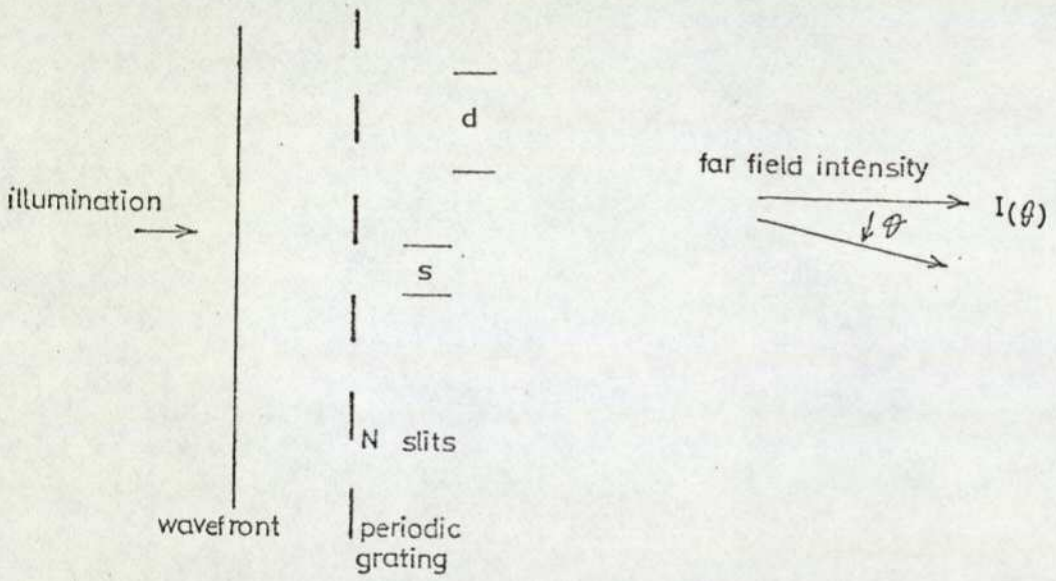


FIG 2.1 FRAUNHOFER DIFFRACTION

$$I(\theta) = I_0 . f_1(\theta) . I_1 \qquad (2.1.)$$

Where I_0 is the slit function (depends on S) , I_1 is the interference function (depends on d, N) and $f_1(\theta)$ is the obliquity factor (depends on θ)

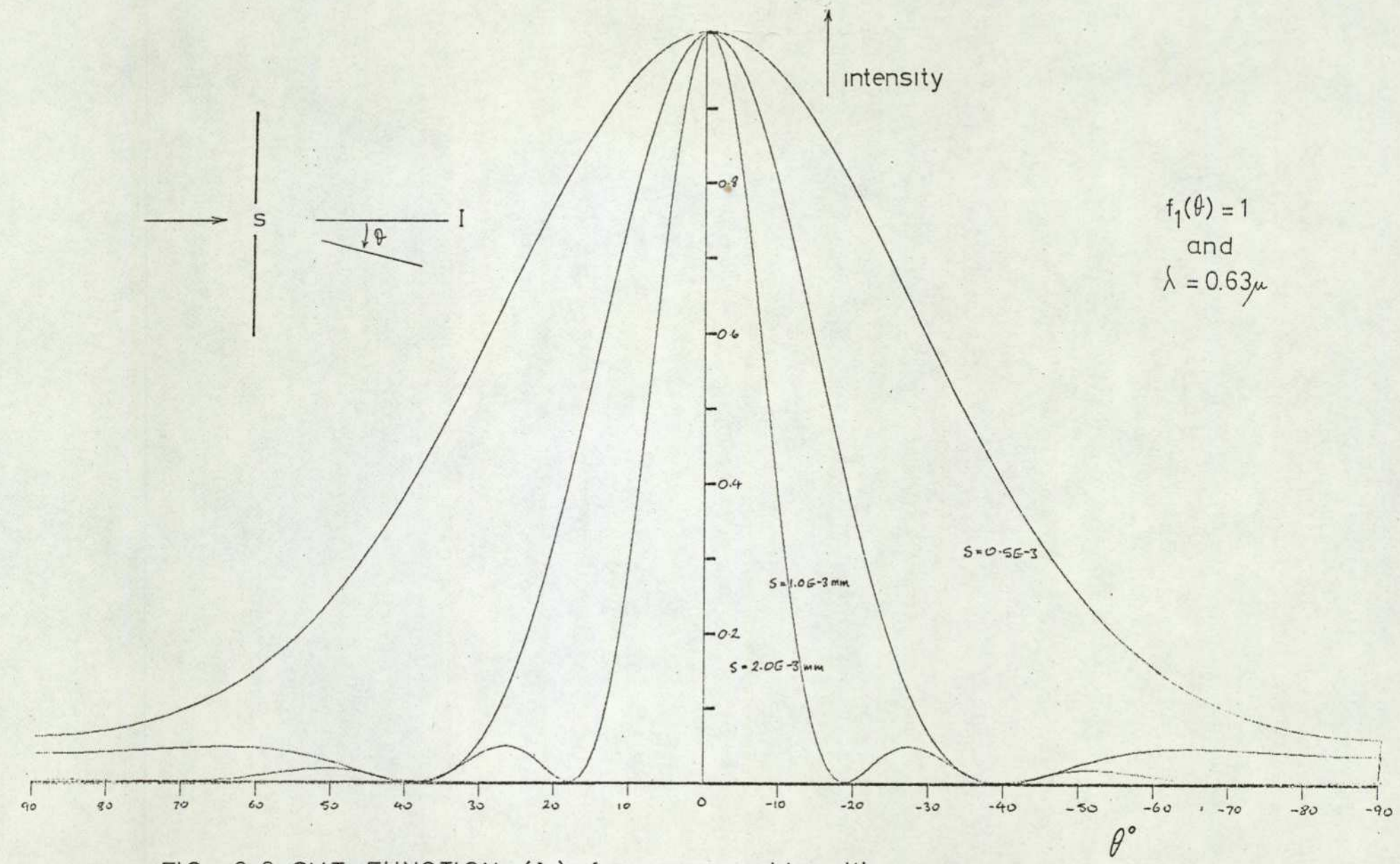


FIG. 2.2 SLIT FUNCTION (I_o) for various slit widths

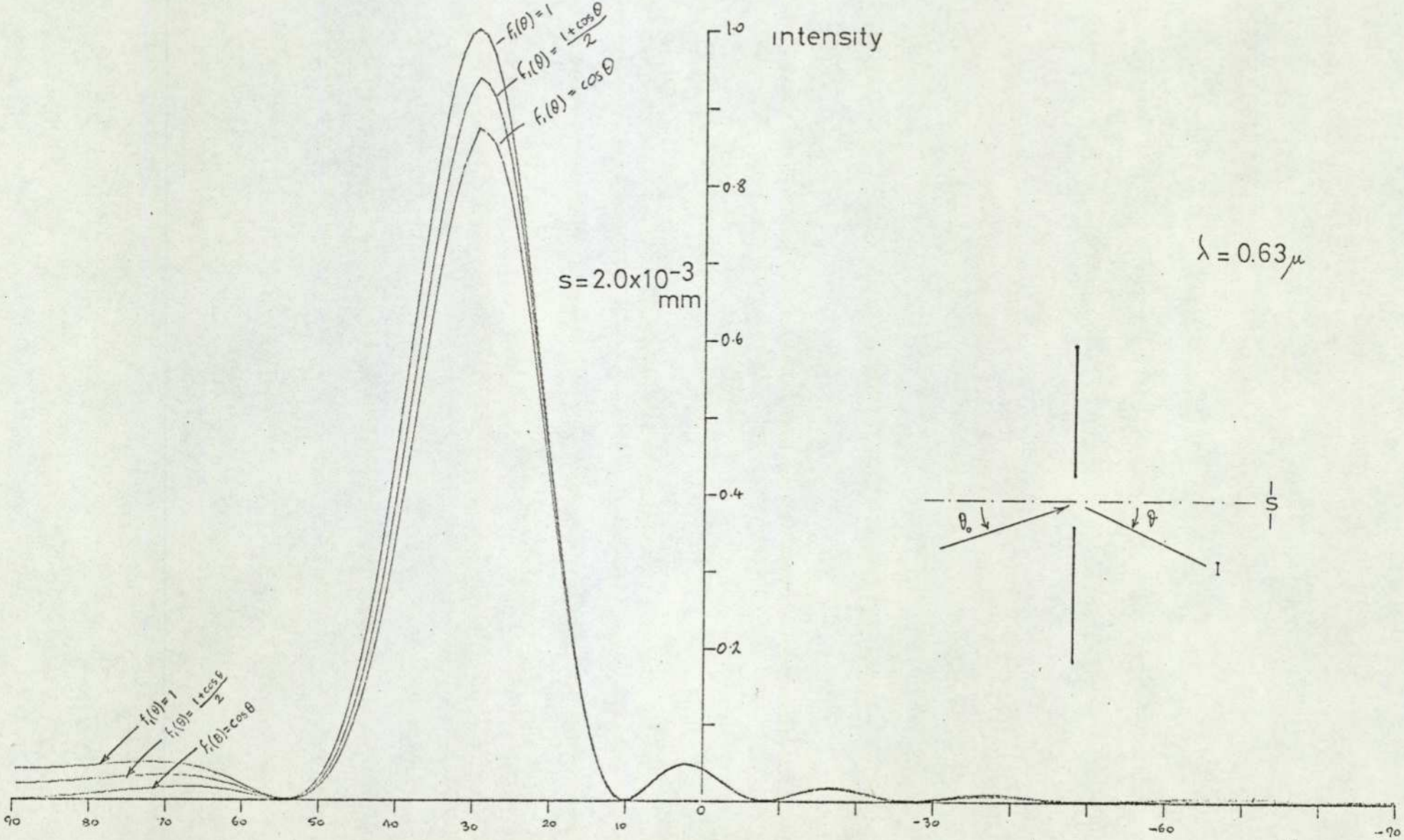


FIG. 2.3 SLIT FUNCTION (I_0) for various obliquity factors

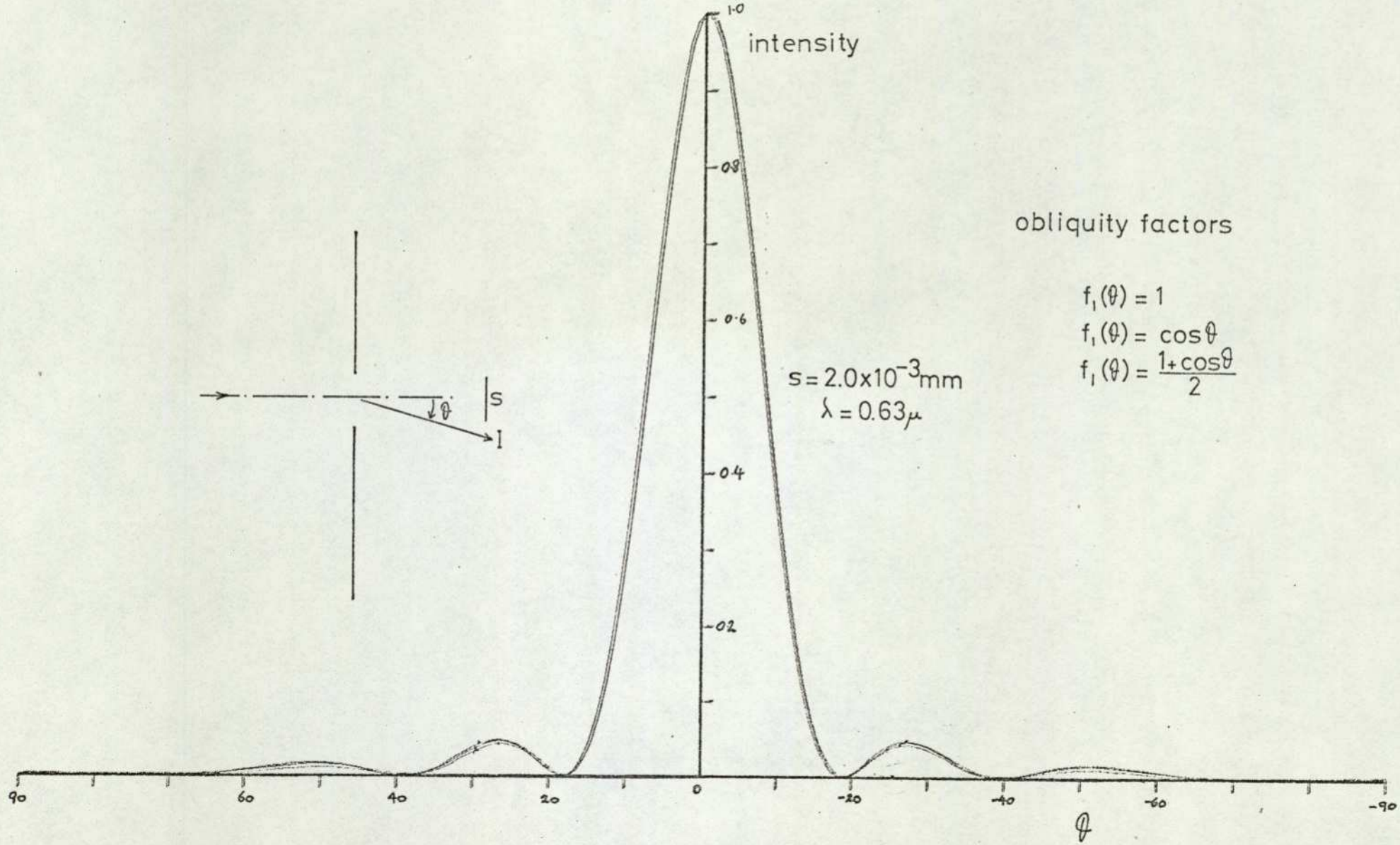


FIG. 2.4 SLIT FUNCTION (I_o) for various obliquity factors

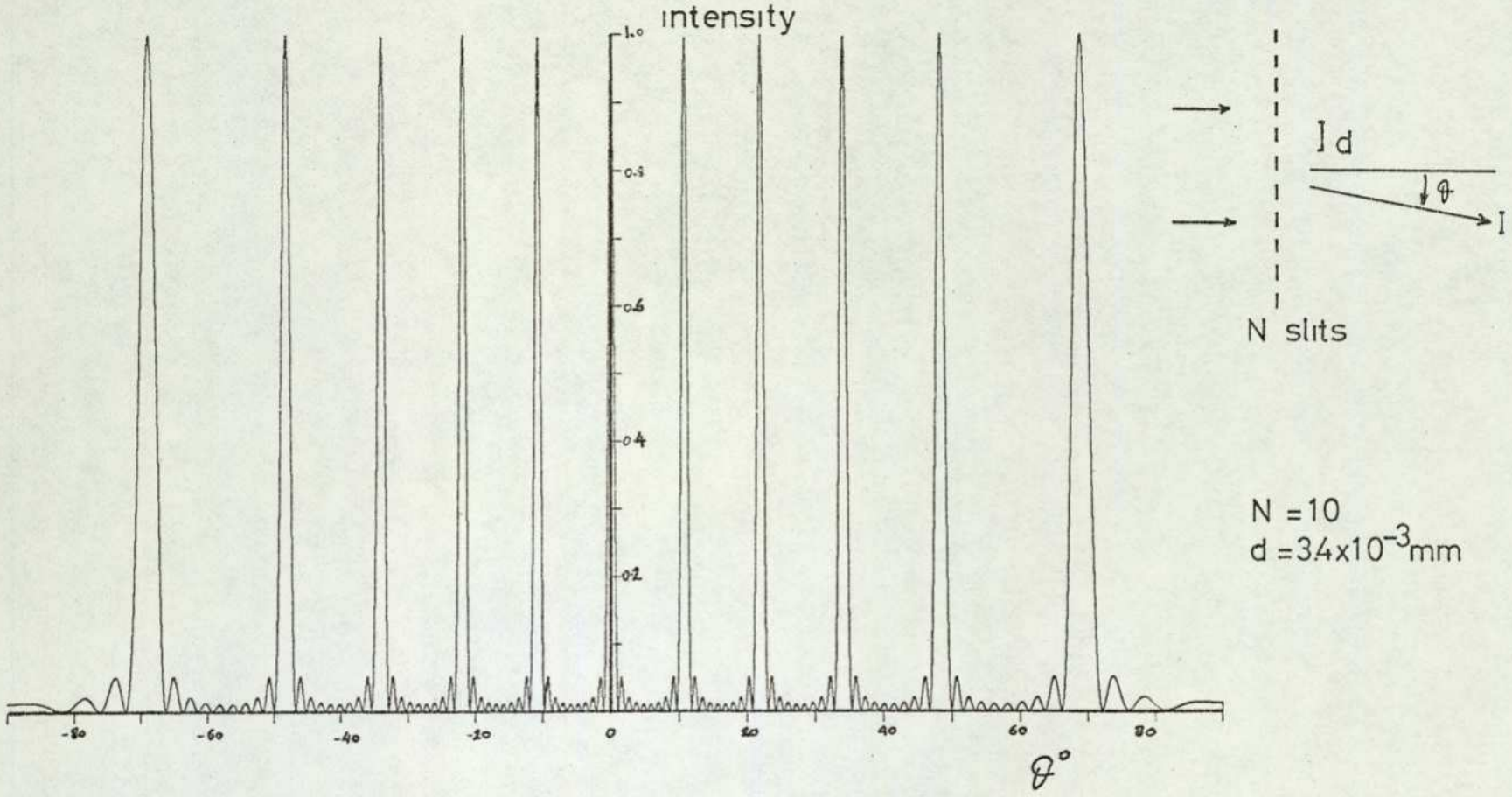


FIG. 2.5 INTERFERENCE FUNCTION (I_1) at $\lambda = 0.63\mu$

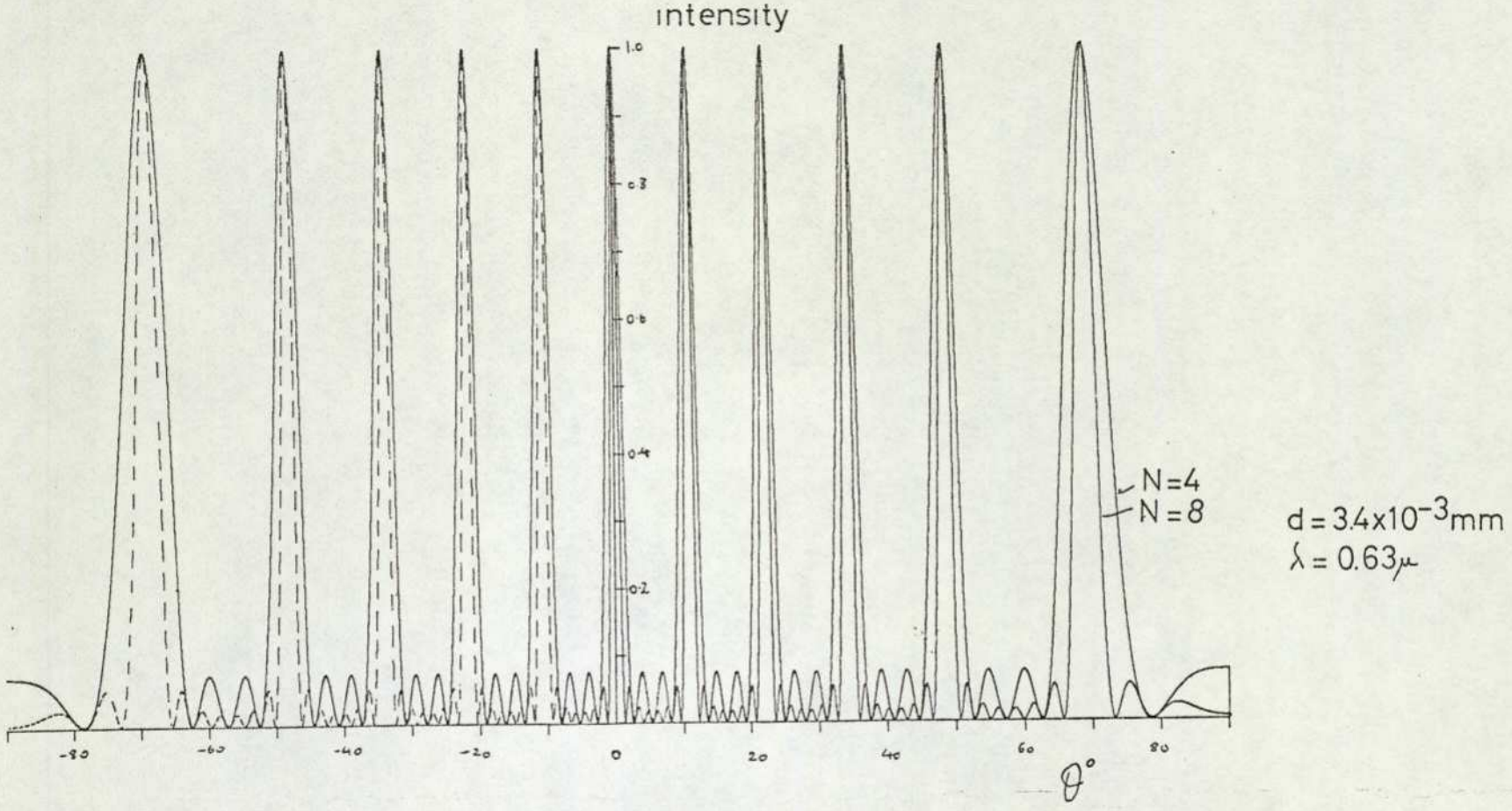


FIG. 2.6 INTERFERENCE FUNCTION (I_1)

The obliquity factor may be used to compensate for the $\theta = \pi/2$ case or to furnish the complete Huygens wavefronts condition, that wavefronts do not propagate for the $\theta = \pm\pi$ direction.

The slit function may be estimated by summing the vector amplitude from increments across a period of the grating as a function of ϑ . The generalised grating form is a periodic perturbation of refractive index or transmissivity of a medium and the multiple slit grating is just an idealisation of it.

Hence
$$I_o = \left[\lim_{m\to\infty} \sum \frac{1}{m} \sin\left((m-1)\frac{2\pi s}{m\lambda}\gamma_1\right)\right]^2 + \left[\lim_{m\to\infty} \sum \frac{1}{m} \cos\left((m-1)\frac{2\pi s}{m\lambda}\gamma_1\right)\right]^2 \qquad (2.2)$$

where $\gamma_1 = \sin\vartheta + \sin i$ and i is the incidence angle and similarly

$$I_1 = \left[\sum_{n=1}^{N} \frac{1}{N} \sin\left((n-1)\frac{2\pi d}{\lambda}\gamma_2\right)\right]^2 + \left[\sum_{n=1}^{N} \frac{1}{N} \cos\left((n-1)\frac{2\pi d}{\lambda}\gamma_2\right)\right]^2 \qquad (2.3)$$

where $\gamma_2 = \sin\vartheta + \sin i + \frac{\Delta n}{2\pi}$ where Δn is a phase modulation term. (2.4)

These forms are presented here because they form the basis of a computing approach and can readily be extended to cope with Fresnel diffraction. The normal expressions for the completed summations are:

$$I_o = \left[\frac{\sin(\pi s\gamma_1/\lambda)}{\pi s\gamma_1/\lambda}\right]^2 \qquad (2.5)$$

and
$$I_1 = \left[\frac{\sin(\pi N d\gamma_2/\lambda)}{\sin(\pi d\gamma_2/\lambda)}\right]^2 \qquad (2.6)$$

but any induced variation in γ_2 requires an incremental approach such as the former. (All these expressions are norma lised to unity.)

Although equation 2.2 can be expanded over the whole aperture and will include the same information as calculating I_o and I_1 separately, it would require more operations (N x M rather than N + M).

Typical computed patterns of simple slit functions are shown in Figures 2.2, 2.3, 2.4 which illustrate the effects of slit width (Fig. 2.2), incidence angle (Fig. 2.3) and the three possible obliquity factors.

Figure 2.5 shows a typical interference function achievable from a periodic structure. Orders recur at angles decided by

$$d \sin \theta = \pm n\pi \qquad (2.7)$$

and order divergence varies with N so that the superposition of interference function will allow N Rayleigh resolvable order directions. Figure 2.6 shows the effects of slit width on I_1.

It must be emphasised that information contained in such a case may be more than the quoted Rayleigh number. The condition that the maximum on one spot coincides with the first minimum of the adjacent spot is essentially a visual criterion and any aperture or intensity threshold detection system can, depending on beam profile extend the number of directions that can be resolved.

So far interference and slit functions have been considered as symmetrical functions, but it is possible and often useful to 'blaze' gratings so that certain orders become preferred and contain a larger amount of enery than in the unblazed case. This blazing effect may be achieved by causing the periodic index or transmission perturbation not to be symmetrical in nature. Hence, a modulation/deflection effect can be achieved either by the establishing of various forms of I_1 for a given I_o, by the modification of

I_o for a given I_1 or by the variation of both functions. So far the diffraction process has been considered as passive but will now be considered in active configurations where some control is exercised over the far field pattern.

2.1. The Controlled Grating Process

Considering a line grating as a phased array of sources, the parameters of each source are phase, intensity and slit function. These can be varied by realisable configurations. The effects of varying intensity or amplitude across a grating aperture are similar and unpromising. This is illustrated in Figure 2.7 and qualitatively diffusion and not deflection is exhibited.

The ideal device that one would wish to realise is a phased array which allows the construction of any phase profile across the device aperture and hence any deflection angle within the slit function of the individual sources. For usable deflections the inter-source spacing must be small, preferably comparable to light wavelength. Unfortunatel individual sources are not yet technically feasible at optical dimensions (unlike microwave dimensions) so the realisation of this can be approximated by two means:

1. Forgoing individually controlled sources and accepting dependent sources.

or 2. Constructing a large array and reducing its effective size by appropriate optics.

Both these approaches are presented in the following simulations constituting viable modulator/deflector approaches.

2.2. Dependent Sources

The simplest configuration comprises adjacent controlled sources where two beams are employed with variable phase between them. Each source then illuminates adjacent slits in a hypothetical line grating. As I_1 is being examined identical, or comparable slit functions are assumed if the illustrated operation is to be achieved.



FIG. 2.7 INTERFERENCE FUNCTION with intensity variation across device aperture

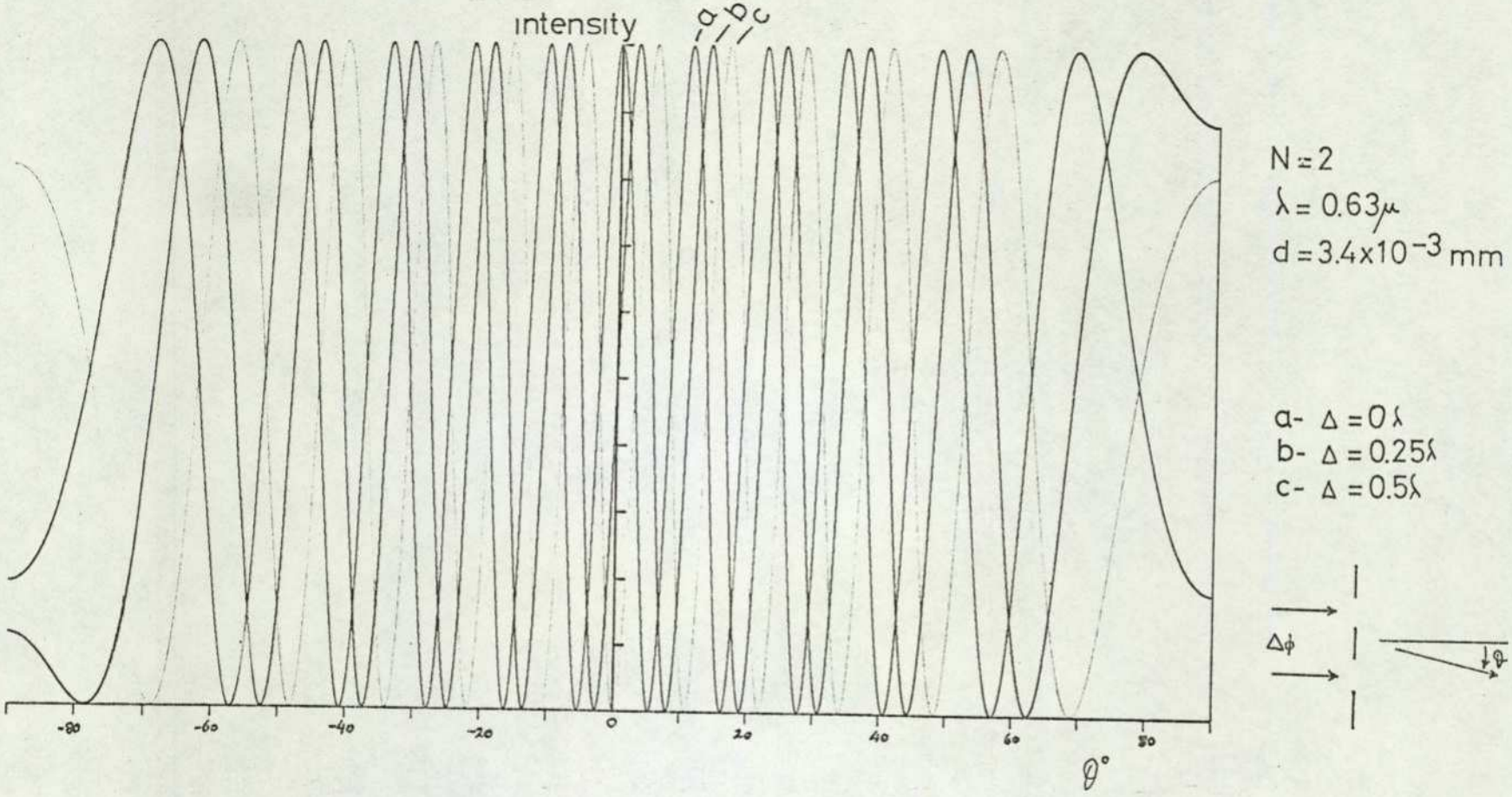
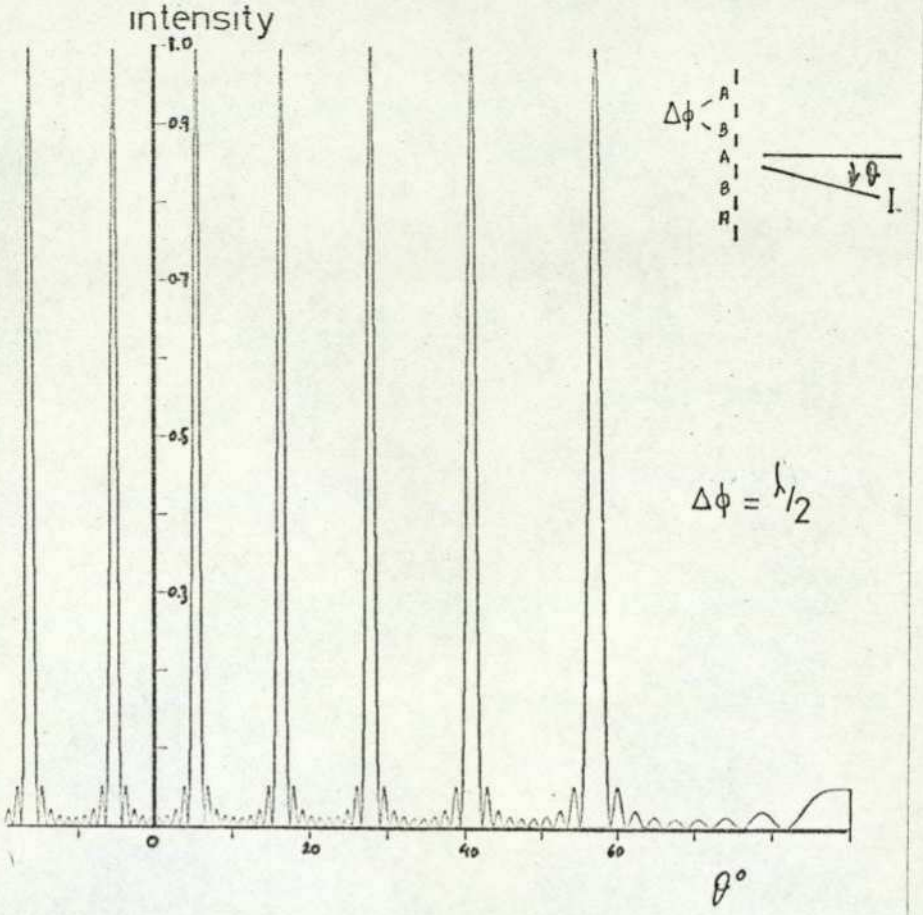
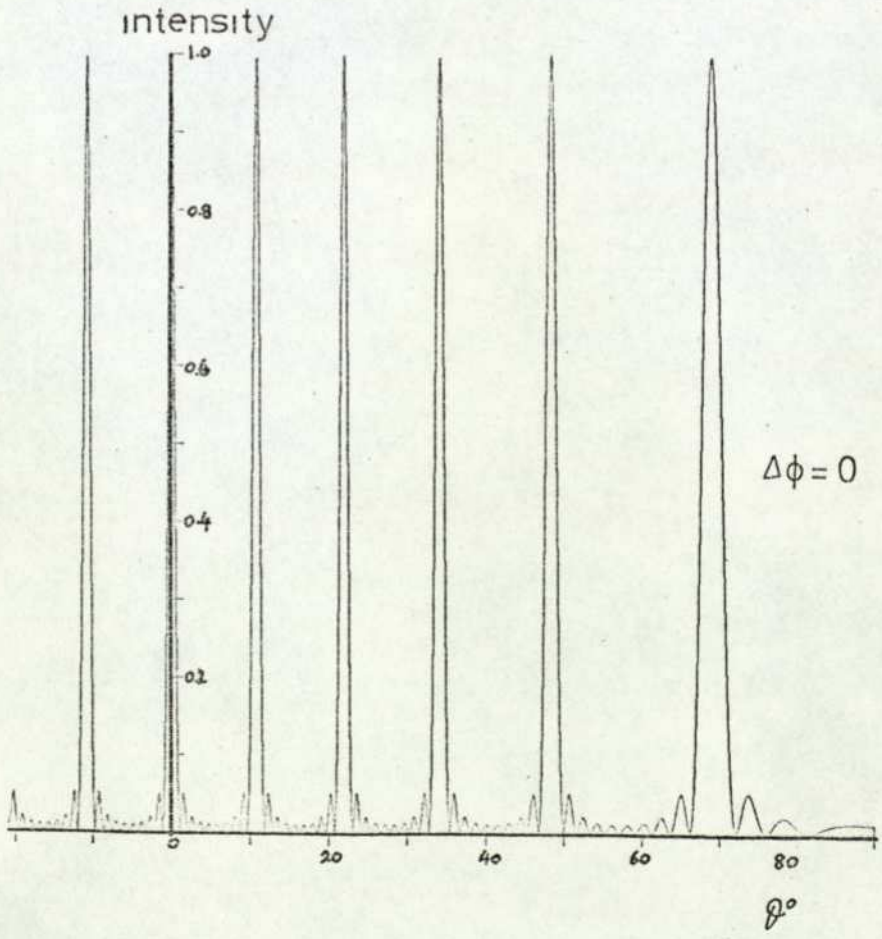


FIG. 2.8 INTERFERENCE FUNCTION (I_1) Youngs Fringes

FIG. 2.9 INTERFERENCE FUNCTION (I_1) adjacent controlled sources





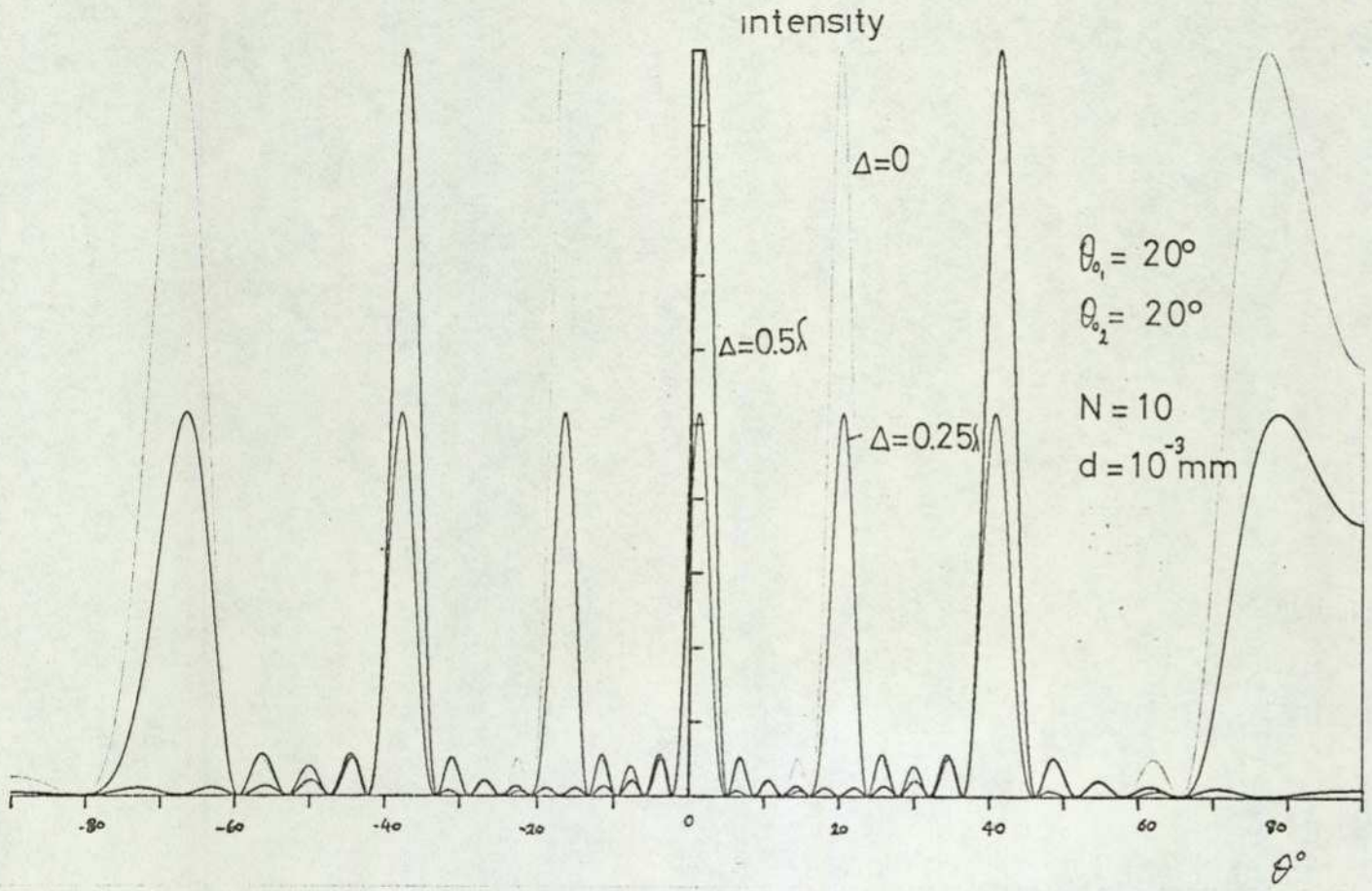


FIG. 2.10 INTERFERENCE FUNCTION (I_1) coupling between orders

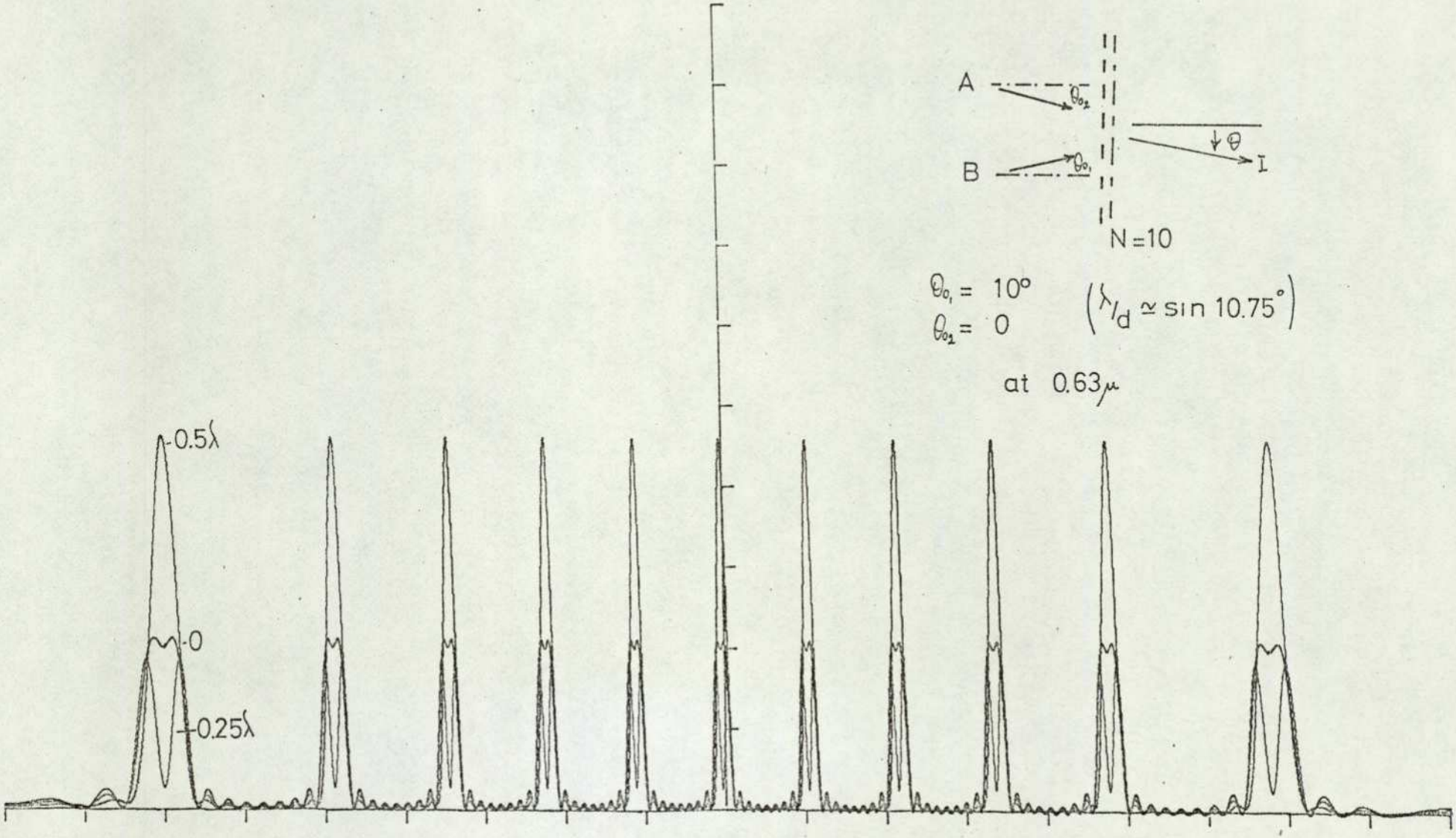


FIG. 2.11 INTERFERENCE FUNCTION (I_1) for $\theta_{o_1} \neq \theta_{o_2}$ and adjacent controlled sources

Figure 2.8 illustrates this effect with two slits which gives a fringe pattern and shows fringe movement with a change of phase and demonstrates the Rayleigh resolution criterion between $\Delta\phi=0, \Delta\phi=\pi$ cases.
Figure 2.9 illustrates the patterns obtained for ten such adjacent slits for $\Delta\phi=0, \Delta\phi=\pi$ and shows good potential for modulation and deflection. This is the nature of the change in I_1 in Raman Nath type interactions. The intermediate phase retardation in Figure 2.10 shows the nature of the coupling between the deflected $(\Delta\phi=\pi)$ and the undeflected $(\Delta\phi=0)$ conditions and demonstrates a digital deflection type of action. This type of operation is characteristic of the thin-film diffraction modulators mentioned in section 1.3. Another aspect of operation is that the slit function also varies with phase profile so that final far-field patterns exhibit more complicated characteristics

2.3. Grouped Controlled Sources

Three configurations were modelled: adjacent controlled sources (ABAB etc.), adjacent controlled sources in pairs (AABB etc.), and adjacent controlled sources in threes (AAABBBAAA etc.). Such systems are realisable with the aid of blazed or holographic gratings but proved to offer little promise. The ABAB case for incident light at the correct inter-order angle for the wavelength acts as a resolver (Figure 2.11) and suggests a modulation of maximum to minimum transmission with a $\frac{1}{4}$ relative retardation. Sources in pairs and sets of three coupled energy into side orders (Figures 2.12, 2.13) without any appealing effect with variation of relative retardation for any combination of incident light angles.

It must be stressed that the slit function for the interference function quoted would not overlap for $\theta_{o_1} \neq \theta_{o_2}$ and these patterns would never be realised but as slit width is reduced and overlap becomes possible, the principles could be demonstrated, albeit with very low efficiency as the S/d ratio would then tend to be small.

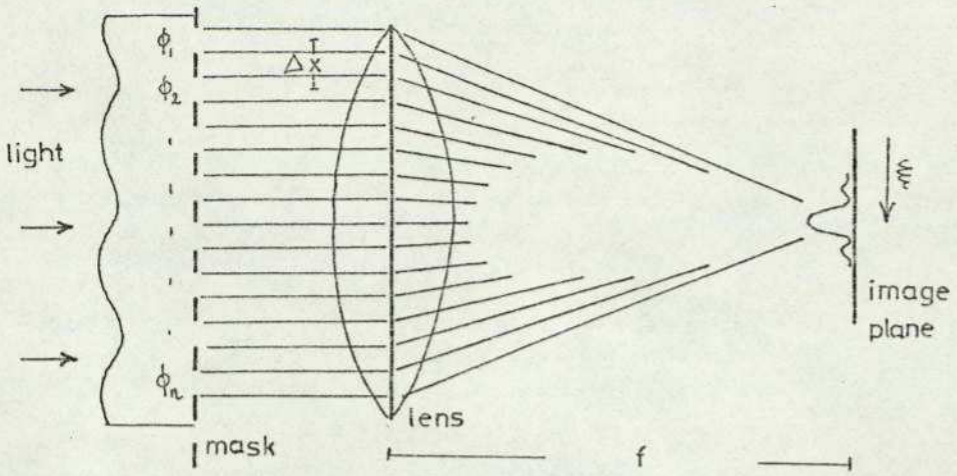


FIG 2.14 TRANSFORMED ARRAY

ARRAY REALISATION

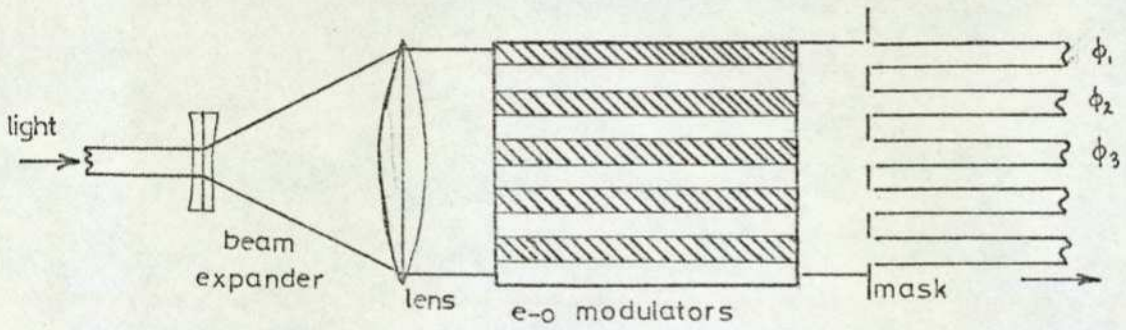


FIG 2.15 INDEPENDENT (PARALLEL)

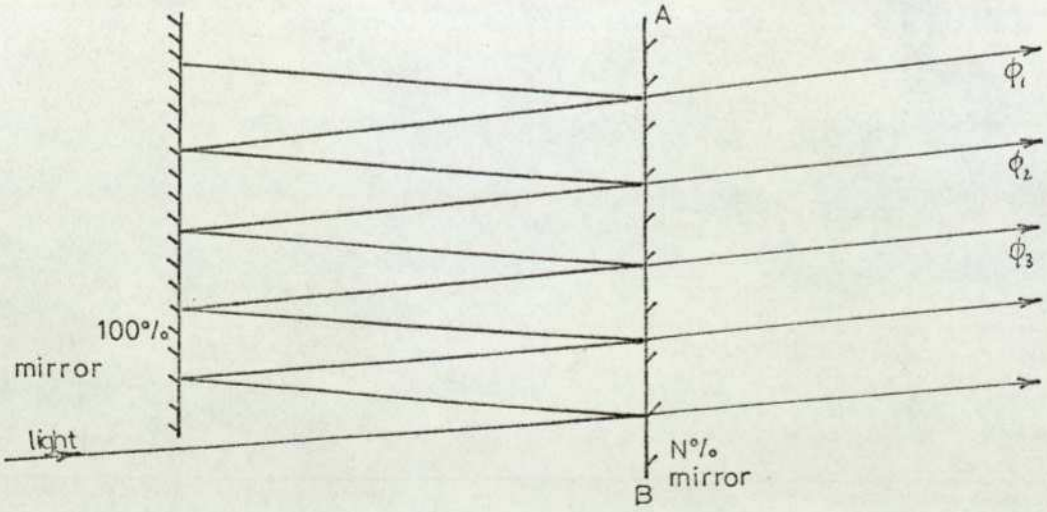


FIG 2.16 SERIES

The conclusions drawn were that adjacent controlled sources of small spacing offer the possibility of coupling energy between orders and for other forms of modulation/ deflection a transformed array appears indicated.

2.4. The Transformed Array.

This device principle (Figure 2,14) has not proved directly useful in either of the forms realised so far (Meyer & Korpel), but offers the possibility of direct development into two dimensional deflection. The deflection mode is continuous with linear impressed phase slope, but the 'slit function' envelope of performance is now little larger than the Airy disc of the individual source images and the deflection is too small to be usable.

The array source generator can be formed in one of two ways:-

1. Parallel Mode (Figure 2.15) as suggested by Meyer. This approach offers the advantage that sources can be individually electro-optically controlled or a single electrode shaped across the whole aperture which will allow various forms of far field operation (collimation, decollimation or deflection, or a combination of these).

2. Series Mode (Figure 216) as suggested by Korpel. In this case the array phases can be controlled by a transverse field in an electro-optic device or by a physical displacement of mirrors (e.g. Grant & Qualkinbush). This series is complicated by uneven source intensities unless the mirror AB is manufactured with a quadratic transmission characteristic to cancel the effect of multiple reflection intensity fall-off. The number of effective sources is limited in either case. Figure illustrates the dimensions of an Airy type pattern obtained from a 1cm beam and a f=10cm lens.

The far field pattern of a transformed array is given by Myer as:-

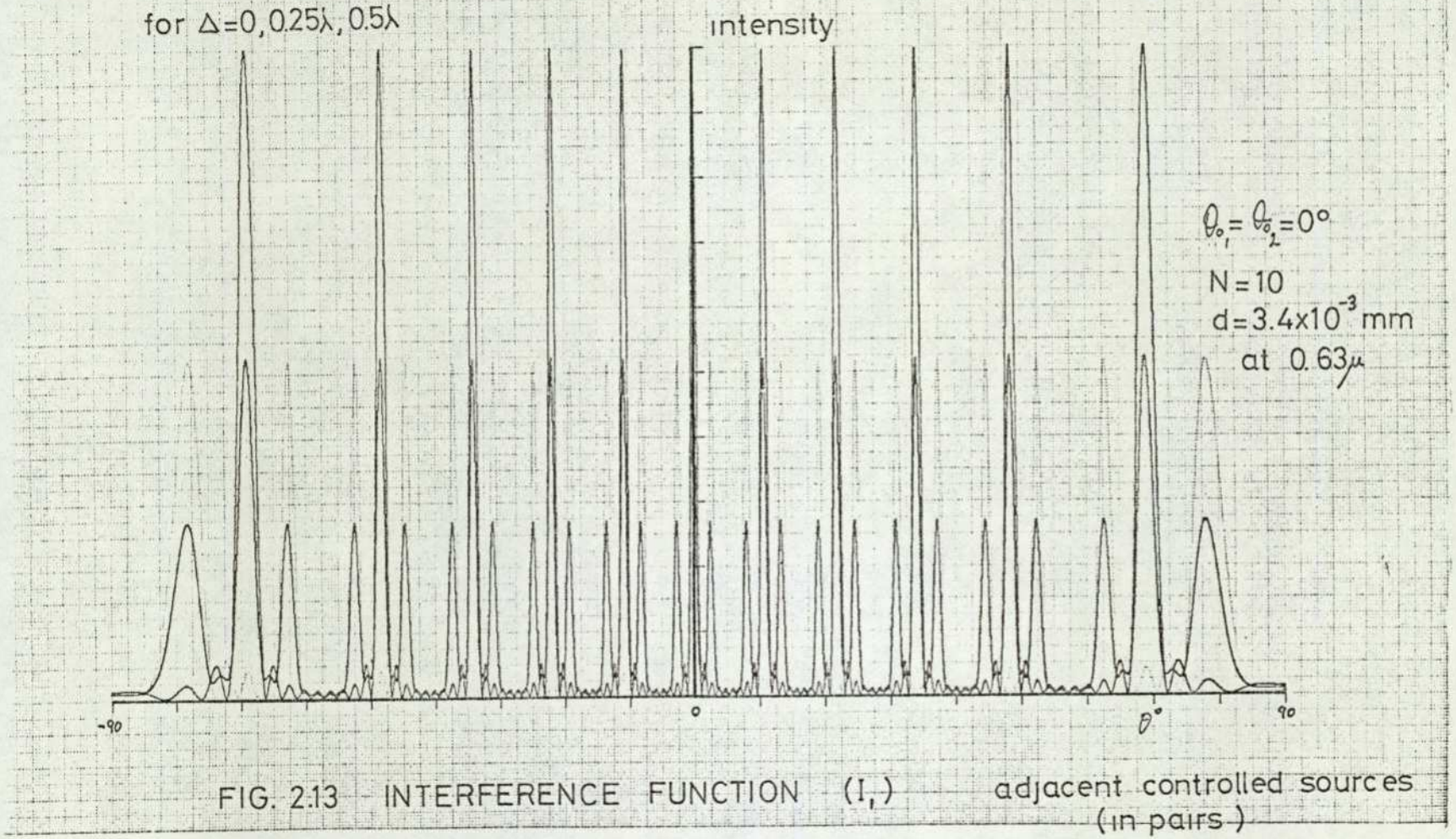


FIG. 2.13 - INTERFERENCE FUNCTION (I_1) adjacent controlled sources (in pairs)

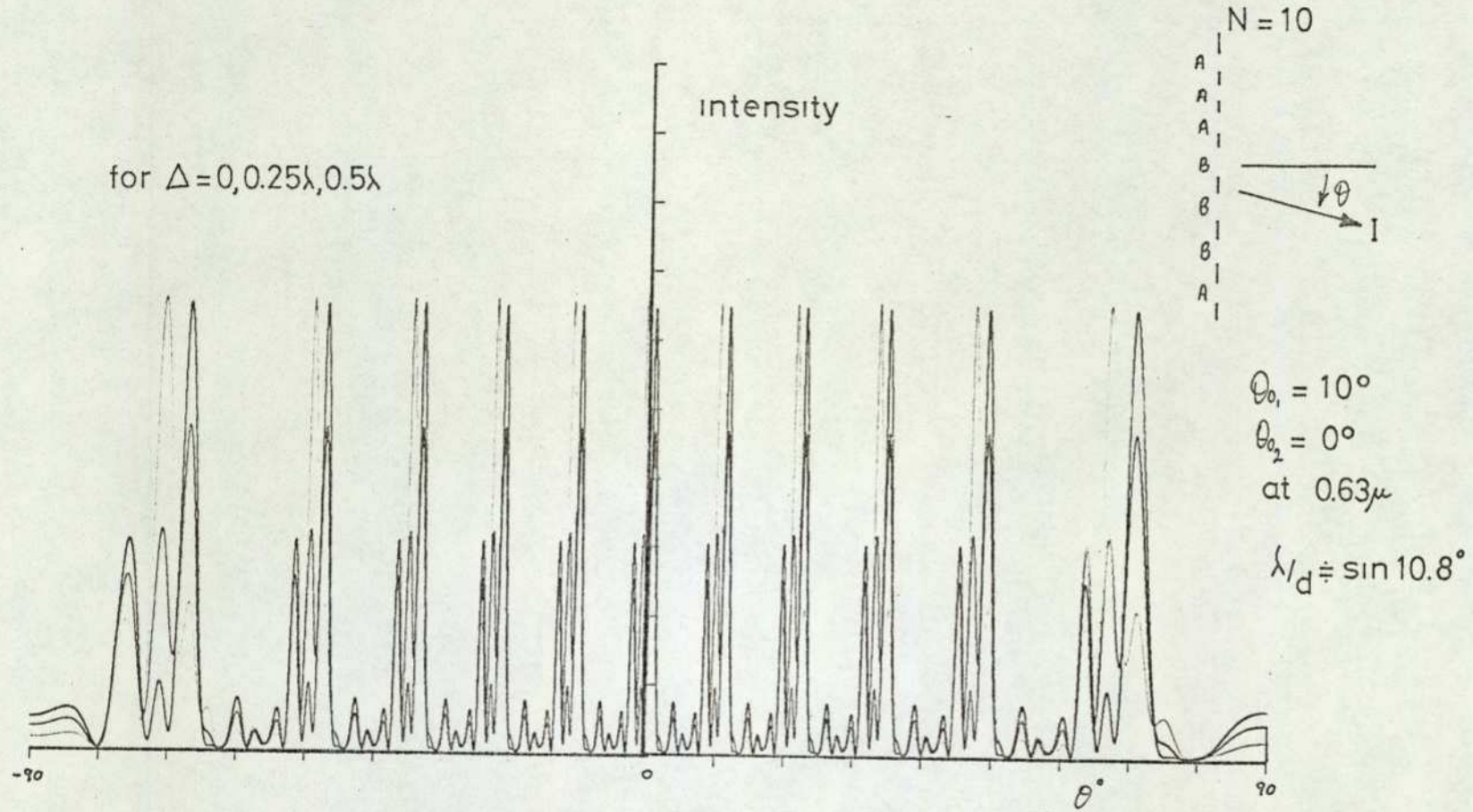


FIG. 2.12 INTERFERENCE FUNCTION (I_1) adjacent controlled sources (sets of three)

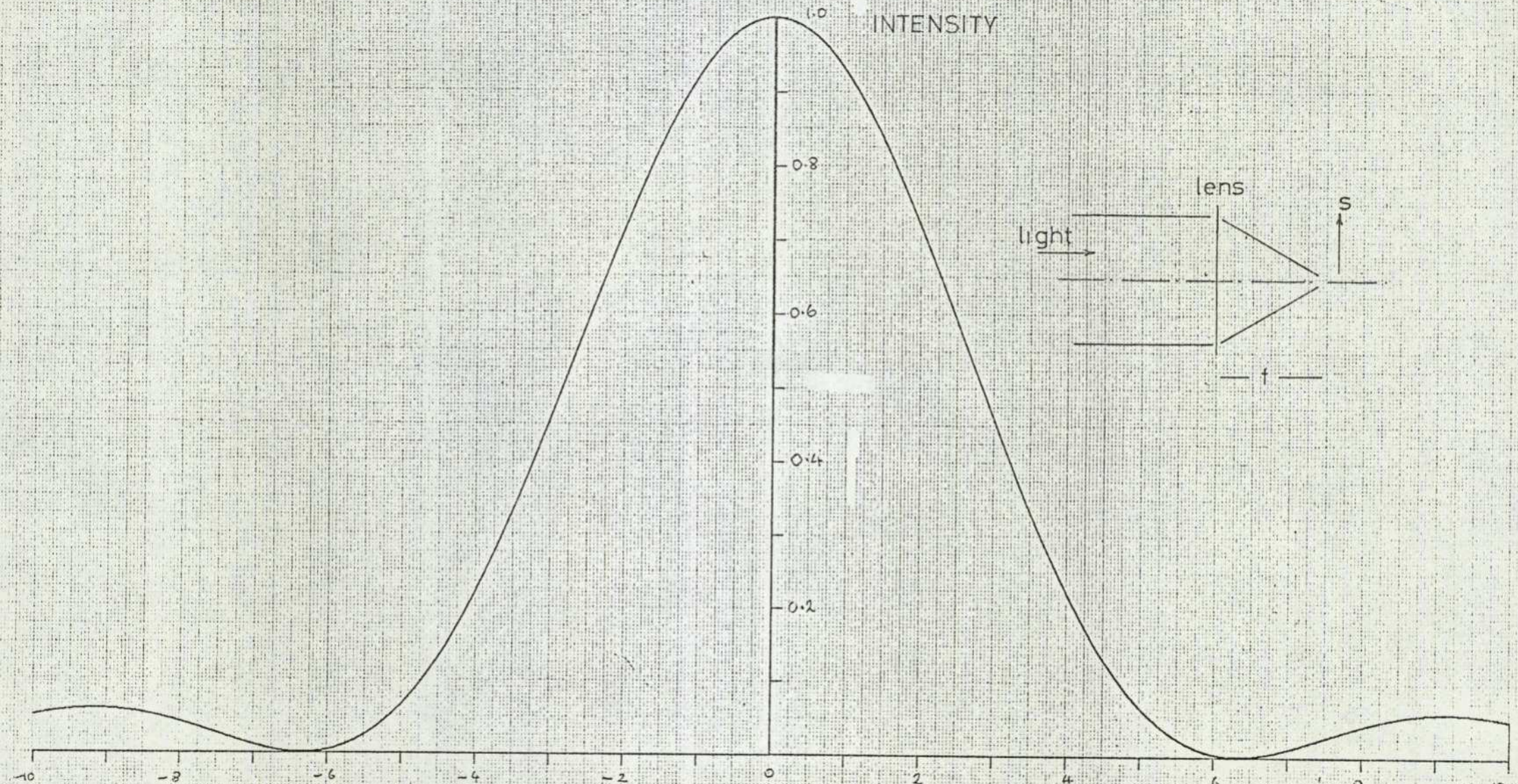


FIG. 2.17 AIRY TYPE IMAGE

$$U(\xi)=Aa^2\left[\frac{\sin(\pi a\xi/\lambda f)}{(\pi a\xi/\lambda f)}\right]\left[\frac{\sin[(M\pi\Delta x\xi)/\lambda f-\pi p]}{\sin(\pi\Delta x\xi)/\lambda f-\pi p/M}\right] \qquad (2,8)$$

Where Δx is source spacing
λ is light wavelength
f is lens focal length
p is maximum of phase slope retardation
A is light amplitude
a is source width
M is the number of sources

In Figure 2.18 the effects of an impressed linear phase profile are illustrated on a 5 source one dimensional grating when imaged by a transform lens. These predictions are experimentally verified in Meyers paper.

In order to render the device of use as a deflector, a grating mask was suggested, placed near the focal point where the grating can be considered to have its slits illuminated by light where phase can be individually controlled so that one condition of a phased array is met. The other necessary condition is that the slit function of the mask apertures should coincide or at least overlap so that interference is possible. To achieve the latter condition slit size may need to be reduced so that the s/d ratio ('metallisation factor') is made smaller. This mask should be placed at a distance from the focal point of not less than l where

$$l \simeq \frac{f\delta}{a/M - s + \delta} \qquad (2,9)$$

where δ is the focus waist diameter.

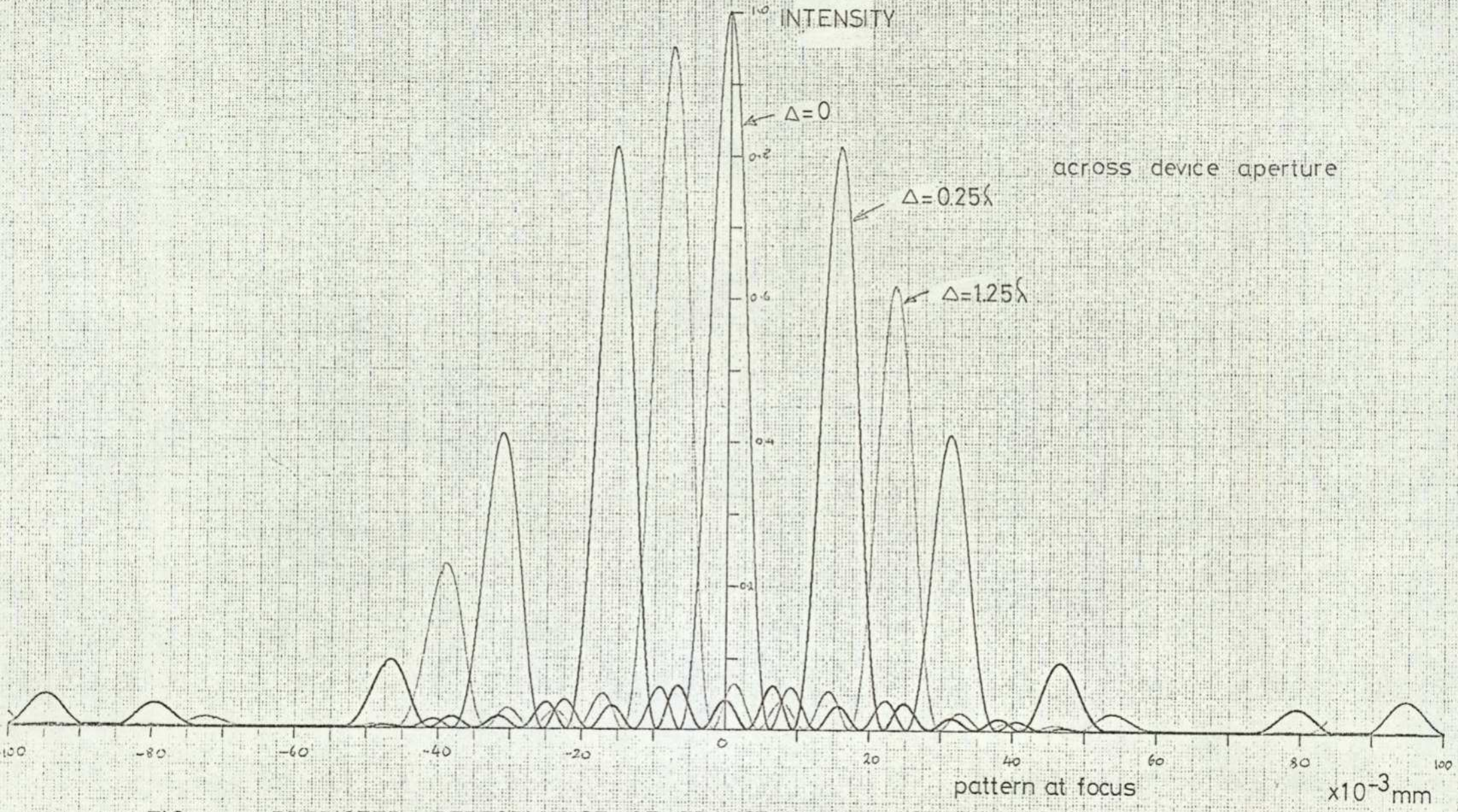


FIG. 2.18 PREDICTED PERFORMANCE OF TRANSFORMED 5 SOURCE ARRAY

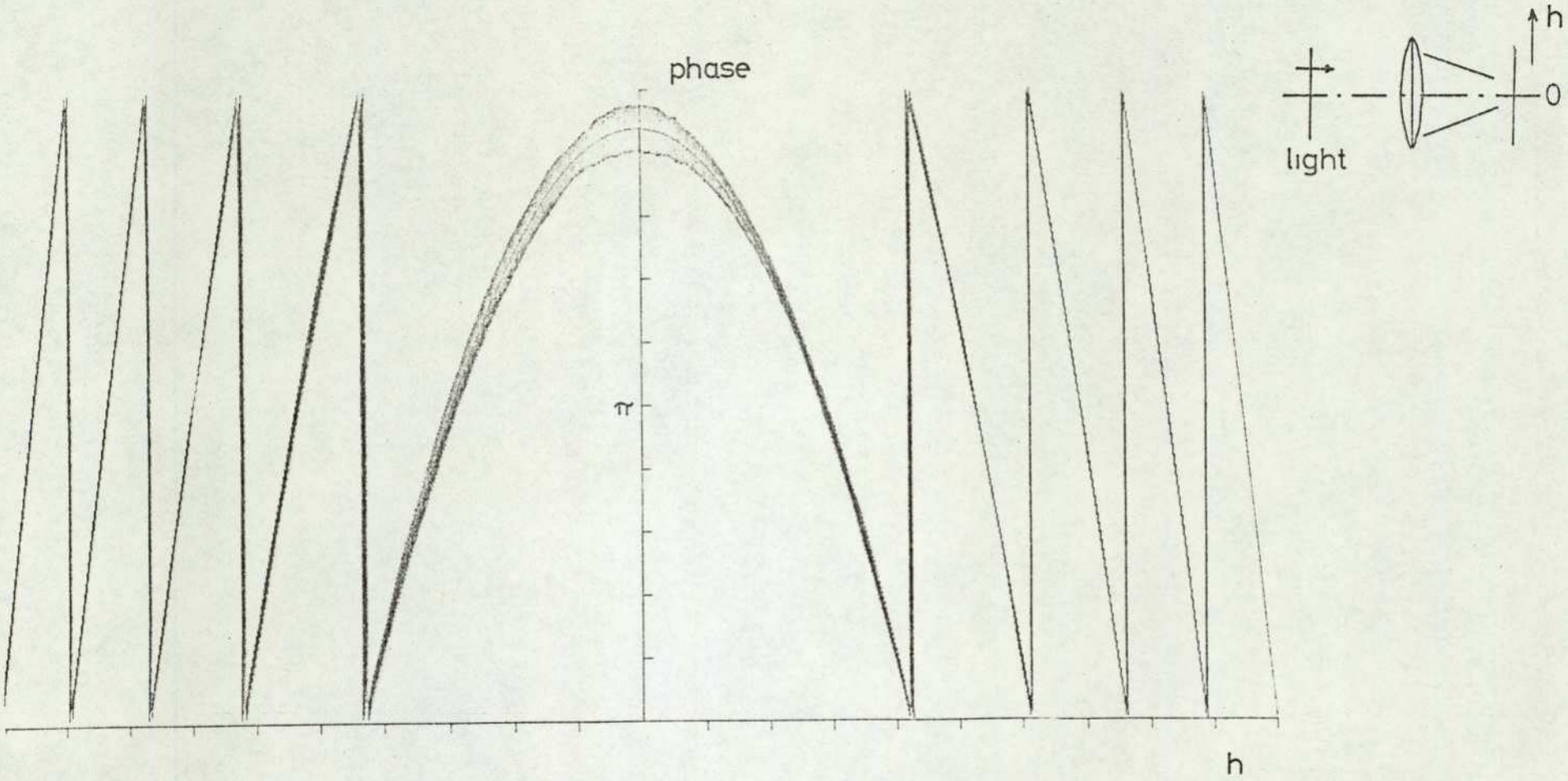


FIG. 2.19 PHASE AT MASK PLANE

The effect of the lens is to impart a curvature to previously plane wavefronts and affect the phase distribution on the mask plane as indicated in Figure 2.19 As the mask apertures can appear at any pitch on this wavefront, electro-optic or optic compensation may be used to recover a plane phase profile or to synthesise any desired profile. As the sources may then be controlled individually, modulation, collimation, and deflection may any, or all be achieved by electro-optic means. As the array may be made two dimensional points can potentially be accessed in three dimensional space by a combination of deflection and focussing.

2.5. Conclusion

Two configurations appeared to show promise

1. A phase corrugation of optical grating dimensions, impressed on the light wavefront offering a variable far field diffraction pattern.

and

2. A 'large' discrete array, transformed onto an optical grating mask, offering a true phased array device.

Both devices are subsequently investigated.

3. REALISATION OF A PHASED ARRAY DEVICE

3. ARRAY REALISATION

a. TEST CELL (Fig. 3.1)

An experimental system was constructed to test the suggested principle. A test cell with Spectrosil windows (Fig. 3.3) was constructed of perspex and a 45° y cut ADP crystal was cut with dimensions 5.5cm x 1.2cm. A five finger electrode structu structure (Fig. 3.5) was constructed by vacuum deposition of copper on chromium onto a glass substrate and subsequent etching from a photoreduced master. (This process is fully described in section 10). An unetched electrode, similarly metallised, was used as a common earthplane. The ADP, crystal polished on both the smallest faces, was then sandwiched between the electrodes (Fig. 3.1.

The combined structure was wired to the cell socket and then the cell filled with Flutec PP9 dielectric fluid. A mask was constructed and photoreduced to offer 1mm apertures as shown in (Fig. 3.3). A Helium Neon Light source (1mW from a Universal Laboratory's laser at 0.63μ) was expanded by a Jodon Beam expander type BET 25 into a collimated 1.5cm diameter beam which was passed through the test cell and mask (Fig. 3.6). A 2.5cm lens of high optical quality, obtained from a SORO collimator, was used to follow the test cell and image the beams onto a screen.

b. DRIVING CIRCUIT (Fig. 3.4)

Array element driving circuitry was constructed on a potential divider principle with a maximum range per source of 0 - +1000v. The electrode was connected to the potentiometer wiper where the 1kV supply was applied across the potentiometer. Five such stages of 4MΩ each were placed across the 1kV supply.

c. THE MASK (Fig. 3.3)

No useful operation could be achieved using photoreduced grating masks of 0.2 or 0.1mm pitch because there was no slit function overlap and there could be no interference. In order to reduce slit width a moire combination of two such masks was

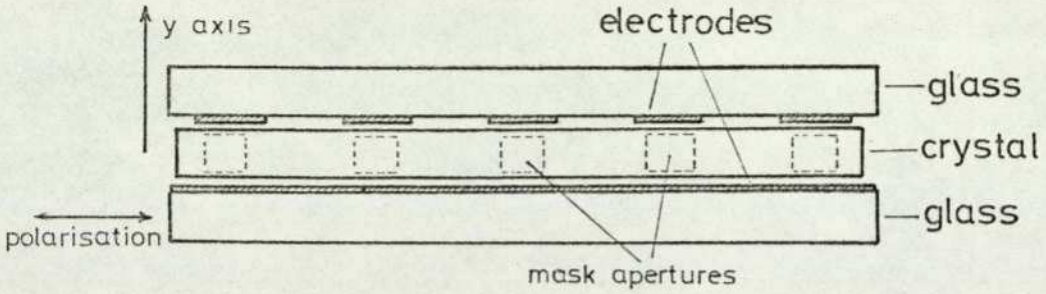


FIG.3.1 CRYSTAL AND ELECTRODES

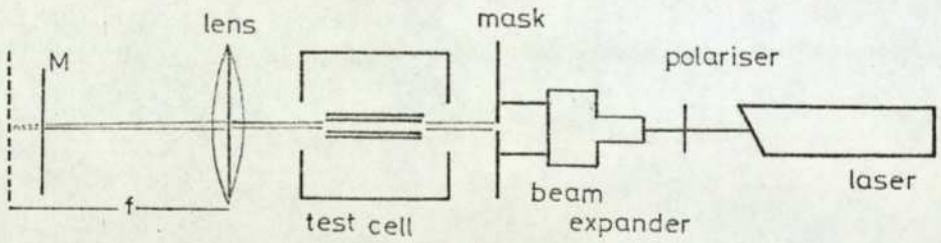


FIG. 3.2 APPARATUS

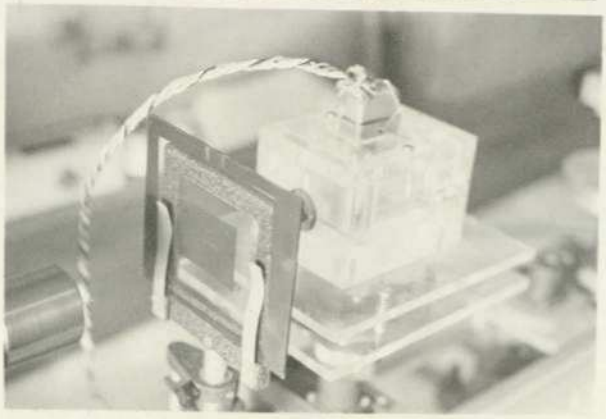


FIG 3.3. TEST CELL AND MASK

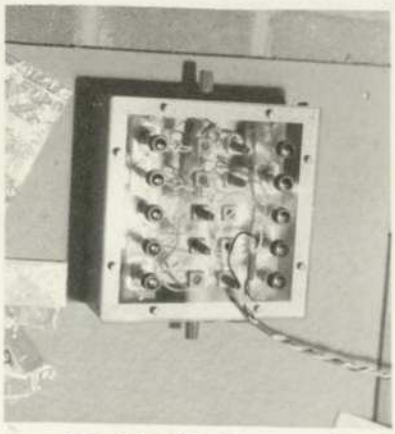


FIG 3.4. VOLTAGE DIVIDER

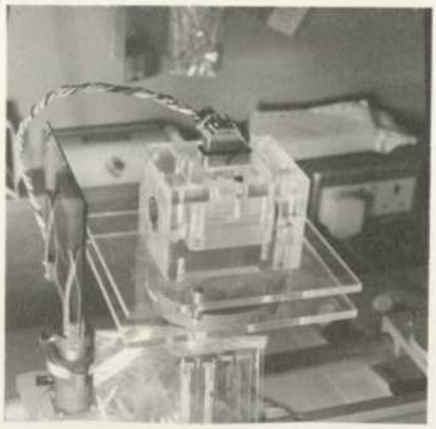


FIG 3.5. TEST CELL AND ELECTRODES



FIG 3.6. LAYOUT

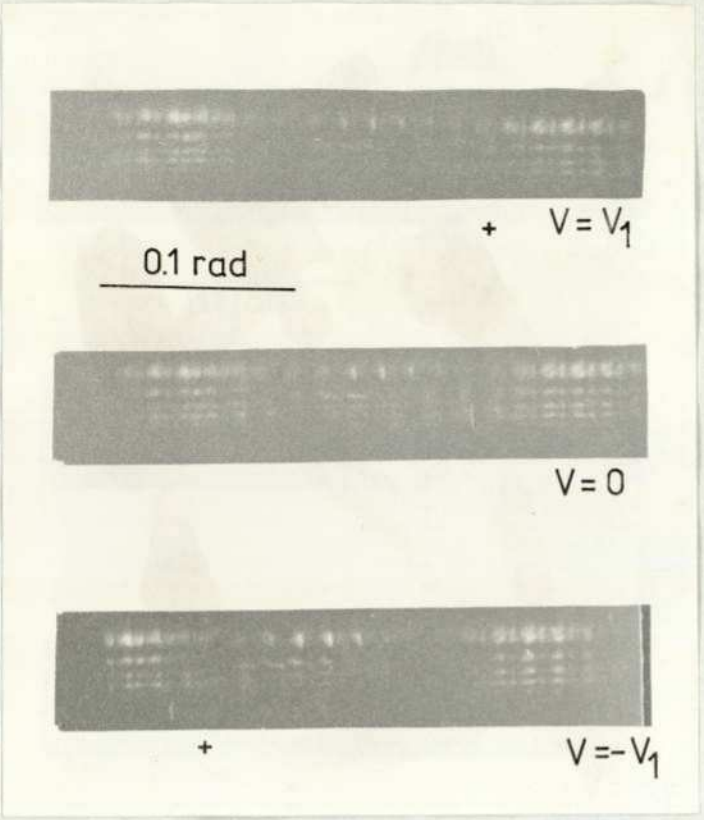


FIG.3.7 ARRAY FAR FIELD PATTERNS

constructed, emulsion to emulsion. A variation of vertical position with reference to the horizontal array now meant a variation of slit width from half the basic pitch to zero. In this manner operation of sorts was achieved and is shown in Fig. 3.7. The far field pattern shows energy coupling with a linear voltage ramp across the device. The areas marked (+) show a continuous deflection of energy with applied voltage. Activation of all electrodes with a voltage ramp across the aperture was necessary to achieve this effect. It did not prove possible to construct a far field pattern by electrode voltage variations because slit function overlap could not be achieved efficiently. A holographic replacement of the moire mask, allowing a blazing action, may be a solution. With operation verified it was decided that due to the inherently

inefficient nature of the process and the difficulty of maintaining phase uniformity across the device apertures, it was not worthwhile to develop or expand the process until fabrication techniques could be made available to implement the device with an acceptable insertion loss and with suitable optical quality components. No solution is immediately evident for the insertion loss problem but the overall principle appears promising for addressing systems.

4. PHASE CORRUGATION DEVICE

4.1 Introduction

It was concluded in Section 2 that a promising device configuration required the impressing of a phase corrugation on incident light wavefronts. This principle is employed in two dimensional aperture light modulation/deflection with acousto-optic interactions and in one dimensional aperture modulation/deflection with thin film diffraction devices (e.g. St Ledger & Ash and Hammer). The gap that appeared here was for a two dimensional device employing electro-optically induced diffraction. The design and instruction of such a device was undertaken.

4.2 Basic Concept of Device

In order to turn the thinfilm St Ledger and Ash type of device into a two dimensional aperture device it was necessary to electro-optically induce a diffraction grating transverse to the path of a light beam. (The term 'diffraction grating' here refers to a periodic variation of transmission or refractive index, not a lossy line grating effect). In order to achieve this without the necessity for a multilayer transparent electrode/crystal combination, it was decided to employ the classic interdigitated electrode structure of surface wave or thin film diffraction modulator origin, and totally internally reflect from the electrode influenced region. (Figure 4.1).

Crystal Configuration

It was decided to use an electro-optically sensitive material with good handling qualities and good availability and so lithium-niobate was an obvious initial choice. The number of orientation variations that were then available were numerous. It was decided that a typical device study with the

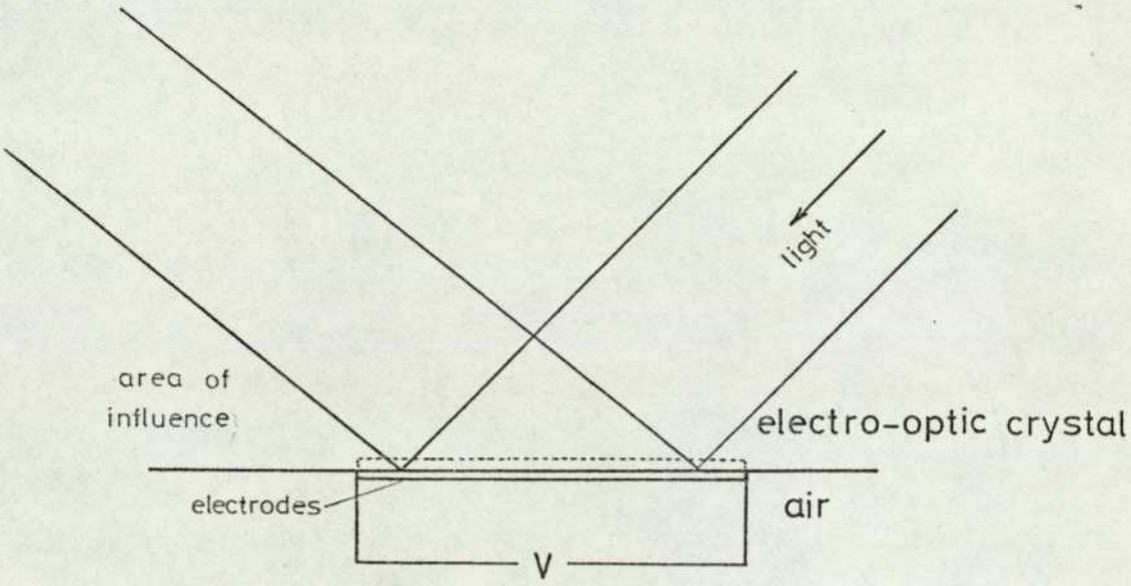


FIG. 4.1 T.I.R. OPERATION

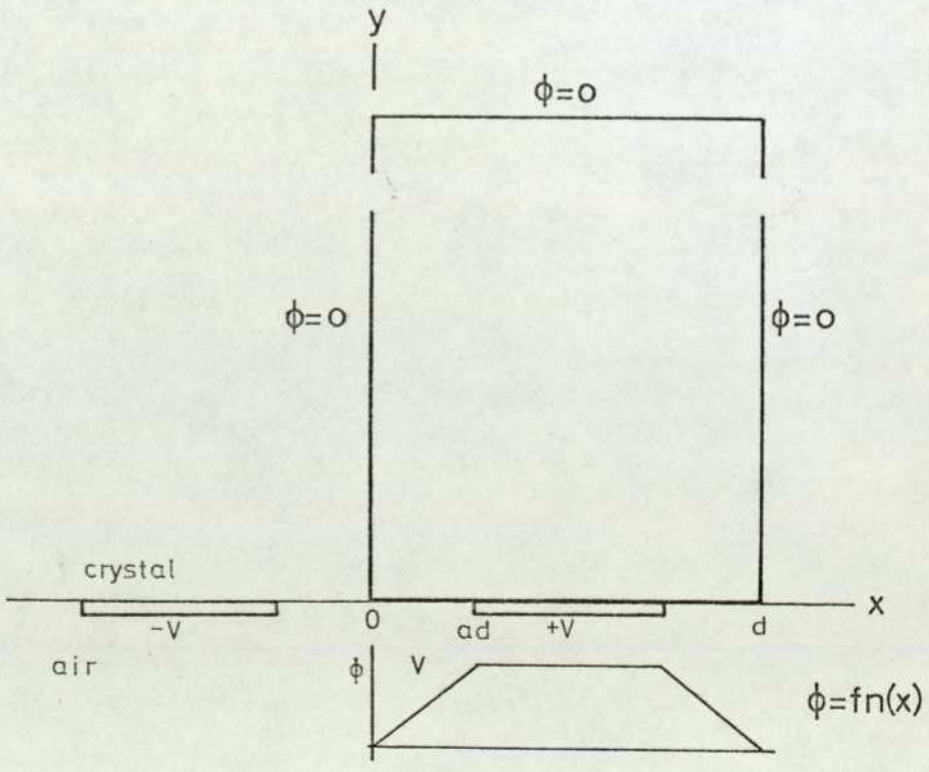


FIG. 4.2 ELECTRODE BOUNDARY CONDITIONS

4.2 Basic Concept of Device continued

intention of identifying the various trade-offs of the device parameters and an estimate of the optimum performance achievable were all that could be attempted initially. With this policy in mind a basic orientation of $LiNBO_3$ was chosen for modelling the device. This assumed that a field was applied along the Z axis and the largest r coefficient used ($r_{33} = 30.8\ 10^{-12}$ m/v @ 0.63μ). A decision about orientation was also necessary at this stage because the field structures would at high frequency be dependent on material anisotropy and the dielectric constants in $LiNBO_3$ form a second rank tensor. These were taken from Lenzo et al as

$$\varepsilon_z^s = 45 \quad \varepsilon_y^s = 27 \quad \varepsilon_x^s = 27$$

(at 9Ghz)

4.3 The Electrode Field Structure

The interdigitated electrode structure is initially assumed to be of equal width and pitch over its whole width. It is characterised by pitch (d) and mark space ratio or 'metallisation factor' (a) as in Figure 4.2. The voltage distribution in the e-o material can be arrived at by modelling, mapping, or a solution of the Laplace equation with appropriate boundary conditions. The former approaches were illustrative and of value only as visualisation aids and the latter approach is outlined here.

4.4 SOLUTION OF THE BOUNDARY VALUE ELECTRODE PROBLEM

The solution to Laplaces Equation can be shown to be unique and if the voltage ϕ is specified around the boundary of the area of interest, the solution is complete. As can be seen in Figure 4.2 the actual boundary conditions are Dirichlet (ϕ specified on boundary).

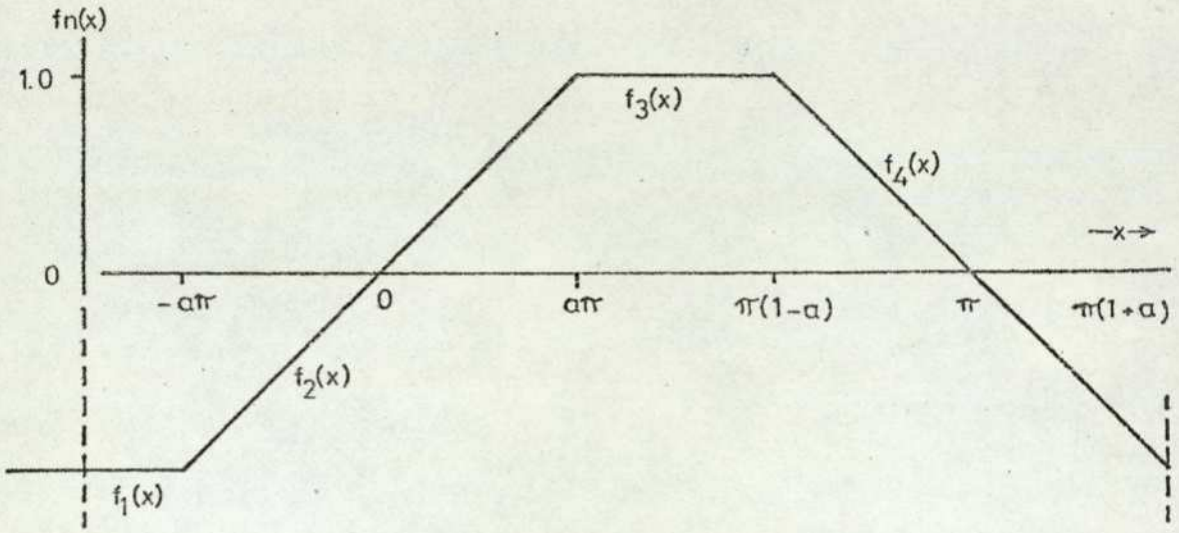


FIG. 4.3 FOURIER FORM BOUNDARY CONDITION

For the cartesian form of Laplace:

$$\frac{\partial^2\phi}{\partial x} + \frac{\partial^2\phi}{\partial y} + \frac{\partial^2\phi}{\partial z} = 0 \qquad (4,1)$$

assume the solution $\phi = f(x)g(y)h(z)$ (4,2)

hence $$\frac{\partial\phi}{\partial x} = f'(x)\,g(y)\,h(z) \qquad (4,3)$$

and $$\frac{\partial^2\phi}{\partial x^2} = f''(x)\,g(y)h(z) \quad \text{etc.} \qquad (4,4)$$

so that (4.1) can be rewritten

$$f''(x)g(y)h(z)+f(x)g''(y)h(z)+f(x)g(y)h''(z) = 0 \qquad (4,5)$$

4.4 SOLUTION OF THE BOUNDARY VALUE ELECTRODE PROBLEM
continued

$$\therefore \quad \frac{f''(x)}{f(x)} + \frac{g''(y)}{g(y)} + \frac{h''(z)}{h(z)} = 0 \qquad (4,6)$$

since each term is a function of only one variable, hence, each term must be equal to a constant

$$\frac{d^2f(x)}{dx^2} + k_x^2 f(x) = 0 \qquad (4,7)$$

$$\frac{d^2g(y)}{dy^2} + k_y^2 g(y) = 0 \qquad (4,8)$$

$$\frac{d^2h(z)}{dz^2} + k_z^2 h(z) = 0 \qquad (4,9)$$

where k_x, k_y, k_z are separation constants.

And $$k_x^2 + k_y^2 + k_z^2 = 0 \qquad (4,10)$$

This reduces the problem to three differential equations. Considering the electrode problem as two dimensional ($k_z = 0$) consider

$$\frac{\partial^2\phi}{\partial x^2} + \frac{\partial^2\phi}{\partial y^2} = 0 \qquad (4,11)$$

and assume a product solution $\phi = f(x)g(y)$ (4,12)

to satisfy $$\frac{d^2f(x)}{dx^2} + k_x^2 f(x) = 0 \qquad (4,13)$$

$$\frac{d^2g(y)}{dy^2} + k_y^2 g(y) = 0 \qquad (4,14)$$

where $k_x^2 = -k_y^2$ (4,15)

These give a general solution:

$$\phi(x,y) = \sum_{m=1}^{\infty} (b_m \sin mx + c_m \cos mx)(g_m \sinh my + h_m \cosh my) + k_1 + k_2 x + k_3 y$$

(4,16)

where b_m, c_m, g_m, h_m are Fourier coefficients and k_1, k_2, k_3 are constants.

4.3 ACTUAL BOUNDARY CONDITIONS

The boundary conditions for the electrode structure from the semi infinite strip in Figure 4.2 are

$$\phi(0,y) = 0 \qquad (1)$$
$$\phi(a,y) = 0 \qquad (2)$$
$$\phi(x,\infty) = 0 \qquad (3)$$
$$\phi(x,o) = fn(x) \qquad (4)$$

Condition (1) implies that $C_m = 0$

(2) that $m = \frac{\alpha\pi}{d}$ where α is an integer

and (3) that $g_m = -h_m$

giving $$\phi(x,y) = \sum_{\alpha=1}^{\infty}\left(b_\alpha h_\alpha \sin\frac{\alpha\pi}{d}x\ e^{-\frac{\alpha\pi}{d}y}\right) \qquad (4,17)$$

Condition (4) requires that

$$f_n(x) = \sum_{\alpha=1}^{\infty} b_\alpha h_\alpha \sin\frac{\alpha\pi}{d}x \qquad (4,18)$$

or that $b_\alpha h_\alpha$ is chosen as the coefficients of the Fourier series for $f_n(x)$.

Hence, for the range 0 - d

$$c_m = b_n h_m = \frac{2}{d}\int_0^d f_n(x) \sin mx\, dx \qquad (4,19)$$

The Fourier Boundary Form

From Figure 4.3 the boundary condition can be expressed

$$f_n(x) = a_o + \sum_{n=1}^{\infty}(a_n \cos nx + b_n \sin nx) \qquad (4,20)$$

The Fourier Boundary Form continued

Where the Fourier coefficients are, in general,

$$a_0 = \frac{1}{T}\int_0^T f_n(x)dx \qquad (4,21)$$

$$a_k = \frac{1}{T}\int_0^T f_n(x)\cos kx\,dx \qquad (4,22)$$

$$b_k = \frac{1}{T}\int_0^T f_n(x)\sin kx\,dx \qquad 4,23$$

$f_n(x)$ values for a piecewise description of $f_n(x)$ are

$$\left.\begin{aligned} f_1(x) &= -1.0 && (x<-a\pi) \\ f_2(x) &= \frac{x}{a\pi} && (-a\pi<x<a\pi) \\ f_3(x) &= 1.0 && (a\pi<x<\pi(1-a)) \\ f_4(x) &= \frac{1}{a}\left(1-\frac{z}{\pi}\right) && (x>\pi(1-a)) \end{aligned}\right\} \qquad (4,24)$$

Hence $f_n(x)$ as chosen in Figure 4.3 can be expressed

$$f_n(x) = \sum_{n=1,3,} b_n \sin x \qquad (4,25)$$

Where n is odd as the function is symmetrical about $x = \pi/2$ and a_o, a_k are zero because of

symmetry about the origin.

Hence
$$\pi b_n = -\int_{-\pi(1-a)}^{-a\pi} \sin nx\,dx + \int_{a\pi}^{\pi(1-a)} \sin nx\,dx + \frac{1}{a}\int_{\pi(1-a)}^{\pi(1+a)} \sin nx\,dx$$

$$+\frac{1}{a\pi}\int_{-a\pi}^{a\pi} x\sin nx\,dx - \frac{1}{a\pi}\int_{\pi(1-a)}^{\pi(1+a)} x\sin nx\,dx$$

(4,26)

The Fourier Boundary Form continued

Which reduces to

$$b_n = \frac{4 \sin n\pi a}{n\pi . n\pi a} \qquad (4,27)$$

$$\text{so that } f_n(x) = \sum_{n=1,3,5,} \frac{4 \sin n\pi a}{n\pi . n\pi a} \sin x \qquad (4,28)$$

$$\text{and } \phi(x,y) = \sum_{n=1,3,5,} \frac{4V \sin n\pi a}{n\pi . n\pi a} \exp \frac{-n\pi y}{d} \sin \frac{n\pi x}{d} \qquad (4,29)$$

for the isotropic case ($\varepsilon_x = \varepsilon_y$) This function will give the voltages in the dielectric or resistive isotropy cases but will need to be modified to give the voltages correctly for an anisotropic case.

4.6 THE ANISOTROPIC CASE

The two dimensional anisotropy expected from a uni-axial medium can be allowed for by a modification of the exponential term in equation 4,29 so that

$$\exp \frac{-n\pi y}{d}$$

changes to

$$\exp -\frac{n\pi}{d} \sqrt{\frac{\varepsilon_y}{\varepsilon_x}}\, y$$

4.7 VOLTAGES DUE TO ELECTRODES

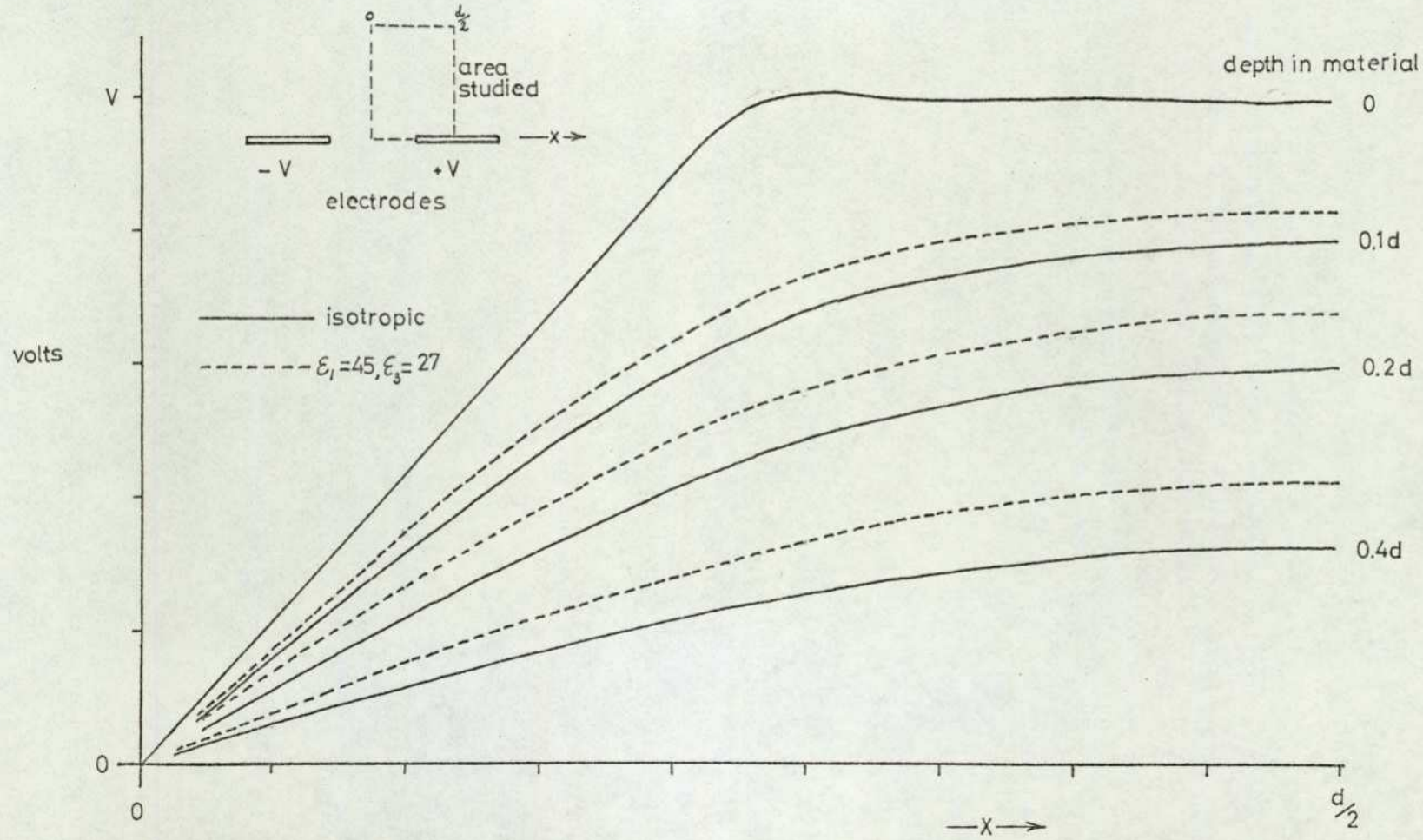
Equation (4,29) gives the voltage distribution between two infinite electrodes as in Figure 4.3 Allowance is made for variation in metallisation factor (a) and provision exists for isotropic and anisotropic field distributions. This equation was not correctly available in published literature but was essential for the development of further stages

4.7 VOLTAGES DUE TO ELECTRODES continued

of device operation predictions. A computer program was written to tabulate $\phi(x,y)$ for various values of a and dielectric constant. This program (Program GRAT) is included in Appendix P and a typical predicted voltage distribution presented in Figure 4.4. Typical cases of interest are presented, for a = 0.25 and an isotropic and a lithium niobate orientation. The problem of whether to employ an isotropic or anisotropic model is never easily resolved if low or medium frequency operation is employed. At high frequency operation in electro-optic materials the field structure may be considered dependent on the dielectric constants but at D.C. some materials with A.C. anisotropy possess resistive anisotropy and some do not. As a D.C. field is determined by the material resistivities this may mean that D.C. and A.C. operation may be far enough apart in terms of operating point that the leading bits of information in word transfer, for example, may be at risk. The resistive values of many electro-optic crystals are dependent on impurity doping and both ADP and lithium niobate exhibit resistive isotropy and dielectric anisotropy. KD*P however is anisotropic in both cases.

Points to stress in Figure 4.4 include the subscript notation of the dielectric constant ($\varepsilon_3 \equiv \varepsilon_z$, $\varepsilon_1 \equiv \varepsilon_2 \equiv \varepsilon_x \equiv \varepsilon_y$) as lithium niobate is isotropic in the x/y crystallographic plane. The chosen configuration shows that the voltage distribution will vary with anisotropy to increase voltages over the isotropic case at a given depth in the orientation shown. If an orthogonal orientation, involving the interchange of dielectric constants was used, then the voltages at a given depth would be decreased with respect to the isotropic case.

FIG. 4.4 VOLTAGES DUE TO ELECTRODES (d=0.1mm)



4.8 THE FIELD STRUCTURE

In order to assess device performance a knowledge of orthogonal fields due to the electrodes is needed. Initially useful axes to choose are transverse to the electrodes and normal to the electrode plane. The fields can be evaluated from equation (4,29) as

$$E_x = - \frac{d\phi}{dx} \qquad (4,30)$$

$$E_y = - \frac{d\phi}{dy} \qquad (4,31)$$

so

$$E_x(x,y) = \sum_{n=1,3,} \frac{-4V}{n\pi} \frac{\sin n\pi a}{n\pi a} \frac{n\pi}{d}\sqrt{\frac{e_3}{e_1}} \exp\left[\frac{n\pi}{d}\sqrt{\frac{e_3}{e_1}}y\right] \sin\frac{n\pi x}{d} \qquad (4,32)$$

and

$$E_y(x,y) = \sum_{n=1,3,} \frac{4V}{n\pi} \frac{\sin n\pi a}{n\pi a} \frac{n\pi}{d} \exp\left[\frac{-n\pi}{d}\sqrt{\frac{e_3}{e_1}}y\right] \cos\frac{n\pi x}{d} \qquad (4,33)$$

A Program to compute these functions was written (Program GRGD- in Appendix P2) and a comparison of predicted fields is presented in Figures 4.5, 4.6. It is to be noted that the normal field case (E_y) contains an infinite field locally at the electrode edge, and that at zero depth normal fields are affected by anisotropy whereas parallel fields are not. Also worthy of notice is the fact that the anisotropy case previously considered has opposite affects on E_x and E_y. Field is reduced in the normal field case and increased in the parallel fields case. Also of interest is the fact that at a depth of $\sim 0.3d$. E_y is the same for the isotropic and the Lithium Niobate anisotropic case. This suggests a possibility that devices can be constructed which exhibit identical ac and dc performance. Peak field strengths are similar in both cases so electro-optic devices using E_x and E_z are expected to be approximately similar in performance on the basis of these results.

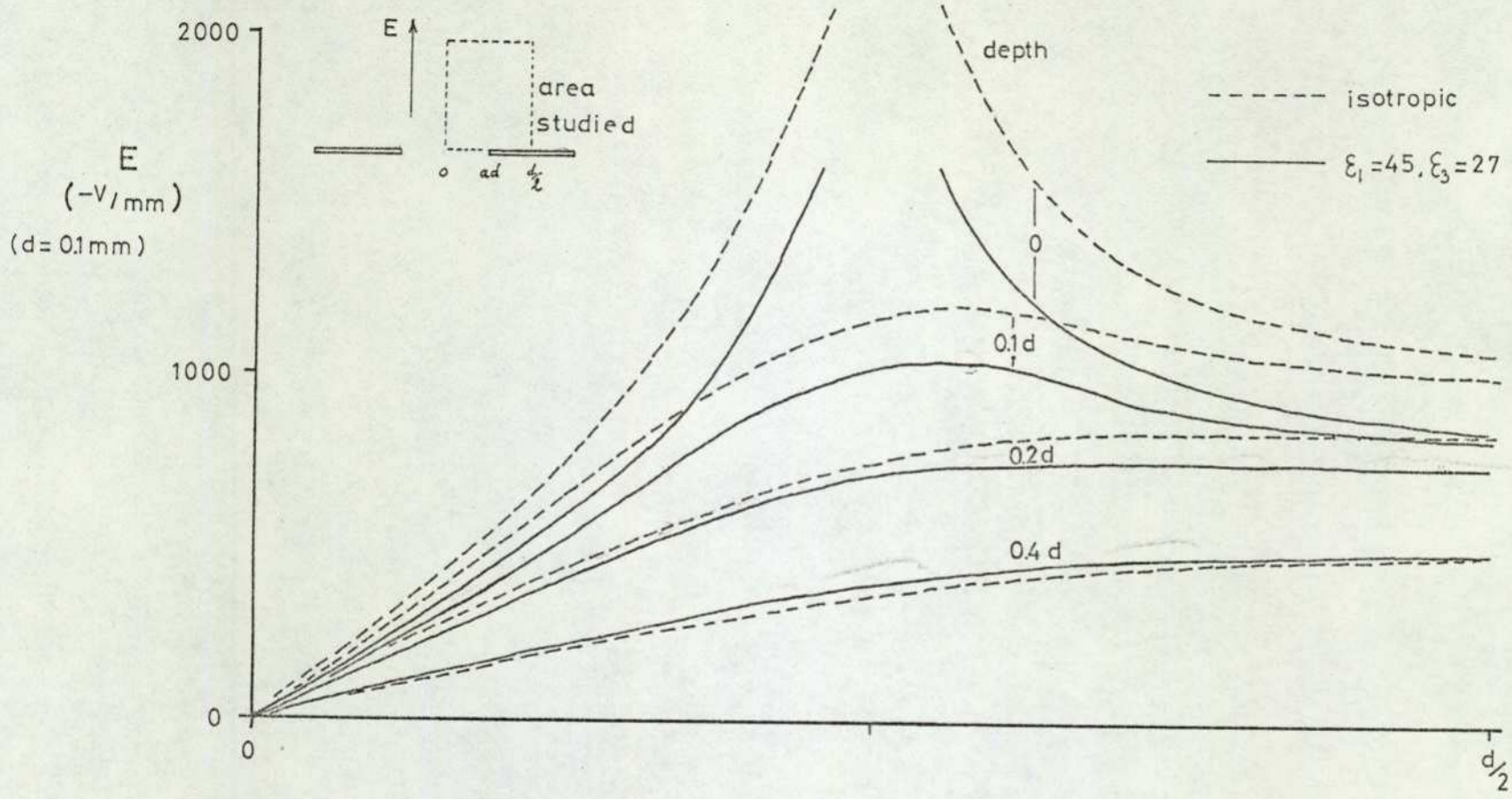


FIG. 4.5 NORMAL FIELDS

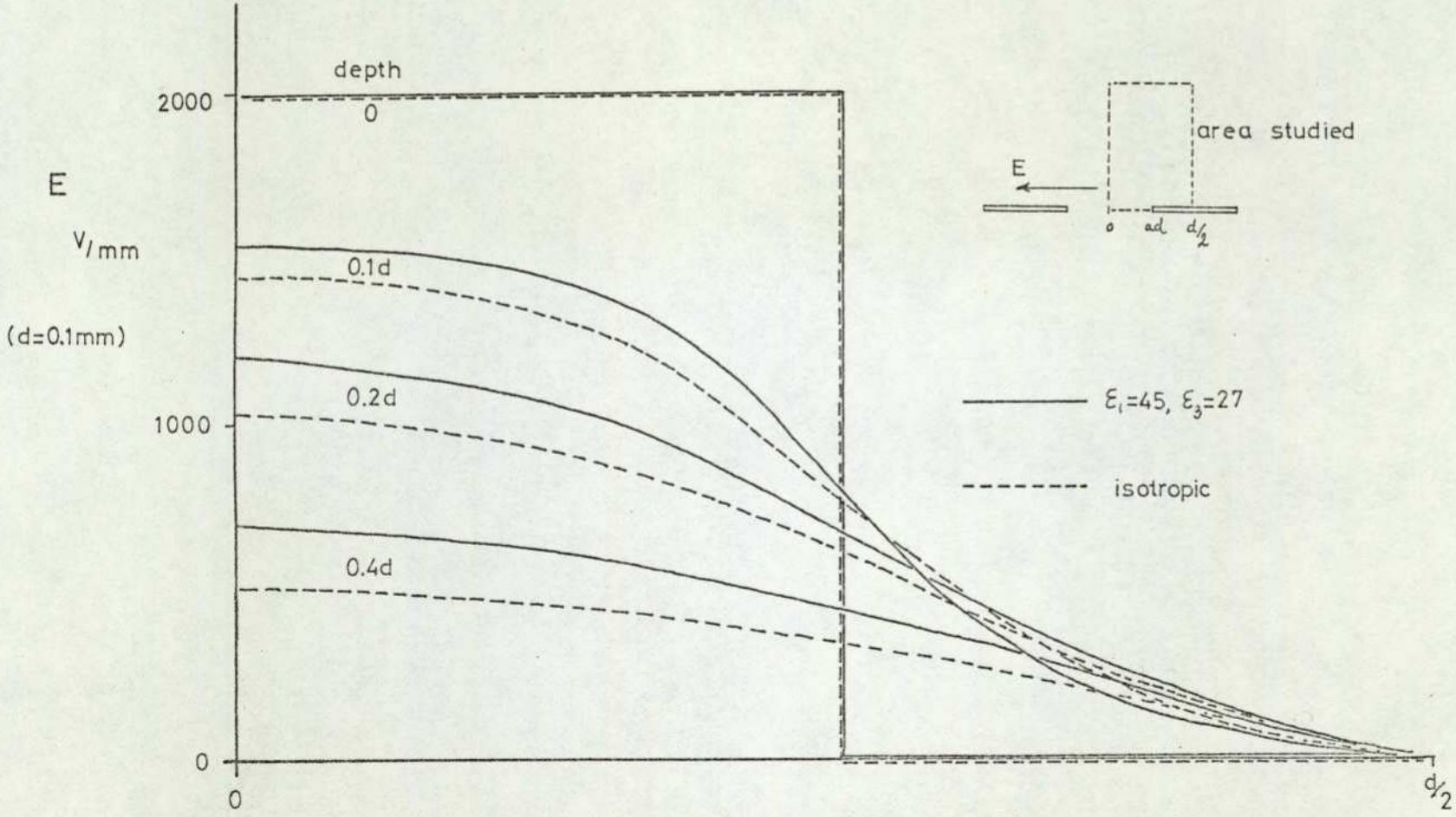


FIG. 4.6 PARALLEL FIELDS

Series Convergence

A Fourier series improves convergence when integrated and is rendered less convergent or even divergent when differentiated. Two differentiations of the voltage expression (4,29) will cause a divergence so that the convergence of field expressions may need to be watched if computation is employed. Figure 4.7 shows the effect of imposing a limit on N, for N = 50 the series summation involves 25 terms and for N = 100 it involves 50 terms. It can be seen that for >100 the function bears a good resemblance to that expected.

4.9 DEVICE CAPACITANCE

The energy stored in the field of an electro-optic device is of paramount importance as the driving circuitry has the job of supplying and discharging in as brief and as efficient a way as possible. An electrode pitch of the interdigitated structure contains a fixed quantity of energy having a capacitance independent of electrode pitch (assuming a constant metallisation factor). This is identical to the case of a parallel plate capacitor of fixed aspect ratio presenting a capacitance constant with size variation.

$$C = \frac{e e_o A}{d} \qquad 4.4.1$$

and stored energy is $\frac{1}{2}CV^2$

Hence if W is energy stored per pitch and N is number of pitches

$$Nw = \frac{C}{2}(2V_o)^2 \qquad 4.4.2$$

Where $\pm V_o$ are the electrode voltages, thus

$$C = \frac{NW}{2V_o^2}\ F \qquad \text{for the device} \qquad 4.4.3$$

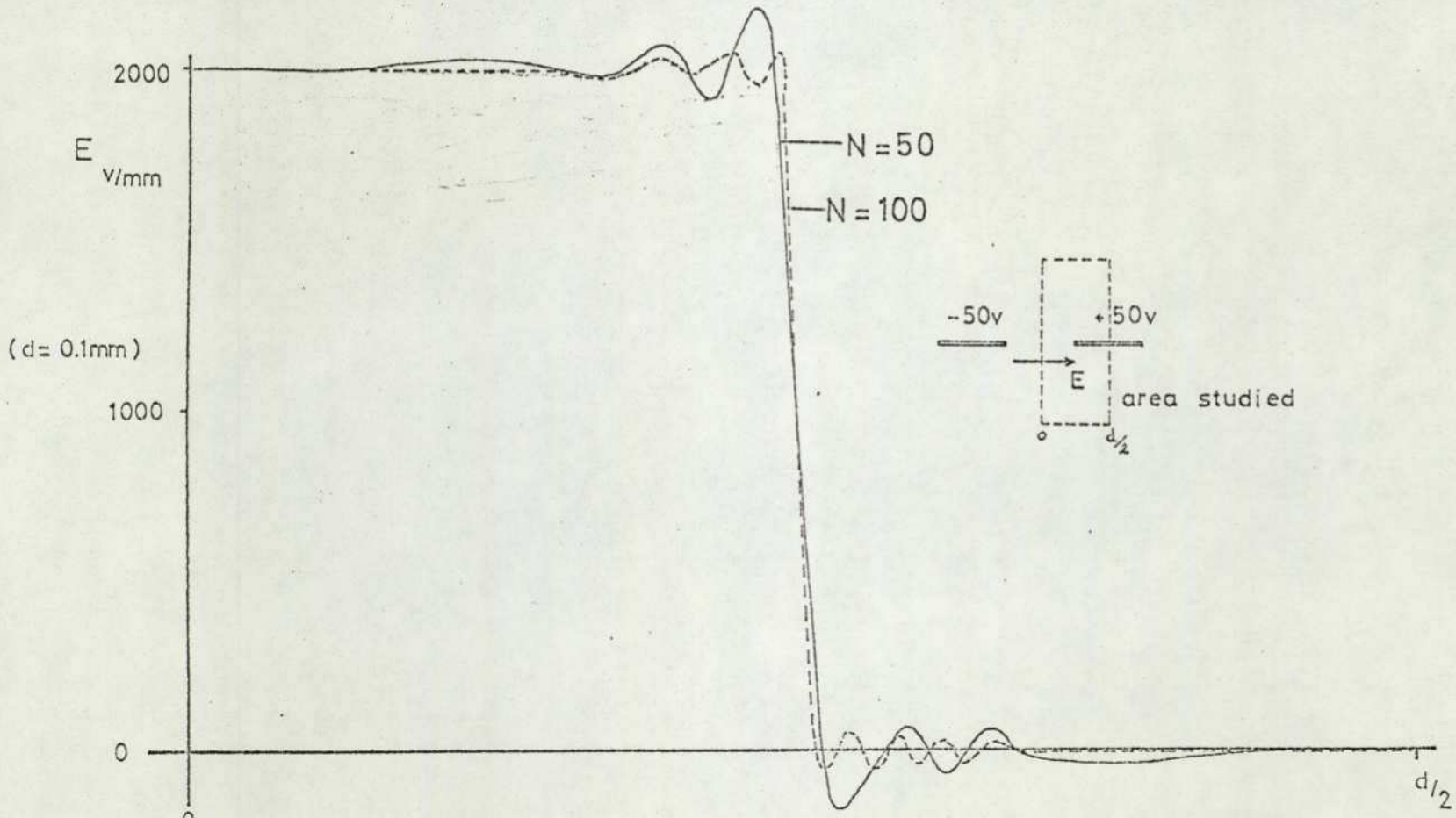


FIG 4.7 SERIES CONVERGENCE

4.9 DEVICE CAPACITANCE continued

Energy in the active material can now be expressed as

$$W = \frac{dl}{2}\int_0^h (e_1 E_1^2(x,y)+e_3 E_3^2(x,y))\,dx \qquad 4.4.4$$

Where l is electrode length, h is crystal depth and $e_1, E_1(x,y), e_3, E_3(x,y)$ are the orthogonal permittivities and respective fields. To comprise the whole device capacitance as assessment is based on an infinitely deep device on one side and an air or glass material on the other.

Thus from first principles, in cartesian co-ordinates

$$W = \frac{1}{2}\int_0^h\int_0^l\int_{-d}^{d}(e_1 E_1^2(x,y) + e_3 E_3^2(x,y))\,dx\,dy\,dz \qquad 4.4.5$$

Where $E_1(x,y)$ and $E_3(x,y)$ are the field expressions for the interdigitated structure previously calculated (equations 4,32 4,33). As E(x,y) appears to the second power, convergence is enhanced to the point where only the first term of the series expansion need be used.

Hence if

$$E(x) = A\sin\frac{\pi x}{d} \qquad 4.4.6$$

$$E(z) = B\cos\frac{\pi y}{d} \qquad 4.4.7$$

are the first terms from equations 4.32, 4.33

then equation 4.4.5 reduces to

$$W = \frac{l\,d}{2}\int_0^h (e_1 A^2 + e_3 B^2)\,dy \qquad 4.4.8$$

if h tends to infinity

4.9 DEVICE CAPACITANCE continued

$$W = 8 l V_0^2 \pi \left(\frac{\sin \pi a}{\pi a}\right)^2 \sqrt{e_1 e_3} \qquad 4.4.9$$

for the crystal and for the other side of the electrode, filled with a material of dielectric constant e_g gives

$$W_g = 8 l V_0^2 \pi \left(\frac{\sin \pi a}{\pi a}\right)^2 e_g \qquad 4.4.10$$

Hence

$$C_{device} = \frac{N}{2V_0^2}(W + W_g) \qquad 4.4.11$$

As expected this function shows no dependence on d.

The above functions were computed by program CAPC listed in Appendix P2 and typical predictions for a given aperture are presented in Table 4.1. A substrate dielectric constant of 7.5 is assumed (this is a typical value for glass). N is the number of electrode fingers.

4.9 DEVICE CAPACITANCE continued

TABLE 4.1 - PREDICTED VALUES OF CAPACITANCE

D_{mm}	A	e_g	e_1	e_3	N	$C_{substrate_{pf}}$	C_{xtal} pf
0.2	0.25	7.5	45	27	10	0.69	3.2
0.1	0.25	7.5	45	27	18	1.2	5.7
0.05	0.25	7.5	45	27	36	2.5	11.5
0.2	0.33	7.5	45	27		0.60	2.7
0.1	0.289	7.5	45	27		1.1	5.3
0.05	0.311	7.5	45	27		2.2	10.2
and for the isotropic case:							
0.2	0.33					0.60	3.3
0.1	0.29					1.1	6.9
0.05	0.31					2.2	13.1

Where electrode area is 2Nd mm^2 (approximately $4mm^2$) and a range of possible values of a and d is presented. It is to be noted that a substrate, if present, may contribute significant capacitance and that device capacitance is invariably proportional to pitch as expected from first consideration (equation 4.4.1). A trade-off is evident here: if ϑ is made small to lower operating voltage, electrode area and capacitance increases.

4.10 ESTIMATION OF PHASE PROFILES (Phase Variation Against Output Aperture)

In order to estimate the phase profile across the TIR device aperture it is necessary to do two things. First to line integrate along the incident beam to evaluate the total effective field and then to assume a favourable electro-optic crystal orientation and hence the resultant phase retardation.

4.10 ESTIMATION OF PHASE PROFILES continued

In general phase retardation Γ can be expressed in terms of refractive index change Δn as

$$\Gamma = \frac{2\pi}{\lambda} L \Delta n \qquad 4.34$$

If the incident and reflected retardation is cumulative and equal then, incrementally:

$$\delta\Gamma = \frac{4\pi}{\lambda} \Delta n \, \delta l \qquad 4.35$$

which, when integrated gives, for the whole device

$$\Gamma(x) = \frac{4\pi}{\lambda} \int_0^{l/2 \tan\theta} \frac{\Delta n \, dl}{\sin\theta} \text{ radians} \qquad 4.36$$

where l is the device electrode length and Δn is a function of Ex, Ey and the crystal orientation. (θ is the incidence angle).

4.11 INDUCED REFRACTIVE INDEX CHANGE

An infinite number of possible crystals and orientation could have been chosen to illustrate this device at this stage. Lithium Niobate was initially chosen in its simplest useful cut, that is using r_{33}, the largest e-o coefficient.

The index ellipsoid of Lithium Niobate, a uniaxial crystal of class 3m is:

$$(n_o^{-2} - r_{22}E_y + r_{13}E_z)x^2 + (n_o^{-2} - r_{22}E_y + r_{13}E_z)y^2 + (n_e^{-2} + r_{33}E_z)z^2 +$$
$$2(-r_{22}E_x)xy + 2r_{51}E_y yz + 2r_{51}E_x xz = 1 \qquad 4.37$$

Where the z, x, y orthogonal axes form a left hand screw system by convention and n_o and n_e are the ordinary and extraordinary refractive indices. Lithium Niobate possesses eight nonzero electro-optic coefficients (r_{ij}) of the possible eighteen. Four of them are independent. Values given in literature are:

4.11 INDUCED REFRACTIVE INDEX CHANGE continued

$r_{33}^{s} = 30.8 \times 10^{-12} m/V$

$r_{22}^{s} = 3.4$ "

$r_{51}^{s} = 28$ "

$r_{13}^{s} = 8.6$ "

It can be seen that r_{33} is the largest and it is chosen for use in the subsequent device analysis. Confusion may arise at this point because of the existence of crystallographic axes (x,y) and the cartesian co-ordinates so far employed in voltage and field characterisation. It may best be avoided by separating orientation transformations from fields operations. In equation 4.37 E_x, E_y, E_z correspond to fields along the x,y,z axes respectively. Refractive indices seen by an incident beam in the crystal are represented by the major axes of the ellipsoid section normal to the beam direction. (A wave-surface ellipsoid can be generated from 4.37 by constructing the reciprocal surface).

Effect of an Electric Field

The application of an electric field to a crystal results in two types of effects in general on an index ellipse. Ellipse axes will change in length, usually differentially and the major and minor axes may rotate. In most cases this rotation is negligible but in some if may render a particular orientation useless. The axes product terms in equation 4.37 give a measure of this affect and if a general ellipsoid is considered as

$$\frac{x^2}{a^2} + \frac{y^2}{b^2} + cxy = 1 \qquad 4.38$$

then by substituting a rotational transformation

$$x = X\cos\eta + Y\sin\eta \qquad 4.39$$

Effect of an Electric Field continued

$$y = Y\cos\eta - X\sin\eta \qquad 4.40$$

the condition for the XY product coefficient to be zero is that

$$\tan\eta = \frac{c}{2\left(\frac{1}{a^2} - \frac{1}{b^2}\right)^2} \qquad 4.41$$

and in practice if C is a term comparable with an r coefficient and a is equal to b, then the rotation is insignificant. (of the order of $\sim 10^{-9}$ radians in practical orientation). An exact analysis of the effect of an applied field on a crystal is therefore a calculation of the relevant index ellipsoid section with a correction made for axes rotation. This is doubly important after a transformation of field or axes when an unfamiliar configuration results.

Rotational Transformation

This may be approached from the fundamental index ellipsoid description

$$B_{ij}X_iX_j = 1 \qquad 4.42$$

(where B_{ij} - impermeability tensor) being translated to the new form by the use of the conventional direction cosines a_{jm} in

$$B_{ij} = a_{il}a_{jm}S_{lm} + a_{il}a_{jm}a_{rn}r_{lmn}E_r \qquad 443$$

in the method outlined by Kalymnios but this approach is shorthand rather than informative, and it was decided to transform the index ellipsoid without recourse to convention rotation and use only orthodox substitution transformation of the form in equations 4.39, 4.40. This leaves field directions unchanged with respect to the crystallographic axes.

Basic Transformations

The r_{33} coefficient may be made use of by the application of an E_z field. The ellipsoid equation is then

$$(n_o^{-2}+r_{13}E_z)x^2 + (n_o^{-2}+r_{13}E_z)y^2 + (n_e^{-2}+r_{33}E_z)z^2 = 1 \qquad 4.43$$

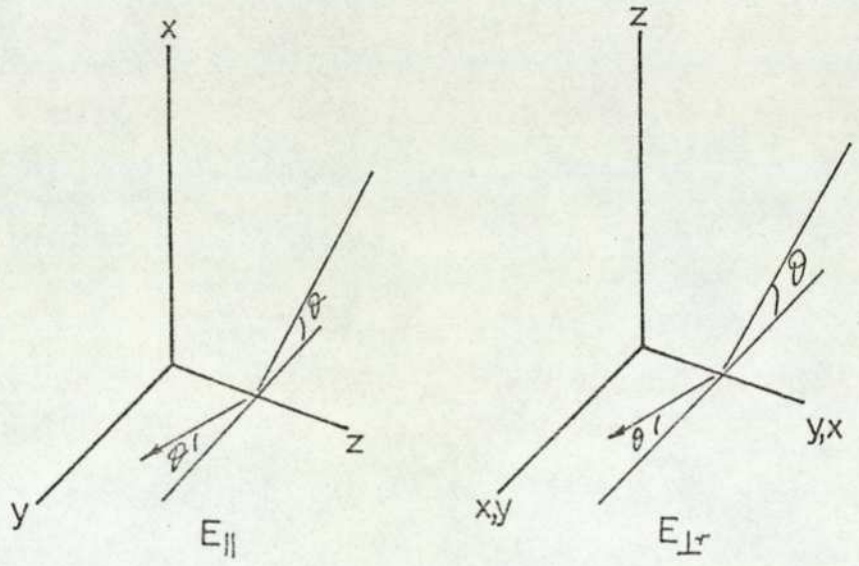


FIG.4.8 BASIC TRANSFORMATIONS

and clearly the resulting field induced refractive index variation of n_e may be used with incident light anywhere in the xy plane and polarisation in the z direction. This example is illustrated in Figure 4.11 in the $E_{\|}$ case where the transverse component of the inter-electrode field is used to represent E_z. The induced refractive index change in the $E_{\|}$ (Δn_z) case may also be used in the polarisation normal to the electrodes whereupon the r_{13} co-efficient is used and is also independent of θ with the index ellipse seen in both cases being

$$(n_o^{-2}+r_{13}E_z)x^2 + (n_e^{-2}+r_{33}E_z)z^2 + 2r_{51}E_x zx = 1 \qquad 4.44$$

Basic Transformations continued

As the product term disappears if $E_x = 0$, axes are not rotated by applied field (E_z) and reducing equation 4.44 by rearrangement and Binomial expansion gives the induced refractive index variations:

$$n_o\Big|_{E_z} = n_o\left(1 - \frac{n_o^2 r_{13} E_z}{2}\right) \quad \text{for all } \vartheta \qquad 4.45$$

$$n_o\Big|_{E_z} = n_e\left(1 - \frac{n_e^2 r_{33} E_z}{2}\right) \quad \text{for } \vartheta = 0 \qquad 4.46$$

giving

$$\Delta n_o\Big|_{E_z} = \frac{-n_o^3 r_{13} E_z}{2} \qquad 4.47$$

$$\Delta n_e\Big|_{E_z} = \frac{-n_e^3 r_{33} E_z}{2} \qquad 4.48$$

A small rotation exists in this case as the electrode fields effectively possess orthogonal components and a rotation term of $2r_{51}$ Ex/y will remain. This corresponds to a rotation of the ellipse axes of 1.9×10^{-6} radians per kilovolt/m.

Alternative Orientations

The case when the fields normal to the electrode plane are used is not as simple. Two cases are involved basically, the z/y and the z/x orientation. The former involves rotation about the y axis by an angle $\emptyset$ and illumination to lie along the new x axis while the latter involves rotation about the x axis and illumination along the y axis

$$\tan \eta = \frac{2 r_{51} E_y}{2(n_o^{-2} + r_{22} E_y + r_{13} E_z - n_e^{-2} - r_{33} E_z)^2} \qquad 4.49$$

again giving a value of η of $\sim 1.9 \times 10^{-6}$ rad /kv-m-1

First Transformation

Two transformations are necessary.

Rotating first about the y axis and using the substitutions:

$$x = x' \cos\theta - z' \sin\theta \qquad 4.50$$

$$z = x' \sin\theta + z' \cos\theta \qquad 4.51$$

Substituting in the general lithium niobate index ellipsoid (equation 4.37) gives the new index ellipsoid form which allows the study of light along of the new axes, x', y', z. The form of this equation is inconvenient in length and this transformation is presented in full in appendix T1. Taking the $x'=0$ section of this ellipsoid - equivalent to considering light along x' - an expression of the form:

$$Ay'^{2} + Bz^{2} = Cy'z = 1 \qquad 4.52$$

is obtained where

$$A = (n_o^{-2} + r_{22}E_y + r_{13}E_z) \qquad 4.53$$

$$B = (\cos^2\theta . n_e^{-2} + \sin^2\theta . n_o^{-2} + \cos^2\theta . r_{33}E_z - \sin^2\theta . r_{22}E_y + \sin^2\theta . r_{13}E_z - 2\sin\theta\cos\theta . r_{51}E_x) \qquad 4.54$$

and

$$C = (2E_x r_{22}\sin\theta + 2r_{51}E_y\cos\theta) \qquad 4.55$$

As Ex = 0 in the configuration under study the product term in C disappears as does the r_{51} term in B. The affect in field on A is not as great as that on B for small θ as small coefficients appear in A. Rewriting B in the form:

First Transformation continued

$$B = \frac{1}{n_z'^2} \qquad 4.56$$

so that refractive index change along z is

$$\Delta n = n_z' - n_o \qquad 4.57$$

and can be expanded , via the binomial expansion from equation 4.54 to give

$$\Delta n = \frac{E_z(r_{33}\cos^2\theta + r_{13}\sin^2\theta) - E_y\sin^2\theta r_{22} - 2\sin\theta\cos\theta r_{51}E_x}{2(\cos^2\theta\, n_e^{-2} + \sin^2\theta\, n_o^{-2})^{3/2}} \qquad 4.58$$

The truncation inherent in taking only the first binomial term in expansion is a practical step as the r_{ij}^2 term will be a factor of 10^9 smaller than the first and the inaccuracy is of that order and is usually acceptable.

Second Transformation

The second transformation required to characterise the case for using the field components normal to the electrodes is to rotate the axes of reference by an angle θ about the x axis. This gives the z/x orientation case. A repetition of the preceding transformation is not necessary in full because of the xy plane symmetry of lithium niobate. As can be seen from equation 4.37 the coefficients of x^2 and y^2 are identical when Ey = 0. This is the case for the z/x orientation so it is only necessary to read x for y in equation 4.58 if ellipse rotation can be neglected. The rotation term proves to be:

$$2E_x r_{22}\sin\theta + 2r_{51}E_y\cos\theta$$

which suggests that rotation is indeed insignificant. Hence the induced refractive index changes are:

Second Transformation continued

a) for the z/y orientation:

$$\Delta n = \frac{E_z(r_{33}\cos^2\theta + r_{13}\sin^2\theta) - E_y r_{22}\sin^2\theta}{2(\cos^2\theta n_e^{-2} + \sin^2\theta n_o^{-2})^{3/2}} \qquad 4.59$$

and b) for the z/x orientation:

$$\Delta n = \frac{E_z(r_{33}\cos^2\theta + r_{13}\sin^2\theta) - 2 r_{51} E_x \sin\theta\cos\theta}{2(\cos\theta n_e^{-2} + \sin\theta n_o^{-2})^{3/2}} \qquad 4.60$$

Combining Orientations and Fields

From combining orientations and fields it can be seen that both field components can play a part in the overall device performance and that the angle θ will affect the nature as well as the sensitivity of the operation. The act of reflection can be considered as the addition of a $-\theta$ phase modulation case. From equations 4.59 and 4.60 it can be seen that this will have no assymetrical affect on Δn as the only resultant sign change (in equation 4.60) causes the Ex component to disappear.

4.12 FIELD INDUCED PHASE PROFILES

It is now possible to combine the quantitative knowledge of the field structure gained in section 4.7 with the knowledge of Lithium Niobate orientations from section 4.6 and predict the phase profile across a TIR device aperture. The phase across the device can be expressed in cartesian co-ordinates as:

$$\Gamma(x) = \frac{4\pi}{\lambda \sin\theta} \int_0^{l/2 \tan\theta} \Delta n_{(x,y)}\, dy \qquad 4.61$$

4.12 FIELD INDUCED PHASE PROFILES continued

where $\Delta n_{(x)}$ can be expressed in terms of the crystallographic orthogonal fields:

$$\Delta n_{(x,y)} = \frac{E_{z(x,y)}(\cos^2\theta.r_{33}+\sin^2\theta.r_{13}) - E_{y(x,y)}\sin^2\theta.r_{22}}{2(\cos^2\theta.n_e^{-2}+\sin^2\theta.n_o^{-2})^{3/2}}$$

for the z/y orientation, and

$$\Delta n_{(x,y)} = \frac{E_{z(x,y)}(\cos\theta.r_{33}+\sin\theta.r_{13})+E_{x(x,y)}\sin\theta.\cos\theta.r_{51}}{2(\cos^2\theta.n_e^{-2}+\sin^2\theta.n_o^{-2})^{3/2}} \qquad 4.62$$

for the z/x orientation. (The E_x term changes sign with $\theta = -\theta$ and so is ignored in overall path summation).

These expressions are of the form

$$\Delta n_{(x,y)} = P.E_{z(x,y)} + Q.E_{y(x,y)} \qquad 4.63$$

and the field structures that represent $E_z(x,y)$ and $E_y(x,y)$ were derived in section 4.7 and considering field components as $E_\parallel$ in the electrode plane and $E_\perp$ normal to electrode plane so that in cartesian form:

$$E_{\parallel(xy)} = -\sum_{n=1,3,5,} \frac{4V}{d}\,\mathrm{sinc}(n\pi a)\sqrt{\frac{\varepsilon}{\varepsilon}}\exp\left[\frac{n\pi}{d}\sqrt{\frac{\varepsilon_3}{\varepsilon_1}}y\right]\sin\frac{n\pi x}{d} \qquad 4.64$$

and

$$E_{\perp(xy)} = \sum_{n=1,3,5,} \frac{4V}{d}\,\mathrm{sinc}(n\pi a)\exp\left[\frac{n\pi}{d}\sqrt{\frac{\varepsilon_3}{\varepsilon_1}}y\right]\cos\frac{n\pi x}{d} \qquad 4.65$$

FIELD INDUCED PHASE PROFILES continued

and the phase profile expressed in series form as:

$$\Gamma_{(x)} = \frac{4\pi}{\lambda \sin\vartheta} \left[P\int E_{1(x,y)}dy + Q\int E_{2(x,y)}dy \right]_0^{\frac{1}{2}\tan\vartheta} \qquad 4.66$$

In the cases we consider the r_{33} coefficient may be operated on by $E_{\parallel}$ or $E_{\perp}$ by the interchange of P and Q, thereby rotating the crystal by 90° around x or y with respect to the electrodes. Thus if

$$\left.\begin{aligned} E_1 &= E_{\parallel}(x,y) \\ \text{and } E_2 &= E_{\perp}(x,y) \end{aligned}\right\} \qquad 4.67$$

then the $E_{\parallel}$ field is used when:

$$P = \frac{\cos^2\vartheta\, r_{33} + \sin^2\vartheta\, r_{13}}{2(\cos^2\vartheta\, \bar{n}_e^{-2} + \sin^2\vartheta\, \bar{n}_o^{-2})} \qquad 4.68$$

and P and Q are interchanged for the $E_{\perp}$ component to be employed. (These orientations are represented in Figure 4.8).

Comments on Device Configuration

This analysis illustrates the complexities of an interdigitated electrode device as the number of variables is greatly augmented by the fact that fringing fields in crystalline media are employed. The interaction of a two dimensional field (in an anisotropic medium) with a three dimensional crystal structure allows for many variations. For the variables are:

1) crystal orientation
2) incidence angle
3) electrode pitch
4) metallisation factor

Comments on Device Configuration continued

and all need to be considered for total device characterisation. It must be noted that consideration of symmetry imposes the condition that the relative sign of the refractive index change terms changes over half the electrode pitch, so that:

$$\Delta n_{(x,y)} = P.E_{1(x,y)} \pm Q.E_{2(x,y)} \qquad 4.69$$

is additive for $x < d/2$ and subtractive for $d/2 < x < d$

This information is inherent in the mathematics but needs to be stressed when an optimised computer program is to be written.

Use of ADP or an Isomorph

Only the usage of Lithium Niobate has been stressed so far but the principle could quite readily have been studied in conjunction with a material such as ADP which possesses a large transverse effect using r_{41} and a different spectral window. ($r_{41} = 23.4 \times 10^{-12}$ m/V) but a lower refractive index than $LiNBO_3$. The latter fact renders the material less sensitive.

The ADP index ellipsoid is

$$\frac{x^2}{n_o^2} + \frac{y^2}{n_o^2} + \frac{z^2}{n_e^2} + 2r_{41}zxE_y + 2r_{41}yzE_x + 2r_{63}xyE_z = 1 \qquad 4.7.1$$

and a potentially interesting cut to make use of the r_{41} coefficient is the 45° x or y cut. In this case a rotation of 45° about the x or y axes and illumination across this direction with field along y gives an induced refractive change of

Use of ADP or an Isomorph continued

$$\Delta n = \frac{\sqrt{2}\, r_{41} E}{\left(\frac{1}{n_o^2} + \frac{1}{n_e^2}\right)^{3/2}} \qquad 4.7.2$$

If light is inclined at an angle ϑ then horizontal field effects are unaffected while the vertical field effect will be

$$\Delta n = \sqrt{2}\, r_{41} E n_o^3 \tan\vartheta \cos\vartheta \qquad 4.7.3$$

4.13 PHASE PROFILE PROGRAMS

Four programs were written (TGWV, GTWV, GTWI, TGWI) Appendix P2 to investigate phase profiles from normal and horizontal field devices. The former were to study horizontal and the latter to study vertical field devices. Data was generated against voltage and incidence angle and the isotropy/anisotropy was noted.

A series of d (pitch) values was examined as was the effect of metallisation factor variation. These dependences were not of great importance at this stage but were necessary for program development towards the far field pattern performance prediction of a realised device.

Typical results are presented in Figures 4.9 , to 4.12 and the points to notice are the general phase profile shapes and the opposite effects of the indicated anisotropy. Device sensitivities do not appear vastly different. The assymetry suggested from the mathematics of the previous section is not immediately evident and is not a serious contribution at such small values of ϑ.

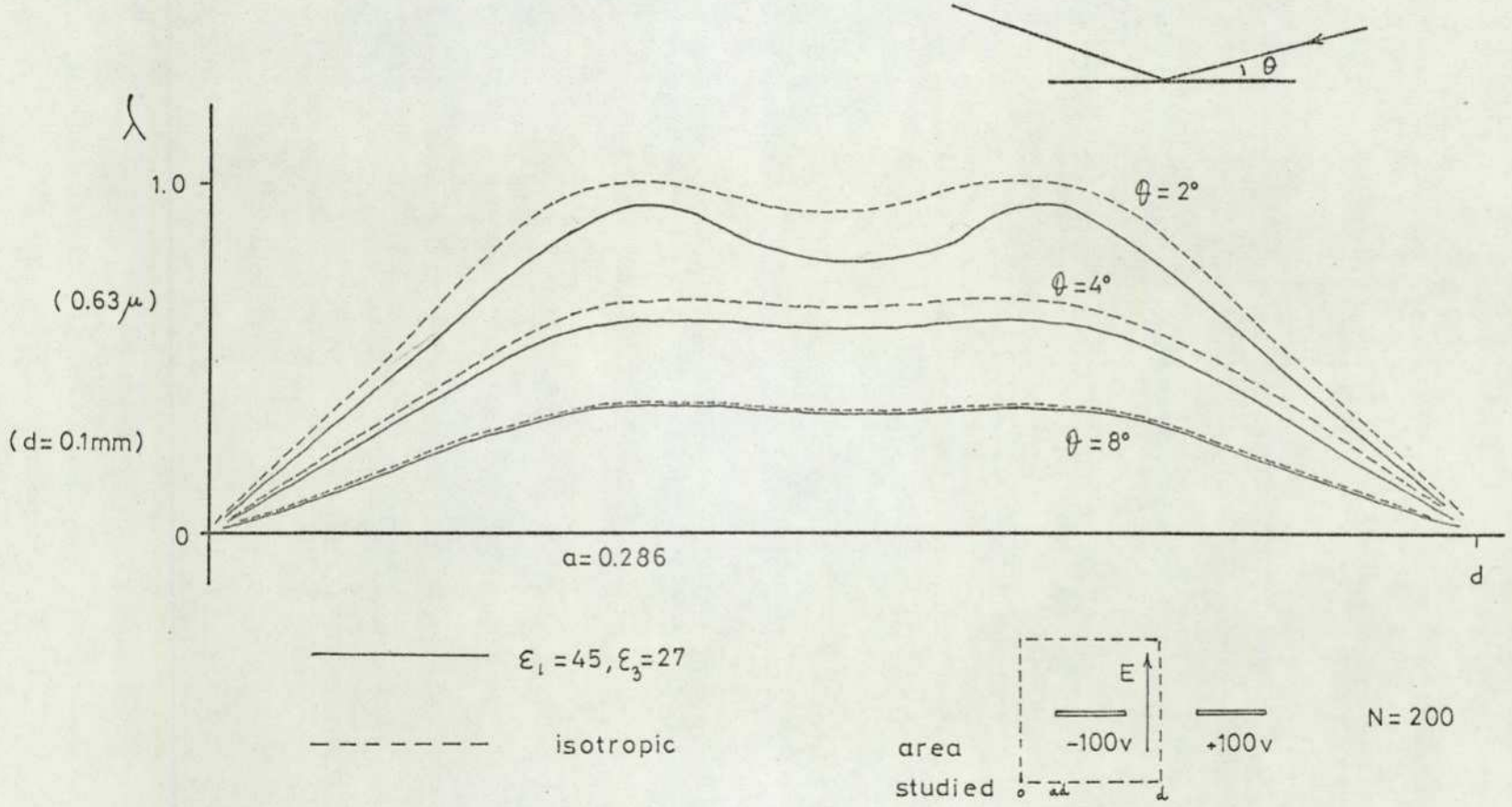


FIG. 4.9 PHASE PROFILES vertical field (d=0.1mm)

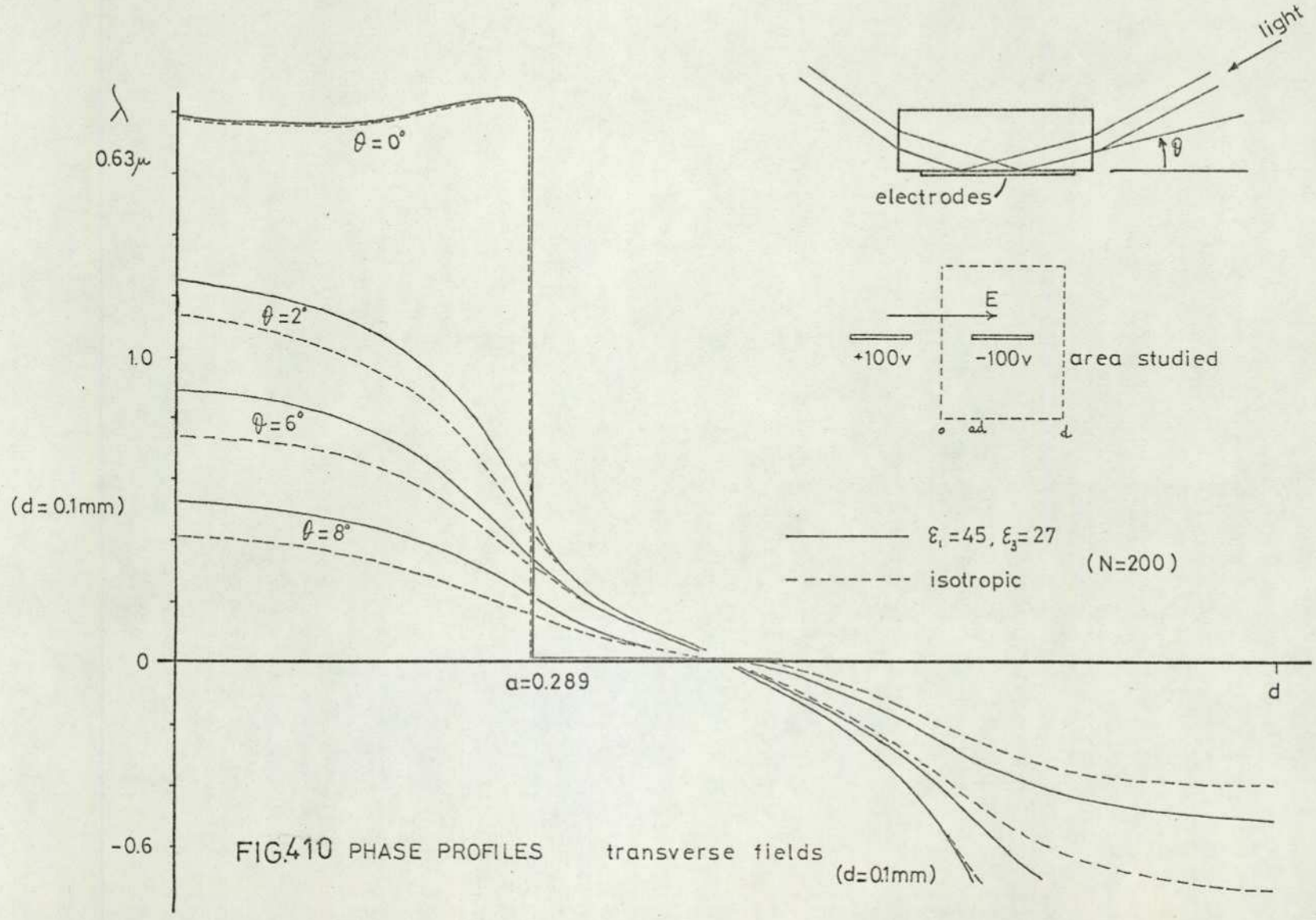
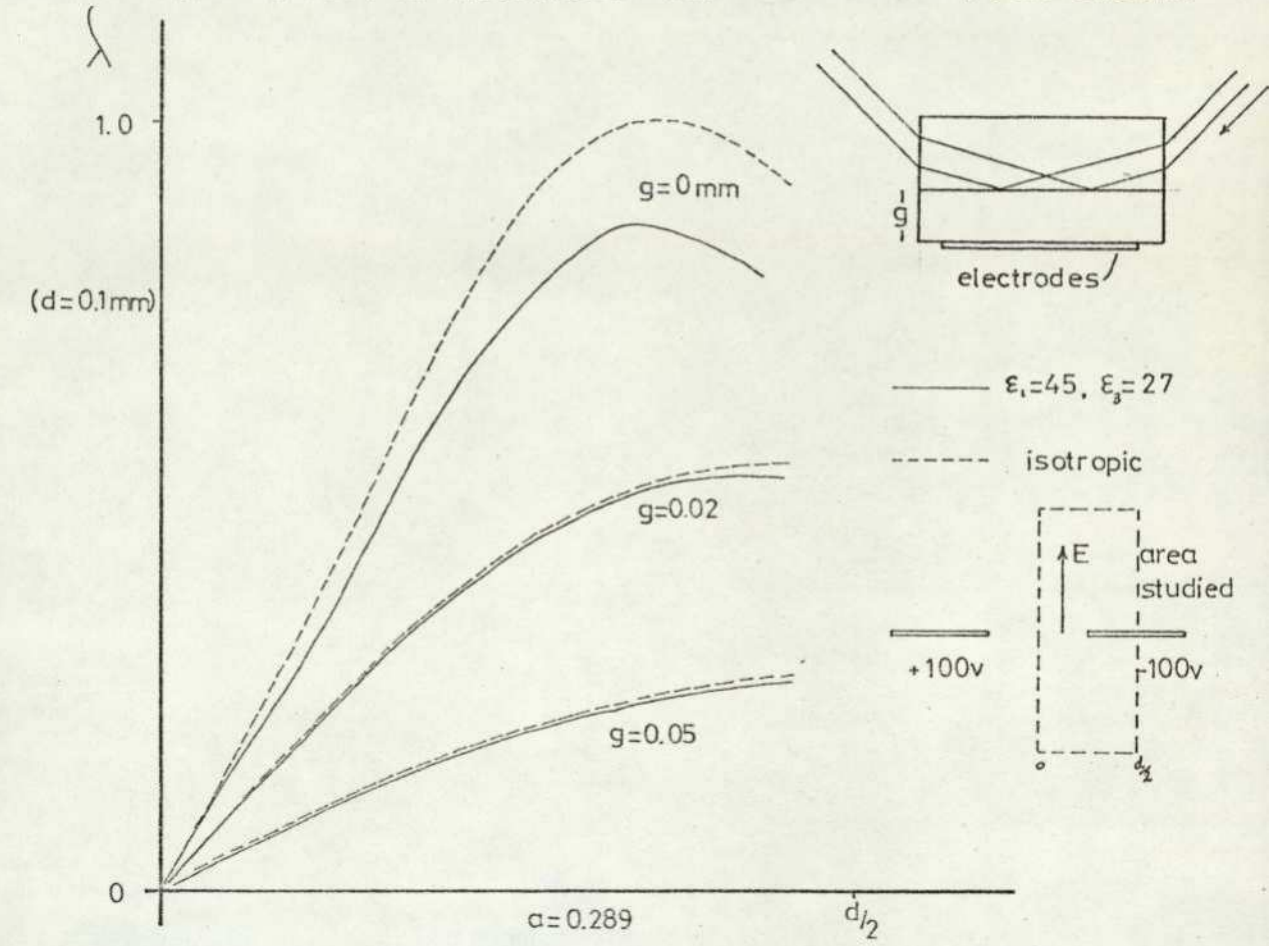


FIG.410 PHASE PROFILES transverse fields (d=0.1mm)

FIG. 4.11 EFFECT OF ELECTRODE GAP ($\theta = 2°$ shown)



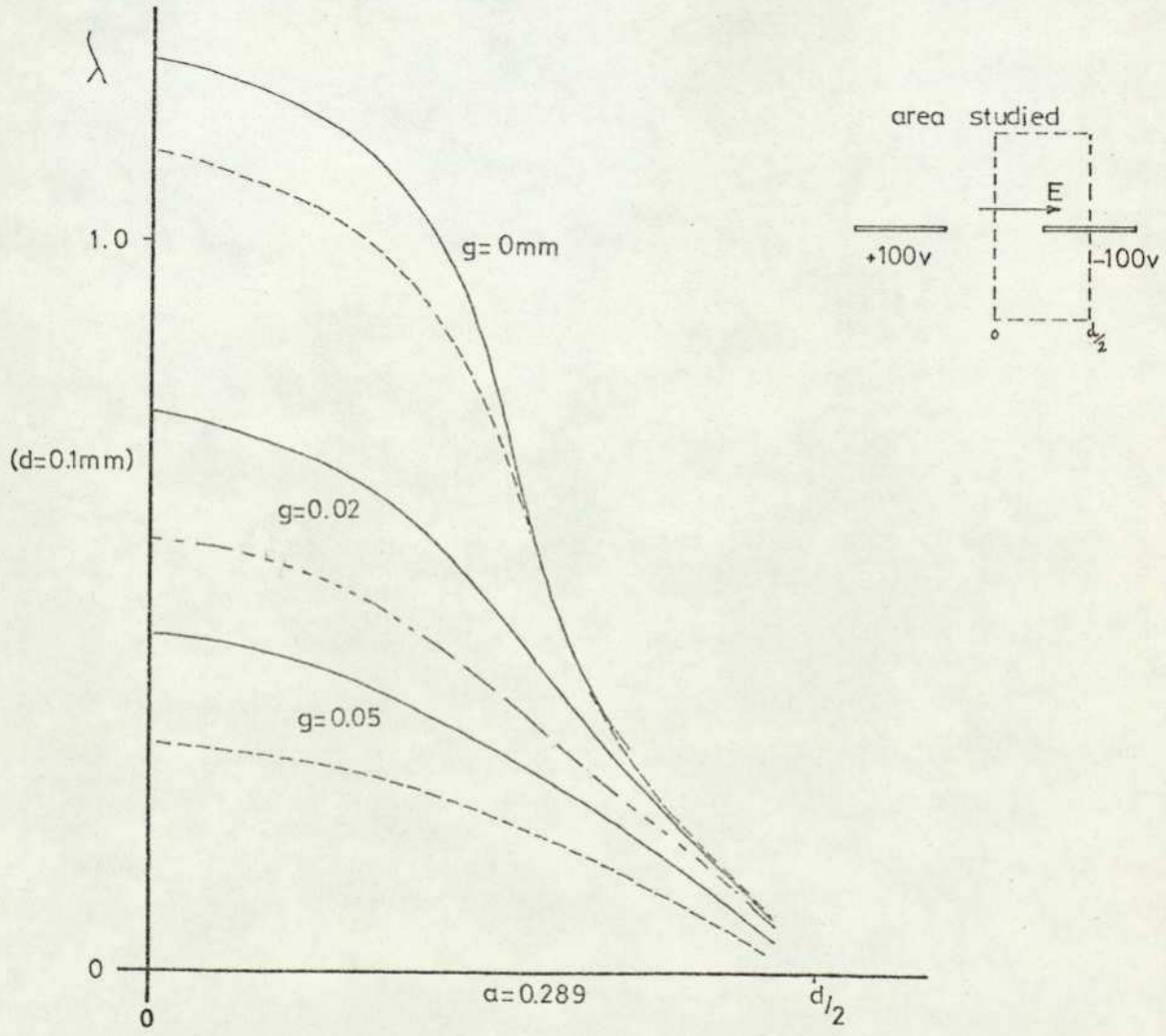
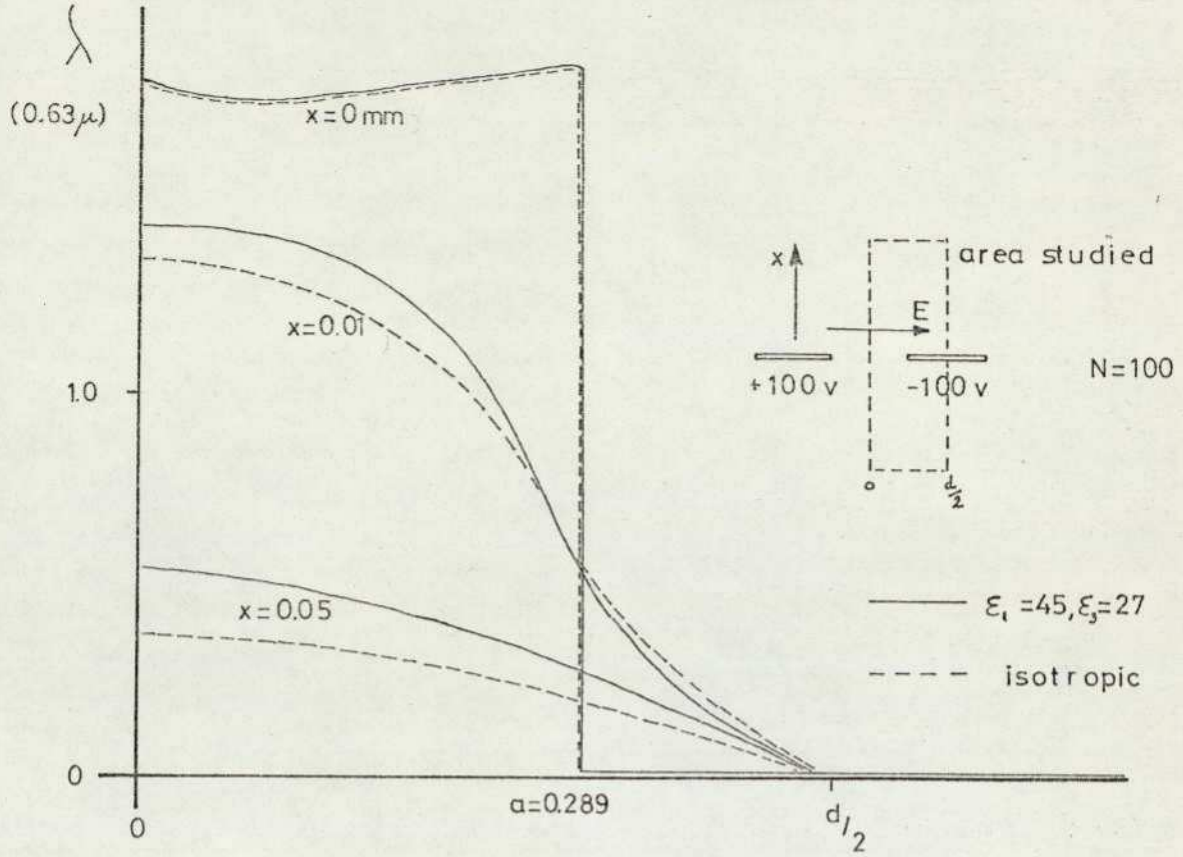
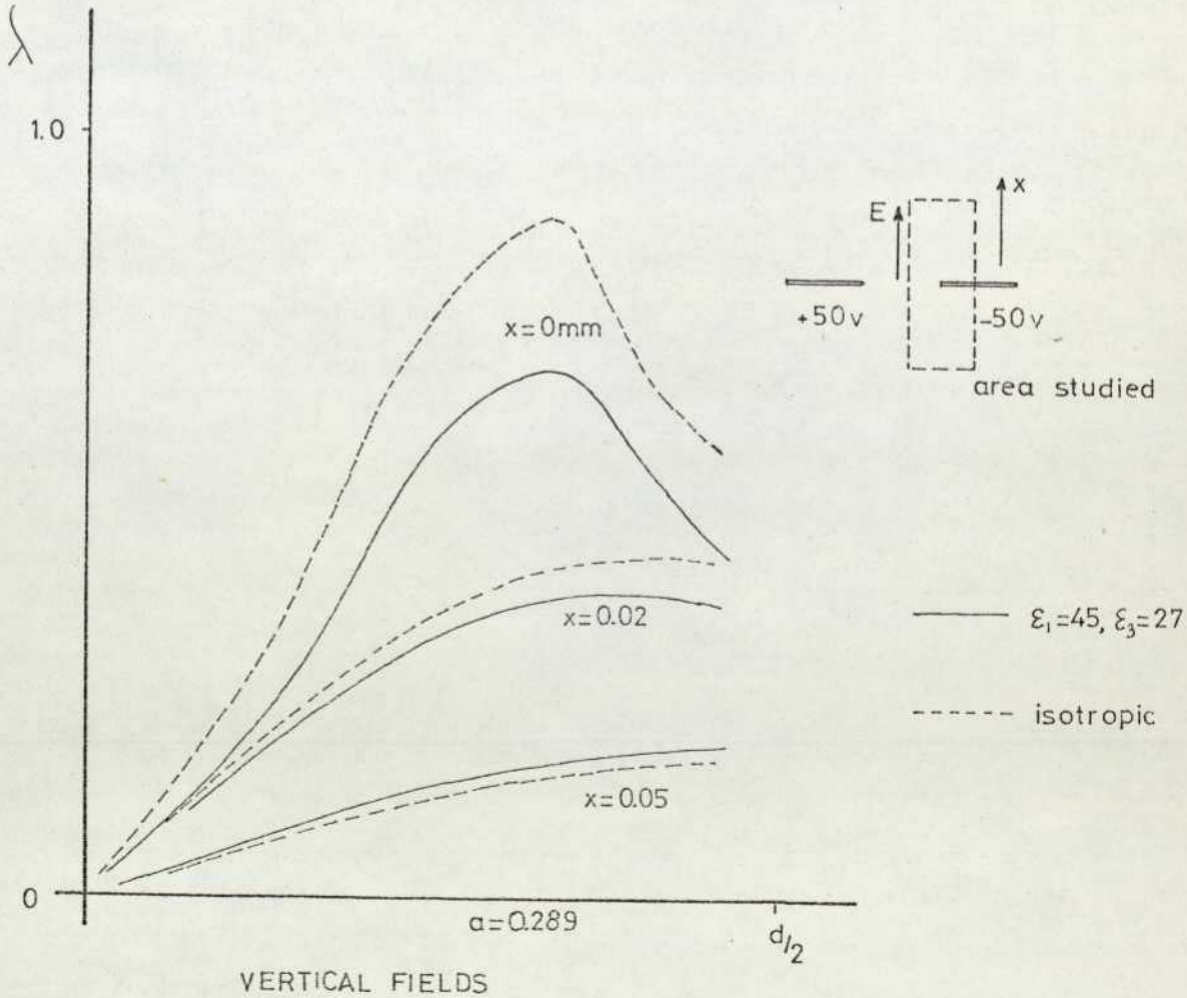


FIG. 4.12 PHASE PROFILES FOR $\vartheta = 0°$, d=0.1mm



HORIZONTAL FIELDS



VERTICAL FIELDS

Effects of Electrode Gap - Figure 4.11

The programs were also used to generate information on the sensitivity of the system to electrode/active area spacing. A matched gap material was assumed and both orientations show that device sensitivity is approximately halved by a gap thickness of 20% of electrode pitch. Such a matched gap could be achieved in practice by a bulk diffusion or implantation type process as well as a deposition technique if either decreased the bulk refractive index. It is interesting to note that such a gap renders the normal fields case less isotropy/anisotropy sensitive.

Phase Profiles for $\vartheta = 0$.

The $\vartheta = 0^{\circ}$ case has been widely used as a thin film device basis but the zero depth case is only approximately attainable when the electrode pitch is coarse compared with the guide depth. This condition calls for an unattainably wide guided beam to make use of the diffraction principle effectively. Hence a glance at the device performance versus depth is not out of place here as both extremes of the available range of ϑ prove to be of interest.

Figure 4.12 shows that a halving of device sensitivity occurs at a depth of approximately 20% of d in both configurations. The anisotropy sensitivity increases depth in the horizontal fields case and decreases in the normal fields case. In the latter case a depth of $\backsim$35%d seems to allow identical ac or dc performance.

Appendix P3 shows the phase profiles computed for various device configurations and gives their fourier content.

4.14 PHASE PROFILE AND MISALIGNMENT

So far device operation is under conditions of
1) collimated light parallel to the electrodes, and
2) uniform phase change in reflection across the device aperture. Information can be gained about device usability if misalignment sensitivity is known as this conveys information about device angular aperture and the importance of incident light collimation.

The problems of the misaligned device case are twofold. Firstly, the field path integral now becomes a three dimensional instead of a two dimensional function and secondly, the index ellipsoid section is changed.

The New Field Line Integral

The basic form of the phase retardation is:

$$\Gamma_{(x)} = \frac{4\pi}{\lambda}\int_{0}^{l/2\tan\theta} \Delta n_{(E_{(x,y)})}\, dy \qquad 4.70$$

for a device of length l. In the aligned case E(x,y) only varies with y during the integration and the value of retardation is evaluated for different values of x across the device aperture. In this case, when reference axes are considered at the electrode midpoint (inset figure 4.13) $\Delta n_{(E_{(xy)})}$ becomes a function of y in both variables and the integration process is made more complex. Another difference is that incident and reflected effects are no longer equal and additive. It can be readily seen that retardation nulls occur at x = 0 or nd for transverse field configurations and at $x = \pm (2n-1)\,d/2$ for normal field orientations because effects are equal and opposite in these cases. Because of this the pre-reflection and post-reflection effects must be computed separately and added to form the final expected phase profile.

The New Field Line Integral continued

Hence phase retardation can now be expressed as

$$\Gamma_{(x)} = \frac{2\pi}{\lambda}\left[\int_0^{\frac{1}{2}\tan} {}^{\Delta n}E(\tfrac{1}{2}\tan\vartheta, x+\tfrac{1}{2}\tan\alpha) + {}^{\Delta n}E(\tfrac{1}{2}\tan\vartheta, x-\tfrac{1}{2}\tan\alpha)\ dy\right] \qquad 4.71$$

by considering the reflected path of light misaligned by α^{o} as a mirror image of light misaligned by $-\alpha^{o}$.

At this point the induced refractive index change can be separated into field and index ellipsoid terms and using the notation in equation 4.63 can be expressed for convenience in the form

$$\Delta n_{(x)} = P.E_1 + Q.E_2 \qquad 4,72$$

where P and Q are of the complicated form expressed in equations 4,62 and 4,63 and can be considered as constants in the integration, being only dependent on ϑ. E_1 and E_2 have been expressed in section 4.7 and can now be considered in generalised form. Thus

$$E_y = \lesssim R_1 \exp(-A_1 \tfrac{l}{2}\tan\vartheta)\cos B_1(x + \tfrac{l}{2}\tan\alpha) \qquad 4.73$$

can be simplified further to:

$$E_y = \lesssim A \exp(-Bl)\cos Cl \qquad 4,74$$

and

$$E_x = \lesssim R_2 \exp(-A_{12}\tfrac{l}{2}\tan\vartheta)\sin B_1(x - l\tan\alpha) \qquad 4.75$$

becomes

$$E_x = \lesssim D \exp(-El)\sin Fl \qquad 4.76$$

Where the cartesian device aperture notation (x,y) is retained.

The New Field Line Integral continued

Next the integrals

$$I_1 = \int_0^{l/2} E_y dl \quad \text{and} \quad I_2 = \int_0^{l/2} E_x dl \qquad 4.77$$

need to be solved, and solving by parts the solutions are:

$$I_1 = \frac{A\exp(-Bl)(C\sin Cl - B\cos Cl)}{B^2 - C^2} \qquad 4.78$$

and

$$I_2 = \frac{-D\exp(-El)(E\sin Fl + F\cos Fl)}{E^2 + F^2} \qquad 4.79$$

and solving the integration limits and substituting for the shorthand the full expressions are arrived at: (see following page - equations 4.80, 4.81, 4.82 and 4.83).

So now $\int_0^l Edl$ can be expressed as

Eqn 4.80 - eqn. 4.82
and
Eqn 4.81 - eqn 4.83

The complexity of these expressions illustrates the need for the shorthand form employed previously. Before these functions are combined with the refractive index terms (P & Q in equation 4.72) they may need to be corrected for the misalignment angle α as this may need to be allowed for by a transformation of the index ellipse.

(See previous page)

$$I_1\Big|_{l/2} = \frac{R\exp(-n\pi/d\sqrt{\varepsilon_3/\varepsilon_1}\,l/2\tan\theta)}{\frac{n\pi}{d}\frac{\varepsilon_3}{\varepsilon_1}\tan^2\theta + \frac{n\pi}{d}\tan^2\alpha}\left[\cos\frac{n\pi x}{d}\left(\frac{n\pi}{d}\tan\alpha\sin\frac{n\pi l\tan\alpha}{2d} - \frac{n\pi}{d}\sqrt{\frac{\varepsilon_3}{\varepsilon_1}}\tan\theta\cos\frac{n\pi l\tan\alpha}{2d}\right)\right.$$
$$\left. -\sin\frac{n\pi x}{d}\left(\frac{n\pi}{d}\sqrt{\frac{\varepsilon_3}{\varepsilon_1}}\tan\theta\sin\frac{n\pi l\tan\theta}{d} + \frac{n\pi\tan\alpha}{d}\cos\frac{n\pi l\tan\alpha}{2d}\right)\right] \qquad 4.80$$

$$I_2\Big|_{l/2} = \frac{-R\sqrt{\frac{\varepsilon_3}{\varepsilon_1}}\exp\left(\frac{n\pi}{d}\sqrt{\frac{\varepsilon_3}{\varepsilon_1}}\,\frac{l}{2}\tan\theta\right)}{\frac{\varepsilon_3}{\varepsilon_1}\tan^2\theta + \tan^2\alpha}\left[\sin\frac{n\pi x}{d}\left(\tan\alpha\sin\frac{n\pi l\tan\alpha}{2d} - \sqrt{\frac{\varepsilon_3}{\varepsilon_1}}\tan\theta\cos\frac{n\pi l\tan\alpha}{2d}\right)\right.$$
$$\left. -\cos\frac{n\pi x}{d}\left(\sqrt{\frac{\varepsilon_3}{\varepsilon_1}}\tan\theta\sin\frac{n\pi l\tan\alpha}{2d} + \tan\alpha\cos\frac{n\pi l\tan\alpha}{2d}\right)\right] \qquad 4.81$$

and for the zero integration limit:

$$I_1\Big|_0 = \frac{-R\left(\cos\left(\frac{n\pi x}{d}\right)\frac{\varepsilon_3}{\varepsilon_1}\tan\theta + \sin\frac{n\pi x}{d}\tan\alpha\right)}{\frac{\varepsilon_3}{\varepsilon_1}\tan^2\theta + \tan^2\alpha} \qquad 4.82$$

$$I_2\Big|_0 = \frac{R\sqrt{\frac{\varepsilon_3}{\varepsilon_1}}\left(\sqrt{\frac{\varepsilon_3}{\varepsilon_1}}\tan\theta\sin\frac{n\pi x}{d} + \tan\alpha\cos\frac{n\pi x}{d}\right)}{\frac{\varepsilon_3}{\varepsilon_1}\tan^2\theta + \tan^2\alpha} \qquad 4.83$$

Index Ellipse in the Misaligned Case

Throughout any study of this aspect of the device two types of operation are considered: transverse field and normal field activation of the electro-optic material. It can be seen readily that the component normal to the electrodes is unaffected by α because the transformation is about that axis. Some second order effect will be felt on the normal contribution but this can be ignored as its significance is very small. This assumption is not so readily made in the case of the horizontal field.

If the index ellipsoid seen when the device is aligned is:

$$Ax^2 + By^2 + Cz^2 + Dxy + Exz + Fyz = 1 \qquad 4.84$$

then the section seen in the x/z plane say after a misalignment α is

$$x^2(A\cos^2\alpha + C\sin^2\alpha + E\sin\alpha\cos\alpha) + z^2(A\sin^2\alpha + C\cos^2\alpha + E\sin\alpha\cos\alpha) + xz(-2A\sin\alpha\cos\alpha + 2C\sin\alpha\cos\alpha + E\cos^2\alpha + E\sin^2\alpha) = 1 \qquad 4.85$$

As rotation is insignificant initially, D, E, F are small and as A and C are almost exactly equal the rotation term is also insignificant. Hence for small α this expression is very close to the original equation 4.84 as $\sin^2\alpha \to 0$ and $\cos^2\alpha \to 1$. Hence for small α no correction was applied to the index ellipse and the phase profile computed. Figure 4.13 shows the field integrals and demonstrates the field profile shapes with misalignment. At a given excitation the given example illustrates that for the d = 0.1 mm case the peak-to-peak phase amplitude is halved by a misalignment of 7°. This information gives a clue how to modify this type of device to cope with convergent or divergent light.

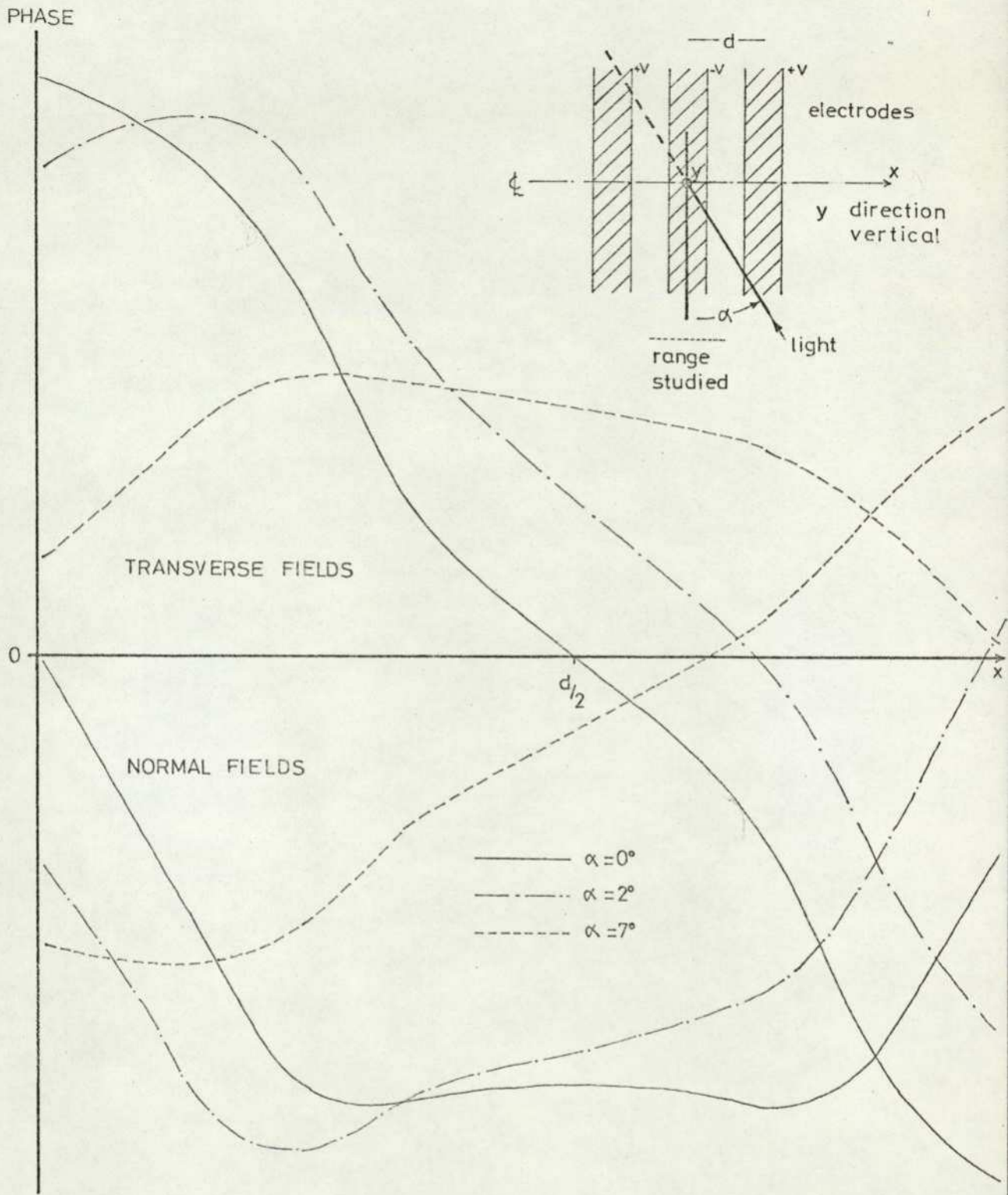


FIG. 4.13 PHASE PROFILE VARIATION CAUSED BY MISALIGNMENT

(ϑ = 3.1° case illustrated)

4.15 PHASE CHANGE ON REFLECTION

So far device modelling has been assembled around the concept of plane wavefronts propagating through the device and experiencing a phase corrugation. Now the TIR reflection needs to be examined to test if any phase corrugation is not electro-optically induced but is caused by different phase changes on TIR reflection than on reflection from the electrode metallisation areas. The problem can be studied from two standpoints. Any electrode system that is further away from the TIR surface than the wave penetrates into the rarer medium can be considered to have no influence on the phase of the totally internally reflected light. A typical penetration obeys an exponential law of the form

$$A = A_o \exp(-\alpha y) \qquad 4.86$$

and is certainly ineffective at depths greater than a wavelength beyond the dielectric interface. In consequence only the case with electrodes in intimate contact with, or deposited on, the dielectric interface is a possible residual phase corrugation situation.

Fresnels Equations

Using Fresnels equations, light polarised parallel and normal to the reflecting plane can be considered in terms of phase and intensity. Thus normalised intensities

$$I_{\perp} = \left[\frac{\frac{n}{n'}\cos I - \sqrt{\left(1 - \left(\frac{n}{n'}\right)^2 \sin^2 I\right)}}{\frac{n}{n'}\cos I + \sqrt{\left(1 - \left(\frac{n}{n'}\right)^2 \sin^2 I\right)}} \right]^2 \qquad 4.87$$

$$I_{\parallel} = \left[\frac{\cos I - \left(\frac{n}{n'}\right)\sqrt{\left(1 - \left(\frac{n}{n'}\right)^2 \sin^2 I\right)}}{\cos I + \left(\frac{n}{n'}\right)\sqrt{\left(1 - \left(\frac{n}{n'}\right)^2 \sin^2 I\right)}} \right]^2 \qquad 4.88$$

Fresnels Equations continued

and the associated phase changes are:

$$\tan\left(\frac{\delta_+}{2}\right) = \frac{\sqrt{\left(\frac{n}{n'}\right)^2 \sin^2 I - 1}}{\left(\frac{n}{n'}\right)\cos I} \qquad 4.89$$

$$\tan\left(\frac{\delta_\perp}{2}\right) = \frac{\left(\frac{n}{n'}\right)\sqrt{\left(\frac{n}{n'}\right)^2 \sin^2 I - 1}}{\cos I} \qquad 4.90$$

Where n and n' are the dense and rare material refractive indices respectively and $I = 90-\theta$ These functions are computed by program REFL (listed in appendix P2) and a pair of typical case studies illustrated in Figures 4.14 and 4.15. Both Lithium Niobate and ADP are shown and a dielectric/air interface is assumed. The higher refractive index difference naturally causes TIR to occur earlier in the $LiNBO_3$ case and the process efficiency is total at angles greater than 30° and 40° respectively. If glass of refractive index of 1.4 is used then the curves of Figure 4.1 are shifted to the right by some 15°. Phase change on reflection is suggested as quite significant from Figure 4.15 but it must be remembered that incidence angles of a maximum of $\sim 10^\circ$ are to be used in suggested devices and this corresponds to phase changes of the order of a few degrees only. In order to assess the differential between this retardation and that caused from reflection from an electrode finger composed of metal film it is now necessary to compare with the case of reflection from a dielectric/metal interface.

Reflection from a Metal Surface

The optics of metals become obscure when thin films are involved and here it is fortunately reasonable to assume electrodes thick in comparison with optical wavelengths and to consider reflection from a material surface of complex refractive index $\hat{n}$ of the form

$$\hat{n} = n + ink \qquad 4.91$$

Two metals were considered for this purpose, copper and chromium, both offering easy deposition and etch suitability. Quoted refractive index values were found (American Institute of Physics Handbook) at helium neon frequencies:

	n	k
Copper	0.62	8.29
Chromium	2.97	4.85

Phase changes (ref. Born & Wolf) on reflection are

$$\tan\phi = \frac{2v n_1 \cos I}{u^2 + v^2 - n_1^2 \cos^2 I} \qquad 4.92$$

and $$\tan\phi = 2n_1 n^2 \cos I \, \frac{2kv - (1-k^2)v}{n^4(1+k^2)\cos^2 I - n_1^2(u^2 - v^2)} \qquad 4.93$$

where $$\hat{n}\cos\theta_2 = u_2 + iv_2$$

and θ_2 is the angle within the metal and is defined as

$$\cos\theta_2 = \sqrt{\left(1 - \frac{(1-k^2)}{n^2(1+k^2)^2}\sin^2 I + i\frac{2k}{n^2(1+k^2)^2}\sin^2 I\right)} \qquad 4.95$$

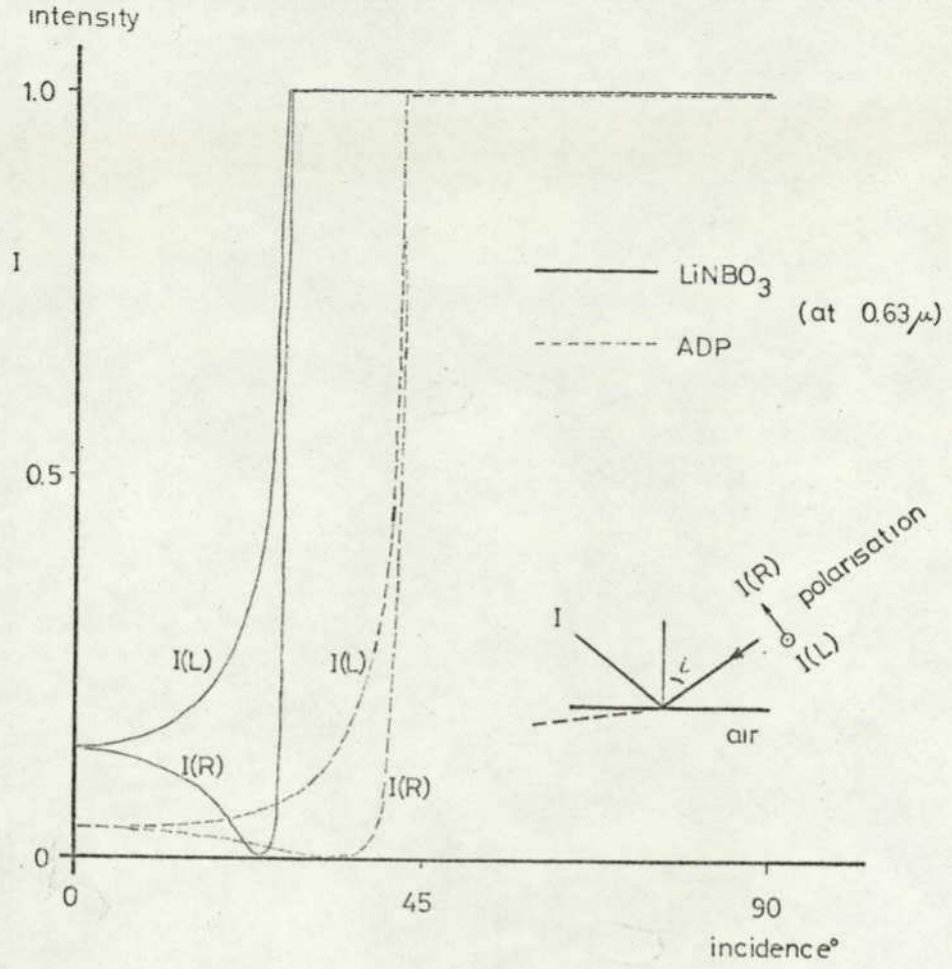


FIG. 4.14 TOTAL INTERNAL REFLECTION INTENSITY

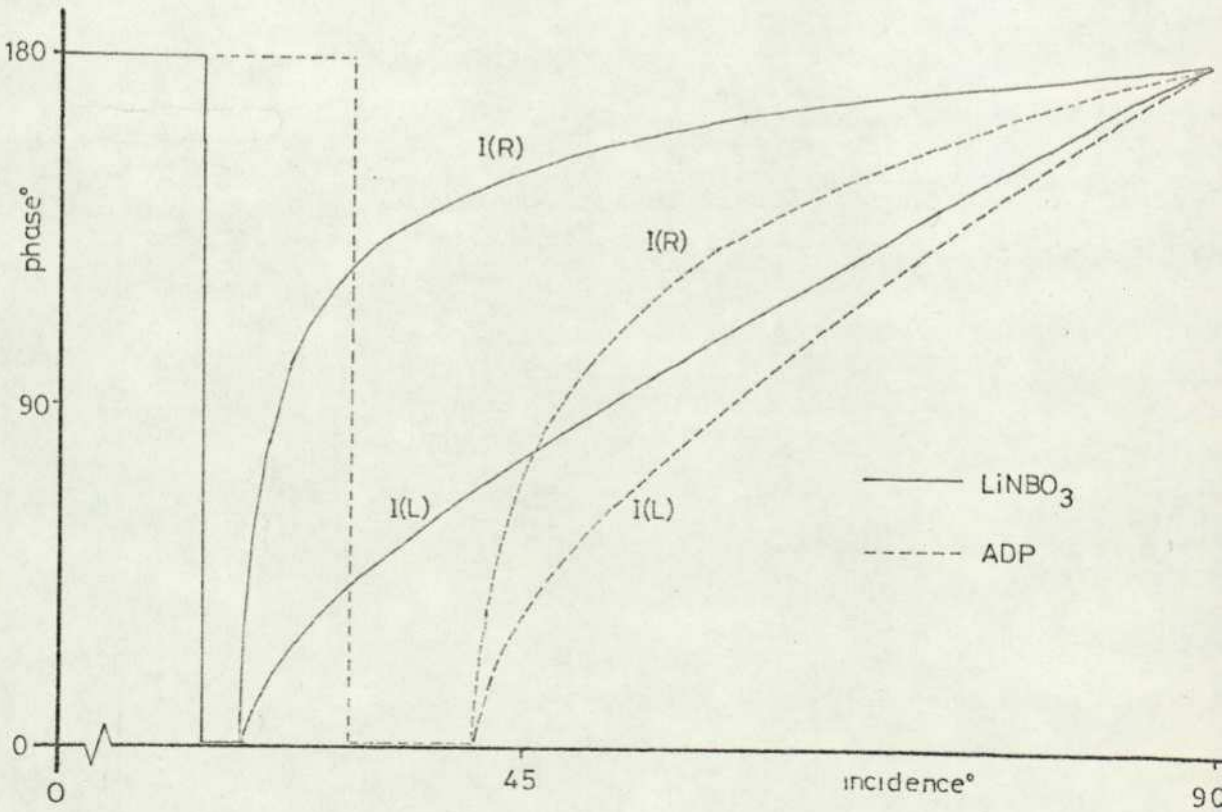


FIG. 4.15 PHASE CHANGE ON REFLECTION

Reflection from a Metal Surface continued

Calculations have suggested phase change values close to 180°.

Using these equations and assuming an I value of 84° ($\theta = 6^{\circ}$)

$\emptyset_{\perp}$ was found to be $\sim 176^{\circ}$ for chromium and $\sim 179^{\circ}$ for copper which effect would not be of significance. It was concluded that, even if metal/crystal configuration causing a residual phase corrugation were employed then corrective measures could be taken. Such a phase profile would be rectangular and could be augmented or counteracted by a transverse field configuration. Hence, if treated as a corrugation phase bias, this potential effect would never threaten device usability at least for quadratic material

4.16 FAR FIELD PERFORMANCE

The Analysis conducted so far has been solely to predict the phase retardation caused across the device aperture. It is next necessary to convert this information into a far field pattern which contains information about the variation in radiated intensity versus deflection angle. Two approaches towards this are immediately apparent:

a) Pursue orthodox diffraction theory for a periodic perturbation (for example see 'Antennas', J D Kraus 1950). This allows an intensity function of ones choice to be impressed across a sinusoidal perturbation aperture. In order to make use of this approach it is necessary to render the mathematics free of Bessel forms for computing reasons and to make modifications to allow non sinusoidal perturbations to be processed.

FAR FIELD PERFORMANCE continued

b) The alternative approach is the fundamental one of amplitude summation of radiated amplitudes across the device aperture. This is identical to the normal vector summation employed in the derivation of interference function and slit function in basic Fraunhofer diffraction. The only difference in this comparison is that the function is effectively continuous across the device aperture.

For total accuracy, an infinite number of increments per pitch would be desirable but a practical value of 100 was chosen in practice as offering sufficient accuracy. It is possible to impose an intensity weighting across the device to express the effect of a non-rectangular profile incident beam.

In fact both approaches were employed.

The Fourier Transform Method (Program DIFT in Appendix P2)

This is so called because the field pattern is the fourier transform of the aperture distribution. The far field radiation of an aperture distribution F(x) is:

$$E(\vartheta) = \int_{\text{aperture}} F(x) \exp(jkx \sin\vartheta)\, dx \qquad 4.96$$

where ϑ is deflection angle and x is a transverse aperture co-ordinate. $E(\vartheta)$ is the fourier transform of F(x). Initially assuming uniform illumination of device aperture we can write for one electrode pitch:

$$F(x) = \exp\left(j\phi \sin\frac{\pi x}{d}\right) \qquad 4.97$$

The Fourier Transform Method continued

Where ϕ is the peak value of phase corrugation, Hence:

$$E = \int_{-d}^{-d} \exp j(kx\sin\theta + \phi \sin(\frac{\pi x}{d}))dx \qquad 4.98$$

which can be written in the form:

$$E = \frac{2d}{\pi}\int_{0}^{\pi} \cos(nu + \phi \sin u)du \qquad 4.99$$

where $u = \frac{\pi x}{d}$, $n = \frac{kd}{\pi}\sin\theta$ 4.100

which, for integral n gives:

$$E = -2d J_n(\phi) \qquad 4.101$$

where $J_n(\phi)$ is a Bessel function of order n

and $\sin\theta = \frac{n\lambda}{2d}$ 4.102

so that, if the aperture involves N pitches

$$|E| = 2d J_n(\phi)\left|\frac{\sin N\psi}{\sin\psi}\right| \qquad 4.103$$

where $\psi = Kd\sin\theta$ 4.104

A practical version for our purposes assumes a general function of the form in equation 4.97, modified to allow an intensity profile across the device aperture.

$$F_{(x)} = f(x)\exp(j\phi\sin\frac{\pi x}{d}) \qquad 4.105$$

Rearranging equation 4.98, using the relationship

$$\exp(j\xi) = \cos\xi + j\sin\xi \qquad 4.106$$

The Fourier Transform Method continued

We arrive at:

$$E = f(o) + 2 \sum_{m=1}^{R} f(\frac{mD}{R}) \cos\left[\frac{mDk}{R} \sin\theta + \phi \sin(\frac{m\pi D}{dR}) \right] \qquad 4.107$$

where f(x) is the distribution (e.g. Gaussian), the aperture is 2D and there are 2R+1 elementary radiators. In order to normalise the results f(0) is equated to zero and

$$k = 2\pi/\lambda$$

Equation 4.107 now needs to be modified to allow non sinusoidal perturbation to be handled and this can most readily be achieved by expanding the second term in the bracket in a Fourier form. (Where $\hat{\rho}$ is peak retardation value, n is number of electrode fingers and F_c = 0,1,2, are the Fourier coefficients, Q in number.) ie. $\sum_{c=0}^{Q-1} \hat{\rho} F_c \sin(\frac{mn\pi}{2R}(c-1))$

The Incremental Amplitude Vector Summation Method
(Program VLTI in Appendix P 2)

In this case only computing problems exist. In previous sections phase profiles are computed fairly readily. Ten or eleven points across the profile of half a pitch are evaluated in previous sections with no difficulty using a CDC 7600 and reasonably efficient programming. The demand that 100 points be calculated in such an aperture was excessive so an intrapolation function was necessary. This was provided by modifying a Gauss-Siedel method for solving N simultaneous equations (ref. D McCracken - 'A Guide to Fortran Programming'). The resulting function provided a curve fit polynomial to the computed points and this polynomial was then employed for the generation of values for the phase summation. Basically the Gauss-Siedel method solves

The Incremental Amplitude Vector Summation Method
continued

$$\begin{aligned} a_{11}x_1 + a_{12}x_2 + \cdots + a_{1r}x_r &= b_1 \\ a_{21}x_1 + \cdots &= b_2 \\ \vdots \qquad\qquad & \vdots \\ a_{q1}x_1 + \cdots &= b_q \end{aligned} \qquad 4.108$$

for x is a very efficient manner. The rewriting processes causes $x_1 \ldots x_r$ to be a power polynomial in x and $b_1 \ldots b_q$ to be the phase retardations. Polynomials of up to powers of 10 were used and the number of equations was therefore also ten per function. The process, based on quickly converging iteration, was then used to find the coefficients (a_{11}, a_{12} etc. in equation 4.108), giving a power polynomial of the form

$$\int = a_{11}x + a_{12}x^2 + a_{13}x^3 + \cdots + a_{110}x^{10} \qquad 4.109$$

over half a device pitch. A normalised form with no constant (x^o) term was used.

Subsequent analysis consisted of an incremental vector summation of amplitudes over a full pitch (2d) and a subsequent summation over the whole device. Thus amplitudes may be summed in cartesian form:

$$A_x = \operatorname{Lt}_{m\to\infty} \sum_{n=1}^{m} \frac{A}{m} \cos\gamma \qquad 4.110$$

and $$A_y = \operatorname{Lt}_{m\to\infty} \sum_{n=1}^{m} \frac{A}{m} \sin\gamma$$

where $$\gamma = (n-1)\left(\frac{2\pi d}{m\lambda} \sin\phi + \int\left(\frac{nd}{m}\right)\right) \qquad 4.111$$

The Incremental Amplitude Vector Summation Method continued

The angle of summation (equation 4.111) consists of geometric path difference (first term) in terms of ϕ, the deflection angle, and the computed phase profile $\Gamma(x)$ as the second term.

Subsequently, this analysis is repeated over the whole device aperture consisting of N pitches. This involves a further N/2 summation terms, one for each full phase wavefront corrugation cycle.

$$A_x = \sum_{r=1}^{N/2} A_X \cos\delta \qquad 4.112$$

$$A_y = \sum_{r=1}^{N/2} A_y \sin\delta \qquad 4.113$$

where $$\delta = \frac{4\pi rd \sin\phi}{\lambda} \qquad 4.114$$

And far field intensity is obtained by adding the squares of the intensities:

$$I_{(\phi)} = A_x^2 + A_y^2 \qquad 4.115$$

In this way a far field intensity can be calculated for each value of ϕ, thus giving a far field profile.

The summation of Equations 4.112 and 4.113 could be executed in small increments across the whole device aperture of N pitches but the illustrated approach was used as less computing was involved (m + N/2 calculation instead of mN/2).

The Incremental Amplitude Vector Summation Method
continued

After ascertaining that both approaches gave equivalent results it was decided to use the fourier diffraction integral form program (DIFT) to describe the far field pattern intensity characteristics and the incremental amplitude vector summation program (VLTI) for zero order intensity characteristics. This means that the former program was used with the computed fourier coefficients of a given device situation while the incremental form, which contains the total device chracterisation, was used to study the zero order extinction voltage with device parameter variation.

Zero extinction voltage (Vx) considerations are rather modulator oriented. At such a voltage all incident energy is distributed symmetrically about the zero order position with no energy in the zero order. This can be considered as equivalent to the halfwave voltage ($V_{\frac{\lambda}{2}}$) as birefringent modulators. The parameters on which V_x is dependent are of importance therefore and are

1. d - electrode pitch
2. a - metallisation factor
3. θ - incidence angle
4. crystal orientation

and typical examples of this dependence are illustrated in this section.

4.17 DEVICE PARAMETERS AND PERFORMANCE

Figure 4.16 illustrates the dependence of this voltage (V_x) for a typical $LiNBO_3$ device an incidence angle (θ) orientation, and for a change of metallisation factor

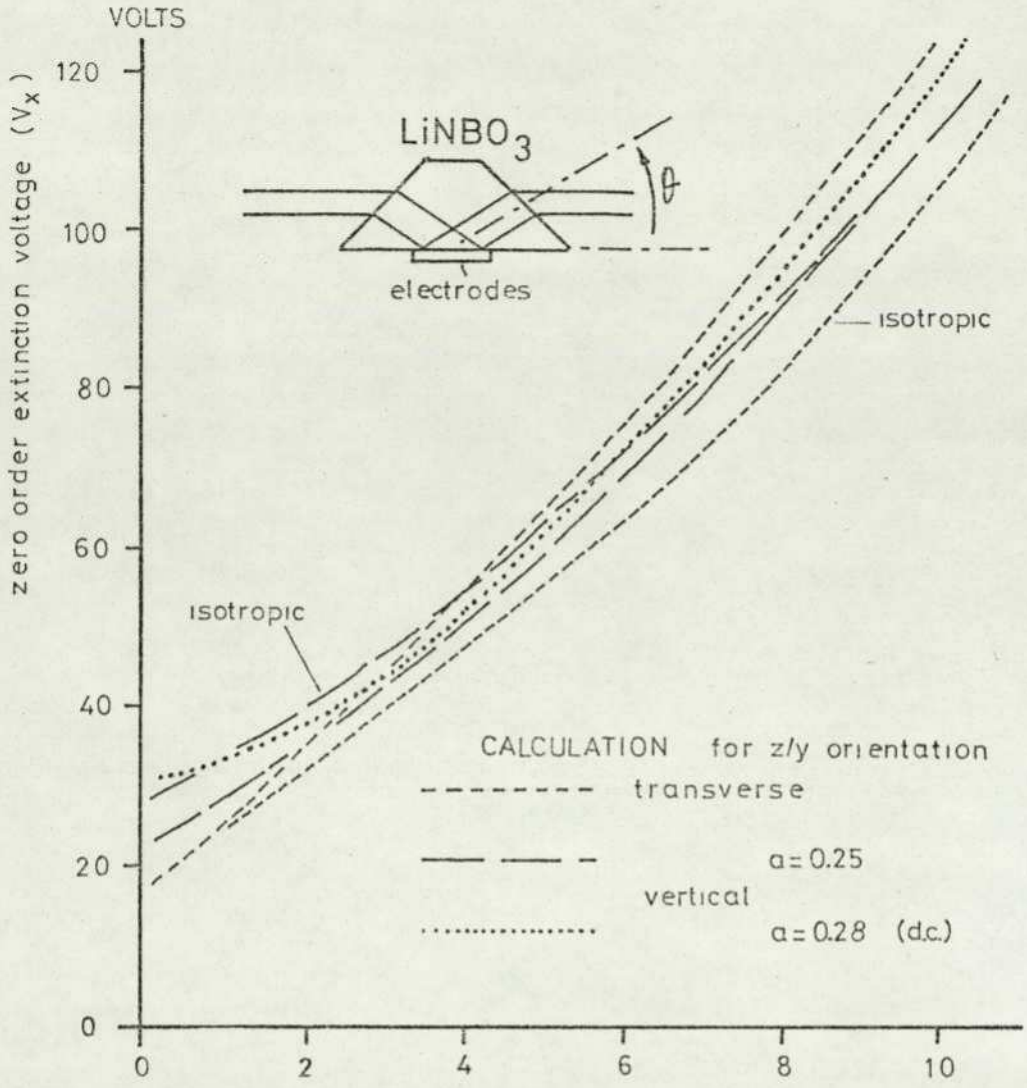


FIG.4.16 DEVICE PERFORMANCE vs INCLINATION for d = 0.1 mm

(a) from 0.25 to 0.29. (Such a change could be expected due to an underetch effect). It is to be noted that the voltages discussed are a factor of ten less than birefringent modulator $V_{\frac{\lambda}{2}}$ magnitudes. A z/y orientation is quoted but x/y orientation would offer a V_x of only $\sim 4\%$ more and of identical characteristics.

Both ac and dc performance in lithium niobate (anisotropic and isotropic) is shown in Figure 4.16 and points to note include the crossover of characteristics at a value of θ of $\sim 2^o$ and the fact that for a practical underetch effect (a change of a from 0.25 to 0.28 is shown) only for very small θ is the effect of any significance.

The dependence of V_x on electrode pitch is illustrated in Figure 4.17. This serves to illustrate one of the major advantages of the TIR device over a thin film ($\theta = 0$) device - the fact that, for reasonably small values of θ ($< 10^o$), V_x falls with pitch (d) reduction. This is of importance because to separate the diffraction orders the electrode pitch may need to be quite fine and the thin film version does not allow the sheet beam to approach the electrode surface very closely because of unavoidable crystal edge effects. Because of this, the overall effect of pitch reduction on the thin film device will in practice be a reduction of sensitivity and the device will in general not be useful if the electrodes are further from the sheet beam than half the electrode pitch. In the TIR version all the 'activated' crystal area can be used and this practical difficulty is removed.

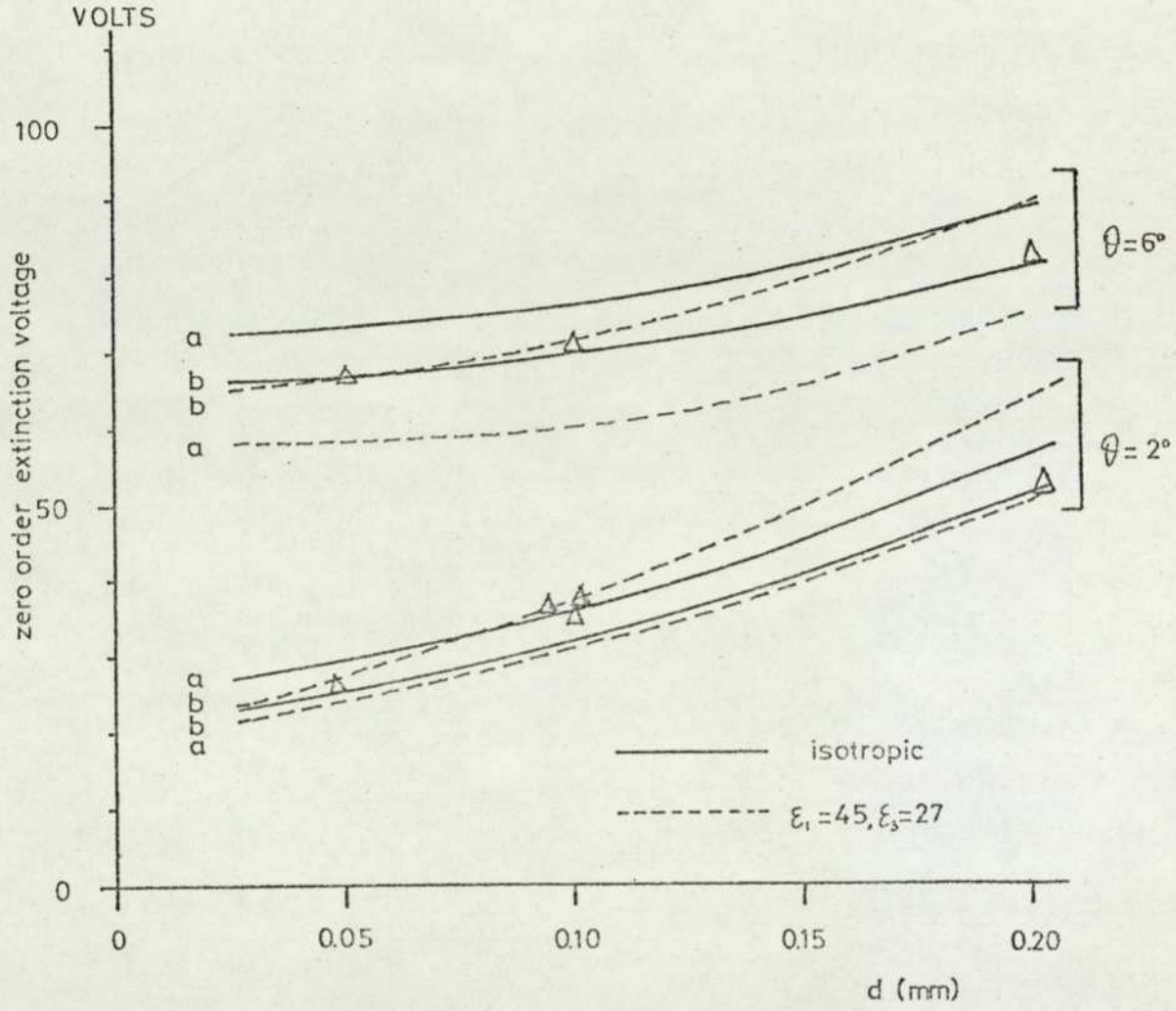


FIG. 4.17 EFFECT OF ELECTRODE PITCH ON DEVICE PERFORMANCE for $a = 0.25$

a transverse orientation

b normal orientation

Δ measured for normal orientation at DC (corrected for metallisation factor variation)

DEVICE PARAMETERS AND PERFORMANCE continued

An essential parameter in device use and modification prospects is a calculation of the sensitivity to misalignment of a practical device. The phase profile associated with a misalignment of the device was shown in Figure 4.13. Only a rotational misalignment in the electrode plane needs to be considered as changes in the other plane are already characterised by a knowledge of performance with collimated light against incidence angle θ. The case depicted in Figure 4.13 and expressed in equations 4.80 to 4.83 is transformed by an incremental summation form (as in section 4.11.2) into a far field pattern. This information is best condensed into the zero order extinction voltage characteristic portrayed in Figure 4.18 and is generated by program VDIV which is listed in appendix P2.

The performance shown in Figure 4.18 for the D.C. (isotropic) case and shows that a practical device has its performance halved by a misalignment of $\sim \pm 6^{o}$. This is a large angle by modulator standards where angular aperture is reduced by the high aspect ratios inherent in devices and in the optical bias that a misalignment may cause. A reduction of sensitivity is not the only expected effect as Figure 4.13 shows an assymetry in the phase profiles and hence a blazing action must also accompany misalignment. The magnitude of β is in part due to the high refractive indices of lithium niobate.

Information about zero order extinction voltage as a function of misaligned angle can be used in a positive way in order to construct a device to work with uncollimated light. This can be achieved by introducing a variation of electrode pitch across the device which compensates for the reduction of sensitivity across the device due to parts of the incident beam being, in effect, misaligned. This point is expanded in section 11.

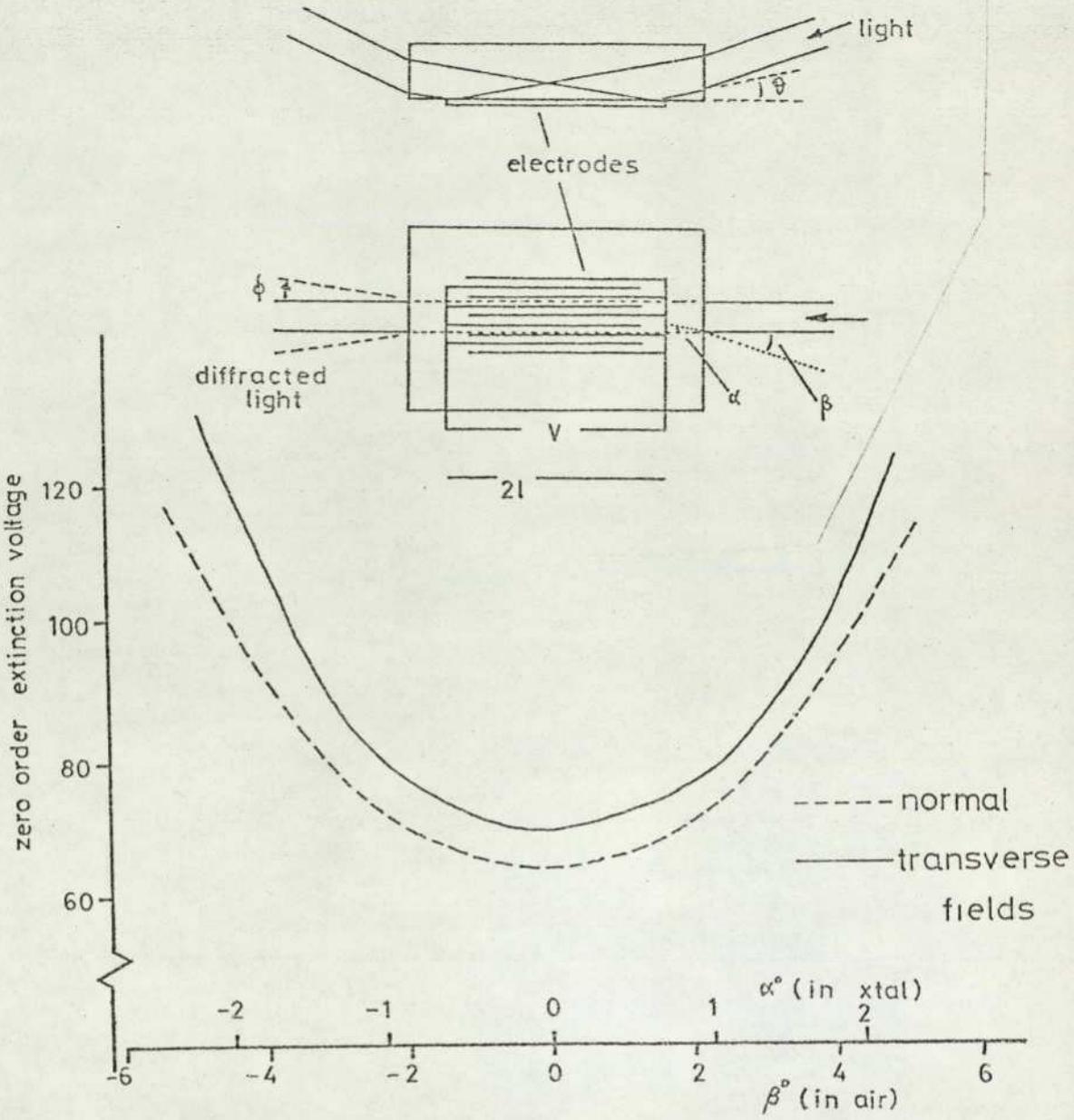


FIG. 4.18 MISALIGNMENT RESPONSE (predicted)

for $\theta = 3°$, d=0.1mm, a=0.29

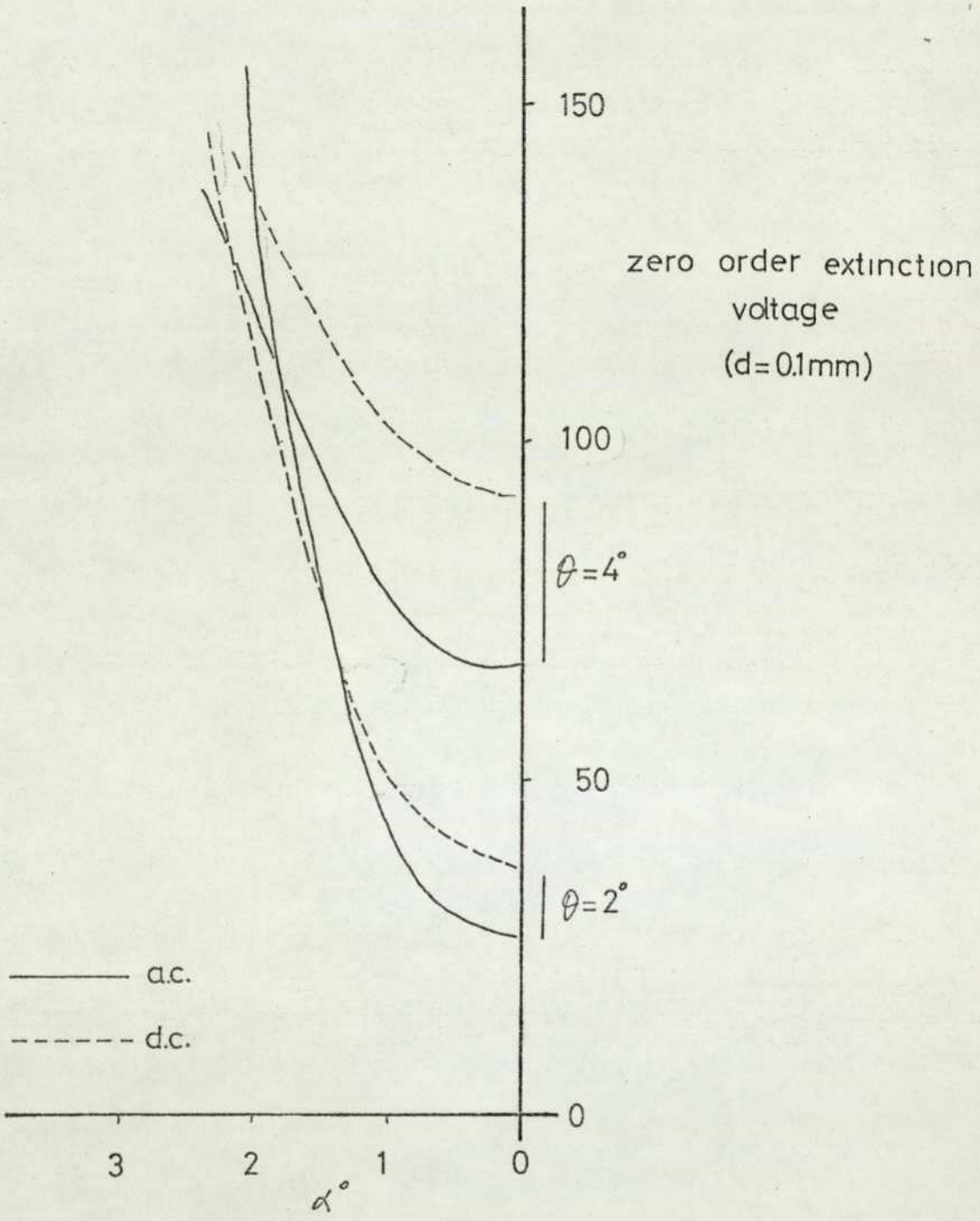


FIG.4.19 MISALIGNMENT vs INCLINATION

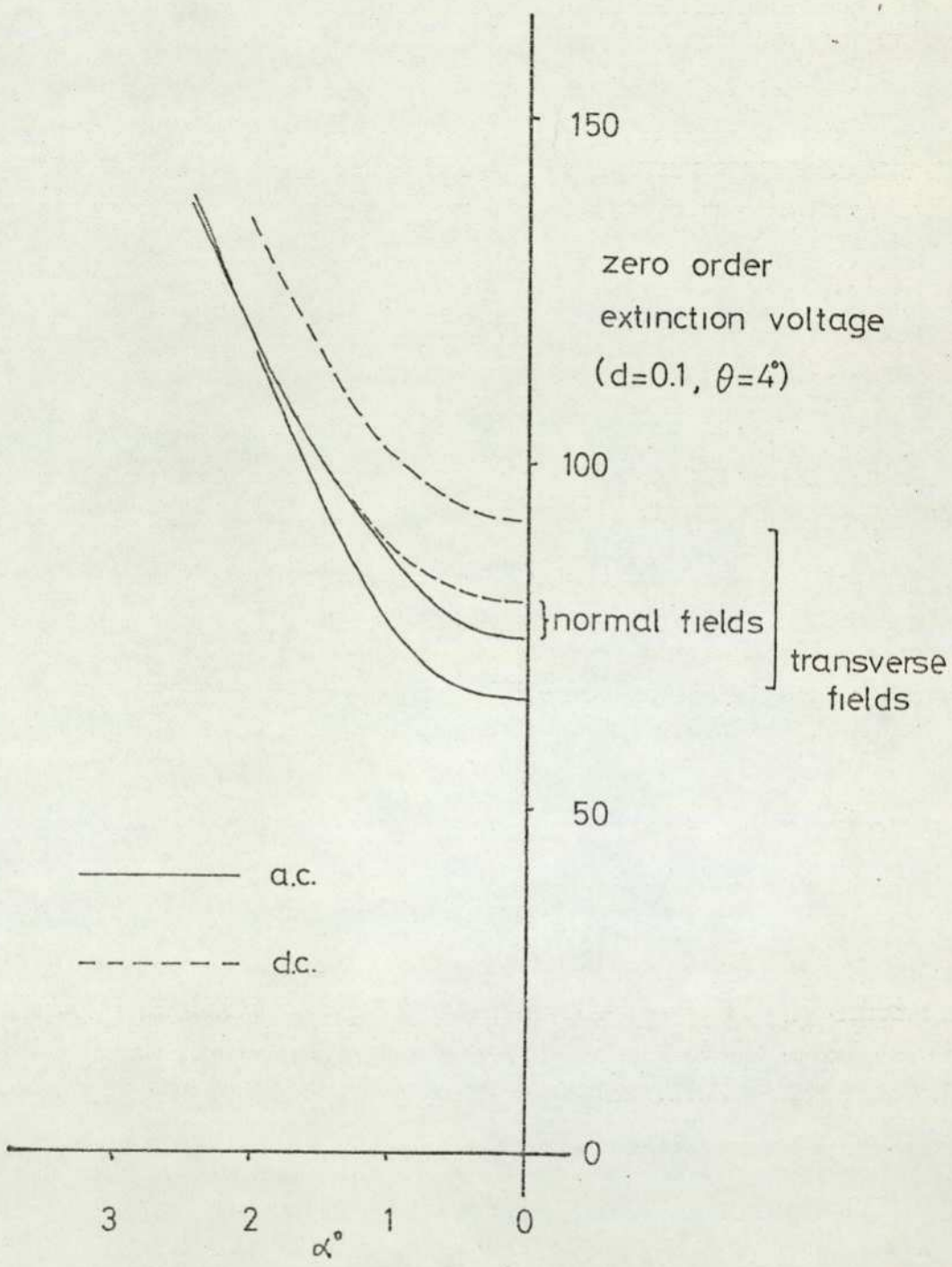


FIG. 4.20 MISALIGNMENT vs ORIENTATION

DEVICE PARAMETERS AND PERFORMANCE continued

An assumption inherent in all far field predictions so far is that the devices are illuminated with plane wavefronts and with a uniform intensity. These conditions are not entirely realistic. The plane wavefronts case requirement is a limiting factor in the situation where the electrode pitch is coarse and an error slope needs to be added to each voltage induced phase step which in turn will serve to degrade the extinction ratio over the device aperture. This could also be counteracted by a pitch variation, across the device aperture. In practice a gaussian intensity profile will be accompanied by a gaussian phase profile and, although the fall-off in intensity with phase change serves to render the effect of less importance, a correction can be made by the above method.

The far field pattern characteristics are complicated in actual devices by the fact that actual phase profiles are in general compound functions of two non-sinusoidal field profiles. Two types of information are necessary about far field patterns. The first is the order intensity characteristic and the second the angular position of the orders. These will be treated in this order.

Figure 4.21 shows the order intensity characteristic obtained from a Raman-Nath type source with a sinusoidal emergent phase profile. Points to note include the relative positions of the orders showing that many may contain energy simultaneously. Modulation action is exhibited by all orders with 100% available from the zero order. The modification that occurs for a practical device is shown in Figure 4.22 where zero and first orders are shown to have shifted in position from the sinusoidal corrugation case which now lies almost exactly between the transverse and normal field

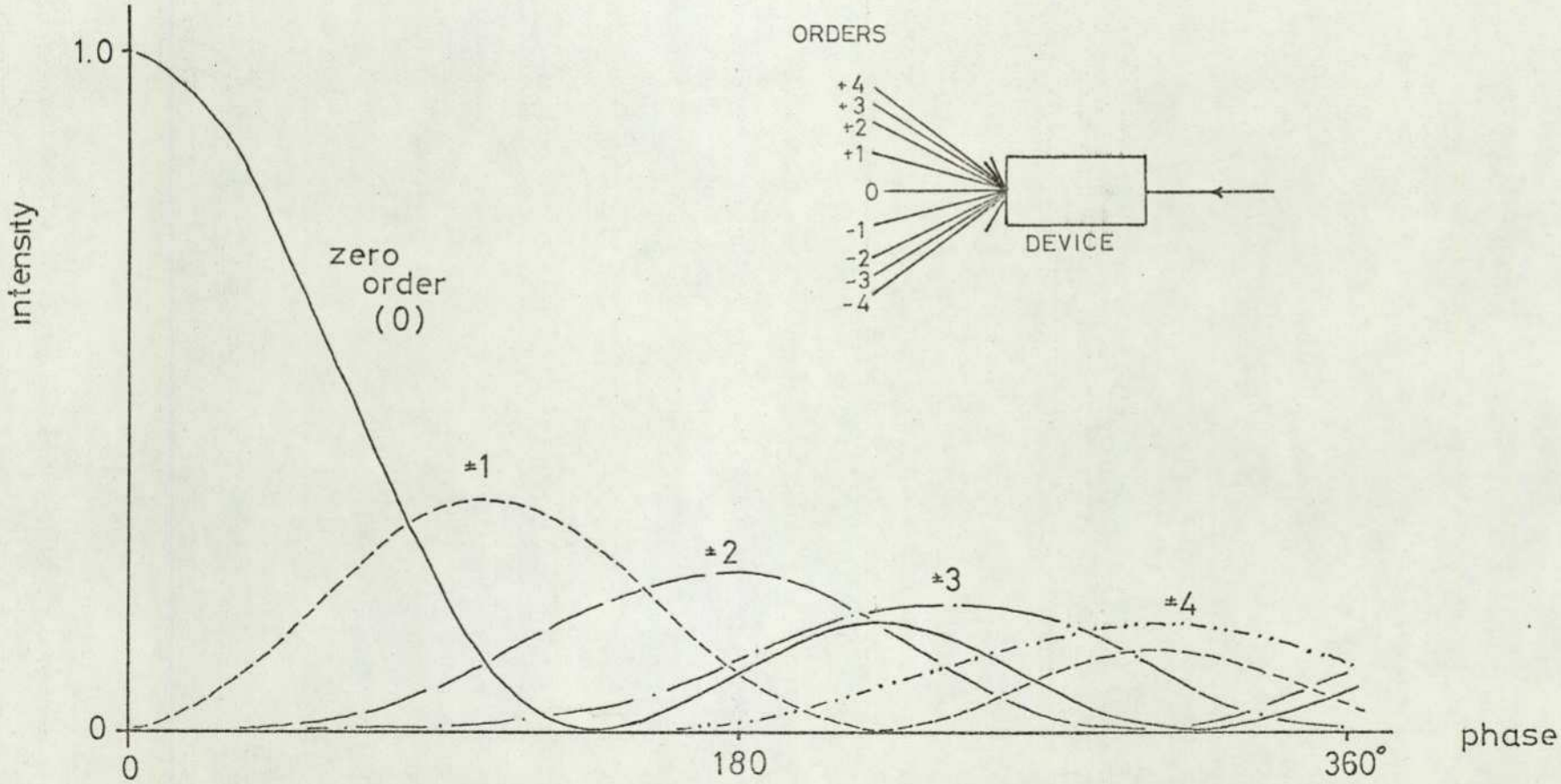


FIG. 4.21 ORDER INTENSITY CHARACTERISTICS (sinusoidal corrugation)

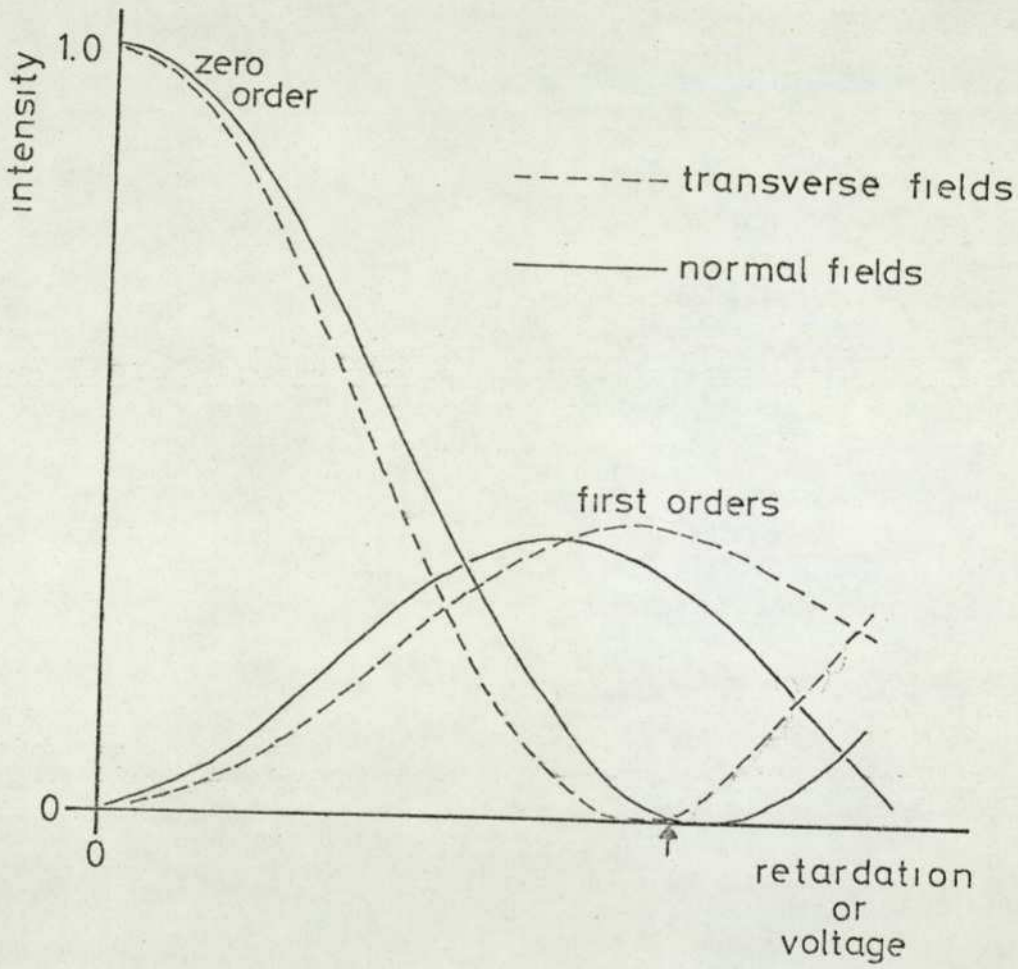


FIG.4.22 ORDER INTENSITY CHARACTERISTIC
for d.c. fields and 0.63μ
at $\theta = 2^\circ$ and d=0.1 mm

DEVICE PARAMETERS AND PERFORMANCE continued

The Fourier coefficients for the phase wavefronts demonstrated in Figure 4.22 are, in normalised form:

a. For transverse field, d = 0.1 mm, $\vartheta = 2^{\circ}$
0.9097 0.0 0.1627 0.0 0.0626

b. for normal field, d = 0.1 mm, $\vartheta = 2^{\circ}$
1.0228 0.0 0.1847 0.0 0.0693
(These are illustrated in Figure 5.2)
(The extinction voltage for the sinusoidal phase corrugation case is shown arrowed). The effect of a lithium niobate device is predicted in this diagram and shows that the effect of the orientation changes is to separate the zero and first order characteristics in the transverse fields case and bring them closer in the normal fields case. This is tantamount to saying that a blazing action is achieved by orientation variation because for first order intensity to be increased means that the order is favoured over the others. This is a definition of blazing.

The magnitude of the peak to peak corrugations involved for zero order extinction in these devices may be of interest. In the event of a sqarewave phase profile the peak to peak phase retardation for zero order extinction is obviously π radians. The case for a sinusoidal phase retardation is rather more ($\sim \frac{\pi^2}{2}$ radians) peak to peak. Figure 4.22 shows that, as may be expected, the transverse and normal field orientations cause the required peak to peak value to be reduced and increased respectively from the sinusoidal phase corrugation case. The first minimum of the sinusoidal phase corrugation case is shown arrowed. Appendix P3 contains a Fourier breakdown of the phase profiles predicted for the TIR device for various realisations.

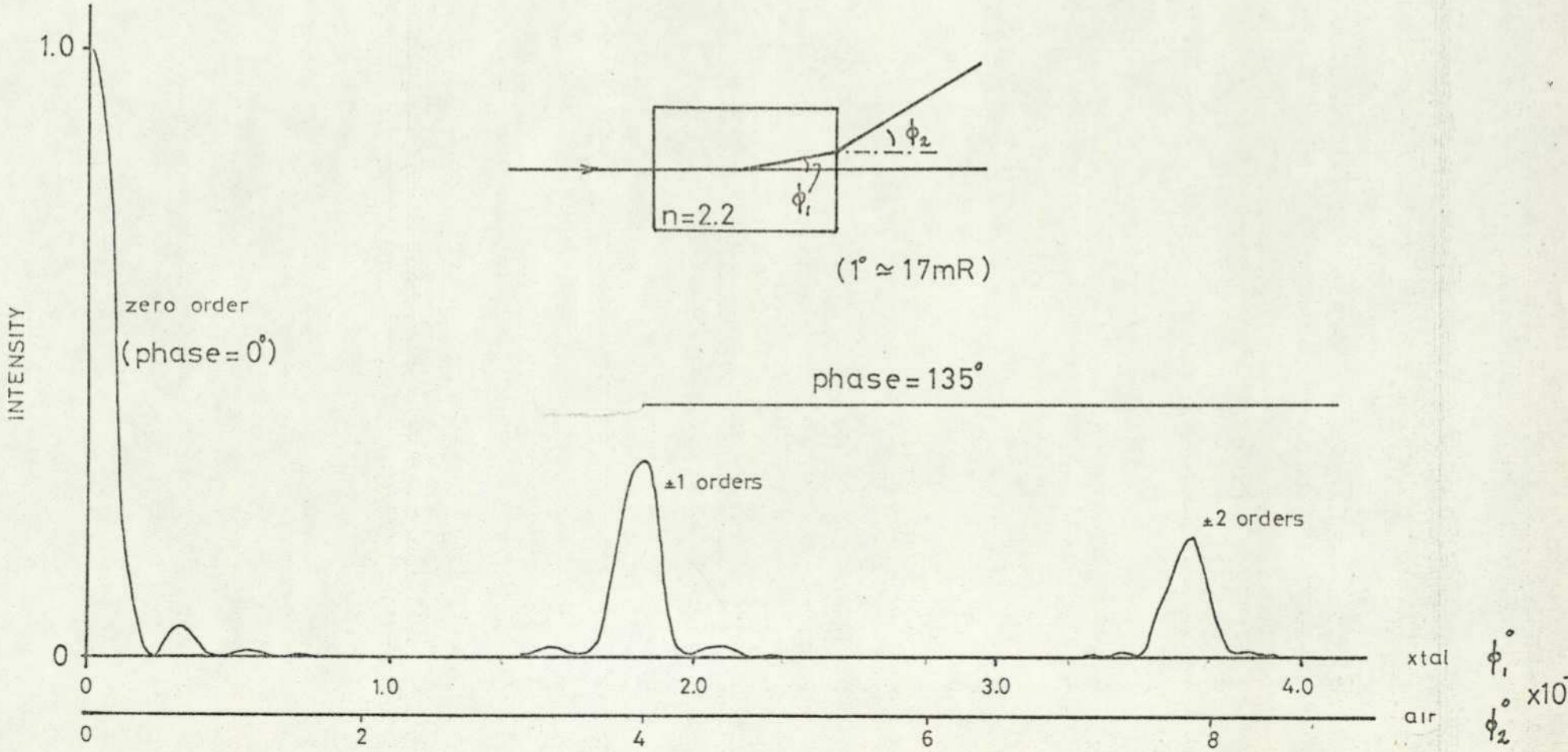


FIG. 4.23 FAR FIELD PATTERN for d = 0.1 mm (0.63μ)

DEVICE PARAMETERS AND PERFORMANCE continued

The Far Field Pattern

The passage of light through the device achieves a phase corrugation across the device aperture. As described previously this may be used to calculate intensity as a function of off-axis angle by two methods. Either classical array theory can be modified to cope with the unusual phase wavefront shapes (ref. Skolnik, Radar Handbook) or an incremental amplitude vector summation (ref. Scibor-Rylski) performed across the device aperture. A third approach can also be invoked which assumes that a phase corrugation emerges from the device and then all propagation takes place in the Poynting vector direction, normal to the phase wavefront, in this way an estimate of device slit functions may be made.

The far field pattern, predicted on either basis, for a sinusoidal phase corrugation is shown in Figure 4.23 for a practical electrode pitch. The advantage of a high refractive index material is shown by the diffraction angle magnification at the dielectric interface. The example given is for an aperture of 1.8mm (i.e. for 18 electrode fingers) and hence the angular resolution is defined. From classical diffraction theory it can be readily shown that the order half-angle varies inversely with the number of aperture total pitches. This is equivalent to the concept in Fraunhofer diffraction of order half angles as a function of the number of grating slits (Section 2).

Calculation of extinction ratios for different phase corrugation shapes gives the results presented in Fig. 4.24. As can be seen no extinction problem exists due to a non-sinusoidal phase corrugation of the variety encountered with these geometries.

The Far Field Pattern continued

An estimate of the slit function associated with this type of device is difficult to achieve but can be shown to vary with device extinction. A program was written (SLFN in Appendix P2) which suggests slit function shape on the basis of assuming that propagation is normal to the computed phase wavefronts.

If the phase profile is considered to be in terms of retardation distance:

$$S = f(y) \qquad 4.116$$

where y is an axis across the device aperture. f(y) is computed by the previously described phase programs (Appendix P2). The relative intensity on the orthogonal propagation assumption can be shown to be:

$$I = \exp\left[\frac{f''(y)}{1+f'(y)^2}\right] \qquad 4.117$$

(assuming light to propagate normal to phase wavefront) and the deflected angle ϕ to be

$$\phi = \tan^{-1}\left[\frac{1}{f'(y)}\right] \qquad 4.118$$

A computation on this basis yielded points which would lie on a slit function of a TIR type device. Analysis on this basis allowed a separation of Slit function and interference functions in the assessment of device performance. The nature of this approach is not rigorous however, and although the results agreed with diffraction generated data, it was decided to use the previously developed techniques.

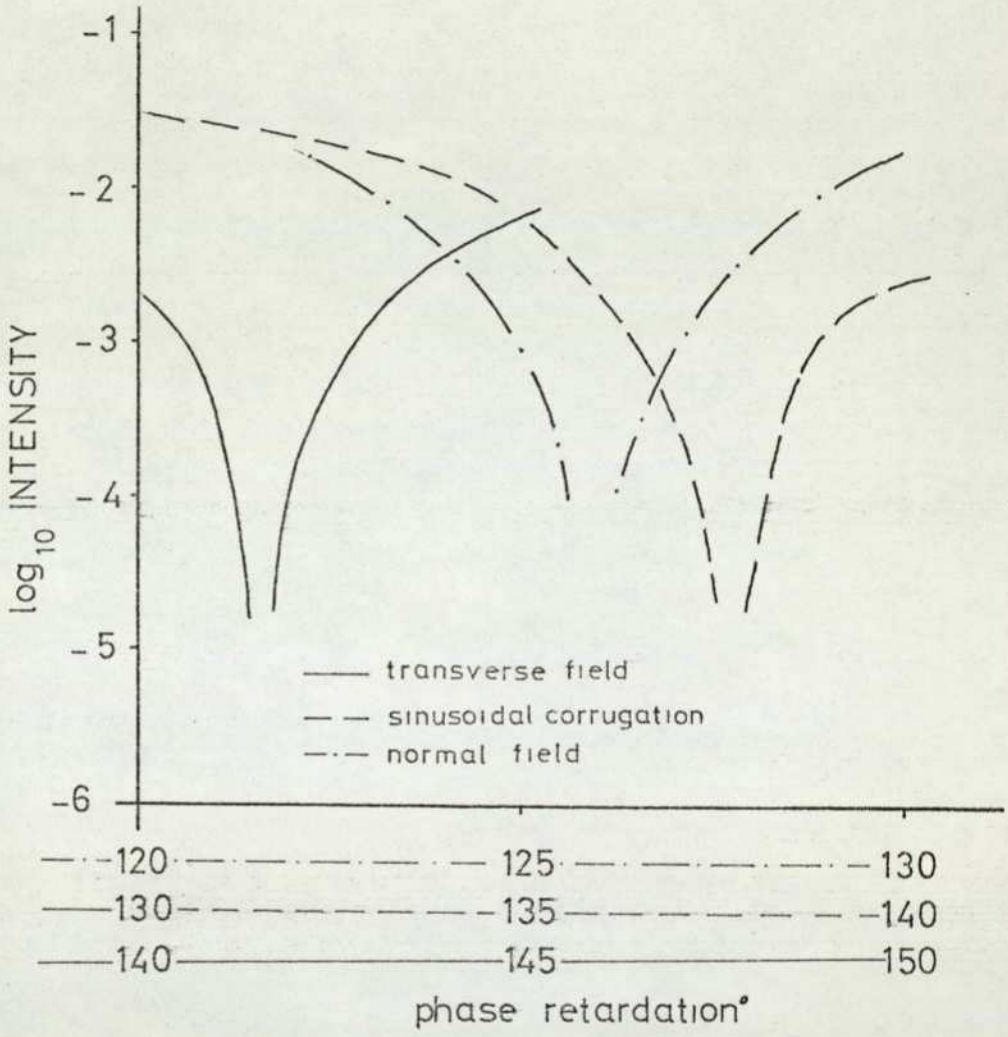


FIG. 4.24 EXTINCTION CURVES

4.18 CONCLUSIONS

The TIR device has been assessed for performance assuming a Lithium Niobate realisation and the simpler cuts associated with that material. This assumption is necessary to render the problem real but an assessment of another material can be made rapidly on the basis of this section if an approximate result is sufficient, whereas some modifications must be made for a rigorous result.

The device characteristics studied have been those of characteristics against excitation, far field performance, and the effects and trade-offs of the various aspects of device geometry. In addition to these, this section also deals with the complexities added by the material orientations for $LiNBO_3$ and an assessment has been made of misalignment sensitivity as part of the information required for further device measurement.

5. SURFACE DEPOSITED DEVICES:

5.1 Measured TIR Device Performance

5.2 Contact Process Electroding

5.3 Analysis of Sub-electrode Layer and Mismatch Effects

5.1.1 Details of Constructed Devices

Lithium Niobate samples were cut from a Roditi boule and polished on three consecutive faces employing procedures described in Sections These samples, shown in Figures 5.1.1, 5.1.2 were intended to allow the construction of transverse and normal field devices as analysed in the previous section. All these crystal samples were therefore cut with faces along the x, y, and z axes thus allowing electrodes in the x, y plane (normal field component activates r_{33}) and x, z or y, z plane (transverse field component activates r_{33}).

5.1.2 The Test Cell Assembly

In order to allow device performance analysis a test cell was constructed with x-y translation and two axis rotation facilities. This is illustrated in Figure 5.1.3,4 and is composed of standard optical bench components with a perspex test cell screwed to a polariser rotator.

5.1.3 Electrodes

The electrodes initially employed are illustrated in Section 10 . They were made by two step photoreduction from a scribed Kimoto strip-film and 0.05, 0.1 and 0.2 mm in pitch. These electrodes were then etched in a copper on chromium film. The thickness of this film was of the order of 1-2 μ and was not found to be critical in any way. (The etching and deposition processes are dealt in detail within a subsequent section).

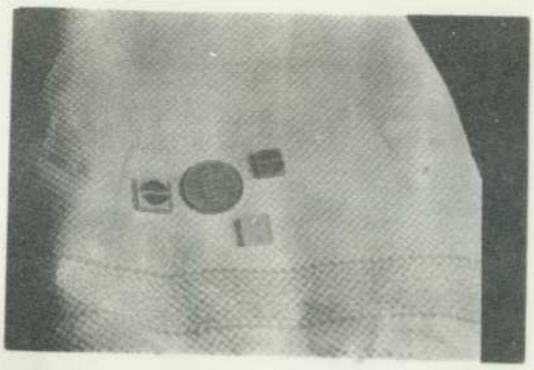


FIG 5.1.1

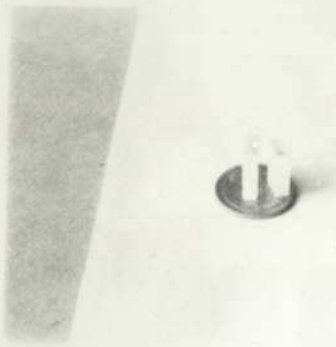


FIG 5.1.2

TYPICAL $LiNBO_3$ CRYSTALS USED FOR TIR DEVICES

PREPARED CRYSTALS

TIR EXPERIMENTAL ARRANGEMENT

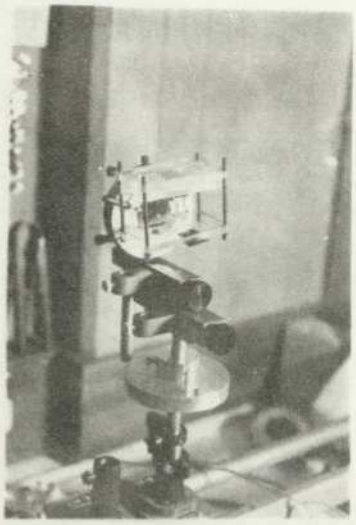


FIG 5.1.3 - TIR TEST CELL

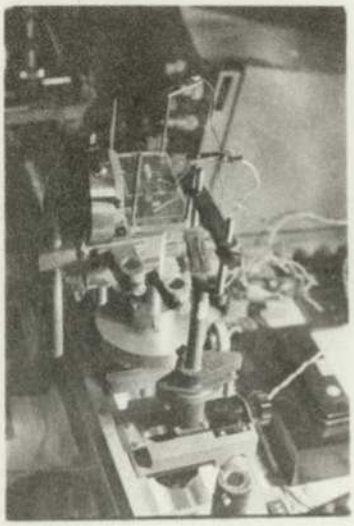


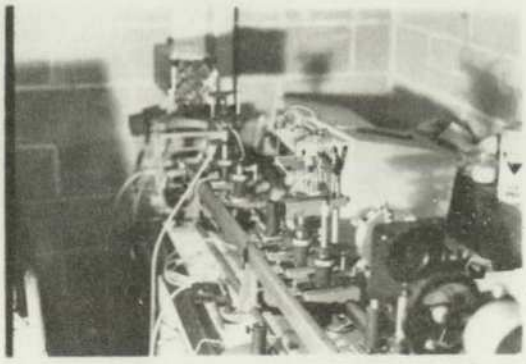
FIG 5.1.4 - LOADED TEST CELL

FIG 5.1.5



TIR TEST APPARATUS

FIG 5.1.6



5.1.4 Crystals

Electrodes were deposited on the samples to investigate:

1. Effect of pitch on performance.
2. Effect of incidence angle on performance.
3. Effect of orientation (normal and transverse fields).
4. Effect of misalignment on performance, and
5. Far field patterns and characteristics.

Typical samples used are illustrated in Figs 5.1.1, 5.1.2

5.1.5 Performance Measurements

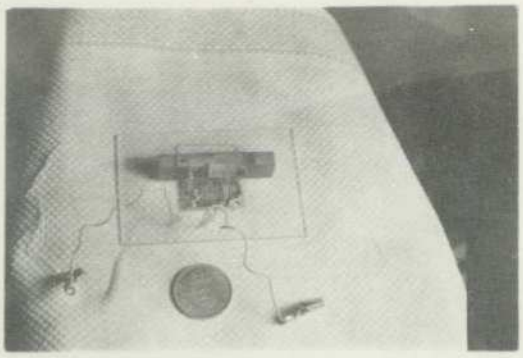
The general experimental arrangement used for these device investigations is illustrated in Figs 5.1.3,4 and schematically in Fig. 5.11 . A helium neon 2mW unpolarised laser was used followed by a dichroic polariser, an iris type stop, a cylindrical lens, and the test cell. Optional detection methods were employed in the far field. These consisted of a pinhole masked Mullard photomultiplier or an SGD 100 PIN diode on a positionally adjustable mounting giving an electrical analogue of position. The lens was used to compensate for the 1:1 electrode aspect ratio and offer a square aperture. Both detectors were complete with their relevant power supplies and the device supply was arranged from a 0-3000 volts supply via a 1MΩ + 1MΩ potential divider thus providing breakdown protection for the device. Initially only d.c. voltages were applied to the device and an isotropic behaviour was assumed.

The test rig configurations employed are illustrated in Figs 5.1.7-5.1.12 and include surface deposited devices (Figs 5.1.8, 5.1.9) and contact process devices (Figs 5.1.10, 5.1.11, 5.1.12).

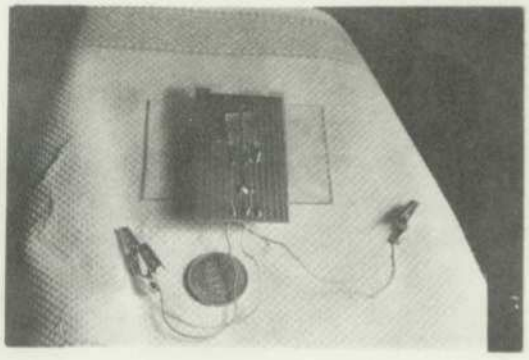
TIR TEST CELLS AND HOLDERS



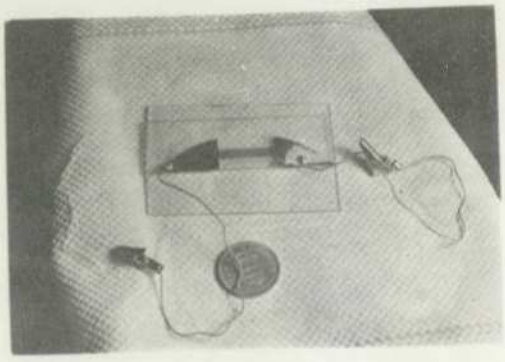
5.1.7 - TEST CELL



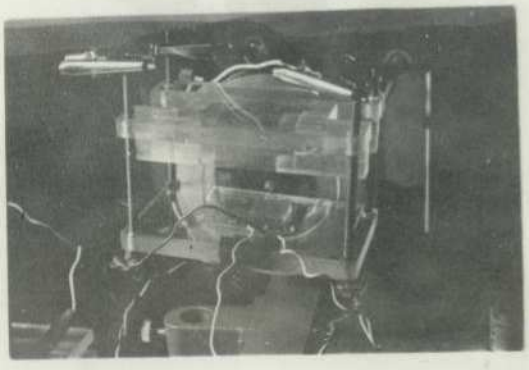
5.1.8 - CRYSTAL HOLDER



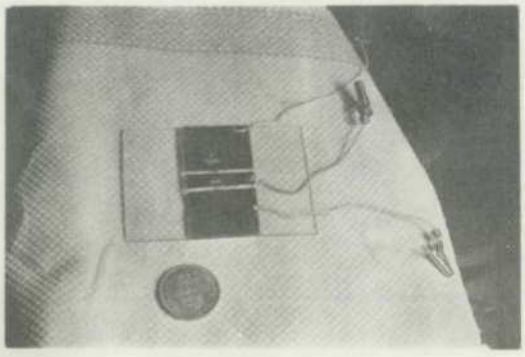
5.1.9 - CRYSTAL HOLDER



5.1.10 - CONTACT ELECTRODES (Q-SWITCH)



5.1.11 - CONTACT ELECTRODED SYSTEM



5.1.12 - CONTACT ELECTRODES

5.1.6 Order Intensity Characteristics

Fig. 5.1 shows predicted order intensity characteristics for a normal field device (z axis and incident polarisation normal to electrode plane) for electrode pitch (d) of 0.1 mm and a value of θ of 2^{o} (within the crystal) the metallisation factor a was 0.239 because of etch effects. As can be seen, excellent agreement is shown by the measured points which were obtained using the photomultiplier and an xy plot against applied voltage. The predictions were obtained from the DIFT program using the information about the expected phase profile shown dotted in Fig 5.2 . All the relevant programs are listed in Appendix P2. A comparison with a $\cos^2$ relationship characteristic of birefringent devices is shown assuming an equivalent $\sim$ 72 volts extinction voltage. It is worth noting that first order maximum occurs at only $\sim$ 42 volts at which point $\sim$ 30% of incident intensity is available. The transverse field case was also investigated with almost identical results but a slight shift of first order characteristics occurred as suggested in section 4. As this shift was comparable to experimental error these curves are not compared here.

5.1.7 Performance Versus Incidence Angle

Device performance versus inclination angle was measured by using the calibrated test cell rotation scale and converting this rotation to incidence change within the crystal using a refractive index value of 2.20 for n_e at 0.63μ. (Hence a tilting of the test cell of 4.3° gave a value of θ of $\sim 2^{o}$). Zero-order extinction voltage was measured using a visual null criterion and the results are shown in Fig. 5.3 . The configuration measured was a normal field component device (z axis normal to electrode plane) with d = 0.1 mm, a metallisation

Performance versus Incidence Angle continued

factor (a) of 0.289 and y axis transverse to electrodes. As can be seen the metallisation factor causes slight degradation of performance for low (comparing solid and dashed lines) while results are again in excellent agreement with prediction. Measurements on transverse field devices (z axis in electrode plane) were also found to exhibit good agreement with prediction but are not included in Fig. 5.3 for the sake of clarity. All these measurements were conducted with d.c. voltages and the relative merits picture should depend on whether the isotropic or anisotropic model applies. Consequently 'best configuration' choices are not the same in d.c. and a.c. conditions.

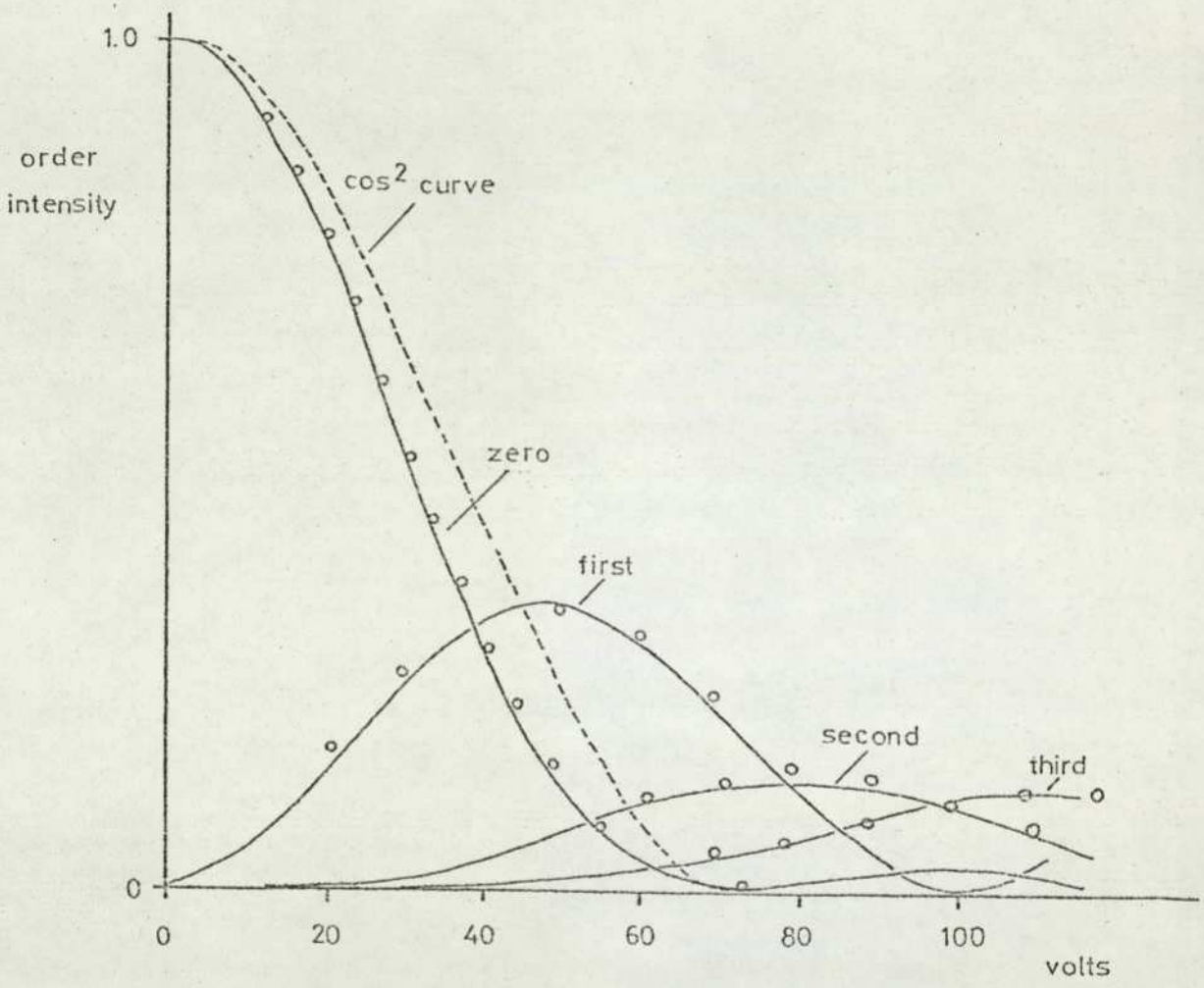


FIG. 5.1 ORDER INTENSITY CHARACTERISTICS

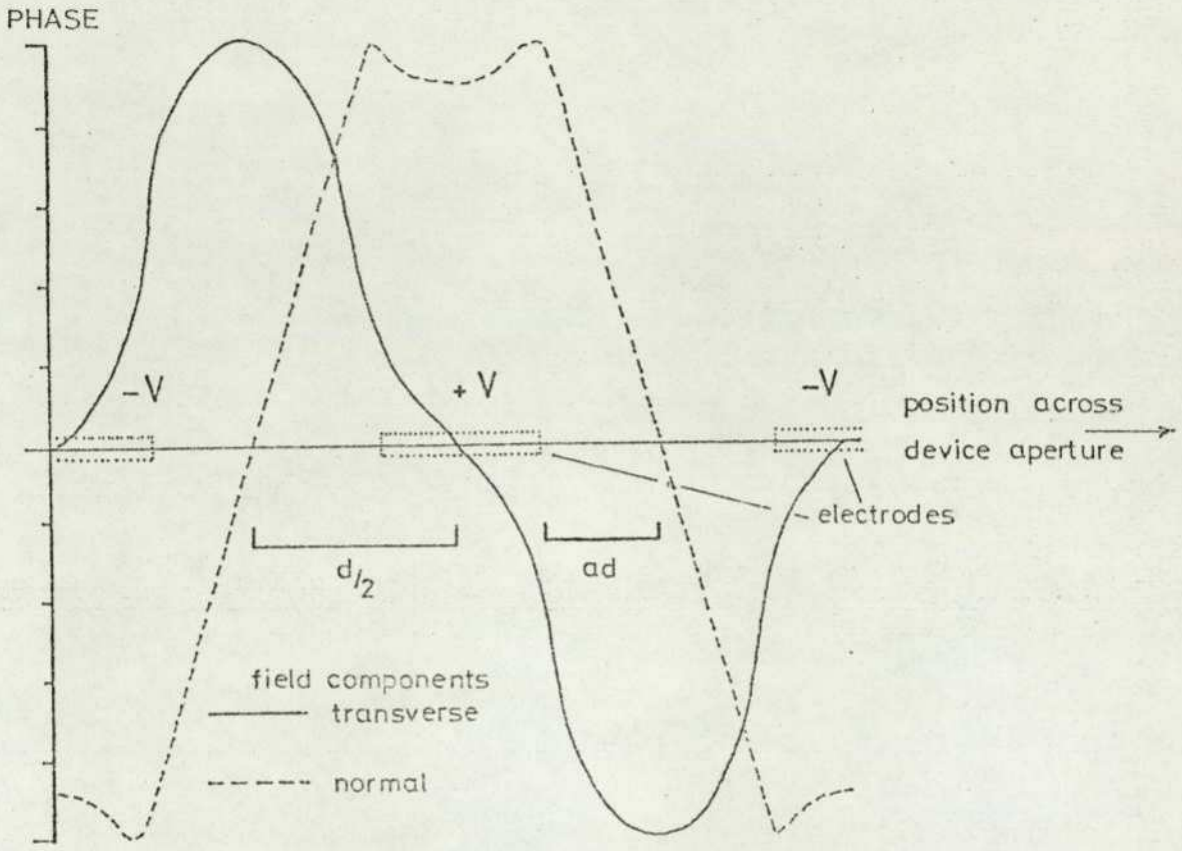


FIG.52 EMERGENT PHASE PROFILES for $\theta=2°$, d=0.1mm

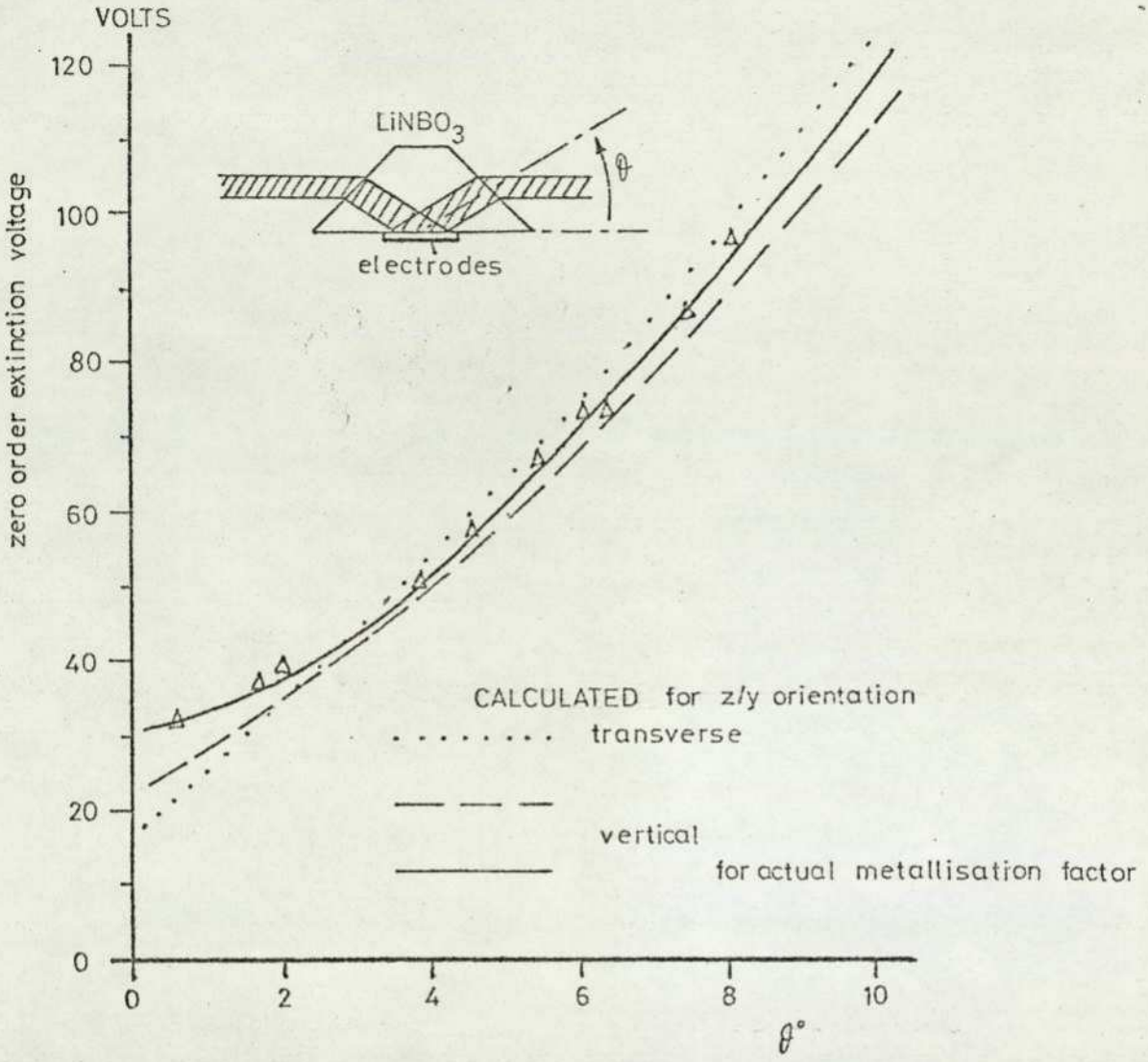


FIG. 5.3 DEVICE PERFORMANCE vs INCLINATION for d=0.1mm

Δ measured for z/y orientation, vertical field

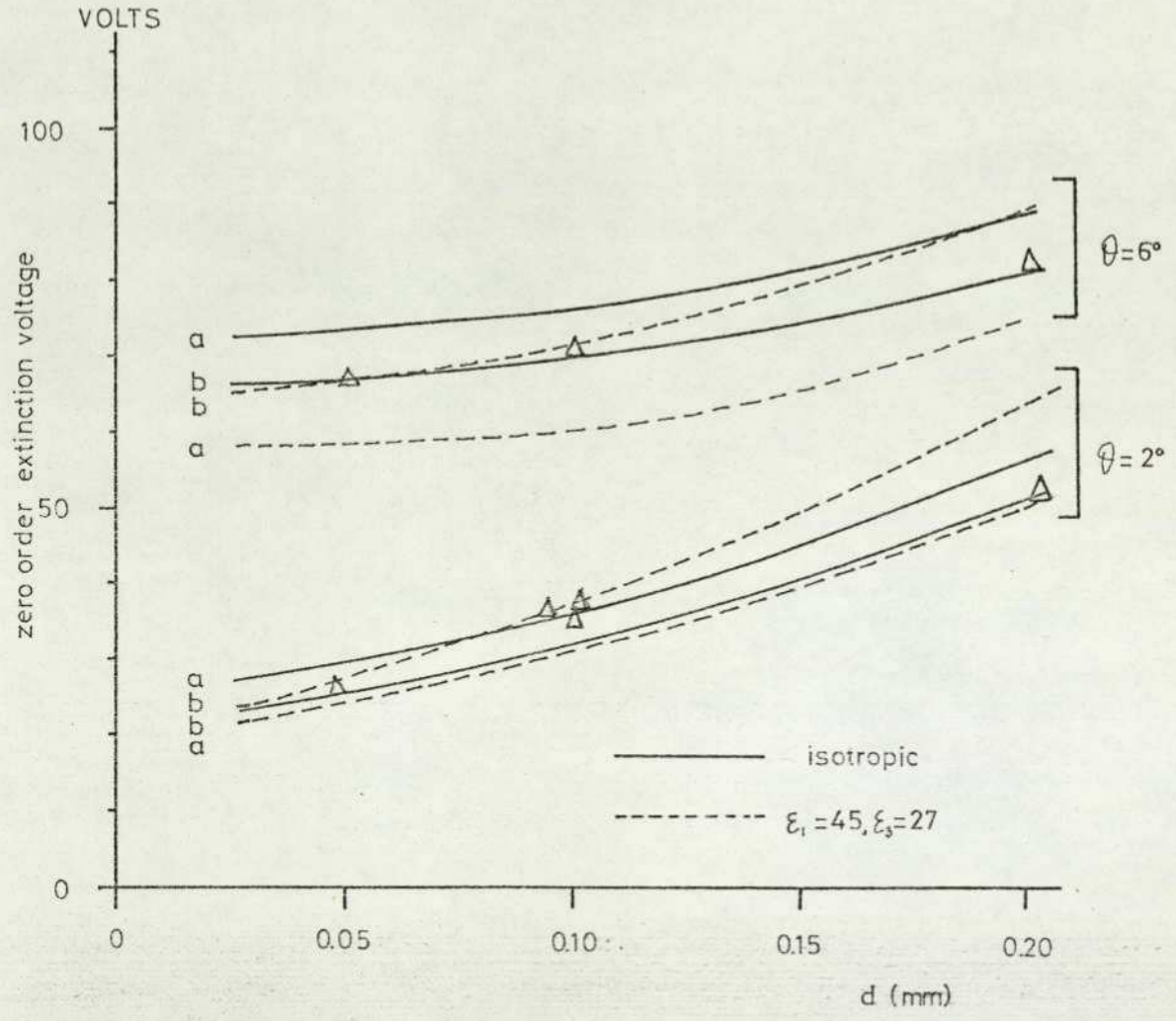


FIG.5.4 EFFECT OF ELECTRODE PITCH ON DEVICE PERFORMANCE
for $a = 0.25$

a transverse orientation

b normal orientation

Δ measured for normal orientation at DC
(corrected for metallisation factor variation)

5.1.8 PERFORMANCE VERSUS ELECTRODE PITCH

Zero order extinction voltage was used as a measure of device performance and the theoretically generated data (Section 4) was experimentally verified for dc conditions and three electrode pitches (0.05, 0.1, 0.2 mm). As was expected it is advantageous to reduce electrode pitch but the benefits are reduced if the incidence angle is increased. Figure 5.4 shows a comparison of prediction and measurement for normal field devices (z axis normal to electrode plane). The experimental arrangement was again as shown in Figures 5.1.5, 6 and the samples used are shown in Figure . A visual assessment of zero order null in the far field was again used giving $\sim$ 5% variation for a detectable change in output. As Figure 5.4 shows information calculated for the a = 0.25 case and with a travelling microscope, the devices mode gave values of a of 0.3, 0.29, 0.28 in order of increasing pitch. Hence it was necessary to compensate the results for this difference and the information, derived from the VLTI program gave the ratios which, when multiplied by the measured voltages, gave the points in Figure 5.4 . These show reasonable agreement with prediction for the two incidence angles shown.

A whole set of three transverse field devices was not constructed but a 0.1 mm pitch (transverse configuration) gave results which also agreed with prediction, This result is not marked in Figure 5.4 for the sake of clarity .

5.1.9 EXTINCTION RATIOS

Theoretical extinction ratios (Section 4) were very high. Measurements, involving light scatter electrode flaws and nonuniform illumination gave results which lay in the 50:1;150:1 region for zero order and > 50:1 in the first orders. A PM tube and mask was used in conjunction with a neutral density filter for these measurements. It was felt that good fabrication would yield results in the 1000:1 class.

5.1.10 MISALIGNMENT PERFORMANCE

In order to assess the critical nature of alignment in the electrode plane and to consider operation with uncollimated light, measurements of misalignment against zero order extinction voltage were made. The experimental arrangement was altered to allow rotation in the electrode plane as shown in Figure and the voltages measured at intervals in the region of the aligned direction. The resultant data for normal and transverse field devices was then centred on the aligned direction ($\alpha = \beta = 0^{\circ}$ in Figure 5.5) and compared with data generated by program VDI2. As can be seen in Figure 5.5 agreement with prediction is excellent. The device used in these measurements involved a pitch of 0.1 mm and an incidence angle of 6°. D.C. voltages were applied.

The order of magnitude of misalignment half angle for this device was $\backsim 6^{\circ}$ but this depends on material refractive index. Because of the sinc function type characteristic with its flatness in the region of zero order extinction, something like $\pm 2^{\circ}$ misalignment can be tolerated at a given voltage while the device as a whole operates satisfactorily with misalignments greater than $\pm 6^{\circ}$. At such large angles sensitivity is down by some 3dB and a blazing action is evident. The Bragg angle is encountered at $\backsim$ 3mR but naturally no Bragg action takes place where no index variations normal to light passage are present. It is worth noting that the alignment sensitivity of orthodox birefringent modulators is high because of the small angular apertures presented ($\backsim \pm 0.5^{\circ}$ generally).

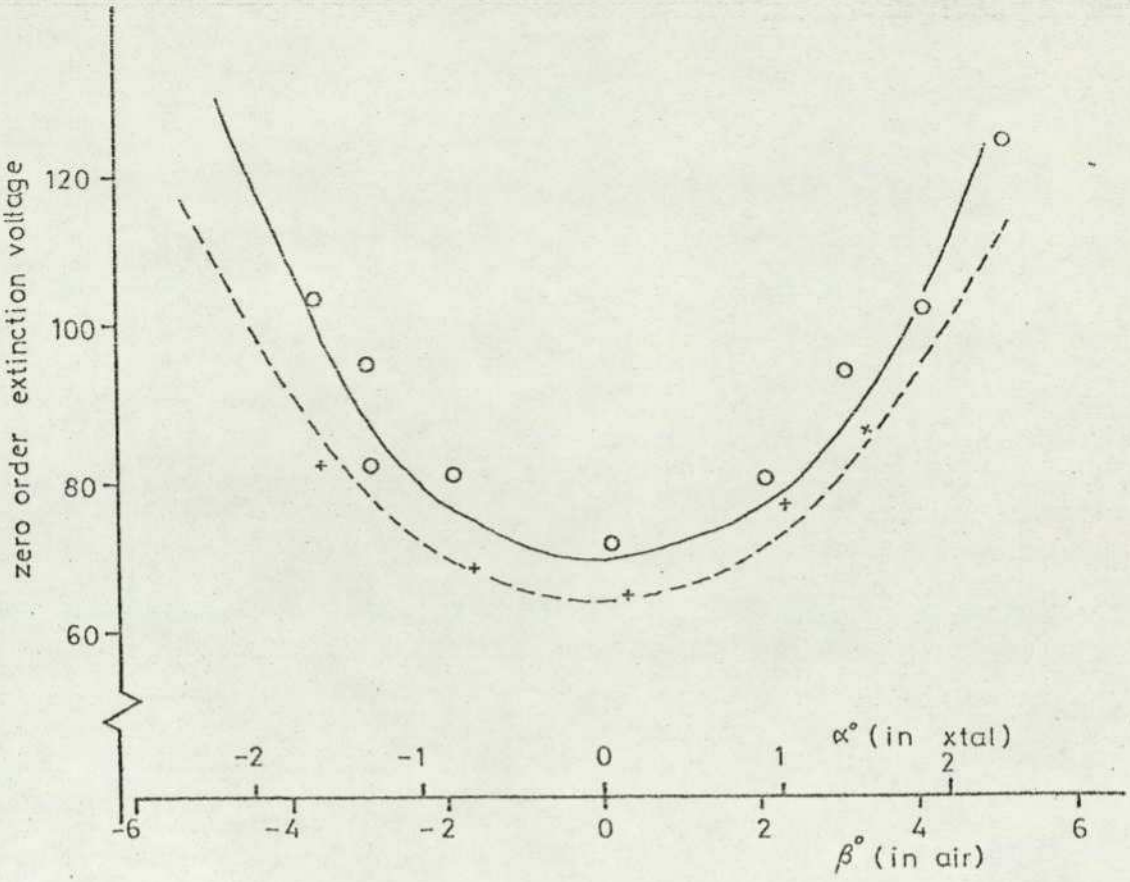


FIG. 5.5 MISALIGNMENT RESPONSE

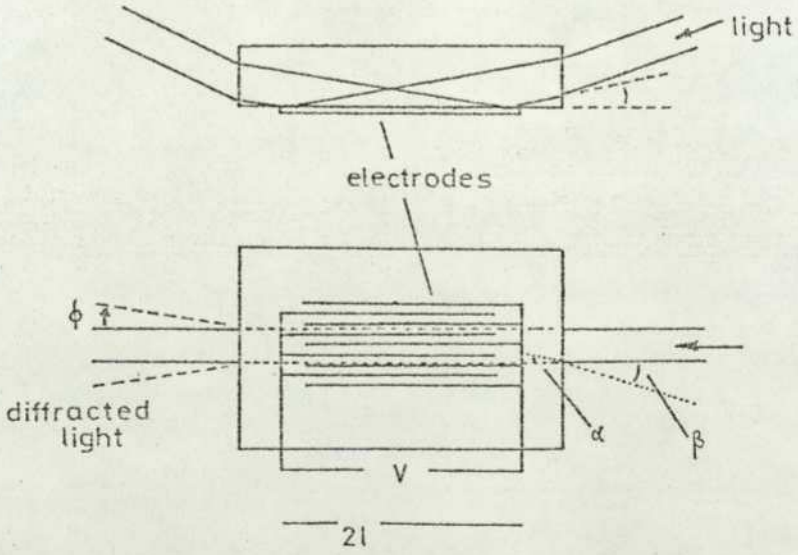


FIG. 5.6 CRYSTAL CONFIGURATION

5.1.11 FAR FIELD PATTERNS AND MODULATION

The far-field pattern is of Raman-Nath type and was examined at a distance of ~0.5 m from the device initially on a projection surface. The far-field with this device is considered to be the distance greater than the minimum required to resolve adjacent orders. (In the case of electrode devices made of linear material this signified a minimum comparable to device aperture).

The nature of the Raman-Nath pattern derived from the devices described in this section, using a cylindrical lens of f=7.5cm are illustrated in Figure 5.7 for the case of d = 0.1mm, $\theta=4^{\circ}$ and at the voltages indicated. Figure 5.7 presents densitometer traces derived from operation of the same device showing zero order modulation action. In all these cases the inter-order angle is found to be in agreement with the predicted:

$$\gamma = \sin^{-1}\frac{\lambda}{2d} = \sim 3 \text{ mR}$$

5.1.12 EFFECTS OF PITCH VARIATION

The device operates as a variable depth phase grating of pitch equal to electrode pitch for quadratic materials, or equal to twice electrode pitch for linear materials. In studying $LiNBO_3$, a linear material, expected and verified inter-order angles are:

d_{mm}	predicted γ°	measured γ°
0.05	0.361	0.357
0.1	0.180	0.178
0.2	0.09	0.094

and Figure 5.8 shows densitometer traces illustrating the effect of pitch variation.

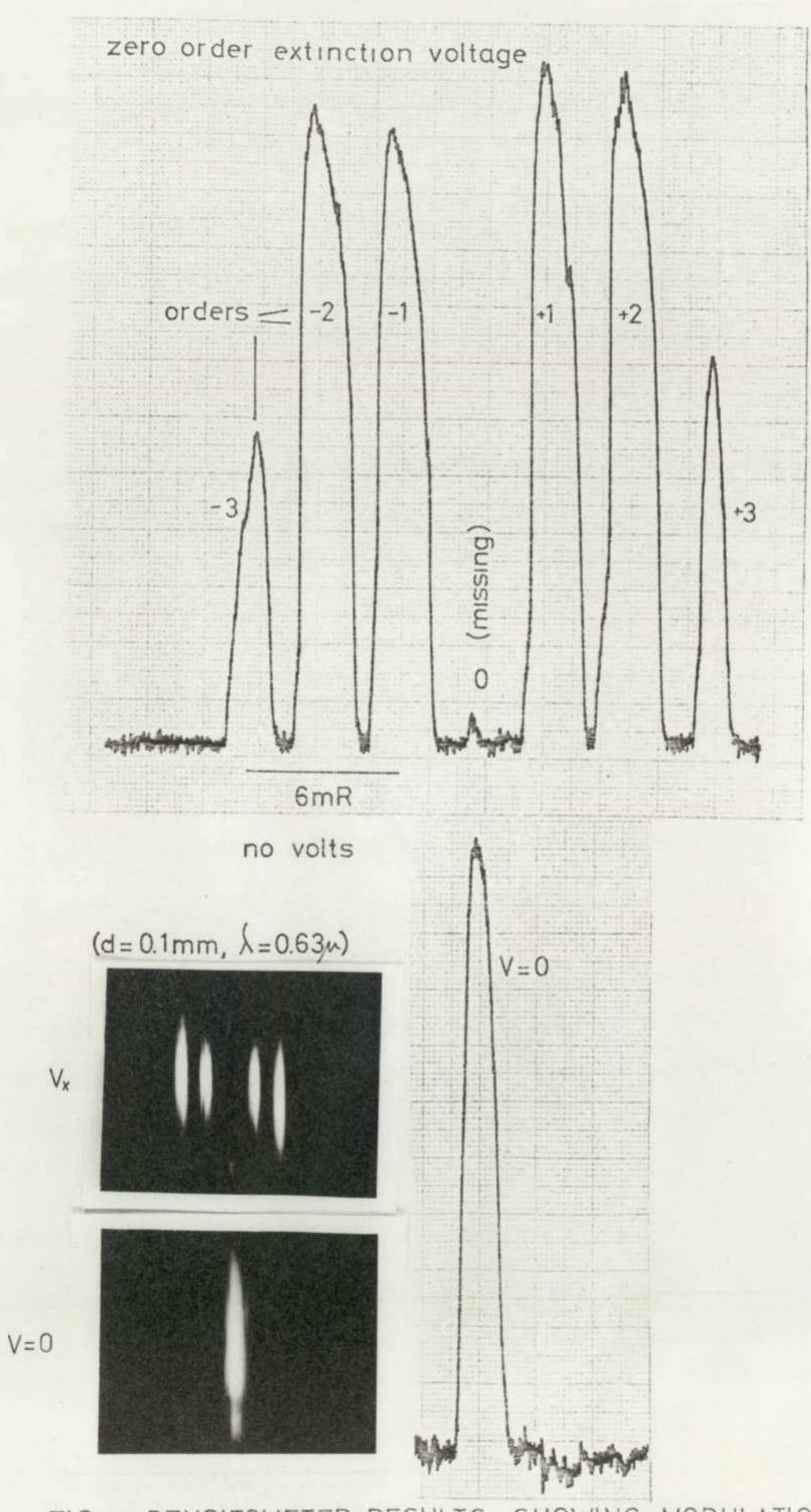


FIG. 57 DENSITOMETER RESULTS SHOWING MODULATION

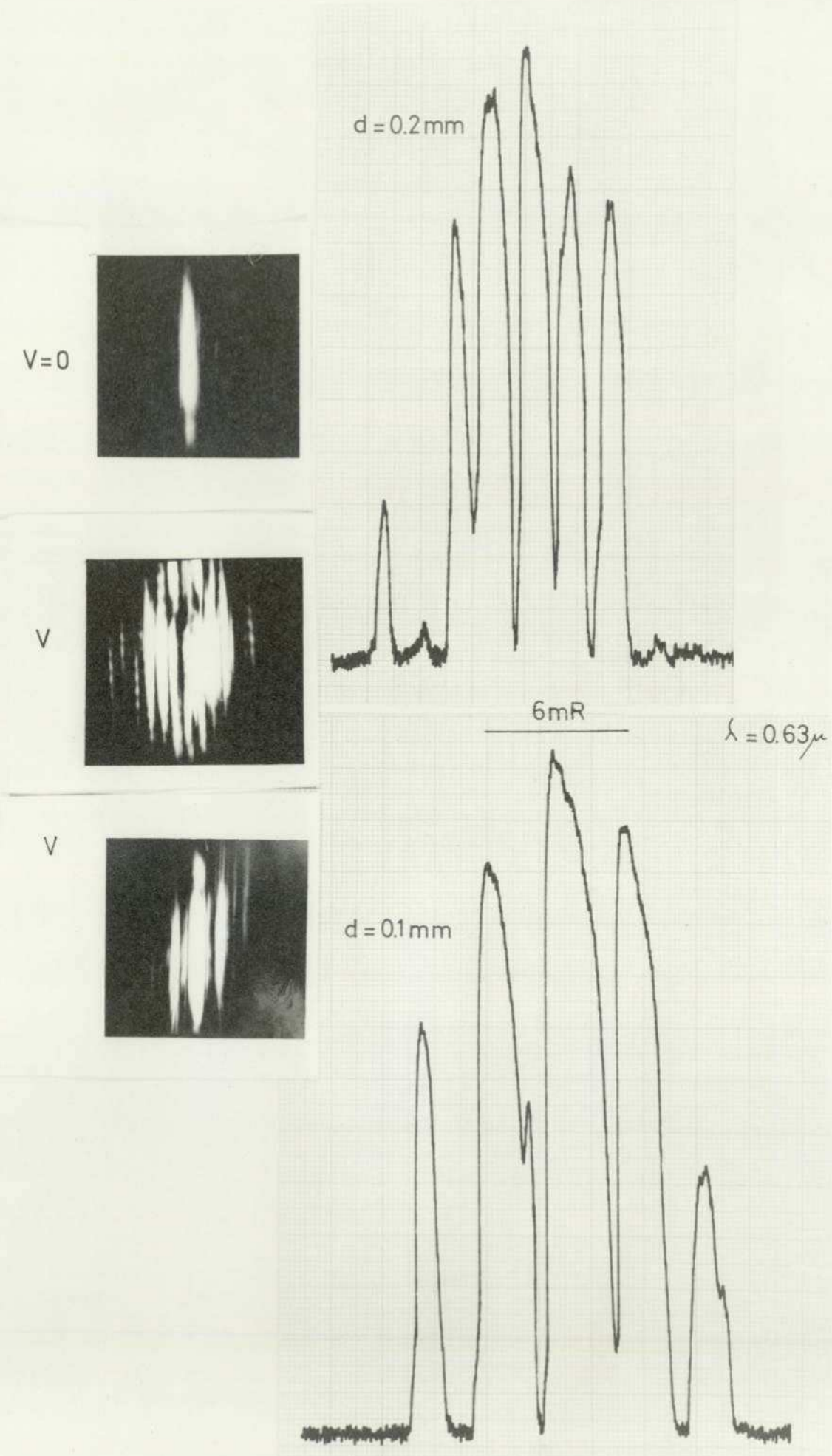


FIG.5.8 DENSITOMETER RESULTS — PITCH VARIATION

5.1.13 COMMENTS ON DEVICE HANDLING, ALIGNMENT, AND ELECTRICAL CONNECTION

As fabricated, no major problems were unearthed at any stage of the orientation, cutting, polishing electroding or etching processes but some care was required in handling if a device with fragile electrode bonding was to be utilised for evaluation. In the event of electrode faults of a bridging variety, it was found possible to evaporate off the shorting area with a d.c. current. Occasionally this caused local damage but on a microscopic scale ($\backsim 10^{-1} mm^2$) thus not detracting from the use of the device. When operated at high voltages (>300 for a 0.1 mm pitch device) tracking breakdown was found to occur. This caused the same effect as the previous technique but lowered the subsequent breakdown level. This breakdown point tended to lie in the 0.25-0.8kV region for 0.1 mm pitch devices and was considered to be a function of surface cleanliness and electrode edge structure only. Because undue electrode area cleaning was avoided to prevent electrode damage, it was not possible to find a reliable surface breakdown value but it is suggested that this lies in the 16kV/mm region and is well outside the 1.4kV/mm usual operating point for zero order extinction. Possibly a dielectric layer of refractive index lower than that of $LiNBO_3$ may raise this level further if necessary.

Alignment was found to be straightforward even with this lensed device because an alignment of several cascaded components was unnecessary. In the case of the lensless device (Section 6) even greater ease is expected. Polarisation directions were easy to identify because of walk-off so that two patterns were exhibited. Upon the application of a voltage the more sensitive (r_{33}) would then be chosen (unless other reasons, such as piezoelectric, dictated the r_{13} coefficient be used with its associated five times reduction in sensitivity). This effect is illustrated in Section 6

COMMENTS ON DEVICE HANDLING, ALIGNMENT AND ELECTRICAL CONNECTION continued

The devices mode were found to present very high resistance (~200 MΩ) and predictable capacitance. Measurements on thin film devices (ref. Barringer) suggest that resonances occur at which the resistance increases and capacitance decreases but no such resonances were found in the dc - 10MHz region on these devices and no ringing was evident with impulse operation (Section 6), for surface deposited devices. Ringing effects were noted, however, with contact electrodes (next section).

Electrical connections to these devices were made using whisker contacts with the crystals held in place either by their spring pressure or by adhesion to double sided sticky tape. These device test configurations are illustrated in Figures 5.1.7 — 5.1.12 and show some of the arrangements used.

An attempt was made to operate this device with electrodes rotated to be normal to the light propagation direction. This effect, in theory, gives a much greater inter order angle but the cost is the loss of the path length integration effect that is achieved with electrodes parallel to light propagation direction. Operation was noted but of insufficient sensitivity to warrant further pursuit.

'White' light operation of sorts was also experimentally demonstrated using a Rank Taylor Hobson tungsten source with collimating lens. Because of the sinc^2 function shape the detuning effect of misregistration from a centre wavelength of 0.525/u is not visually important over the visible range 0.4/u-0.65/u. Hence, if a 15,20:1 extinction ratio is sufficient, a white light operation can be assumed. (The nonzero orders naturally contained the dispersed colours in the incident light).

5.2 CONTACT PROCESS ELECTRODING

Fundamentally the electrode structure does not need to adhere to the crystal surface and, in the case of water soluble crystals or the case where satisfactory electrode adhesion cannot be achieved, it is only possible to apply the electrodes to a substrate and contact the electrodes to the crystal. This principle, illustrated in Figure 5.9 was attempted to assess its practicability as a device configuration.

The same range of crystals as used for the surface deposited devices were employed for these tests and the electrodes were manufactured on microscope slides. These slides offered a refractive index of 1.48 and the electroding was of chromium, copper or copper on chromium.

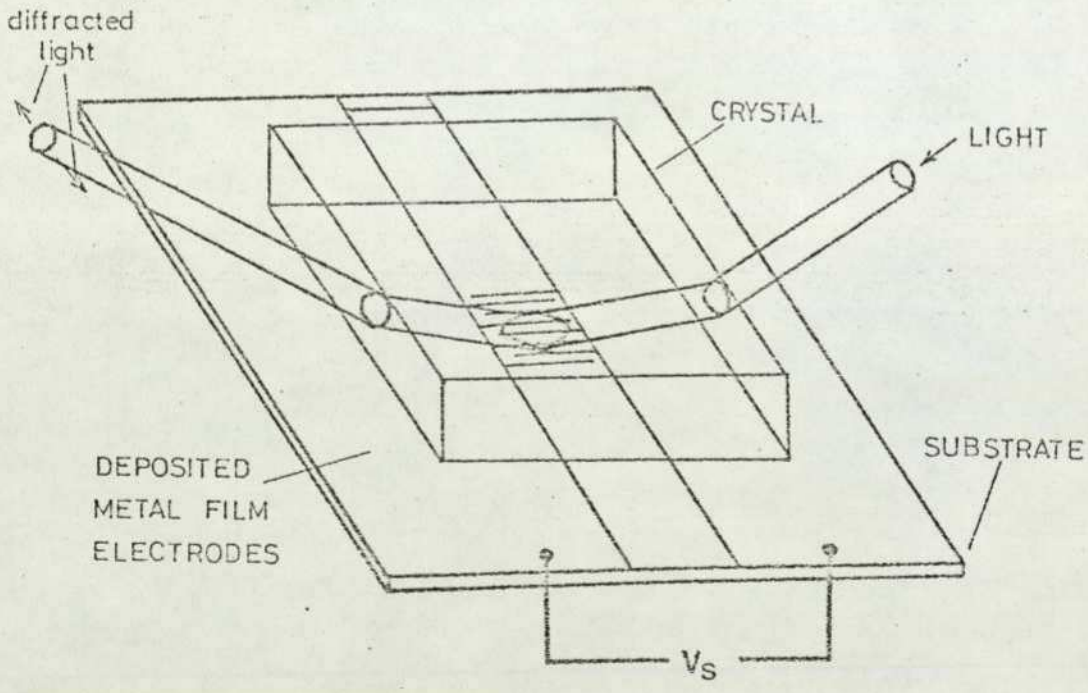


FIG. 5.9 CONTACT ELECTRODES

Contact electroding offered considerably reduced sensitivity with a considerable decay effect with a time constant in the tens of seconds region. This effect and its significance is analysed in this section.

5.2.1 EXPERIMENTAL LAYOUT - FAR FIELD PROFILES

The experimental layout employed is illustrated in Figure 5.11 (and shown in a previous photograph). The components are:

LZ	0.63μ HeNe Laser
P	Dichroic Polariser
S	Aperture Stop
L	Cylindrical lens (f = 7.5 cms)
C	$LiNBO_3$ Crystal + Electrodes
M	Mask ($\begin{cases} 0.5 \\ 0.05 \end{cases}$ mm aperture)
D	Detector (SGD 110 diode or S20 PM tube)
T	Translation Sensor (position-polarity conversion).
PL	HP X-Y Plotter.

The resulting far field pattern profiles are shown in Figure 5.10 and illustrate modulation operation on a 0.1 mm pitch device with two mask apertures. Reduced sensitivity, as compared with a surface device, is exhibited. ($\sim$ 36% modulation for 135 volts with d.c. excitation).

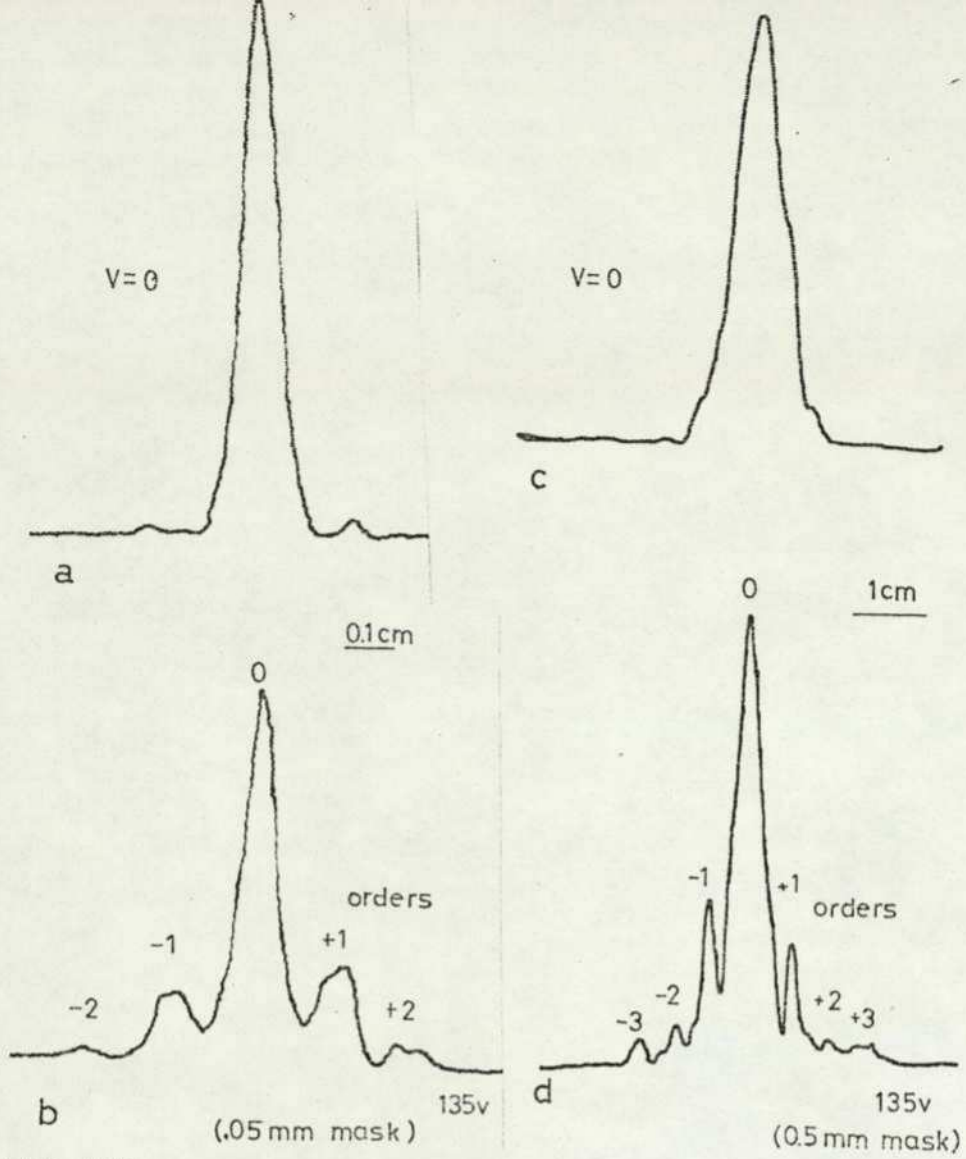


FIG. 5.10 FAR FIELD PATTERN PROFILES

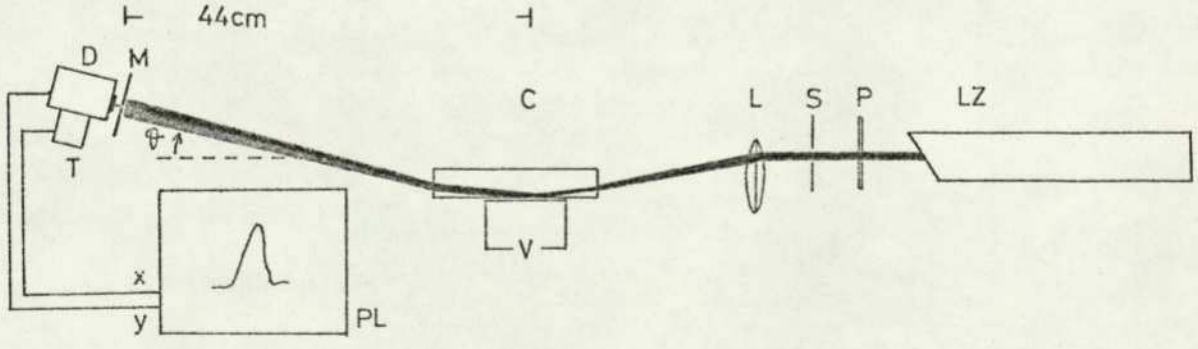


FIG 5.11 EXPERIMENTAL LAYOUT

EXPERIMENTAL LAYOUT - FAR FIELD PROFILES continued

It was not found possible to apply a zero order extinction voltage to these devices because sensitivity was reduced in many cases to a state where this voltage was near to breakdown. Furthermore, the spacing effect of imperfect contact caused no repeatable results to be obtained of this parameter. For repeatability it would be necessary to apply a known pressure to the crystal substrate combination in dust free conditions.

5.2.2 TIME CONSTANT ANALYSIS

Response time constants in electro-optic materials can be done to several effects, among them being:

1. Photoconductivity (e.g. ref. Doughty)
2. Resistivity/capacitance bulk time constant

and 3. Heating effects

and the first step was to identify the dominant cause of these effects.

5.2.3 τ VERSUS INTENSITY (FIG. 5.12)

In order to assess the influence of photoconductivity on the decay of the pattern intensity an illumination at known levels was made. 0.63μ light was used through an 0.1 mm pitch device at an incidence angle of 6°. A TPI attenuator allowed six intensities to be produced from the 2mW laser. As can be seen the time constants, lay in the region of 1 minute and intensity variation did not affect their magnitude. From this it could be concluded that photoconductivity was not the cause of the decay effects.

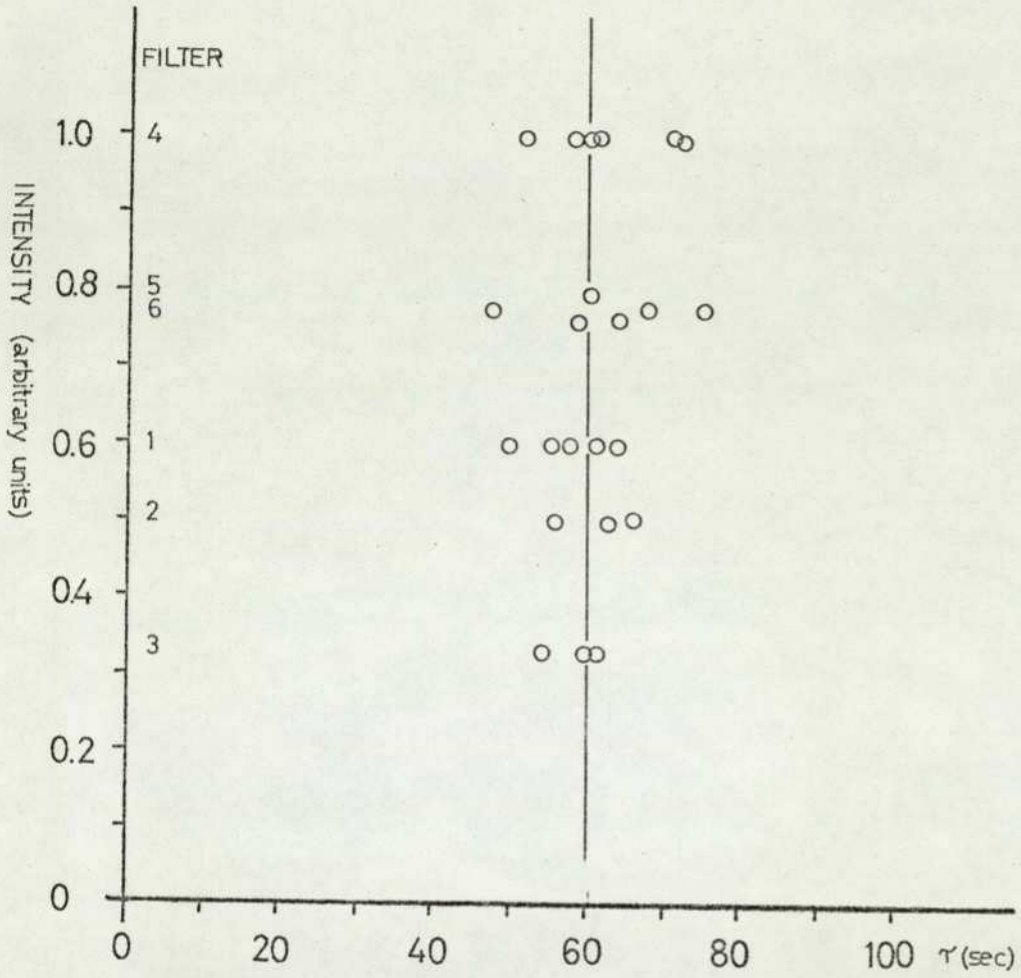


FIG.5.12 FIRST ORDER TIME CONSTANT vs INTENSITY

FILTER	TRANSMISSION
1	0.6
2	0.51
3	0.33
4	1.0
5	0.8
6	0.78

TABLE NORMALISED

TPI ATTENUATOR DETAILS

5.2.4 DECAY CURVE STUDY

The first order decay was studied for two reasons. One, that the PM tube would tend to saturate with zero order even with the pinhole mask used, and the other, that the decay in the zero-order was between two illumination levels and hence more noisy. Applied device voltages lay in the 150-300 volts range. The measurements of decay curves were made using an HP X-Y plotter modified to use a Rotring pen with PM output as the vertical scale and a Tektronix timebase as the horizontal scale. A typical decay of intensity (to about 15% of zero order intensity) is shown in Figure 5.13 and was derived as above.

5.2.5 τ VERSUS APPLIED VOLTAGE (FIG. 5.15)

In order to ascertain the existence of heating or ionisation contribution to the time constants of decay τ was measured against applied voltage. As can be seen, the time constants exhibit an inconclusive reduction with increasing voltage. The intuitive explanation of this suggests an ionisation effect due to the electrode edges. In order to ascertain the space charge current characteristic a picoammeter was used to measure conduction of the device but either the result was swamped by substrate conduction, or else the characteristic space charge current/voltage power law was not in evidence.

5.2.6 ANOMALOUS EFFECTS

Several device/electrode combinations exhibited non-exponential shapes which required postulated explanations. One such is the discontinuous type of characterisation (Figure 5.14) which appears to switch time constants at one point. The most obvious explanation seems to be the part played by ionisation and any space-charge present in the crystal so that the effective resistance term in the time constant is increased by the cessation of ionisation contributions.

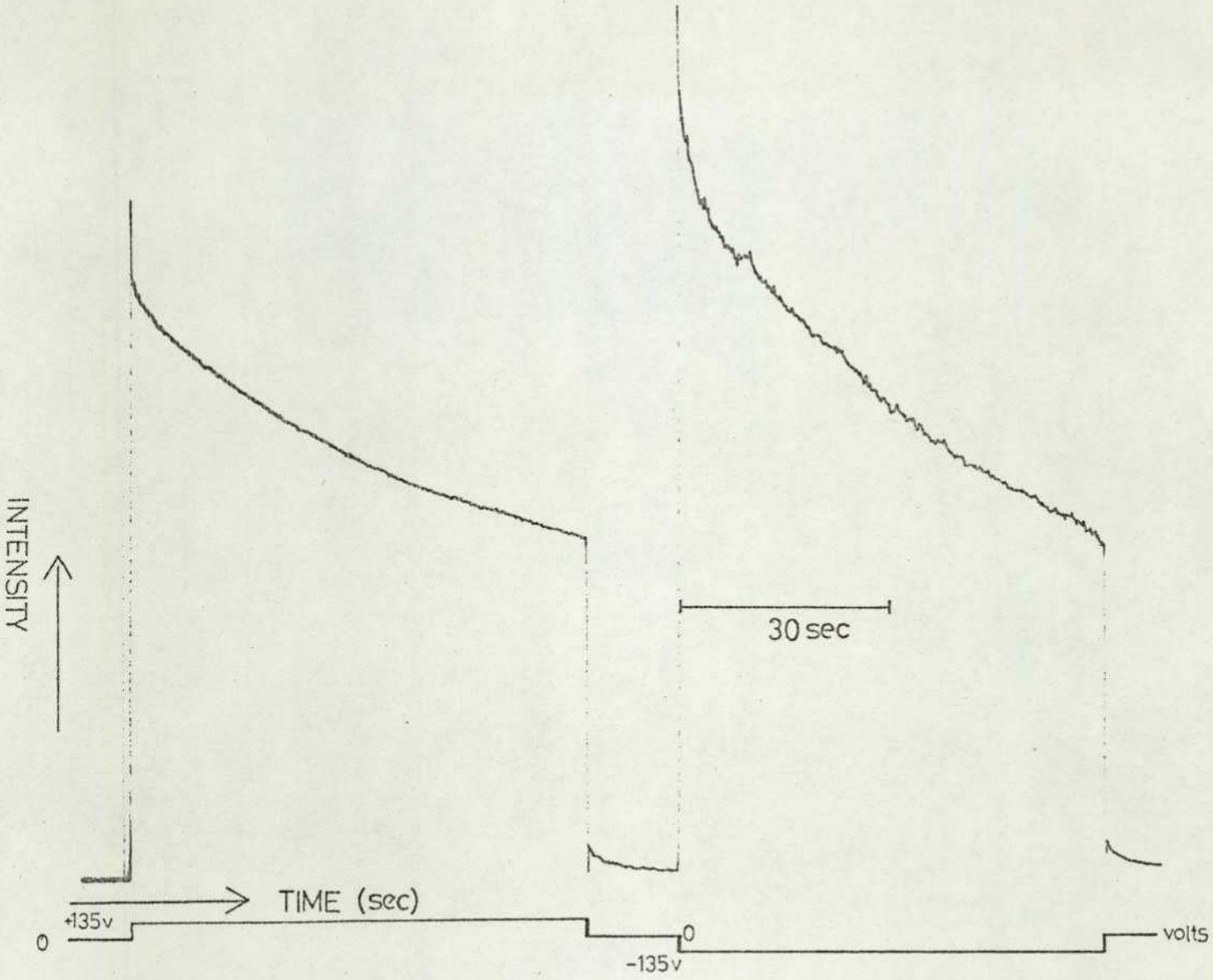


FIG.5.13 DECAY OF FIRST ORDER INTENSITY WITH TIME

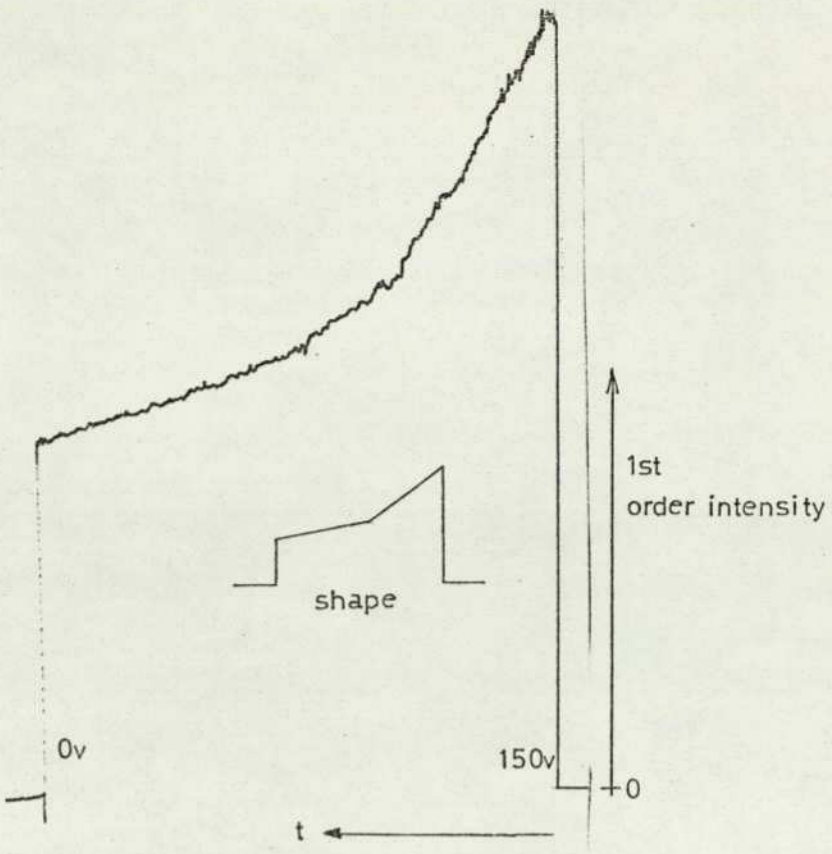
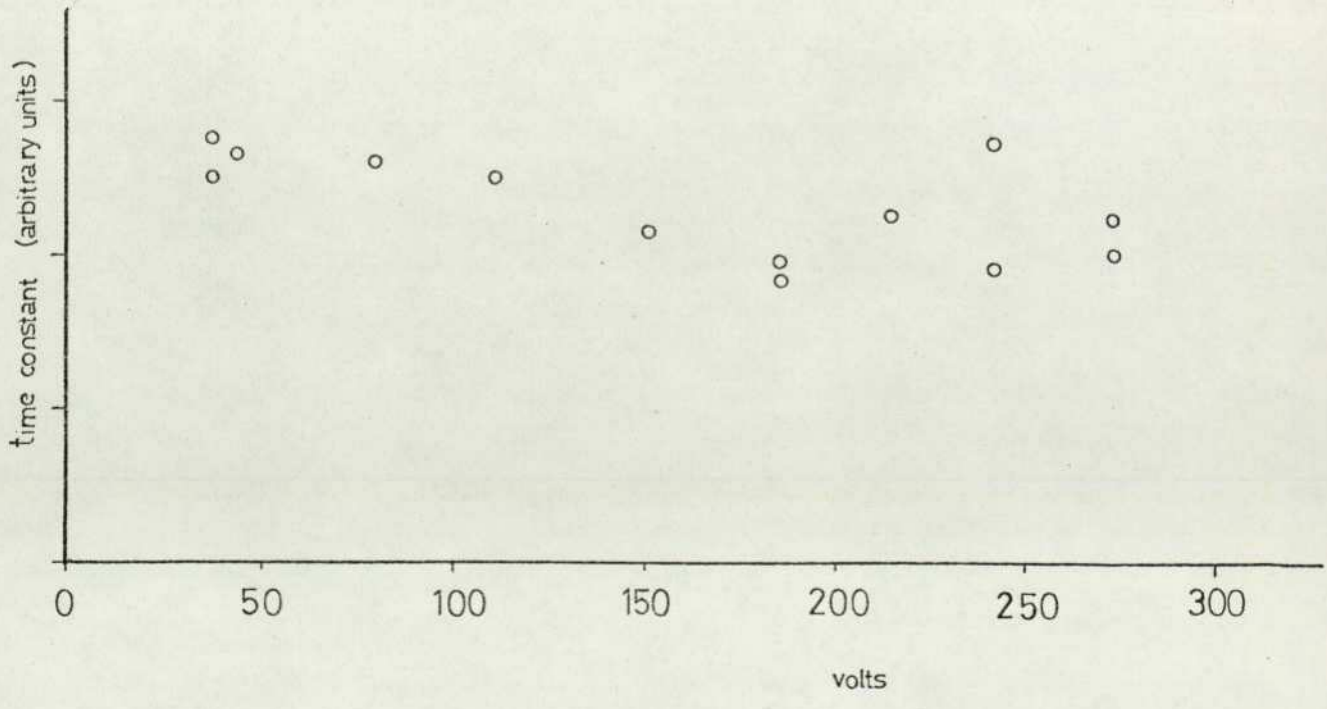


FIG. 5.14 DISCONTINOUS EFFECT (d=0.1mm)

FIG. 5.15 FIRST ORDER TIME CONSTANT vs VOLTAGE



ANOMALOUS EFFECTS continued

Two other effects that were noted and are shown are the short time constant effect (Figure 5.16) and the linear effect (Figure 5.17). The former shows the effect of slight spacing of electrode/crystal and suggests that reasonable operation can be hoped for for non d.c. conditions.

The linear effect in Figure 5.17 is not so clear in cause but a space charge effect is evident in the charge memory effect seen on the lefthand side of the diagram. The linear effect can then be caused by a variation of the effective capacitance so that partial tracking takes place.

The assymetrical effect shown in Figure 5.18 exhibits another phenomenon that was noted, that of unilateral operation. This suggests a charge effect again but with some non-ohmic contact effect superimposed. This latter may be caused by semiconductor or electrode edge effects.

5.2.7 EFFECTS OF PITCH VARIATION

The transit time effect of charge is suggested in Figure 5.19 for the larger pitch case (d = 0.2 mm) and is yet another effect worthy of notice. Performance seen for the finest pitch case (d = 0.05 mm) shows a gradual rise instead of the initial overshoot. This is illustrated in Figure 5.20 and this effect can be explained by a form of ionisation breakdown occurring across the electrodes at that level.

Figure 5.21 illustrates a superimposition of several of the above mechanisms in one device.

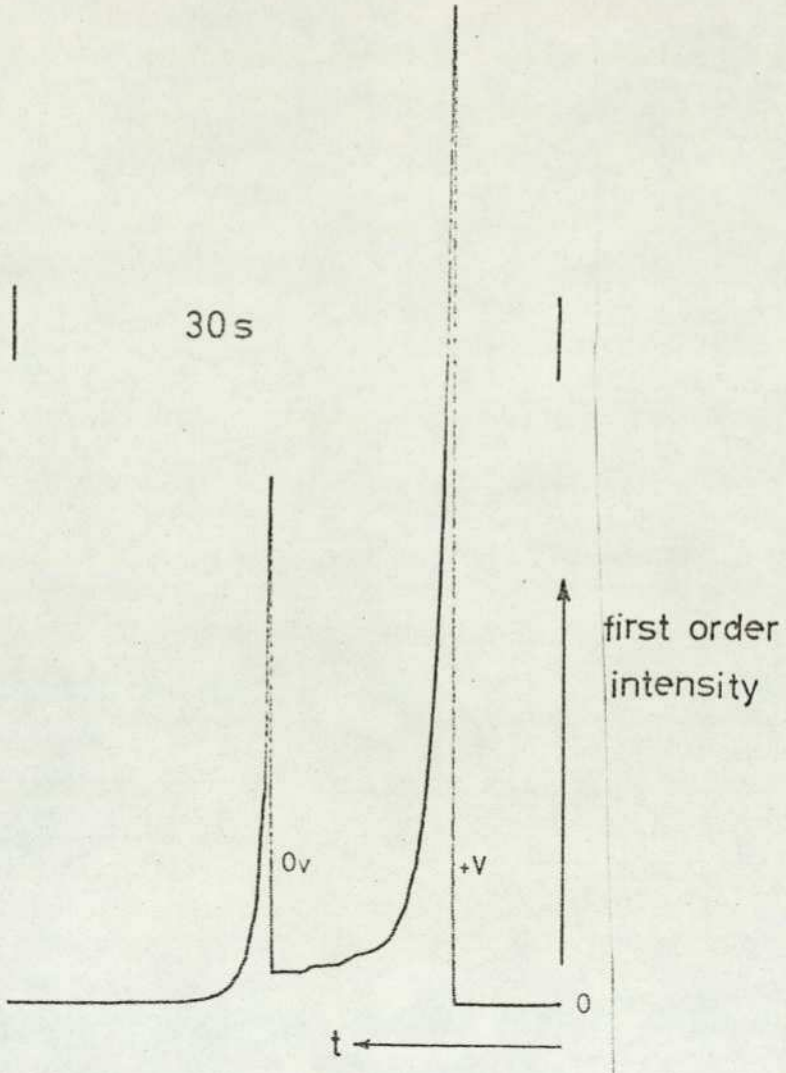


FIG. 5.16

SHORT τ ($r_{33}\|$ electrodes, d= 0.1mm)

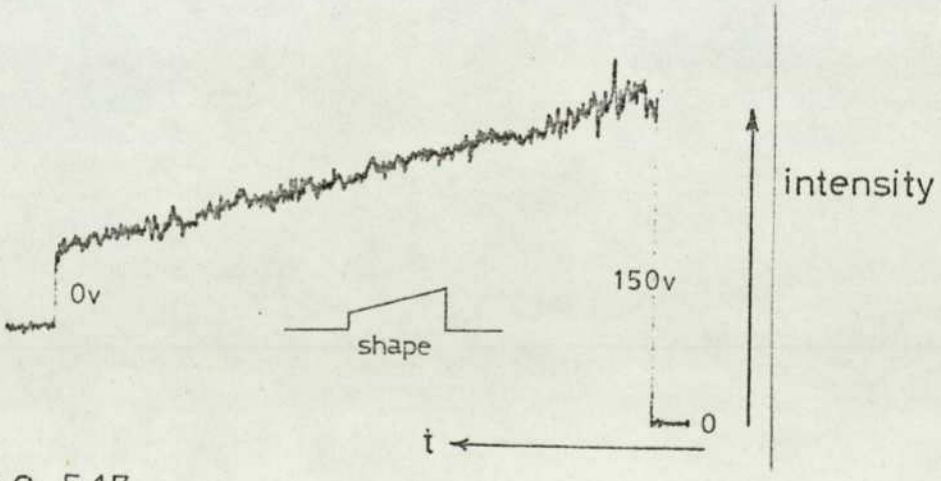


FIG. 5.17

LINEAR EFFECT ($r_{33}\perp$ electrodes, d= 0.1mm)

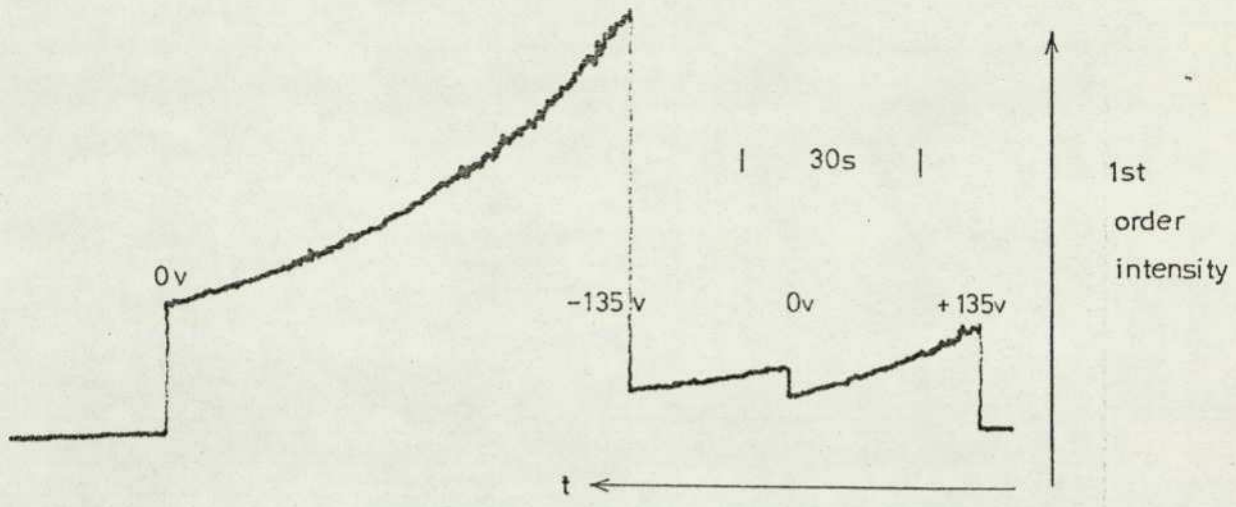


FIG. 5.18 ASSYMETRICAL EFFECT (d= 0.1mm)

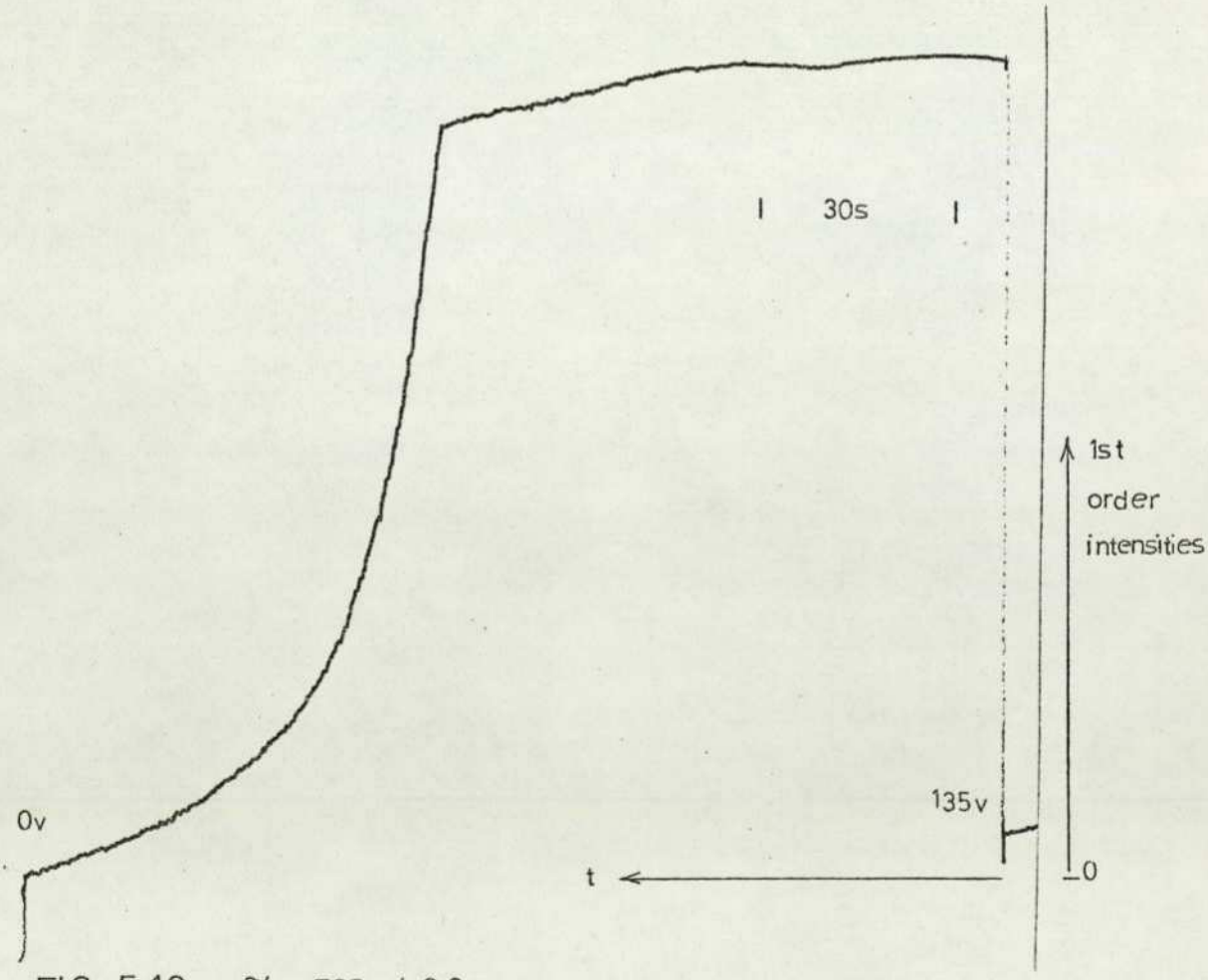
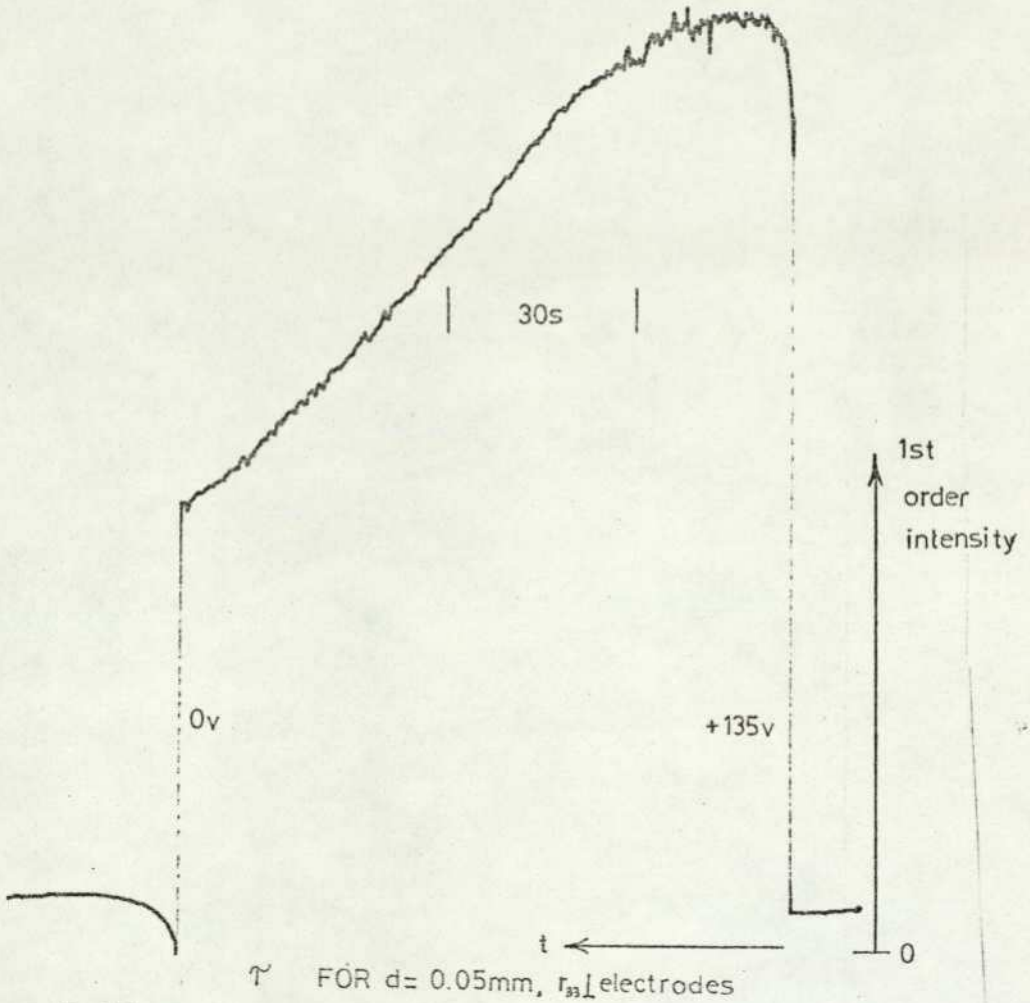


FIG. 5.19 τ FOR d=0.2mm



τ FOR d= 0.05mm, $r_{33}\perp$ electrodes

FIG. 5.20

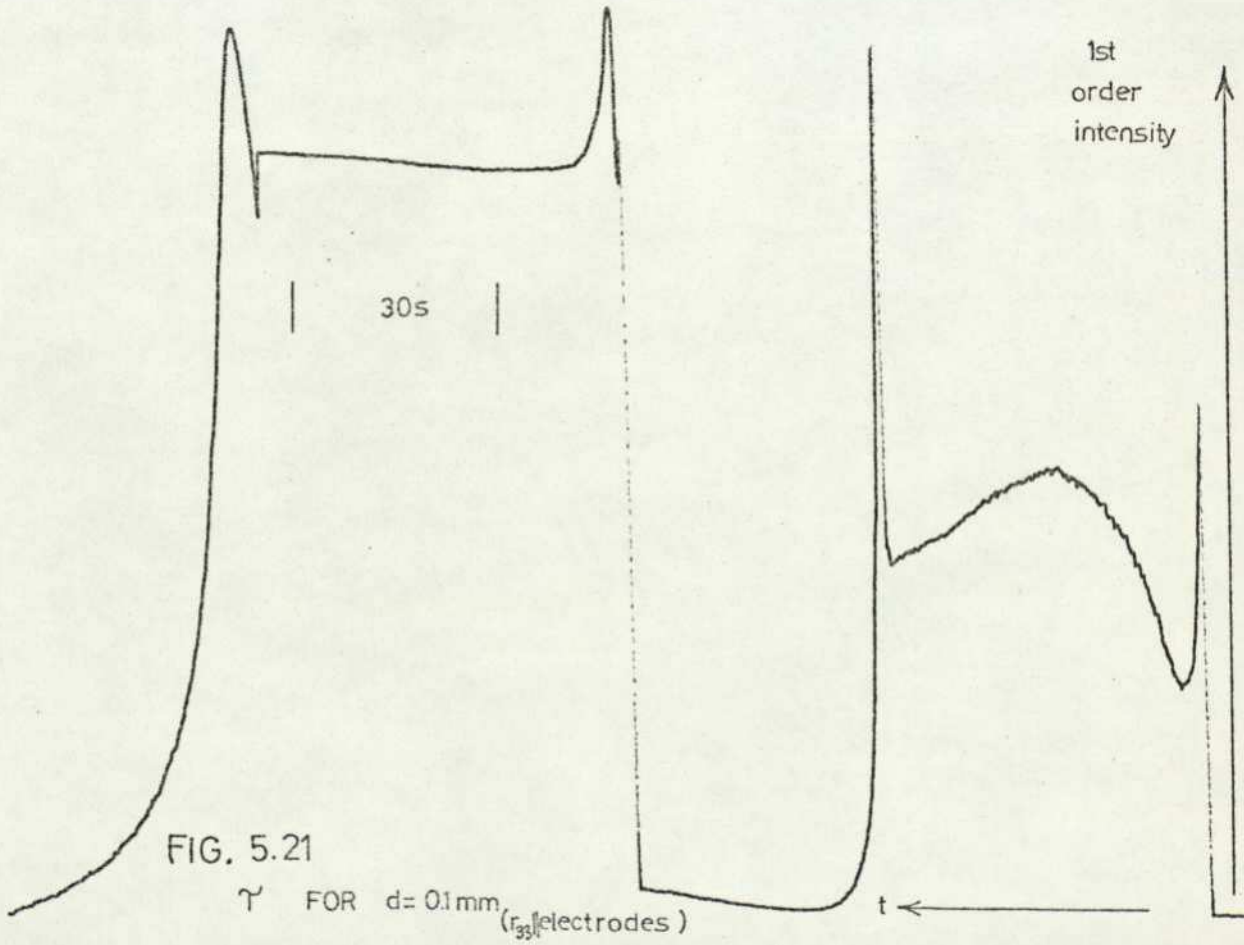


FIG. 5.21

τ FOR d= 0.1mm ($r_{33}\parallel$ electrodes)

5.2.8 ELECTRODE MATCHING

The techniques used in this contact process involved either dry contact of electrodes to crystal or contact in the presence of a resistive/dielectric match fluid. For this purpose PP9 or acetone were used and, whereas resistive matching was improved over the airspaced case, breakdown level was lowered.

These tests were conducted at d.c. conditions and so a d.c. (resistive) match of electrode/crystal gap was attempted. (An a.c. match would suggest a dielectric matching of interelectrode dielectric to crystal dielectric). It was necessary to maintain a matching fluid that offered a lesser refractive index than the crystal so that total-internal reflection could take place.

Tests were made with ADP, using a contact process and PP9 fluid (an inert fluorcarbon). Because of small refractive index variation between ADP and PP9 only small incidence angles were possible and an effect was noted. This was not of sufficient sensitivity to allow a useful device to be constructed but the effective application of electrodes to ADP is a desirable matter as this material has a good optimised performance and a large window as well as low cost.

5.2.9 CONCLUSIONS

A study of the TIR device configuration suggests that surface deposited devices are of immediate use while the contact electrode process does not extend its operation to D.C. Basic TIR tradeoffs are as expected, sensitivity is reduced by pitch reduction or increased incidence angle and the disadvantage of decreasing sensitivity with electrode pitch often encountered in thin film devices, is removed. Zero order extinction is shown to be excellent theoretically and good experimentally. The difference probably being attributed to fabrication imperfections. Far field patterns are found to be predictable in the basis of the Raman-Nath/diffraction models, taking into account the non sinusoidal phase profiles achieved for these devices. Resonances are not in evidence in the expected wavelength range in the surface deposited realisation but abound in the contact process configuration.

Insertion loss of these devices is heavy as no AR coatings are used but as the practical device minimum of two dielectric interfaces is involved it is felt that losses can be made very low. The more so as polarisers are not necessary. Driver considerations are favourable for this device as the CV^2 product for these devices is low, rather because of low operating voltages than capacitance reductions.

It is concluded that the TIR device configuration offers an alternative approach to light modulation. As an electro-optic form of what is usually an acousto-optic device, the TIR modulator/deflector fills a real void - the need for an electro-optic discrete diffraction device.

5.3 ANALYSIS OF SUB-ELECTRODE LAYER AND MISMATCH EFFECTS

In order to analyse the device sensitivity to electrode/crystal spacing layer, a theoretical study of field penetration into the crystal was made. This analysis was based on the AGAP program, listed in Appendix P2, which calculates voltage and field distributions in the electro-optic material due to the voltage applied to one electrode pair.

5.3.1. Fields in the Material:

Using the field expressions derived in Section 4 it is possible to compute fields on the far side of a sub-electrode layer of permittivity ε_a. Hence the voltage in a material of permittivity ε due to an electrode pair ($\pm V_o$) on the far side of an electrode sublayer of thickness t, with the notation used previously, is:

$$\phi = \sum_n \frac{8 V_o \varepsilon_a \sin n\pi a \exp\frac{n\pi t}{d} \exp\frac{-n\pi x}{d} \sin\frac{n\pi z}{d}}{n\pi\, n\pi a\left((\varepsilon+\varepsilon_a)\exp\frac{n\pi t}{d} - (\varepsilon-\varepsilon_a)\exp\frac{-n\pi t}{d}\right)} \qquad 5.2$$

and the resultant field components are:

a) Horizontally

$$E_z = \sum_n \frac{8 V_o \varepsilon_a \sin n\pi a \exp\frac{n\pi t}{d} \exp\frac{-n\pi x}{d} \frac{n\pi}{d} \cos\frac{n\pi z}{d}}{n\pi\, n\pi a\left((\varepsilon+\varepsilon_a)\exp\frac{n\pi t}{d} - (\varepsilon-\varepsilon_a)\exp\frac{-n\pi t}{d}\right)} \qquad 5.3$$

and b) Normal to the electrodes

$$E_x = \sum_n \frac{8 V_o \varepsilon_a \sin n\pi a \exp\frac{n\pi t}{d} \exp\frac{-n\pi x}{d} \frac{-n\pi}{d} \sin\frac{n\pi z}{d}}{n\pi\, n\pi a\left((\varepsilon+\varepsilon_a)\exp\frac{n\pi t}{d} - (\varepsilon-\varepsilon_a)\exp\frac{-n\pi t}{d}\right)} \qquad 5.4$$

Fields in the Material: continued

The results of assessing a few cases for various $\varepsilon/\varepsilon_a$ ratios are presented in the following graphs with the assumption that the electro-optic material is isotropic. Although of limited validity for the A.C. case as shown previously, nevertheless this assumption allows some idea of the device performance degradation to be expected from consideration of the field structures suggested.

The $\varepsilon/\varepsilon_a$ ratio is presented here as the ratio of dielectric constants of the materials. If, however, the device operation is under D.C. conditions, a resistive model will be necessary and instead the appropriate function of the resistivities will need to be employed to describe the field structure correctly. With this in mind the sensitivity of the crystal fields to the $\varepsilon/\varepsilon_a$ ratio can be examined.

Figures 5.22 and 5.23 show the effect of the $\varepsilon/\varepsilon_a$ ratio on the maximum voltage and fields on the crystal surface for a given sublayer thickness. The effects of varying sublayer thickness are shown in Figure 5.24 It can be seen from these computed results that the field structure is very sensitive to $\varepsilon/\varepsilon_a$ ratios not being equal to unity.

5.3.2. Device Dynamic Measurements

Although zero order extinction voltages were not safely achievable on many contact devices, some measurements of modulation were made, on a contact device with d = 0.1mm and $\vartheta=6^{\circ}$, and $\sim$ 100v excitation.

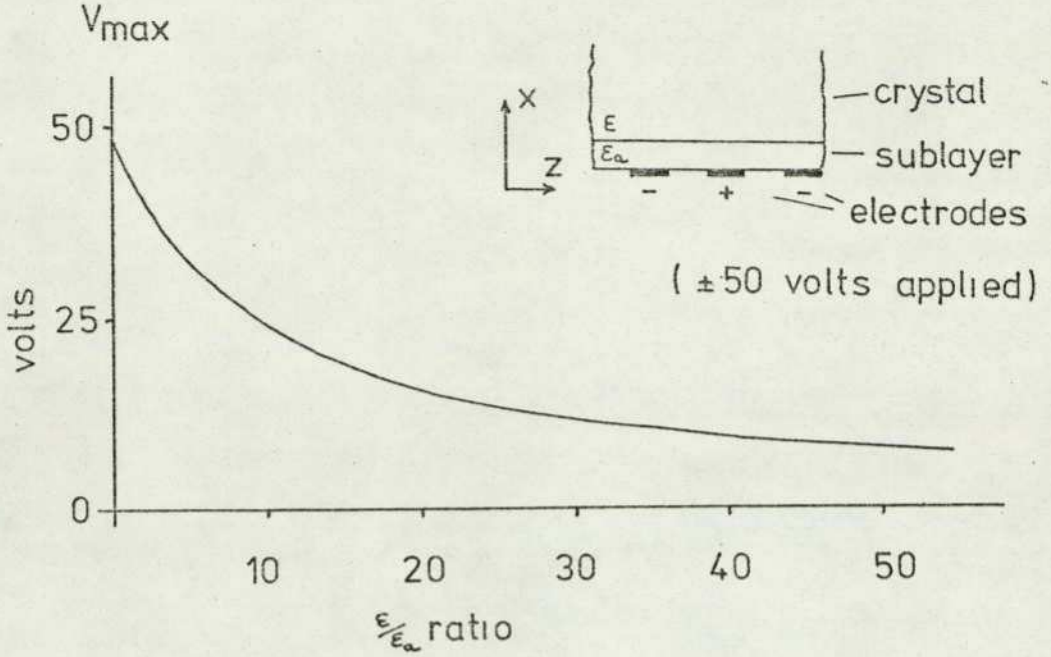


FIG. 5.22 PEAK VOLTAGE IN CRYSTAL vs DIELECTRIC RATIO for d= 0.1mm

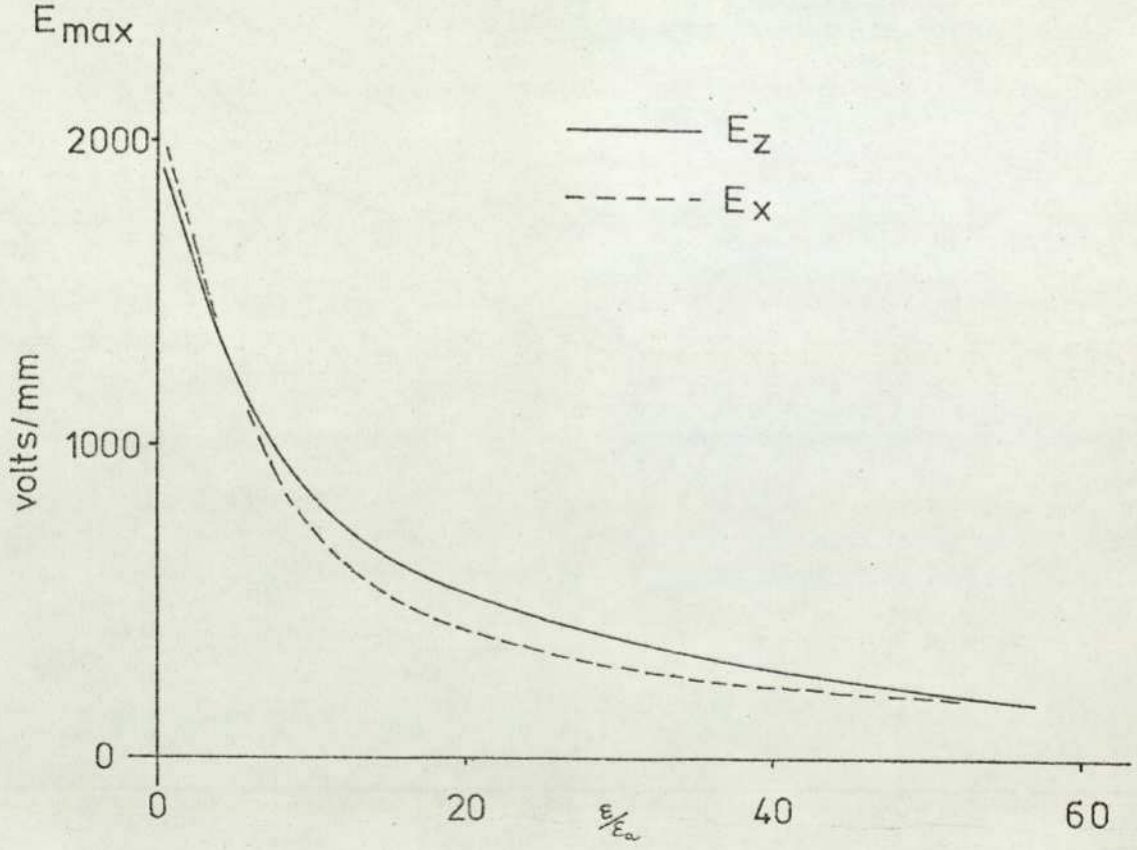


FIG. 5 23 PEAK FIELDS vs DIELECTRIC RATIO (d=0.1mm)

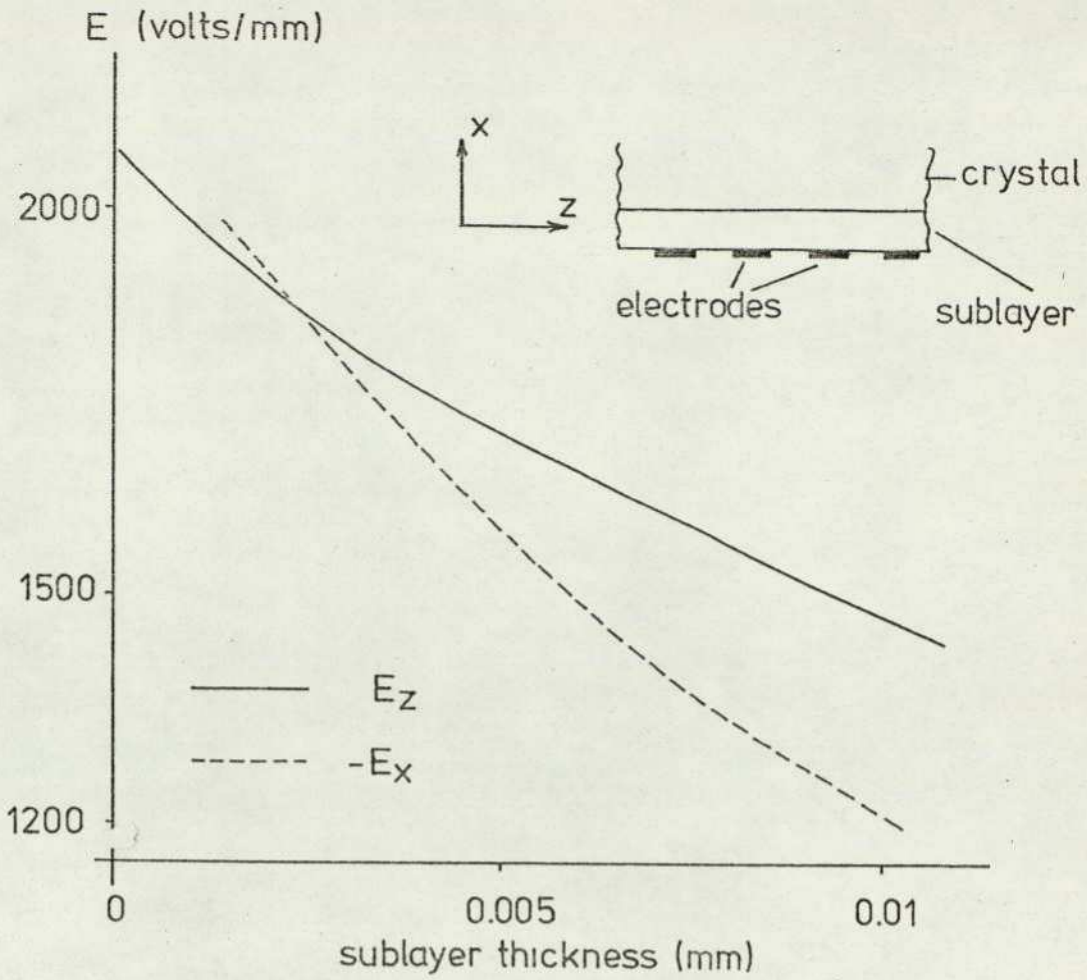


FIG. 5.24 PEAK FIELDS IN CRYSTAL vs SUBLAYER THICKNESS

($\varepsilon/\varepsilon_a = 1$, d = 0.1mm)

5.33 Resonances

Deposited devices were not found to exhibit resonances in the expected regions ($\ll$ 1MHz) while the contact process devices did exhibit them. These are illustrated in Figure 5.25 and two resonance regions are seen in the vicinity of 175KHz and 325KHz in the first order intensity.

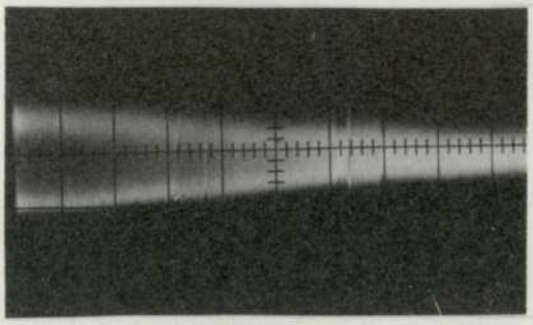


FIG. 5.25 - RESONANCES

The latter, more pronounced region corresponds approximately with the sound transit time, across the Lithium Niobate sample which was 9mm x 9 mm x 1.5mm. Assuming wave velocities of $3.6.10^3$m/s and a shear wave a 360KHz resonance is suggested. The modes are not identified but their existence merely noted. They are unlikely to be simple. A particularly bad resonance is shown in Figure 5.26.

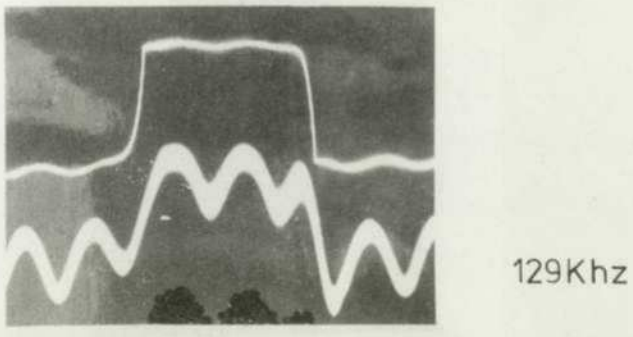


FIG. 5.26 - RINGING

These measurements were made with a totem pole output twin-tetrode amplifier driven by a Hewlett Packard swept function generation (3310A). The sweep voltage ramp was provided by the oscilloscope. Amplifier roll-off caused the trace non-uniformity seen in Figure 5.25.

5.3.4. Bottom End Cut-off:

Using the same equipment as previously a test was made to ascertain VLF effects compared with the known decay effects illustrated earlier in this section. Figure 5.27. illustrates the effect of a VLF sweep on first order intensity at 18 sec/cm and shows that, even at ~ 0.01 Hz no LF cut-off effect is apparent.

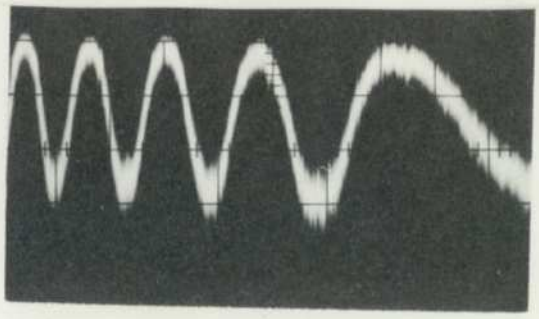


FIG. 5.27 - CUT OFF AT L.F.

Some enhancement is in fact seen at the lower frequencies and this is due to the ac/dc transition or an autobiassing effect or the combination of these effects.

5.3.5 Modulation Characteristics:

Using the tetrode amplifier and HP Function generator generating a ramp waveshape, the modulation function was illustrated. A Photomultiplier (S20 response) was used with a ~ .05mm pinhole mask positioned in the first order. Figure 5.28 shows the device characteristic initial shape. A full range is not shown because of PM saturation.

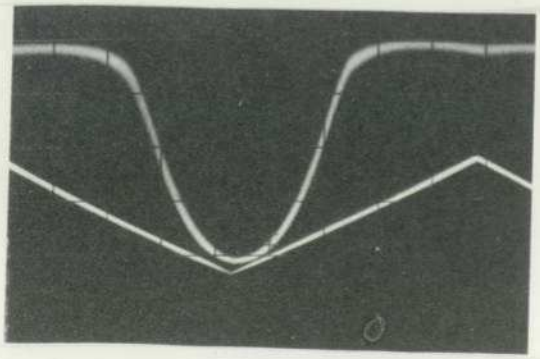


FIG. 5.28 - CHARACTERISTIC

Modulation Characteristics: continued

Device performance is finally illustrated by a 24 KHz, 100V squarewave drive, giving 50% modulation suggesting a zero order extinction voltage of 180-200 volts. (Figure 5.29). Zero order output is shown.

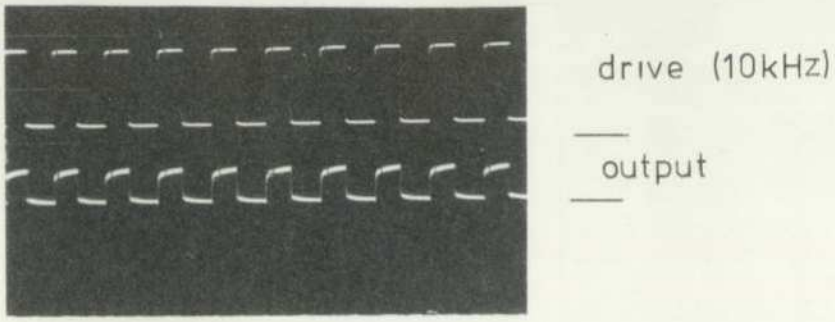


FIG. 5.29 - 50% MODULATION

6. THE TIR MODULATOR/DEFLECTOR AS Q-SWITCH

THE TIR MODULATOR/DEFLECTOR AS Q-SWITCH

All operating parameters in modulators will be enhanced by including the device within a laser cavity. A Bragg or Debye Sears type diffraction device, when included in a laser cavity, causes first transversemodal control type effects and when sufficient energy is coupled out in the zero order direction, it prevents oscillation totally. This is a useful form of intra cavity control and in principle offers possibilities of Q switch operation, mode selection, and selective chromatic control over multiline operation. The latter two effects are likely to be complex in nature and are expected to be difficult to characterise. The nature of the diffraction device is cumulative so many passes through it would imply a high amount of energy in the non zero order direction for even small excitation voltage. As a first order approximation, if n% of energy is removed from the zero order then N passes would suggest a zero order energy (I) of

$$I \leqslant \frac{I_o n^N}{100^N}$$

The assumption made here is that all nonzero order energy does not couple back into the zero order direction. In practice the far field pattern will not contain discrete orders for large N but will approach a continuous intensity distribution. This cumulative effect illustrates the enhancement that will occur within a laser cavity and suggests that, for a device requiring 100 volts for a single pass zero order extinction, Q switching may be possible with only a very small voltage, probably of the order of 10-15 volts necessary to increase cavity loss over the single pass gain level, provided that the diffracted light is lost to the laser.

In order to study these criteria a Q-switch constructed of $LiNBO_3$ was proposed. In such a Q-switch the usual parameters are of importance:

(1) Low insertion loss L_{on}
(2) Fast reponse τ
(3) Good on/off ratio L_{off}/L_{on}
(4) Small CV^2 product for ease of driving
(5) High damage threshold

These parameters are illustrated in Fig. 6.1 and tabulated in Fig. 6.2 against the presently available types of Q-switch.

All the high insertion loss devices are restricted to high gain lasers which tend to be of the pulsed variety. Devices with poor on/off ratio tend to limit the degree of inversion that can be achieved before pre-lasing occurs. A low reponse speed can cause multipulse outputs which deplete energy from the intended initial pulse.

A further significance of high response speed lies in the possible use of an intra-cavity device as a mode lock modulator which is required to Q-switch at round trip intervals and produce a synchronous pulse train. This would require nanosecond type responses of the kind only achievable with electro-optic devices.

The TIR device offers considerable advantages because of high speeds, moderate capacitance, very low operating voltage, low insertion loss, and low damage threshold. The latter two parameters require further comment.

6.1.1 DEVICE INSERTION LOSS

A TIR device consists of three dielectric interfaces, one of which can be considered lossless as total internal reflection takes place. Hence insertion loss is composed of

(1) Reflections at the dielectric interfaces
(2) Material absorption/scattering
(3) Finish flaws causing scattering

For Lithium Niobate absorption is $< 0.002/cm$ and polishing techniques allow flatness of $\lambda/10$ and good inclusion-free boules are readily available. Hence the dielectric losses are of greatest significance. An air/crystal interface causes a

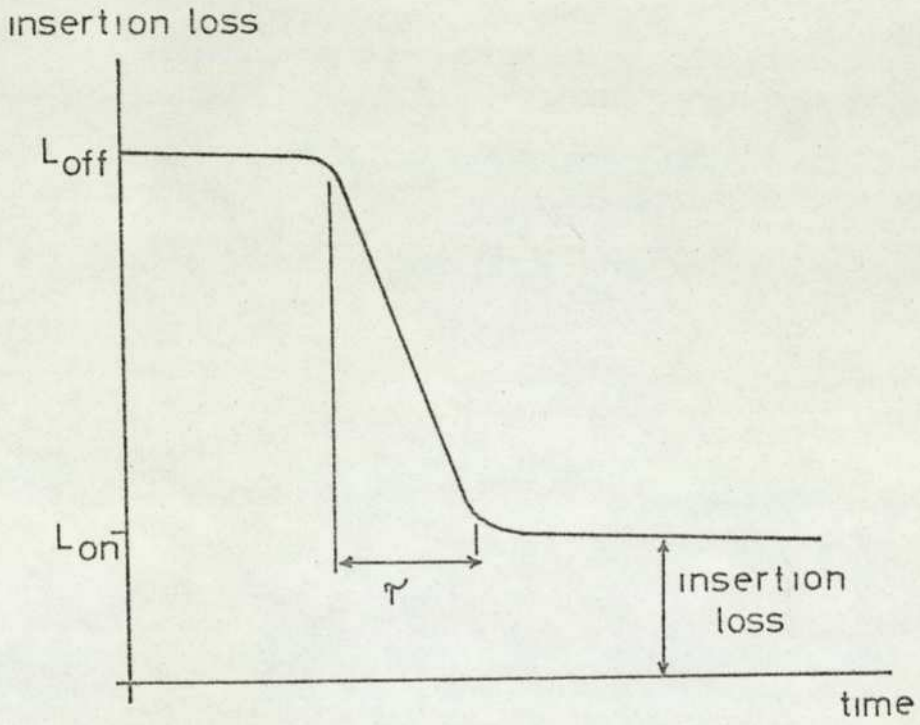


FIG. 6.1 Q SWITCH PARAMETERS

FIG. 6.2 - CHARACTERISTICS OF THE MORE COMMON TYPES OF Q-SWITCH

TYPE OF Q-SWITCH	INSERTION LOSS	ON-OFF RATIO	SWITCHING SPEED	APPLICATION	REMARKS
Spinning Reflector	Low (if speed is optimised)	High	Fairly Fast	Most types of Laser	Cannot be synchronised with external event
Dye	Fairly High	Large	Fast	Mainly Ruby Lasers	Cannot be synchronised with external event
Acousto-Optic	Low	Small	Slow	Continuous or Continuously Pumped High Rep Rate Lasers	
Pockels / Kerr Cells	Fairly High	Large	Fast	Mainly Pulsed Lasers	Most Common Method
Total Internal Reflection	Low	Large	Fast	All Lasers	Possibility of Mode control

reflection loss of ~15%. Fortunately antireflection coatings are usually possible and this can be reduced to a few percent or less. Where lasers exhibit a high gain, then a high insertion loss device may be borne with the penalty of a raised pumping threshold.

6.1.2 DEVICE RESPONSE

Electro-optic operation is the fastest in response of all controlled modulator actions and is dependent on two factors only; the time taken to establish the field and the time taken for light to pass through the device. The former is dependent on travelling wave type considerations and the latter on transit time. Both considerations are of subnanosecond variety in well designed devices.

Practical considerations complicate matters a little because of material effects and driving problems. Effects noticed in diffraction devices suggest that space charge effects may combine with trapping or low mobility to give incomplete extinction. (Residues of ~3% in first orders have been noticed in some devices). A further complication may arise with driving circuits where the unavoidible modulator capacitance renders instantaneous driving signal responses to be impossible and causes overall systems to be slow. A travelling wave approach may allow this capacitance to be invisible to the driving system because of matching and this approach becomes necessary for VHF systems. Practical devices have been reported with nanosecond response speeds. (For example see De Barros & Wilson, who measured ~1.5nS response from a thin film device, thereby approaching measuring system limits extremely closely).

6.1.3 ON/OFF RATIO

The extinction ratio of an intra-cavity device can be quite critical in high gain pulse lasers where even a low percentage

transmission is sufficient to maintain lasing. Electro-optic Q-switches offer extinction ratios of up to 800:1 but require both polariser and resolver. TIR devices have so far yielded extinction ratios of 100-140 : 1, although it is felt this was optical quality limited. Generally speaking an extinction ratio of 2:1 may suffice for a continuous intra-cavity system but better than 10:1 may be required for a pulsed system.

It seems that extinction ratios as large as those offered by acousto-optic modulation should be expected from TIR devices (~1000:1).

6.1.4 THE CV^2 PRODUCT

The point about the relative importance of capacitance or operating voltage improvements has already been made (section 1) but in considering Q-switches the problem is slightly eased because switching is generally employed. The switching systems associated with Q-switch control are required to operate at most in the tens of nanoseconds range. This limits the available methods to spark gaps or avalanche processes and in fact krytrons and avalanche transistors tend to be used for high and medium voltages respectively. Krytrons and avalanche transistors are often used in a pulse cable system whereby either the optical effect is doubled by a multipass system or the controlled voltage is effectively doubled across the Q-switch, or both are done simultaneously. With TIR devices of zero order extinction voltage of 100 volts or so, single avalanche or non avalanche devices may be used and if voltage is lowered further, intergrated circuitry driving becomes a possibility. This trend assists in the potential inclusion of the TIR device in a mode-locked system.

For a given material and orientation the capacitance is constant per unit length of pitch (A typical value for $LiNBO_3$ is 0.174 pf/mm.). Hence, ignoring alignment problems, it is feasible to employ electrodes to cover the beam total internal

reflection ellipse area. This ellipse has major and minor axes of d cosec θ ,d, where d is the beam diameter. The second criterion is then to select a pitch value to give an inter order angle that is sufficiently large to cause a cessation of lasing in the cavity to be Q-switched.

As shown in Fig. 6.3 this choice does not appear to need to be a precise one as energy outside a certain angle, continues to increase with applied voltage. Hence in theory, it is possible to achieve Q-switching with a device whose lowest or lower orders lie within the cavity lasing profile, merely by increasing voltage until the orders lying outside the profile contain sufficient energy to stop oscillation. Fig. 6.3 illustrates the effect that would be expected from a sinusoidal phase perturbation and is in this sense an idealised approximation. The orders up to ±10 are considered and a symmetrical pattern is assumed. The assumption is also made that order energy is proportionaly to peak order intensity. The program generating this information is listed in appendix P2. (Program QSIN)

The operating voltages of Q-switches may be varied by the need to keep electrode area reasonably small for practical reasons such as the available material quantities. In order to minimise electrode area it is necessary to increase the TIR incidence angle and the analysis of this case in $LiNBO_3$ is presented in Fig. 6.4 . It is interesting to note that electrode pitch does not appear to be a significant factor at larger values of incidence angle. This is not a fact which may be used to reduce device capacitance by reducing the number of electrode pitches, however, as any pitch reduction causes a reduction of the far-field pattern inter-order angle and reduces the chances of the device acting as a Q-switch for a given voltage. A TIR incidence angle of more than 60° is possible with a $LiNBO_3$/air interface.

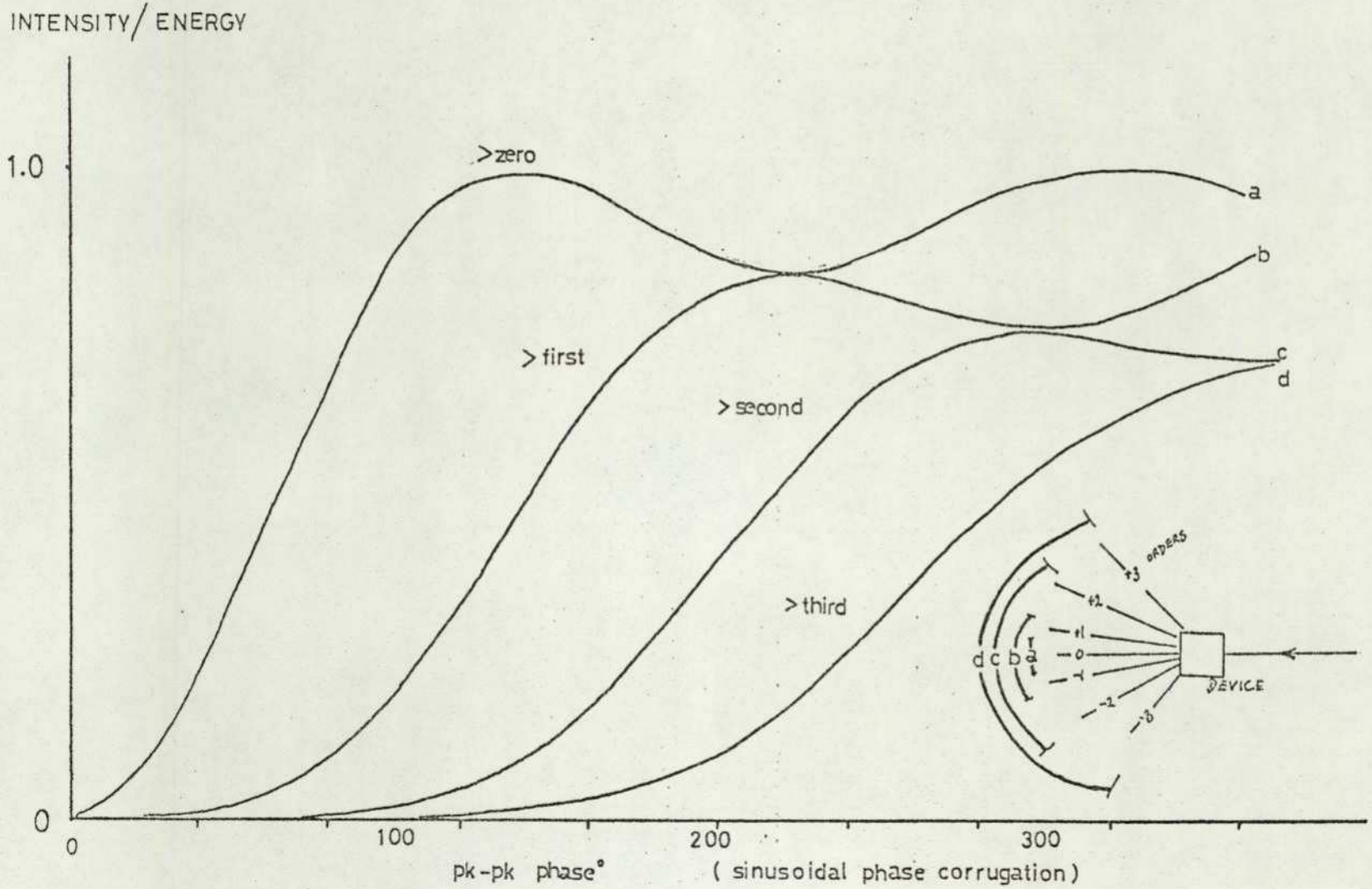


FIG 6.3 ENERGIES OUTSIDE ORDERS

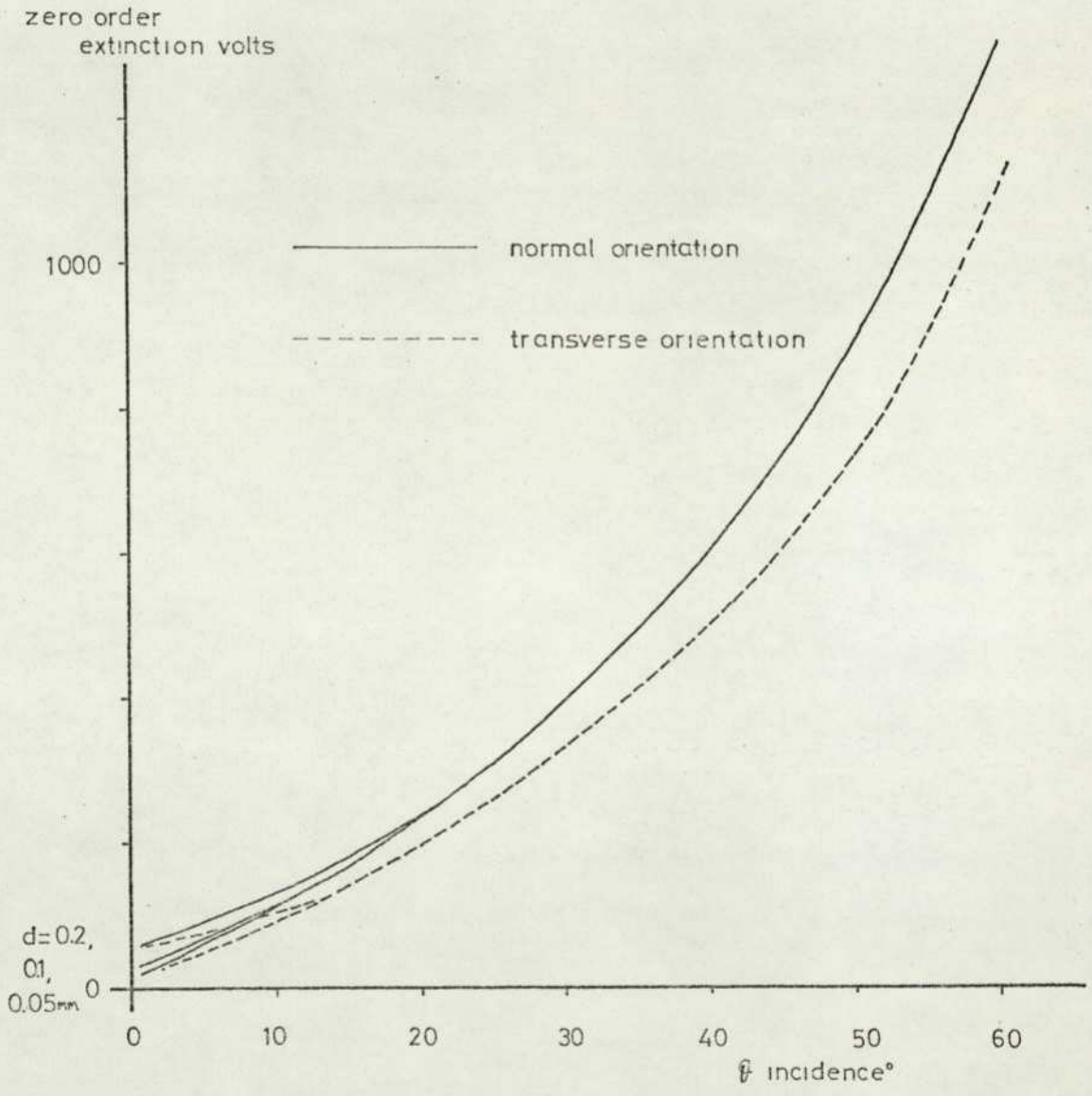


FIG. 6.4 DEVICE PERFORMANCE FOR LARGE INCIDENCE ANGLES
(for DC fields and 0.63μ light)

6 1.5 DAMAGE LEVELS

The questions of damage thresholds and insertion loss are never entirely separable because the absorptive portion of insertion loss is dissipated within the material and may cause damage. This may take the form of surface or bulk damage and is a possible limiting factor in the use of a given device. Observed damage thresholds for Lithium Niobate and Tantalate appear not to be very wavelength dependent. Reported values are 120Mw/cm^2 and 240Mw/cm^2 respectively over 0.5μ to 1μ (ref. Zverev). Published work on damage to transmissive and totally internally reflecting surfaces (ref. Boling and Crisp) suggests that the TIR damage thresholds are dependent on material refractive index and beam polarisation.

The (experimentally verified) ratio of damage thresholds for the entrance and TIR surfaces (45° incidence angle) is

(1) for polarisation normal to TIR plane

$$1 : \frac{n^2-1}{2}$$

(2) for polarisation parallel to TIR plane

$$1 : \frac{n^2-1}{2n^2}$$

It can be seen from these expressions that the existence of a TIR region will not be the limiting factor in the power handling of such a device if

$n^2-1 > 2$ for case (1)

and $n^2-1 > 2n$ for case (2)

For Lithium Niobate $n_o = 2.29$ and $n_e = 2.20$ at).63μ and the possible ratios are:

(1) 1:2.12 for n_o and 1:1.92 for n_e

(2) 1:0.40 for n_o and 1:0.39 for n_e

A material of lesser indices yields rather different results for the same conditions, i.e. for ADP where $n_o = 1.53$, and $n_e = 1.48$ at 0.63μ, the ratios are:

(1) 1:0.67 for n_o and 1:0.60 for n_e

(2) 1:0.29 for n_o and 1:0.27 for n_e

Hence it may be concluded that the damage levels of a TIR Q-switch are dependent on material refractive index. The values quoted are for an incidence angle of 45°. For angles nearer to grazing, the TIR thresholds are increased so even in the ADP case the device may be made normal entry limited. For example in the case of lithium niobate an incidence angle of 5° changes the predicted damage thresholds to

(1) 1:5.7 and

(2) 1:2.6

6.1.6 PHASE CHANGE ON REFLECTION

This aspect of device performance (previously studied in section 4), is of greater importance in the application because the residual diffraction caused by a phase mismatch between totally internally reflected and electrode reflected light will increase device insertion loss significantly. Although combinations that possess a match have been constructed and analysed in previous sections, it may prove necessary to avoid this problem in Q-switches by the inclusion of a low refractive index layer between the crystal and the electrodes. The total internal reflection then takes place from the dielectric interface while the field is generated by distant electrodes. Advantage is taken in this case of the fact that penetration into the rarer medium is very much less than the penetration range of the field. A possible coating of SiO_2 onto $LiNBO_3$, of a thickness of a few microns to about 25% of electrode pitch, will yield a useful device. The layer, which could be deposited or sputtered, requires to have resistivity and/or dielectric constant. which are preferably less than those of the electro-optic crystal. A Q-switch requires to exhibit both A.C. and D.C. operation so both resistivity and dielectric constant need to be considered. Another advantage of this approach is that materials on which electrode deposition and fabrication is

difficult or impossible become possible to use in TIR devices. The isomorphs of KDP still pose problems as lesser refractive indices are hard to come by and probably only low incidence angles may be supported on a glass/ADP type combination. (The analysis of a TIR configuration with a surface spacer layer is presented in section 4).

6.2.1 Q-SWITCH - DEVICE CONSTRUCTION

A lithium niobate modulator was constructed for use as a Q-switch. A Roditi boule was the source of the crystal and an orientation with z axis, normal to the electrode plane, was used. Laue x-ray photography was used to verify orientation and a diamond saw machine (section 9) used to cut a 19×6×3.5 mm crystal. In order to create a "straight line" device such that the input and output beams were collinear, the end faces were cut at a bevelled angle of 8.1°. This, together with a TIR angle of ~10° offered collinear operation at 0.69μ. (Original operation was intended for a continuous Ruby system).

The end faces were polished on the TCU machine (section 9), while the largest face was given a final polish at the Applied Physics department of Hull University.

A copper on chromium layer (~50μ and ~1μ) was deposited onto the largest face and an electrode pattern etched using Shipley photoresist. A photo master of the electrode pattern was produced for this purpose using the TCU reduction camera. An electrode pitch of 0.2mm was chosen as being well within the range of available equipment to produce and because the inter-order angle requirement for a Q-switch could be relaxed for reasonably long cavities. Predicted zero order extinction voltage of this configuration was ~100 volts at 0.63μ and capacitance of the electrode area (18×3 mm) was 47 pf. The aperture was 3mm×3mm. This device is shown in Fig. 6.5.

SAMPLE DEVICE

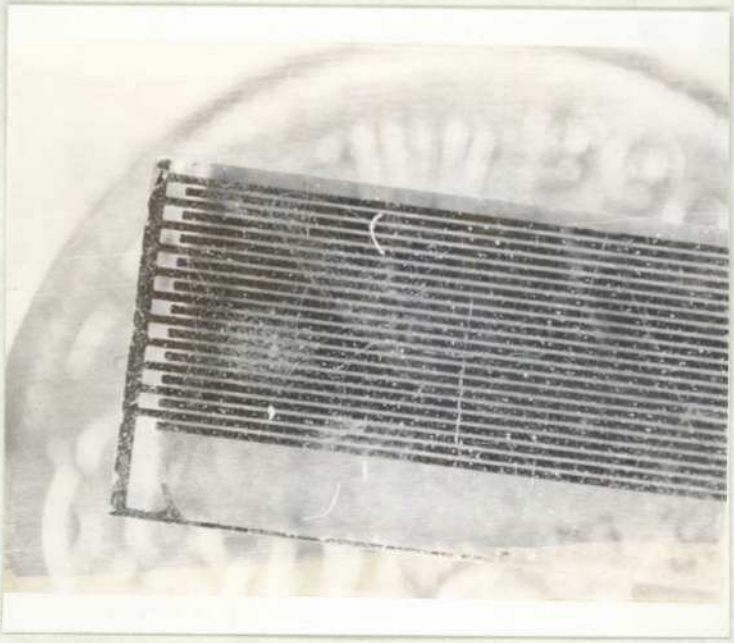




1cm

BOTTOM and SIDE VIEWS

Z axis



1cm

FIG. 6.5 ELECTRODES

6.3.1 DEVICE OPERATION

The operation of this device as a modulator was assessed first. Measurements involved:

(1) Zero-order extinction voltage
(2) Insertion Loss
(3) Speed of Response
(4) Far field pattern

6.3.2 Operating Voltage

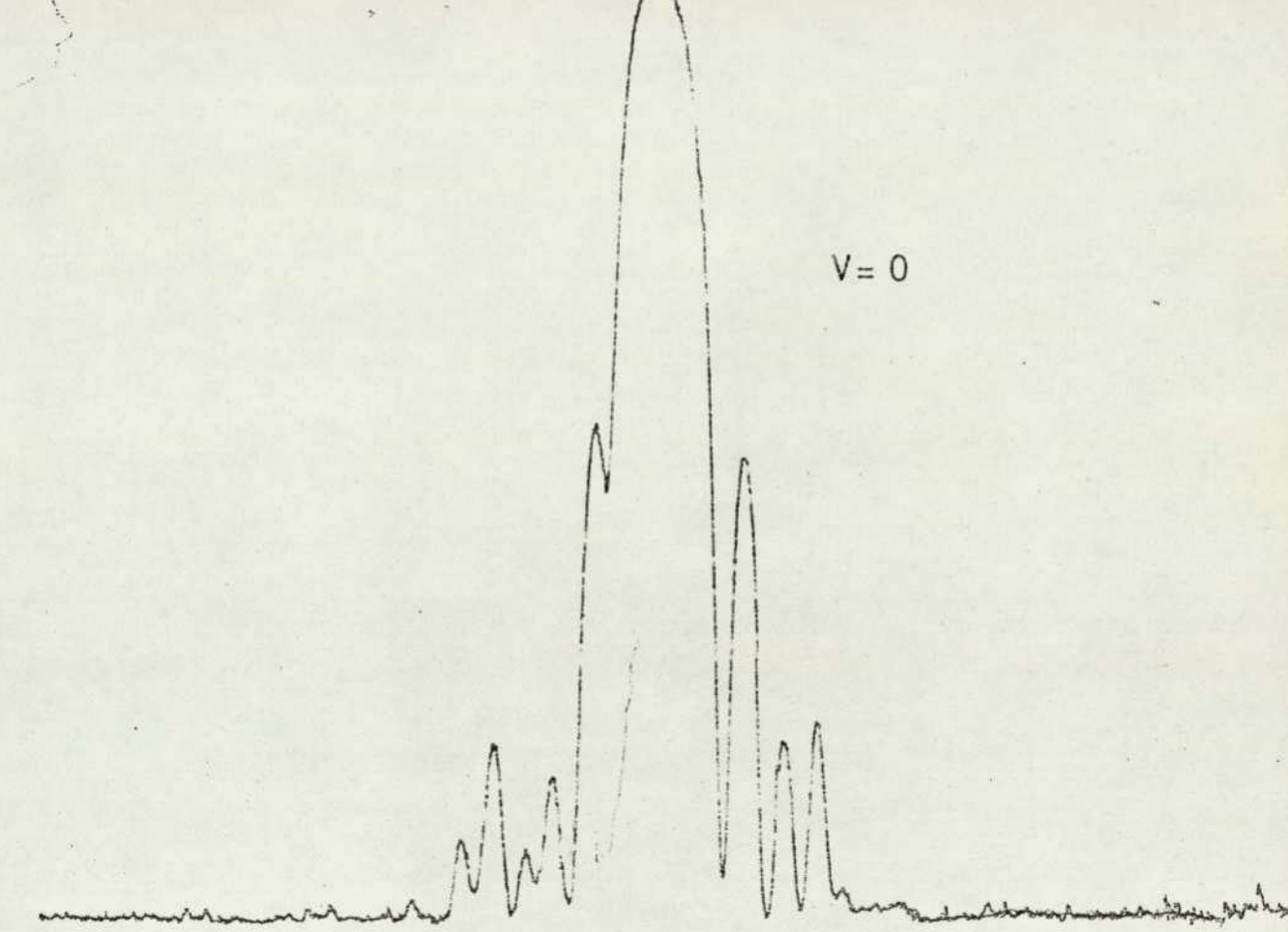
This device design was initially intended for Q-switching a continuous ruby laser (0.69μ) and these extra cavity tests were made at 0.63μ. The zero-order extinction voltage was measured at ~90 volts at this wavelength. This involved an incidence angle of ~8° and was in agreement with values predicted from section 4.

6.3.3 Far Field Pattern

This is shown in Fig. 6.6 and illustrates modulation of the zero-order by ~90 volts and exhibits the inter-order angle expected at 0.63μ - 1.6mR. Microdensitometer traces are shown in Figs. 6.6 and 6.7 , and illustrate the intensity profiles from Figs. 6.6a and 6.7a. These show the zero-order modulation effect of 90v. and the undiffracted beam (Fig. 6.6). and the effect of 90v. in the two polarisations (ordinary and extraordinary) in Fig. 6.7 . The information of Fig 6.6 is also presented in Fig 6.8 where the pattern of higher orders is shown more clearly at the cost of saturating the detection system by the lower orders. Extinction is not ideal in the former case as the applied voltage is not exactly the zero-order extinction value.

6.3.4 Driving System and Operation

Zero-order switching was tested by driving the 50pf device by a 2N2219 transistor with a supply of 90 volts and the



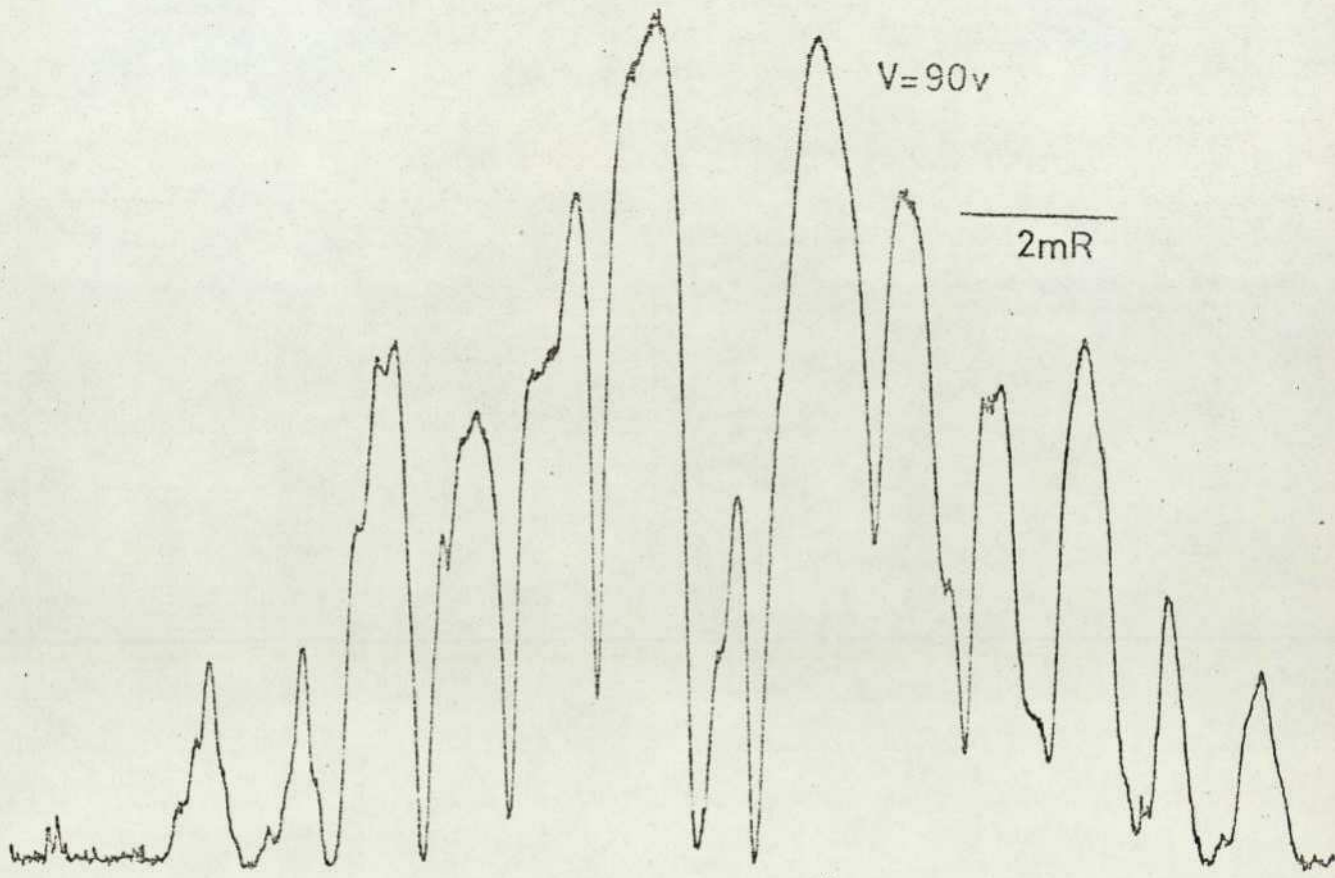


FIG.6.6 PATTERN TRACES (pol. ∥ z axis, $\lambda = 0.63\mu$, d = 0.2mm)

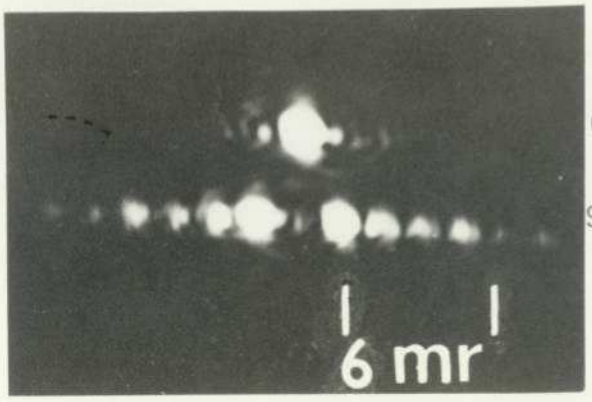
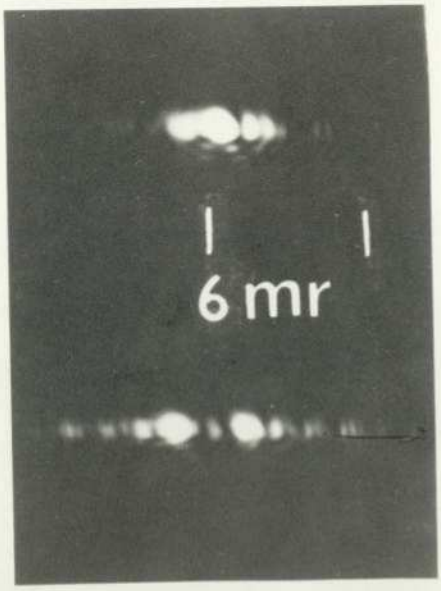


FIG. 6.6a

ZERO ORDER MODULATION
at 90 volts and 0.63μ



r_{13}

r_{33}

FIG. 6.6b

EFFECT ON BOTH POLARISATIONS
(at 90v)

FAR FIELD PATTERNS

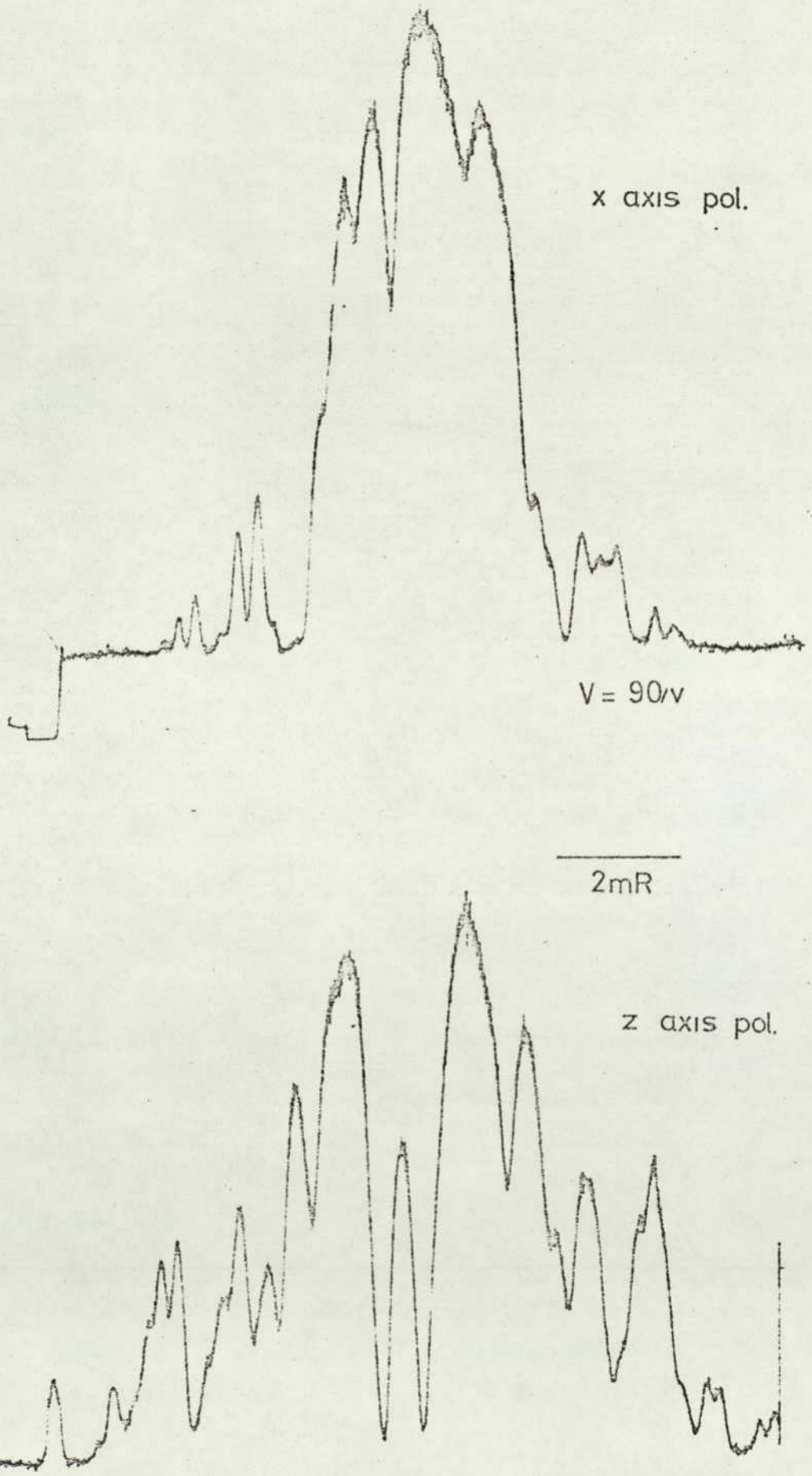


FIG. 6.7 PATTERN TRACES (pol. at 45 to z axis)

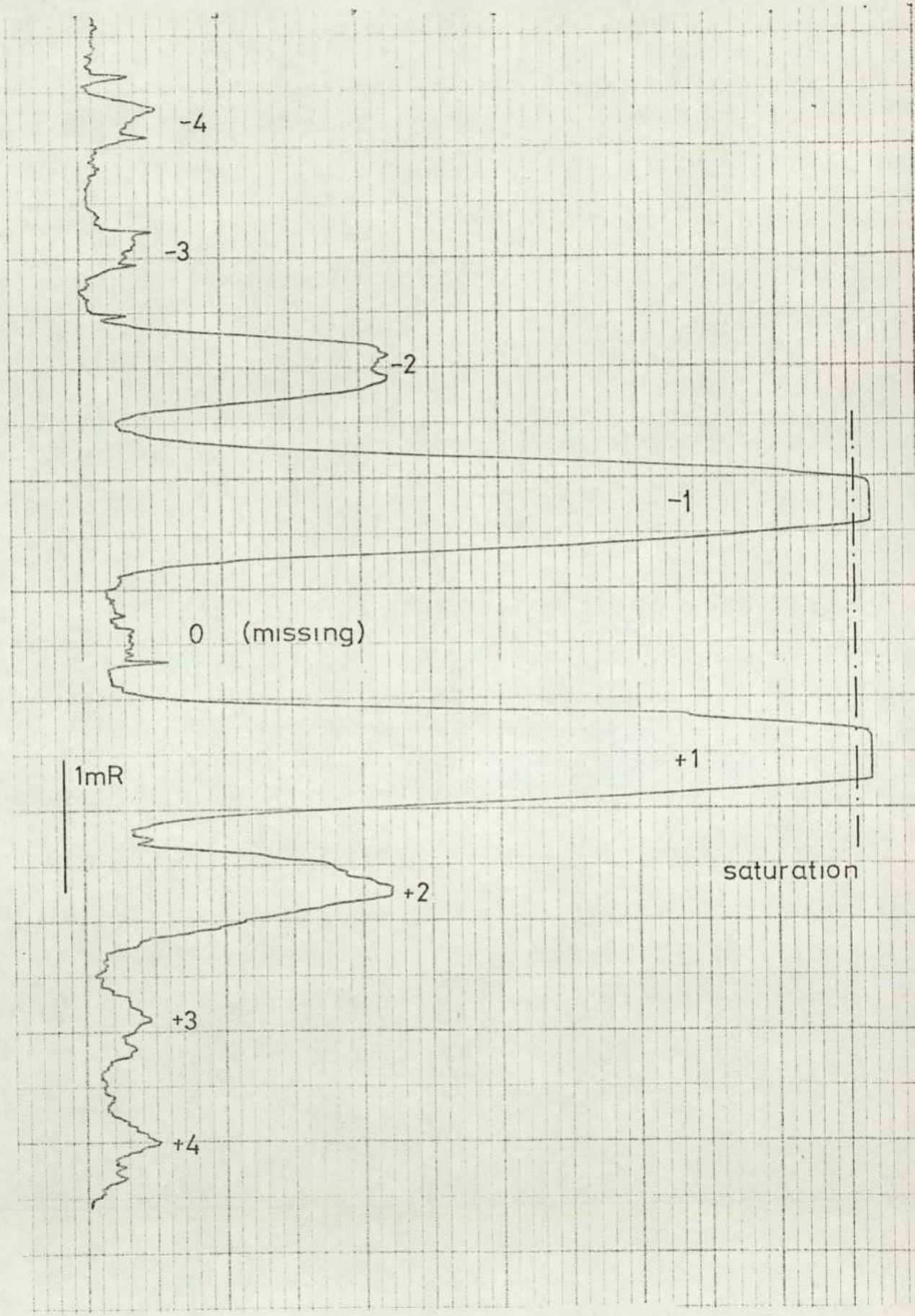


FIG. 6.8 Ddensitometer results —— 90 volts

resultant performance shown in Fig. 6.9 . The relatively slow rise-times are due to the non-avalanche operation of the driver transistor. The actual device reponse can be seen to be much faster than the timescale considered and this agrees with reported results for thin film devices

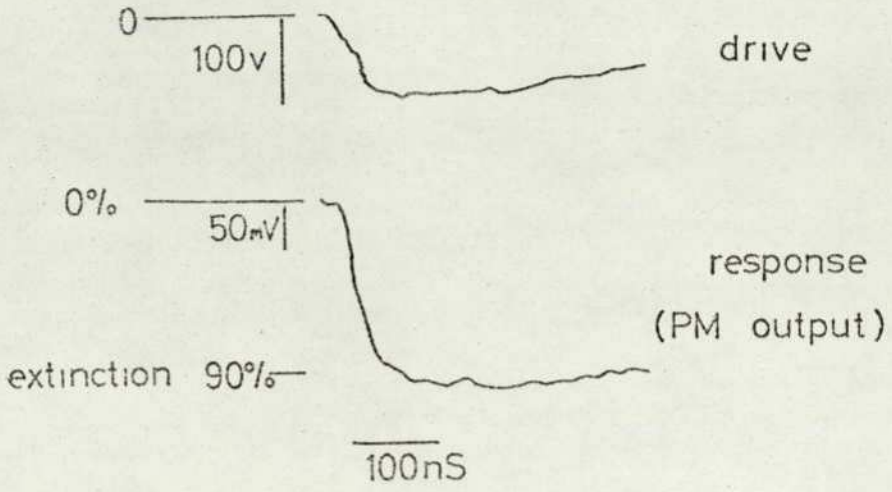


FIG. 6.9 STEP RESPONSE at 0.63μ

(ref. de Barros and Wilson). The nonlinear reponse characteristic of the device is suggested by the shape difference between the driving and light waveshapes in Fig. 6.9.

6.3.5 Insertion Loss

The insertion loss of an anti-reflection coated crystal can be as little as 1%. (Lithium Niobate allows a single layer AR coating). Alternatively loss can be reduced by employing a brewster angle face.

The uncoated normal entry device should exhibit 14% loss per face but the device as cut involved entry at an angle of 66°. This raised the measured total insertion loss to-40%. (The predicted value in this case was 32%). The device was

installed in a PTFE base and whisker contacts made to the electrode common strips. This configuration served to minimise stray capacitance. In this way only two dielectric interfaces were presented to the light beam, not counting the TIR face. Because the continuous ruby laser was not available, it was decided to use a Nd-Yag 1.06μ pulsed laser and, because of the inherently much higher gain, no AR coatings were deposited on the crystal.

6.3.6 Q-Switching Operation

The cavity into which the TIR device was introduced used a 3"x $\frac{1}{4}$" Nd^{+3} Yag flash pumped laser rod, plane mirrors, a 4m focal length lens at the brewster angle, and a mode selecting aperture. The configuration is illustrated in Fig. 6.11

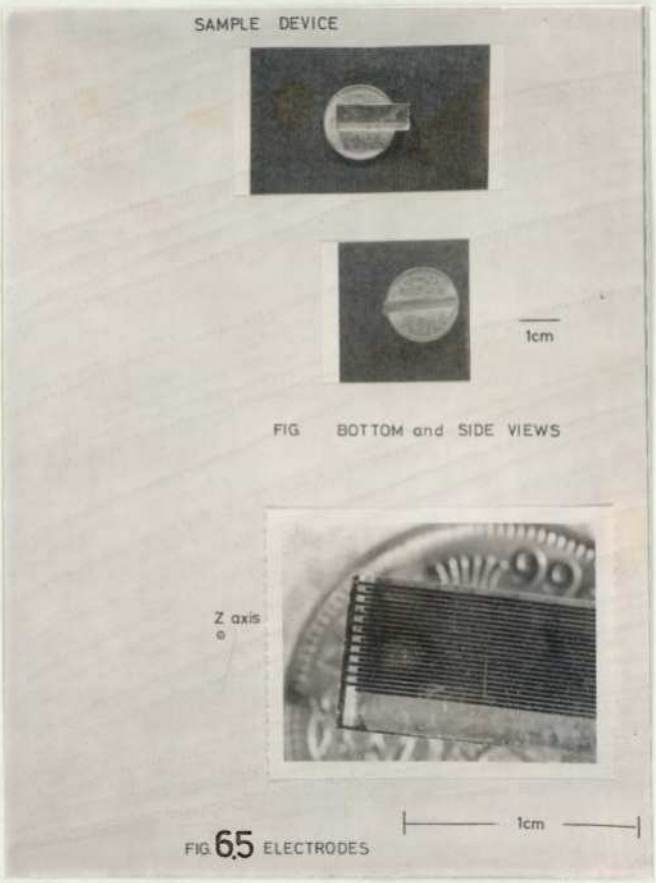
Using 60% output coupling the single mode laser threshold was found to be 15J. When the TIR device or a 50% neutral density filter were inserted into the cavity this was raised to 55J. This is illustrated in Fig. 6.10b.

Q-Switching action was achieved by the removal of voltage (90 volts) normally applied to the TIR device while the rod was at maximum inversion. This was about 100μs after flash initiation and a delay circuit was used for triggering.

At a pump energy of 68J, a single 60nS, 5mJ Q-switched pulse was obtained. Two illustrations of this are presented in Figs. 6.10c and 6.10d. Fig. 6.10c shows the shape and duration of this pulse while Fig. 6.10d shows it to have been a unique event and Q-switching to have truly taken place. The detector used for these results was a photomultipler preceded by a diffuser.

6.3.7 Conclusion

It was shown that Q-switches, with TIR devices can be achieved readily and with very favourable operating characteristics such as single transistor driving and low voltage operation.


SAMPLE DEVICE
1cm
FIG BOTTOM and SIDE VIEWS
Z axis
1cm
FIG 6.5 ELECTRODES

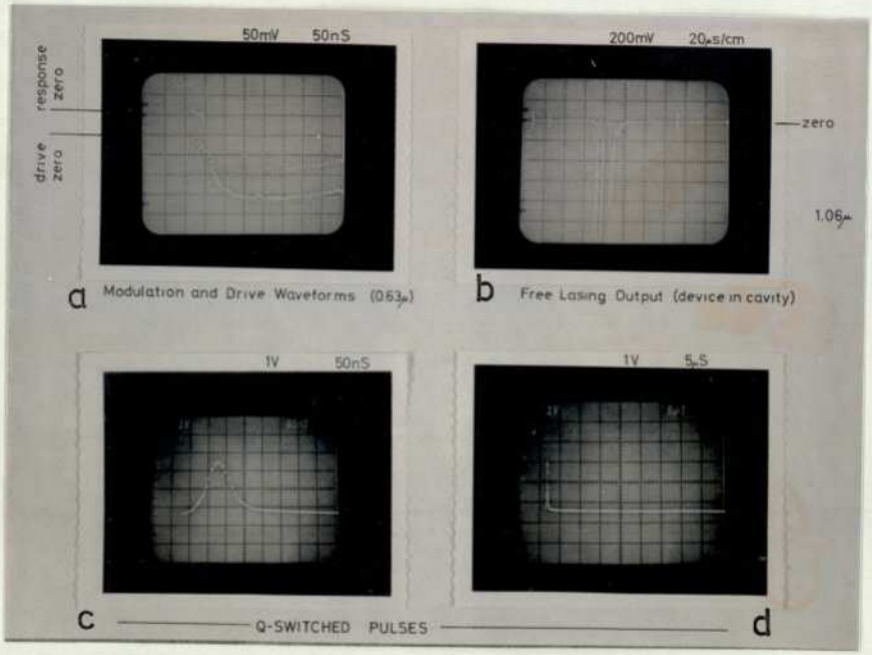

50mV 50nS
response zero
drive zero
a Modulation and Drive Waveforms (0.63μ)
200mV 20μs/cm
zero
1.06μ
b Free Lasing Output (device in cavity)
1V 50nS
1V 5μS
c Q-SWITCHED PULSES d

FIG. 6.10

Q-switching of high gain (pulsed) lasers requires a device offering a superior on/off ratio, while low gain (continuous) lasers require a low insertion loss. The former case has been demonstrated but it should be noted that even lower voltage operation is suggested for the latter case if antireflection precautions are taken.

Pulse widths and risetimes were limited by the non avalanche driver used but 5 - 10nS risetimes are possible and some hope of even higher speeds may be offered by reducing electrode pitch and/or aperture. Another advantage of this type of device is that a polarising element may be rendered unnecessary within the cavity because of brewster faces and the fact that the unwanted polarisation will be deflected out of the cavity. The latter was in fact the case in this experimental verification.

It must be concluded that a promising new Q-switch has been born and that considerable work still needs to be done, to render the device losses low, and assess high power operating prospects.

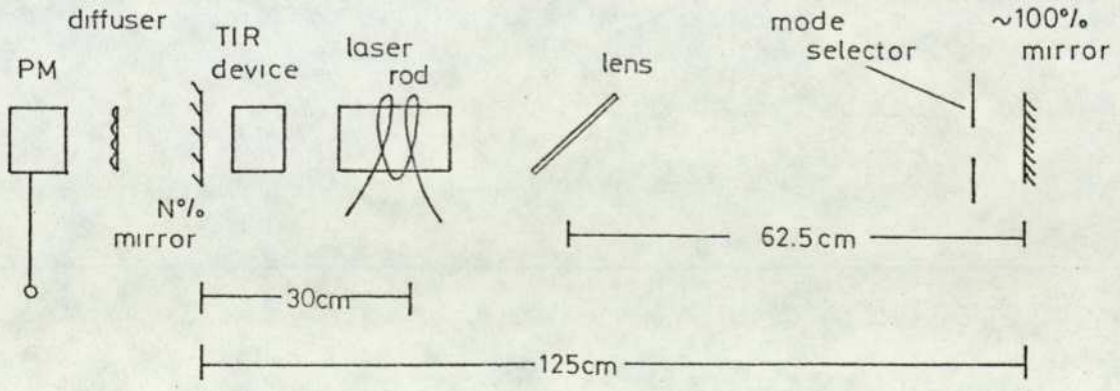


FIG.6.11 Q SWITCHING CONFIGURATION

7. OPTIMISATION OF CRYSTALS

All device configurations considered hitherto have used only one electro-optic coefficient. This has been the most significant single coefficient, e.g. r_{33} in lithium niobate and r_{41} in ADP. Device operations can be augmented, however, by choosing an orientation where other coefficients add their effects to the major coefficient and the overall effect is enhanced. This section shows the magnitude of this optimisation effect for both $LiNBO_3$ and ADP.

Two cases are considered in this section, using a computing approach, giving optimised phase and birefringent modulator information. The configuration considered the transverse field case only, and transformed the index ellipsoid to every orientation in the half solid angle, finding the most sensitive one. Two simultaneous transformations are necessary, of orientation and field, so that light propagation direction and field remain normal.

Taking an index ellipsoid and substituting the direction cosines for each transformation about one axis gives the new ellipsoid form. Resolving the field expressions according to the same rotational transformation gives the effect due to a transverse field. This computation may be executed in this longhand form or in the abbreviated notation (ref. Kalymnios). A full description of the optimisation process is not included here as this is a well referenced area.

Programs were written to search for a best orientation in both $LiNBO_3$ and ADP and are listed in Appendix P2 as LINO and PHOP respectively. The $LiNBO_3$ optimisation was executed using the notation of François (ref. François & Librecht) and subsequently (as in the listed program) from first principles. PHOP was a modification of a previously developed program (ref. Kalymnios). The results are shown in Figures 7.1 and 7.2 . Both phase and intensity information is shown in these diagrams and the optimised orientations for phase modulation are seen to be:

$\theta=30^\circ$, $\phi=38^\circ$ for $LiNBO_3$

and $\theta=37^\circ$, $\psi=90^\circ$ for ADP

The improvement in performance is $\sim$ 40% in the former case, but only $\sim$ 4% in the latter. It is to be noted that the TIR configuration offers a complex field structure and that the orthogonal field components may augment or detract from any improvements resulting from optimisation.

In order to obtain a full picture, therefore, it is necessary to examine the optimisation regions under conditions of a fringing field, rather than the simple transverse fields considered here.

FIG 7.1 $LiNBO_3$ OPTIMISATION

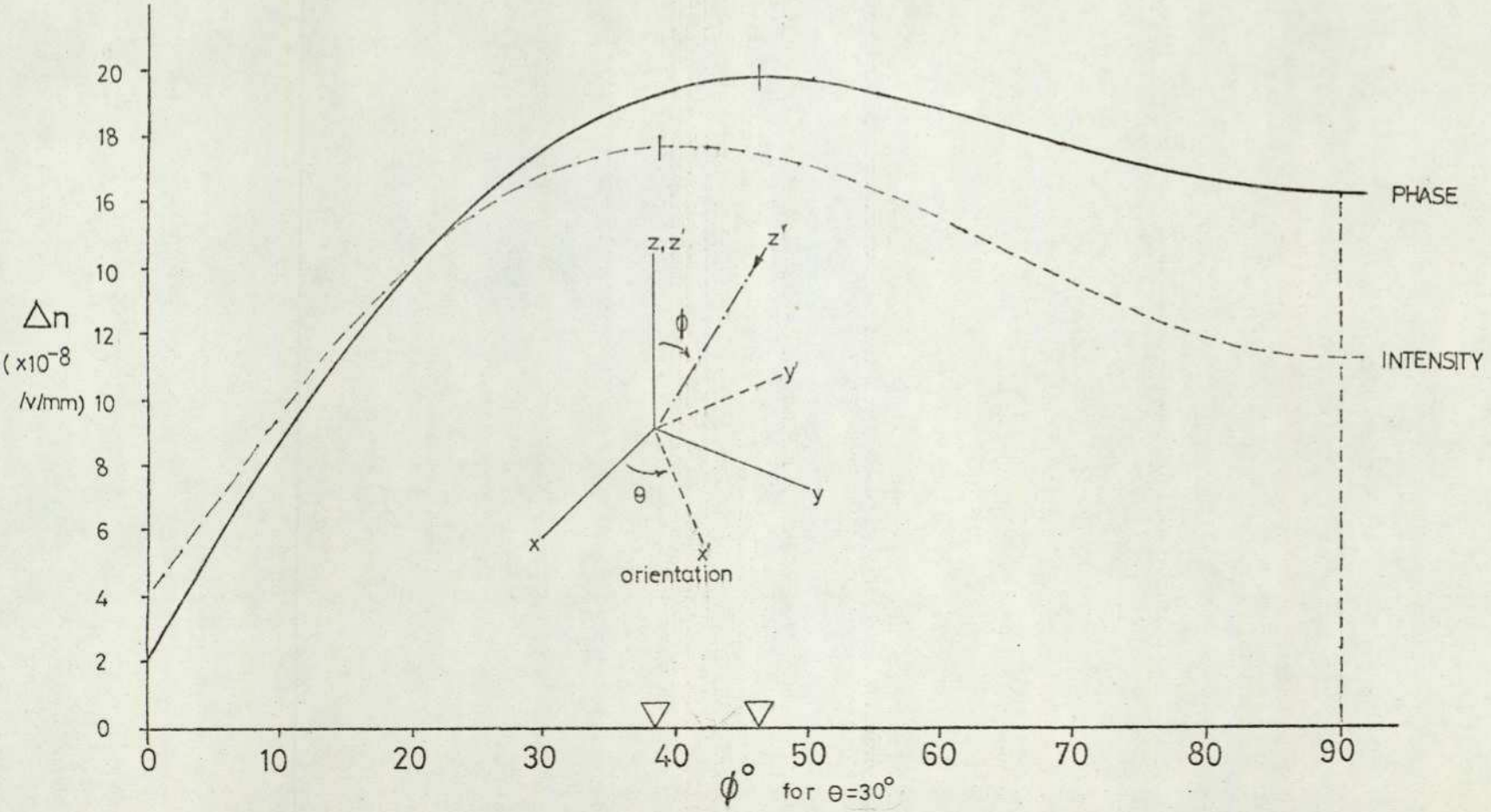
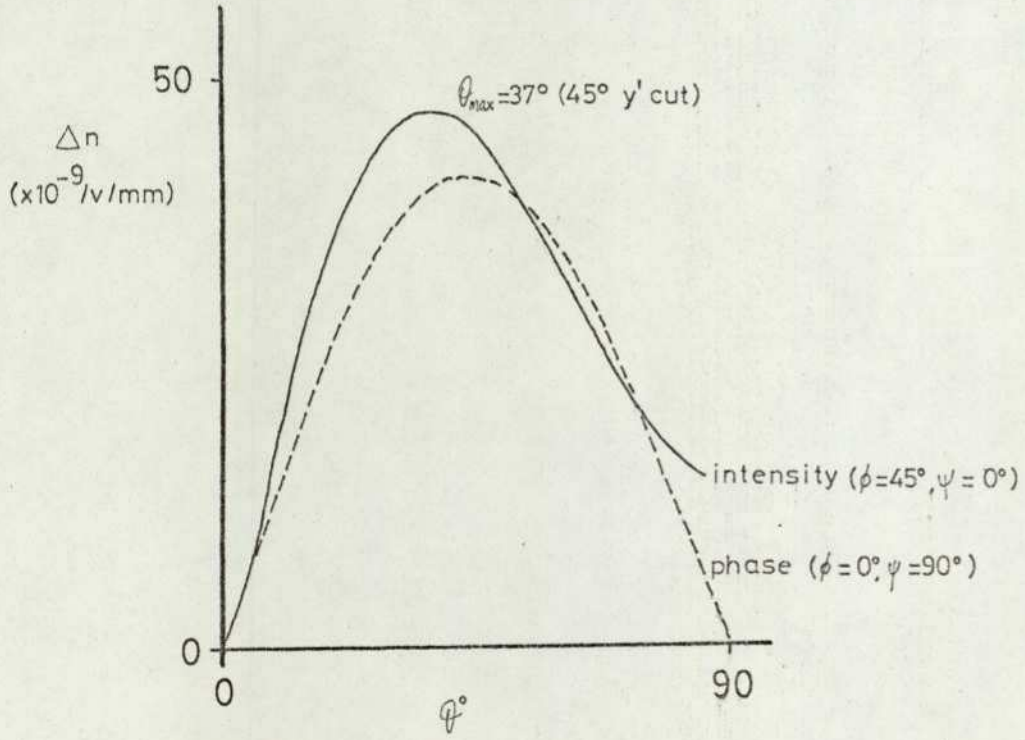
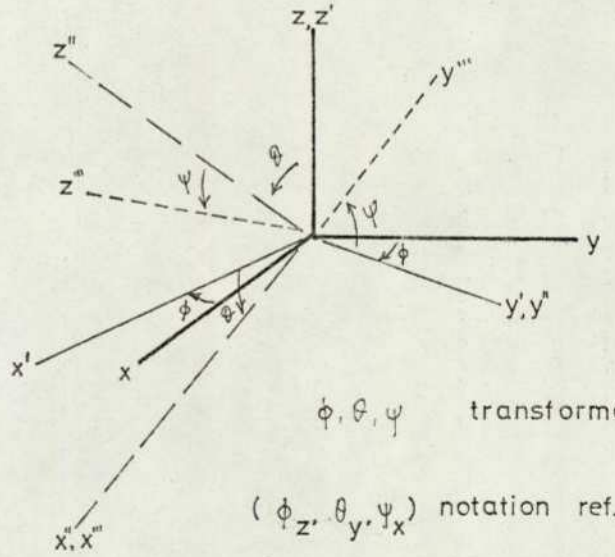


FIG. 7.2 ADP OPTIMISATION



PHASE RETARDATION



ORIENTATION

8. CRYSTAL ORIENTATION

and

9. CUTTING AND POLISHING PROCESSES

8. CRYSTAL ORIENTATION

The lithium niobate samples were cut from a Roditi supplied boule, with polished end faces and with the c axis longitudinal to the boule. A 90° x/y cut was prepared by initial cutting of a boule wafer normal to the c axis slice, after identifying the c axis optically by the maltese cross method. The maltese cross obtained between crossed polarisers shows good extinction and symmetry and suggests a good quality strain free crystal (Fig.81).

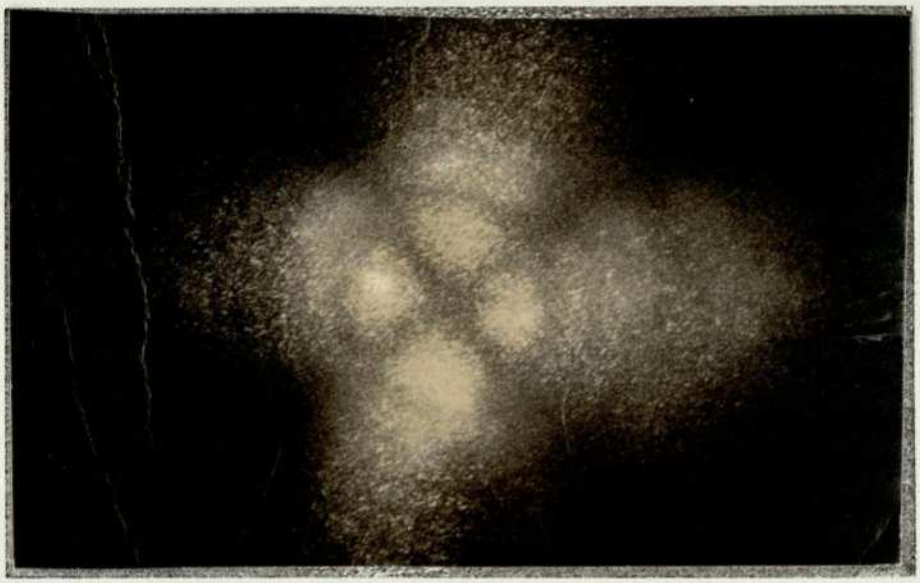
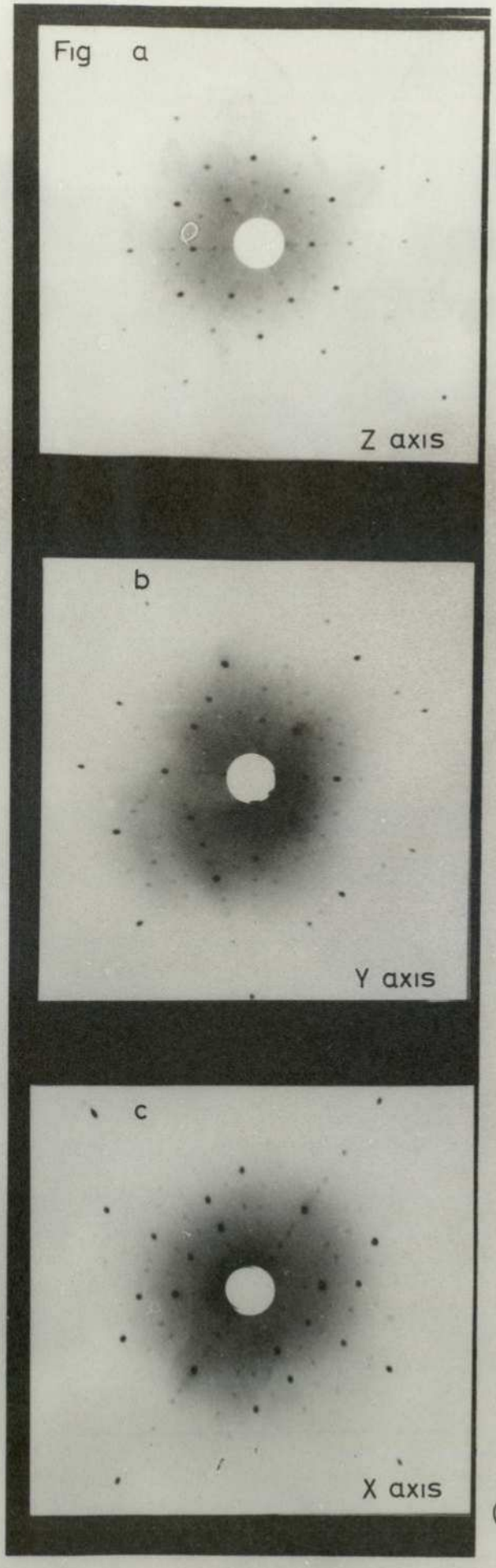
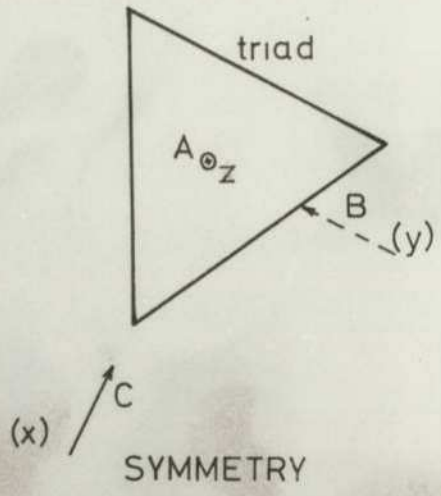


FIG 8.1. $LiNBO_3$ MALTESE CROSS

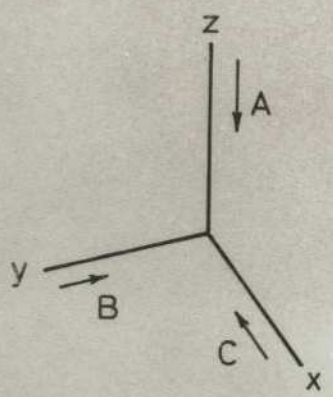
Identification of x and y axes was achieved by X-ray photography using a Phllips x-ray machine and a 3cm sample/source spacing. (Fig. 9.2) A 30 minute exposure was used with Ilford x-ray film using a copper or molybdenum x-ray source. The crystal was aligned so that x-ray illumination occured normal to the slice face, i.e. along the z axis. The resultant photograph is presented in Fig.8.2) where the threefold symmetry to be expected of a crystal of class 3m is shown. The triad of symmetry is illustrated



CLASS 3m



SYMMETRY



AXES

(Ilford X ray film)

FIG. 8.2 LAUE PHOTOGRAPHS

and sign conventions (reference Nye) are superimposed. Any symmetry plane can be chosen as an direction and a y direction then chosen at right angles to form a left hand screw system. Three choices are possible and the chances of one of these being convenient for good materials usage are high. The rarely seen y and x axis views are seen in Fig. 8b and8c, and show the assymmetry and two-fold symmetry respectively to be expected from the geometrical lattice constraints suggested by the optic axis triad of symmetry. It is worth noting that x-ray diffraction techniques are not promising in the location of the optic axis and this is best achieved optically. The reason for this is the ambiguity inherent in Laue x-ray photography which does not distinguish depth and causes threefold symmetry to appear at regular angles and thus conceal the true z axis. For this reason boules are usually supplied with a known z axis direction and x-ray techniques only used to identify (and choose) x and y direction. In the event of more complex orientation, the use of an accurately calibrated goniometer is needed and the starting orientation identified by optical and x-ray means. The required transformation is then executed on the goniometer.

The alternative crystal type that can be studied for the application is the XDP group. These are of class 42m and exhibit a two-fold symmetry. In this case x and y axes are evident from the "as grown" crystal shape.

9. CUTTING AND POLISHING PROCESS

Two types of crystal need be considered for device fabrication, the XDP class or the lithium niobate class. Their classification is morphological and the differences are that the former class is grown from solution, soft, and difficult to handle with a manual polishing requirement, while the latter materials are Chochralski grown, hard, easy to handle and can be automatically polished. The latter group tends to offer smaller crystals. Lithium niobate also presents a high sensitivity with the largest

available coefficients in a commonly available electro-optic material. ADP is an inexpensive material and allows greater device apertures. The handling of these two materials is subsequently considered.

9.1 CRYSTAL CUTTING

Two basic techniques exist, the 'wet string' method for soluble crystals, and the diamond saw technique. The latter is universally useful and was employed for the scope of this work. A Swiss quartz cutting machine (Fig.9.3) was used with a cutting oil blade lubricant/coolant. A warning from personal experience - cutting oil vapour is a serious irritant and should not be inhaled because throat infections will result.

The crystal was first araldited to a balsa block which was in turn araldited to the goniometer table. This goniometer (Fig.9.1) allows rotation so that cuts can be made to form the required crystal. The diamond disc saw can cut into the balsa without damaging the stainless steel goniomter. After cutting (rate 4 to 5 for either crystal) the goniometer table is removed and the araldite dissolved in dichloromethane (contact with this must also be avoided). Alternative bonding methods are less ideal as wax is softened by cutting oil and Evo-stick does not provide an unmobile bond. ADP will crack if removed suddenly from the dichloromethane because of the considerable temperature drop caused by the volatility of the solvent.

9.2 POLISHING

Crystal polishing is an empirical science and only the methods that were found effective can be reported here. Three classes of polishing were employed for the preparation:

(a) Manual pitch lap/polishing rouge process.
(b) Automated lead lap, diamond dust/lubricant system.
(c) Automated Citon process.

The former method involves the greatest skill and is particularly suitable for the XDP group, the members of which have not yet

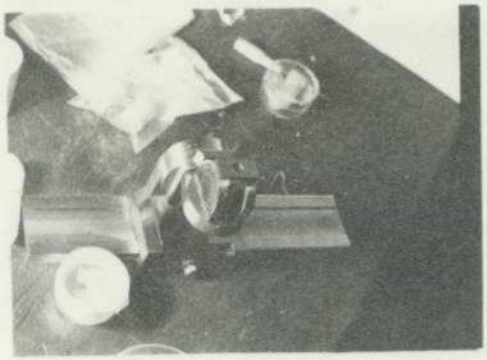


FIG 9.1 - GONIOMETER



FIG 9.2 - LAUE X-RAY MACHINE

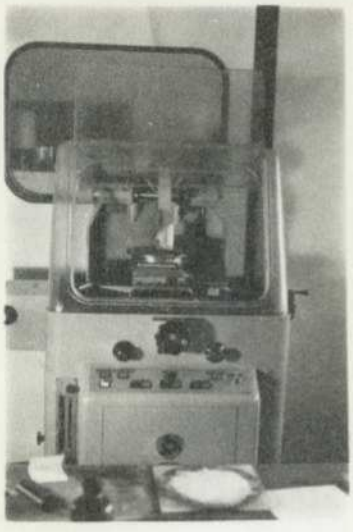


FIG 9.3 - CRYSTAL CUTTING MACHINE



FIG 9.4 - POLISHING MACHINE



FIG 9.5 - LEAD POLISHING LAPS



FIG 9.6 - CRYSTAL IN POLISHING HOLDER

been successfully automatically polished. The lead lap process was used extensively for $LiNBO_3$ in conjunction with the City University polishing machine (Fig.9.4)on its slowest speed of and on a lap with a spiral lubricant distribution groove of pitch ~4mm (Fig.9.5). A workholder was used which required an insert to hold the crystal (Fig.9.6),and brass holders were fabricated for each type and shape of samples and the crystals to be polished waxed in place. The polishing solvents used were of the Hyprez range. They include the polishing diamond paste and solvent or the Hyprez diamond spray. Only the latter range was found to give good results and the 1μ diamond dust suspension used for all work. It is essential to use a lead lap only with one grade of polishing abrasive. The reason for this is the embedding of diamond particles in the lead and the harder material (work holder plus crystal) is in fact polished by the softer lead lap.

The pressure of the crystal on the lap during polishing was found to be uncritical. It was found faster therefore to use quite high pressure after initial contact was established, As device parallelism is not important in the TIR configuration, no polishing towards a geometrical shape was necessary. It was only essential to render existing surfaces polished and transparent. To achieve this it was necessary to keep initial polishing pressures very low via the spring adjustment on the crystal holder, so that misalignment could be corrected before unwanted levels were polished onto the crystals.

The polishing process was found to exhibit a flow effect. This meant that a short polishing process (~1 hr) gave a reasonable finish while continued polishing, towards a better finish, caused a deterioration of the surface, and only a very slow improvement was seen with continued polishing. This effect was aggravated with larger crystal areas ($\geq$1cm) and proved a limiting factor in these cases: with slight surface scratches only sometimes being avoided by constant lap cleaning and copious use of fresh polishing spray. A 1μ spray was used for

S.E.M. SURFACE FINISH PHOTOGRAPHS
($LiNBO_3$)



1μ

FIG. 9.7a



10μ

FIG. 9.7b

LEAD-LAP POLISHED (1μ diamond dust)



1μ

FIG. 9.7c



10μ

FIG. 9.7 d

CITON POLISHED

polishing as this gave a better finish, due to particles being embedded in the lap, than suggested by the particle size. As the finish achieved was of good experimental quality a finer particle polish was not attempted. This appeared doubly unnecessary in view of the fine surface scratches often in evidence on the larger faces. While these did not interfere with device evaluation (except degrading extinction ratio results a little), a possible explanation was postulated and another process attempted. It was felt that these scratches were caused by minute crystal particles, either detached from the crystal edge or the polished surface, and as edge bevelling did not appear to help, so Citon polishing was attempted.

The Citon process was employed and performed by kind permission of the GPO Research. This was a slow removal rate process, designed for materials harder than Lithium Niobate (5 on Moh scale), and employing a leather lap and a weak alkali lubricant with minimal abrasive. The action of the alkali is to consume minute particles quickly with their attendant large area to mass ratio, and hence no scratches are caused by dragging such particles across a previously polished surface. The results of a Citon polishing sample, previously polished on a lead lap, are presented in Fig.9.7. These pictures were taken by the GPO Scanning Electron Microscope (SEM) and show the lead lap polish finish with minute scratches (Figs.9.7 a,b), and the post Citon finish (Figs.9.7 c d) The improvement is self-evident (the loose particles in Figs 9.7c,d are dust particles used to facilitate focussing.

10. MASK PRODUCTION AND ELECTRODE PRODUCTION

10. MASK PRODUCTION

The photomask required to expose the desired electrode pattern can be made in several ways. The Shipley photoresist used is of the positive variety, i.e. the exposed area will not be etched away. This means that the mask will also need to be a positive of the desired electrode pattern. The general technique is to create a large version of the desired pattern and subsequently photoreduce to the desired magnitude. The photoreduction may be of one or two stages. If two stages are employed the second stage will usually be a photograph of several internegatives in order to make efficient use of available film area. A major advantage of the photoreduction process is that any flaws in the master tend to go below the resolution limit in the final photograph, and so disappear. The edge quality retains a high level by the use of line film (containing a steep γ function).

The process employed for mask production involved the use of Kimoto strip-film to make the photomasters via a scribing table (Fig. 10.1). A two or one step photoreduction process followed. The Array masks and electrode patterns were made by a one stage reduction on Ilford line film (type N4E50, 4x5 plates), which has a mylar base. The TCU reduction camera was used (Fig. 10.2). This was a reconstructed Polaroid MP3, modified to use an optical bench, a plate film holder and to work horizontally. As the line film used was blue sensitive, a red strip-film was used and a blue lightbox (with fluorescent illumination) (Fig. 10.2).

Two step photoreduction was employed for the mask production, for all the TIR devices. The assistance of the GPO Research must be acknowledged for the manufacture of the first masks, which were reduced from strip-film masters to provide square electrode patterns 3x3mm in area and 0.05, 0.1 and 0.2mm in pitch. These were attempted on a mylar film but the practical

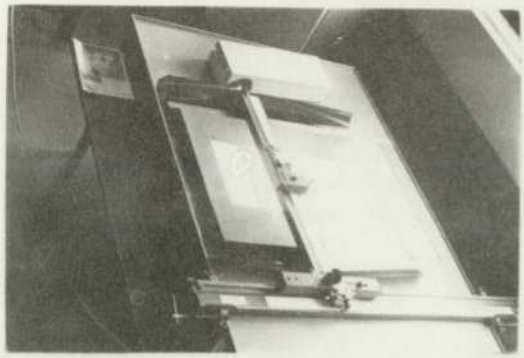


FIG 10.1 - MASTER PREPARATION

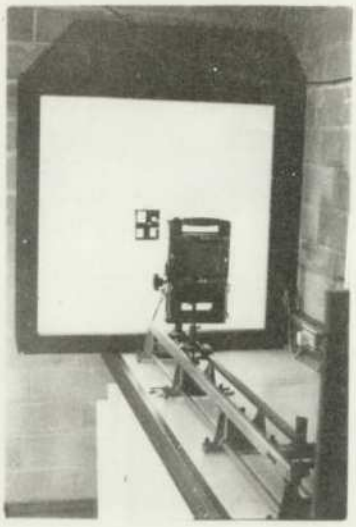


FIG 10.2 - PHOTOREDUCTION



FIG 10.3 - SPINNER IN CLEAN-ROOM

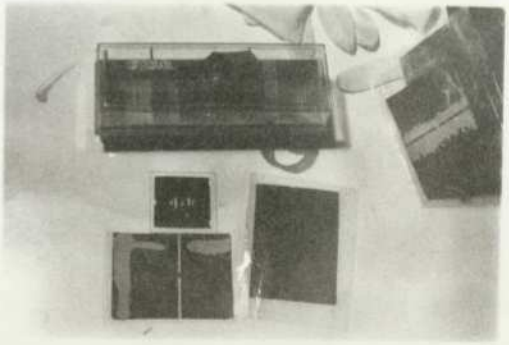


FIG 10.4 - PHOTOMASKS

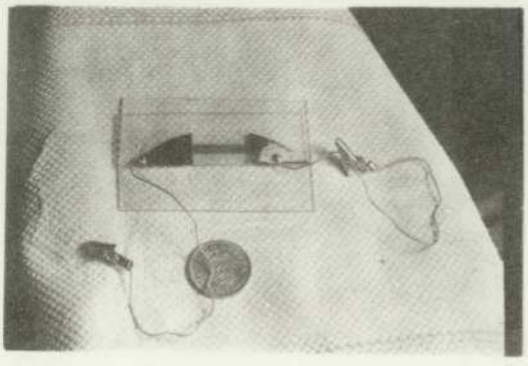


FIG 10.5 - Q-SWITCH ELEC-TRODE (on GLASS)

FIG 10.6 - ETCHED ELECTRODES/ MASTERS

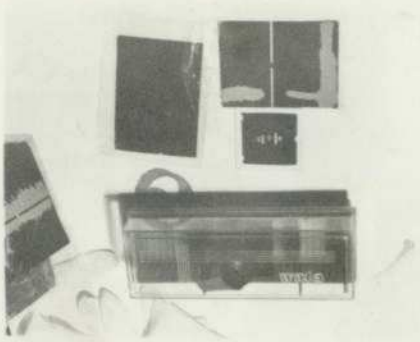


FIG 10.6a - 2^2mm ELECTRODES

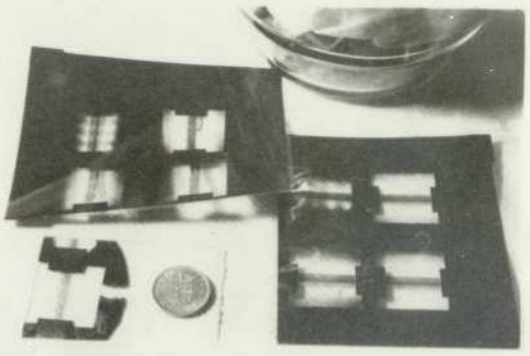


FIG 10.6b - Q-SWITCH ELECTRODES

FIG 10.6c - ARRAY ELECTRODES

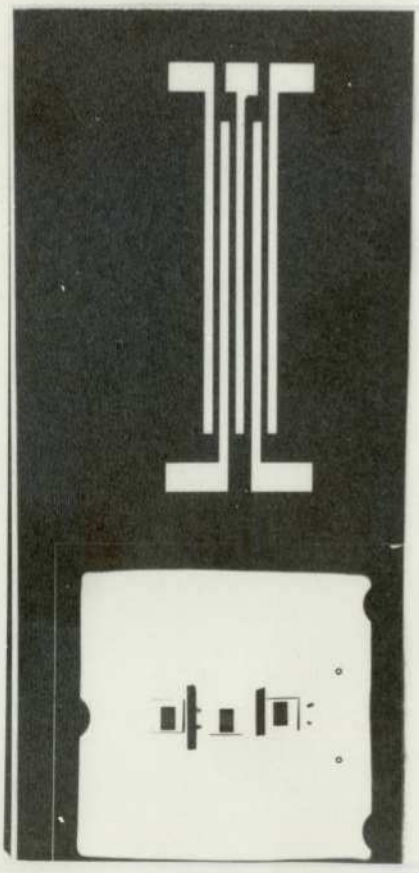


FIG 10.6d - 2^2mm ELECTRODES (0.05, 0.1, 0.2mm pitch).

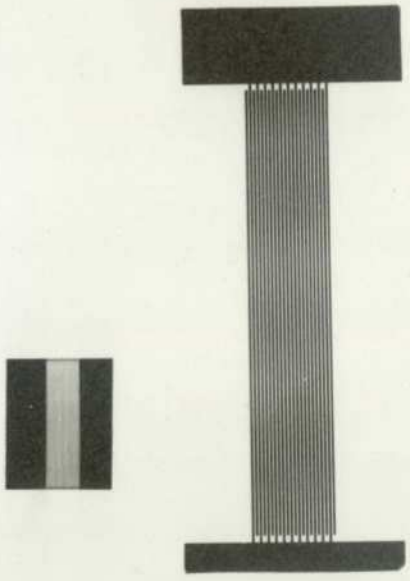


FIG 10.6e - Q-SWITCH ELECTRODES (Internegative & Final)

resolution limit was reached on the finest pitch grating and it proved necessary to use a 2"x2" glass final master to achieve good results.

Long electrodes for subsequent devices were made using the TCU photoreduction facility with mylar base film (Ilford N4E50) and a two stage reduction process. In order to avoid resolution problems caused by system imperfections only 0.2mm pitch devices were actually attempted. These were entirely sucessful.

Further masks were also made using Polaroid positive projection film. These were intended for the production of lecture slides and had a claimed 30 lp/mm resolution. Because achieved results were less than this, it was decided to use them for a secondary mask in conjunction with the GPO masks. These masks are illustrated in Figs.

10.1 METAL DEPOSITION

In the course of this work it was necessary to deposit electrodes onto substrates or crystals. Several techniques were available: electrodes could be painted, or, deposited through a mask; they could be placed on a substrate and brought into contact, or etched in a metal film. The latter two techniques were employed. Both approaches require a metal deposition and an etch. The deposition/photoresist operation can be approached from two sides. The electrode pattern negative can be placed on the crystal or substrate surface in photoresist and the deposition completed on top of this. Subsequent bathing in a photoresist solvent would cause the photoresist to swell and carry off the unwanted deposited metal resulting in only the desired electrode pattern being left behind. This method is fully described for surface wave device production (ref. H. Smith). The standard technique involves the deposition of a metal electrode film and a subsequent etching away of unwanted metal to leave the desired pattern behind. This approach was followed because of

the more uncritical nature of the process and because it was well tried. The reported deposition processes for lithium niobate or even glass were either gold or copper on chromium. It was felt that the chromium copper combination would offer a superior adhesion as the chromium oxygen bond is generally a strong one. In this respect a gold on chromium combination is just as good a solution to the adhesion problem experienced by several workers in this area (ref. Barringer). Using a vacuum deposited copper on chromium metal deposit, either on the crystal or a substrate, no untoward adhesion problems were experienced. It was found that the cleaning process was most effective with a detergent or caustic cleaning of the surface, followed by thorough washing and oven drying. Results obtained by boiling samples in trichlorethylene and postbaking were not as good. Drying marks were hard to avoid but were not found to affect the electrodes within the realm of the experiments involved. In general it was found most effective to avoid all contact with the surface after washing. Attempts to clean further with acetone or an ultrasonic cleaner were not found to improve results. Of all cleaning methods Decon 70 or Shipley Photoresist Remover (a fairly strong alkali) were found the most effective.

Vacuum deposition was found to present two operating problems:

(a) Evacuation difficulty

(b) Deposition thickness measurement.

The former difficulty could cause problems if a porous material such as asbestos, rubber, or even sticky tape was present in the chamber. The presence of unevaporated acetone or water could similarly slow down evacuation or even render it impossible. Evacuation was achieved by a two stage process: mechanical pumping (to ~ 0.01 cm mercury) followed by ion pump action to 10^{-5} cm . The ion pump stage was sensitive to poisoning by undue outgassing of the contents of the chamber, so it was necessary to maintain material cleanliness and that of the associated support hardware. For this reason crystals

were held by springs on a purpose designed aluminium mask and substrates were held by a wire frame at a distance of 10-15cm from the crucible and boat.

The measurement of deposited metal thickness was normally achieved by the use of a frequency determining quartz crystal with a known size of hole in its casing being placed among the samples to be plated. The crystal is made a part of an oscillating circuit where it is the frequency determining element. As metal is deposited, a mass is placed on the crystal and the oscillation frequency reduced. The metal thickness can then be evaluated from a knowledge of metal density and the frequency shift. This approach was found unreliable for the source to target distances involved, where the two sources (boat and crucible) deposited from different directions. This difficulty was not found to be important, as electrode thickness was not a critical factor and a visual assessment of chromium deposition, which was slow, proved quite sufficient. After a gradual outgassing of the tungsten filament (100mA, 1kV), the chromium was evaporated by electron bombardment (15mA, 3kV), until the target was visibly silvered. Then the molybdenum dc heated boat, which contained a pellet of pure copper was heated by a 90A current, and the boat contents evaporated off onto the sample (and elsewhere). During the relatively fast evaporation from the copper boat the chromium heater and anode supplies could be switched off. When the boat current had fallen to 80A, showing the copper to have been driven off and the boat resistance to have increased, the boat current was switched off and the system allowed to cool down, before being opened briefly for the extraction of the samples.

A typical deposition, measured by the crystal frequency shift method, gave ∿ 4kHz shift due to the Chromium and ∿ 50kHz due to the copper. As 1Hz → 1Å deposited of a material of density 1, this corresponds to 600 Å of chromium.

10.2 Photographic and Etch Processes

The metal deposited surface was coated with Shipley A21350 Positive-Working Photo-Resist (Semiconductor Grade) by a spinning process. This was done within half an hour of being taken out of the evaporator to avoid oxidation and contamination problems. The spinner was constructed from a shaded pole motor with a turntable, controlled by a Variac. Using a moistened soap holder, the substrate, or a substrate with crystal attached, was pressed onto the soap holder which was placed on the turntable. The resulting combination was then held in place by suction. The area to be etched was placed off the spin centre to ensure that the photoresist is thrown clear. The metal surface was then covered with AZ1350 from a syringe. No advantage was found in using a micropure filter and a Swinney Adaptor as the solids content of the photoresist was not a limiting factor as the resolution limit of ∿ 0.6 μ was not even being approached. A 120 second spin followed.

This phase was followed by an uncritical drying period for which a cool (40°C) oven was employed. A photomask of the electrode structure was then placed in intimate contact with the coated crystal or substrate surface and an ultra-violet exposure made. An aged sunray lamp (Pifco) was used for this purpose, giving a 10 minute exposure at a range of 40 cm. The development process involved a 45-60 second bath in Shipley developer (diluted 2:1) under conditions of agitation and a temperature of 15°C. The developed photoresist was

then dried and hardened at 90°C and the copper etched away with very dilute ferric chloride. (A 1+7 dilution of printed circuit etching strength). This was followed by a chrome etch composed of 5 ml sodium

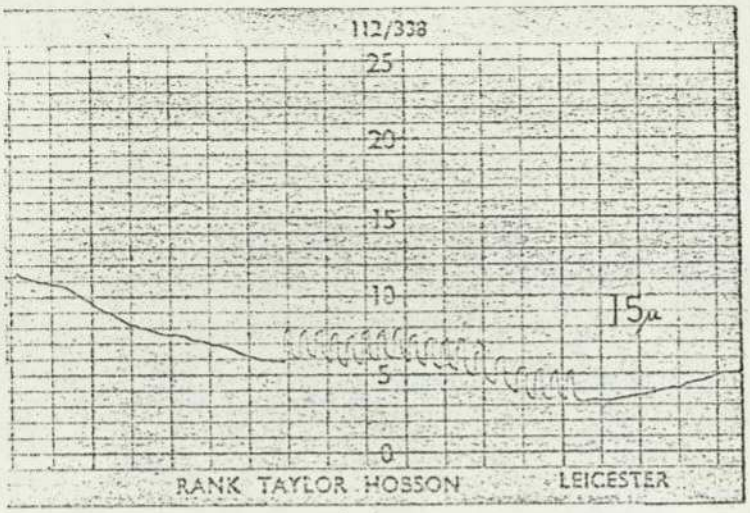


FIG.10.1 TALYSURF TRACE

hydroxide, 30 ml distilled H_2O, 10 gms potassium ferri-cyanide. The result is the etched electrode pattern as seen in Figure

A Talysurf trace from an electrode pattern etched on glass is shown in Figure 10.1 (A Rank Taylor Hobson Talysurf 4 was used). Only a rather thick chromium film was present in this case.

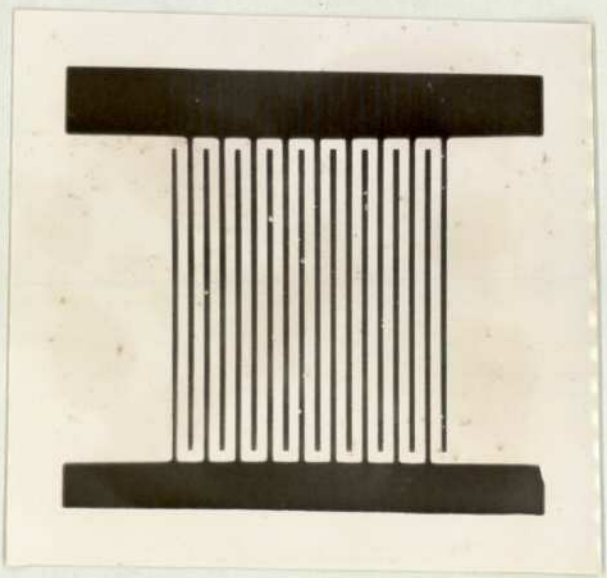


FIG 10.8

ETCHED ELECTRODES

(0.1mm pitch)

11. FURTHER WORK

A large further work range is included here as it is felt that a device with unique application has been born and only categorisation has been achieved. Almost the whole applications aspect, and the modification feeding back from practical usage, remains to be studied.

Device prospects are studied in two aspects;

(1) device development towards desirable characteristics, and

(2) novel device applications

DEVICE DEVELOPMENT

11.1 Infra-red Operation

Infra-red modulators and deflectors are relatively rare because operation voltages tend to be high and not all electro-optic materials offer a suitable window. TIR devices appear promising as the sine of inter-order angles varies linearly with the wavelength of light in the material. Because dispersion is not very large this relationship can be approximated by

$$\sin\theta \doteq n\lambda$$

Phase retardation generally varies as

$$\Gamma \propto \frac{2\pi}{\lambda} E r_{ij} n^3$$

and n, r and $1/\lambda$ are decreased with increasing incident wavelength with the major contribution from the $1/\lambda$ term, so that the necessary voltages increase. This effect can be counteracted by a reduction of electrode pitch to increase the value of E (and the inter-order angle). In this way 10.6μ modulator/deflectors which offer difficulties at present in cadmium telluride, gallium arsenide, or zinc sulphide may prove greatly advantageous used in a diffraction modulator form rather than a transverse form. It

should be noted that the values of E that the material needs to withstand are nearly equal, with the diffraction modulator about 18% less. This means that only a slight advantage, if any, could be expected if the materials limitation was that of surface breakdown. (Infra-red operation at 1.06μ is reported in section 6).

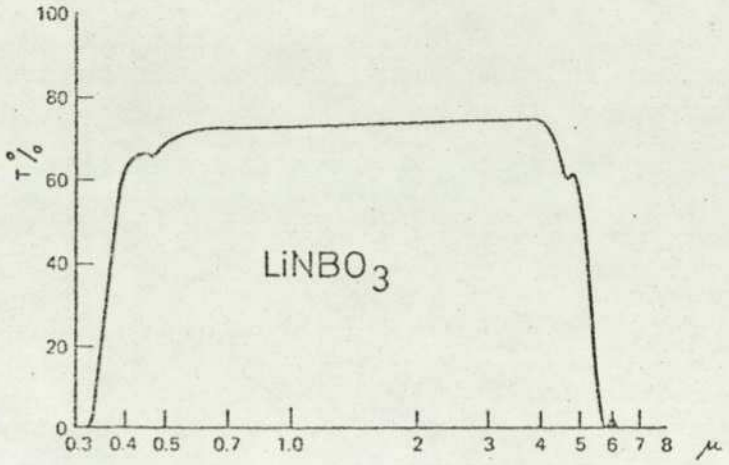


FIG. 11.1 SPECTRAL TRANSMISSION
(no a.r. coating)

11.2 Chromatic Considerations

Because the device operates in a diffraction mode there is a wavelength-sensitive dispersion effect in the non-zero orders.

$$\text{inter-order angle } \theta = \sin^{-1}\left(\frac{n\lambda}{d}\right)$$

In addition to this basic effect there are also the facts that

(1) refractive index of the material varies with wavelength e.g. Sellmeyer equation for Lithium Niobate

(2) retardation varies linearly with wavelength in the material.

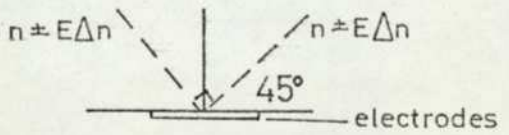
This causes the extinction voltage to vary with incident wavelength and suggests that extinction ratio in the zero-order

would suffer greatly in a white light case. This effect is not serious however because the characteristic sinc function is almost exponential at the zero-order extinction voltage (Vx) point and hence is not very sensitive to small Vx changes.

11.3 Criteria for an Unpolarised Light Device.

Two possible operation modes can be proposed and realised. Incident light can be considered to separate into orthogonal polarisations coinciding with the major and minor axes of the relevant index ellipse. These components create separate diffraction patterns in the far field. These patterns may be coincident, overlapping or separate, but no interference between them is possible because of the polarisation difference. Hence it is merely necessary to choose an orientation with identical performance in both polarisations. This can be achieved by many approaches:

(1) An orientation may be found in which the polarisations in the crystal are at 45° to the electrode plane. In this case the contribution of fields along both polarisation directions is equal so that if a symmetrical



plane of a crystal (such as the x/y plane in lithium niobate) is used such a device will exhibit unpolarised operation

(2) In cases where polarisations are parallel and normal to the electrode plane then effective field contributions, are dependent on crystal resistivities or permittivities and an incidence angle. In this case a device can be made with equal zero-order extinction voltages for transverse and normal field component excited electro-optic operation. In this case the resulting far field patterns will not be identical because of the difference in phase

wavefront shapes causing different far-field intensity characteristics for the two cases. Hence registration and tracking of the order intersities with excitation will never be exact for all orders simultaneously.

(3) The devices constructed from lithium niobate in the z/y and z/x orientation illustrate that another variable may be used to make an unpolarised light device from the transverse/normal orientations that have been studied. This variable is the incidence angle and this can be seen from inspection of a typical induced refractive index change for lithium niobate (Eqn. 4.58) in this case variation of

$$\Delta n = \frac{-E_z(\cos^2\theta\, r_{33} + \sin^2\theta\, r_{22}) + E_y \sin^2\theta\, r_{22}}{2(\cos^2\theta\, n_e^2 + \sin^2\theta\, n_o^2)^{3/2}}$$

causes the Ey contribution to increase and the E_z contribution to decrease. The orthogonal refractive index change in the other ellipse axes can be shown to be:

$$\Delta n = -\frac{n_o^3}{2}(r_{13}E_z + r_{22}E_y)$$

and is independent of θ . These quantities are equal for a value of θ where θ is approximately the solution of

$$\tan^2\theta = \frac{E_y r_{22} - E_z r_{33}}{E_z r_{13}}$$

This suggests that θ can be made of realisable proportions for suitable Ez/Ey combinations.

11.4 Far-Field Pattern Control

Control can be exercised on the far-field pattern in two ways:

(1) The crystal orientation can be altered to react with the available fields so as to change the far-field pattern by deflecting more or less energy into a given class of order. This is a symmetrical blazing action.

(2) The pattern may be affected assymetrically by an assymetrical electrode configuration. If adjacent electrodes are spaced unevenly, the phase wavefronts exhibit an even harmonic component and hence an assymetrical blazing

action is exhibited.

It is worth investigating the possibility of combining these two effects to approach the Bragg device type of operation which cannot be obtained from the TIR device because incident wavefronts cannot propagate through transverse index striations. Practical Bragg devices in acousto-optics often give ~60% energy in the first order. The symmetrical Raman-Nath case gives ~35% in each first order. It seems possible that performance could be improved to render performance comparable. At the time of writing no non-thin film electro-optic Bragg type device exists.

11.5 Uncollimated Light Operation

An extension of the preceding concept of electrode spacing variation can be employed to allow the device to operate with convergent or divergent light by making the electrode pitch to vary symmetrically across the aperture. Coarsest pitch would then be in the centre and finest at the edges of the device aperture for convergent incident light. In this way device operation can be made to exhibit the same zero-order extinction voltage over the whole aperture for a reasonably wide range of incidence angle. The effective loss of sensitivity experienced by misaligned rays is thus compensated for and a good extinction ratio assured.

11.6 Sub-Electrode Layers

As mentioned in the section on Q-switching, the value of a sub-electrode layer may be threefold:

(1) Possible breakdown at high power levels in the region of the electrodes may be avoided.

(2) Residual phase changes and their consequent contribution to insertion loss in non-quadratic materials can be eliminated.

(3) Materials on whom electrode fabrication poses

problems can be electroded normally.

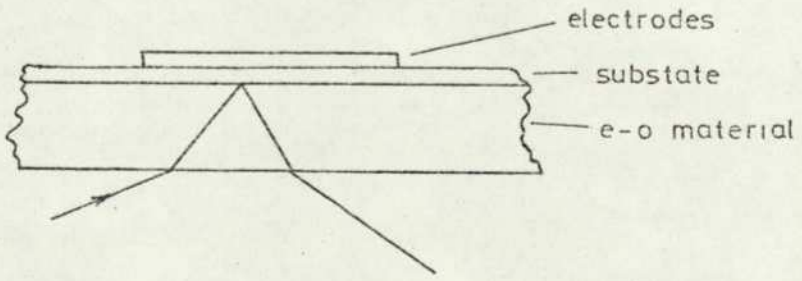
As penetration into the rarer medium is of the order of a wavelength, it is possible to apply an electrode sublayer without any significant deterioration in performance.

11.7 Use with Quadratic Material

The result of constructing a TIR device using quadratic material is to halve the effective phase wavefront pitch over the linear material case and hence double the sine of the inter-order angle. On top of this accrues the advantage of increasing sensitivity with applied voltage. As the use of very small quantities is readily achieved with TIR configurations, small samples of KTN can be used as very interesting devices.

11.8 Use of Thin Films

Thin film samples may be used for effective modulators using the TIR principle. Such samples may be achieved with low material cost and may even be assessed by the TIR method. Another possible advantage may be to allow the use of other otherwise ungrowable materials. As the film thickness need only be greater than or equal to half the electrode pitch, it is possible to use the fact that material volume usage is extremely low (eg. a 10mm . 5mm . 0.1mm pitch electrode area needs only 2.5mm . of material). Three possible device configurations are suggested in Fig.11.2 in order of increasing sensitivity:



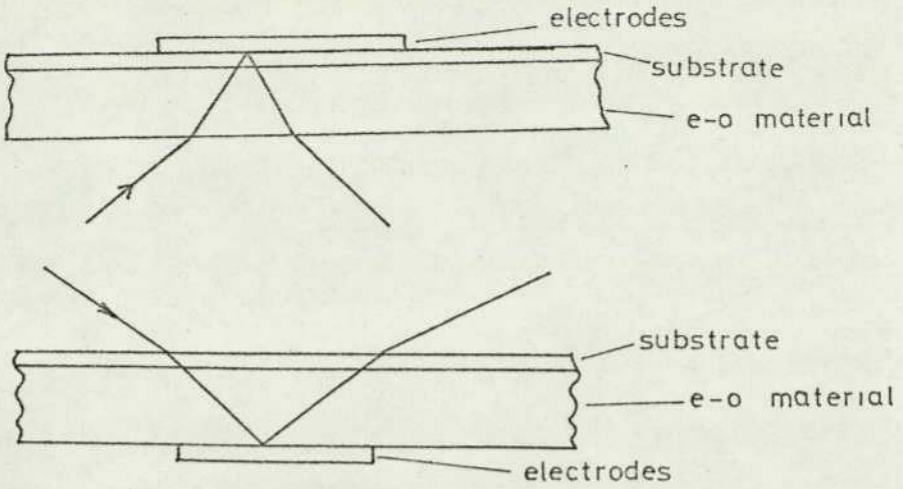


FIG. 11.2 THIN FILMS

11.9 Q-Switching Considerations

Apart from power handling considerations, two intra-cavity aspects of the device merit early analysis. The former is the possibility of mode control and the latter the possibility of reducing the CV^2 product, especially for continuous (low gain) laser operations.

(a) Mode Control: The operation of the device as a Q-switch is to deflect energy into off-axis directions. This may be directly harnessed at an intermediate level of excitation, and used as a variable mode stop or mode control as a slight excitation will enhance off axis orders and possibly raise the mode of operation of the laser. The Q-switch in section may be considered to work in this way in conjunction with a mode-stop.

(b) Reducing the CV^2 Product: It seems possible to Q-switch a continuous laser by only a partial spoiling (~8%?) within the cavity and this may be achieved with one or two electrode pitches so that a 40 volt 10pf device seems possible for, say, intracavity Helium Neon control, thereby offering excellent prospects of mode locking.

11.10 Access to Transistor Action

The electro-optic action of transistor materials may allow the interdigitated structure of HF transistors to be used for light modulation or the transistor action investigated by this method. The orientation of the crystal may prove a difficulty if unfavourable, and the illumination generated carriers may render this concept unworkable at some wavelengths. Nevertheless UHF modulation may be achieved by this means, using a new 4 terminal device.

11.11 Far-Field Pattern Changes

The Raman-Nath type pattern generated by the TIR device renders writing and reading uses impossible. A possible way of changing the far-field pattern is by a far or near field grating/hologram to alter the far-field variation with excitation to a more useful form. Such forms involve switching or preferably scanning.

Far-field changes can also be achieved by cascading devices, probably within the same crystal. In this way a far-field pattern may be synthesized by assembling a phase profile through subsequent TIR interactions. Alternatively a sequence of an X device followed by a Y device will give an interpretation when used for writing or reading.

11.12 A Controlled Thin FIlm Coupler

The effect of a transverse electrode configuration is very small because the light suffers only very small overall phase changes but the principle can be used (Fig.11.3) for an electro-optic thin-film coupler. This allows control on thin film coupling and is believed to be a unique application. Because unused light is not lost the principle could be used intra-cavity as a variable 'mirror' for output coupling.

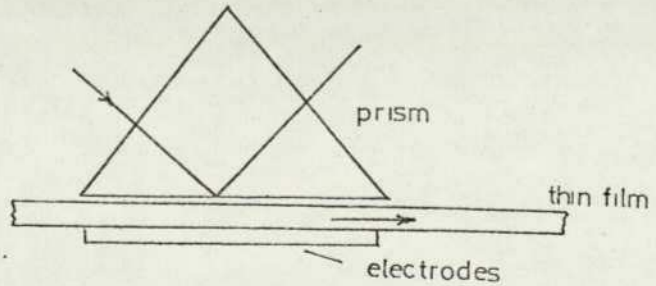


FIG. 11.3 COUPLER

11.13 FAR FIELD PATTERN INFORMATION CONTENT

Raman-Nath type devices do not find ready applications in information addressing and reading systems due to the complex nature of their far field patterns. These patterns, however, can be considered to contain information about the excitation applied to the device and can, therefore, be thought of as parallel 'words', associated with a given voltage. In this way the Raman-Nath device can be considered as an analogue-to-code conversion system. Unfortunately, the code is obscure and non-digital and translation is necessary. However, a coding system built on this principle would have excellent response speed, but only a small number of bits. Such a system would involve a TIR device, a PIN diode array, and MECL II type logic. Overall analogue to parallel word times would be < 5nS in this principle and words would be equivalent to about 3 binary bits.

It may prove promising to develop the signal/data processing applications of fast diffraction devices and make use of the Raman-Nath type pattern which has hitherto not been exploited.

ACKNOWLEDGEMENTS

The author wishes to acknowledge the considerable encouragement and support of Dr F C Widdis, who supervised this project and to extend grateful thanks to [redacted] for the use of GPO Research facilities. The author also wishes to thank [redacted] for consistent crystal preparation work of a very high standard. Thanks are also due to [redacted] of the City University, for their advice in the course of this work.

The author also wishes to acknowledge SRC support.

APPENDIX F1

COMPUTED PHASE PROFILES FOR THE TIR DEVICE AND THEIR FOURIER CONTENT

APPENDIX F1

This appendix includes information about the nature of the phase profiles for various configurations of the device. These phase profiles were computer generated by program GTWV and TGWV (Appendix P2) and the resultant profiles digitised into 20 points over one cycle (2d). This profile was then analysed by a Fixpac Fourier analysis program and run on a Ferranti FM1600B minicomputer. Output on a line plotter allowed a spatial harmonic content of the phase profile to be displayed. Of the options open in this program, the harmonics were chosen to be displayed in a logarithmic amplitude manner in order to enhance the information about the higher orders. As the phase profiles are symmetrical for aligned devices, even harmonics are obviously missing. (Waveform assymetry would indicate far field pattern assymetry).

The importance of the deviation of these profiles from the sinusoidal is the 'blazing' effect that accompanies the presence of harmonics. In such a case a class of order is enhanced or depleted without far field assymetry being introduced. In this appendix the significant phase profiles are shown and contrasted, together with their harmonic content. The 'blazing' action by device orientation or configuration changes is suggested by the following phase profiles and their associated spectra. Each phase profile is referred to an origin consistent with previous notation, zero is a midpoint between electrodes. Of the harmonics shown only the first few are of significance and a straight line plot from value to value is given, and not the usual 'comb' notation.

Fig.F1 and Fig.F2 show the theoretical thin film realisation in both orientations (normal and transverse fields). The harmonic contents vary considerably with the former case being a nearer approximation to the sinusoidal case. The nearest approximation of all to the sinusoidal case is shown

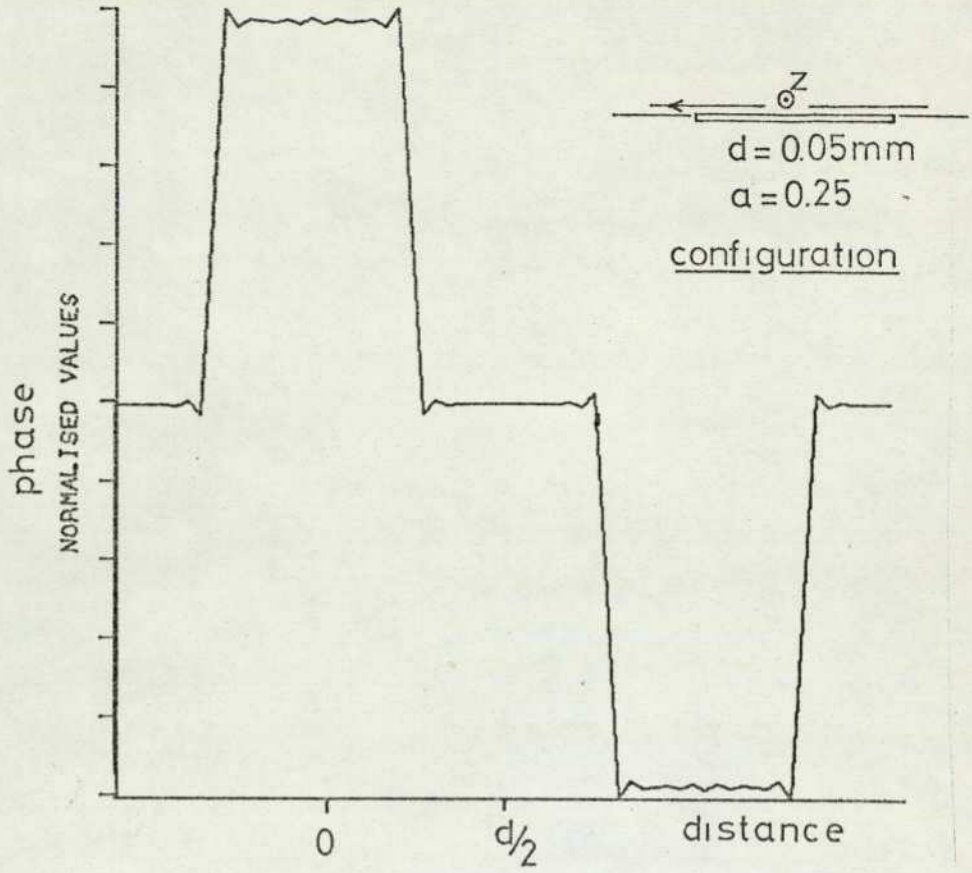
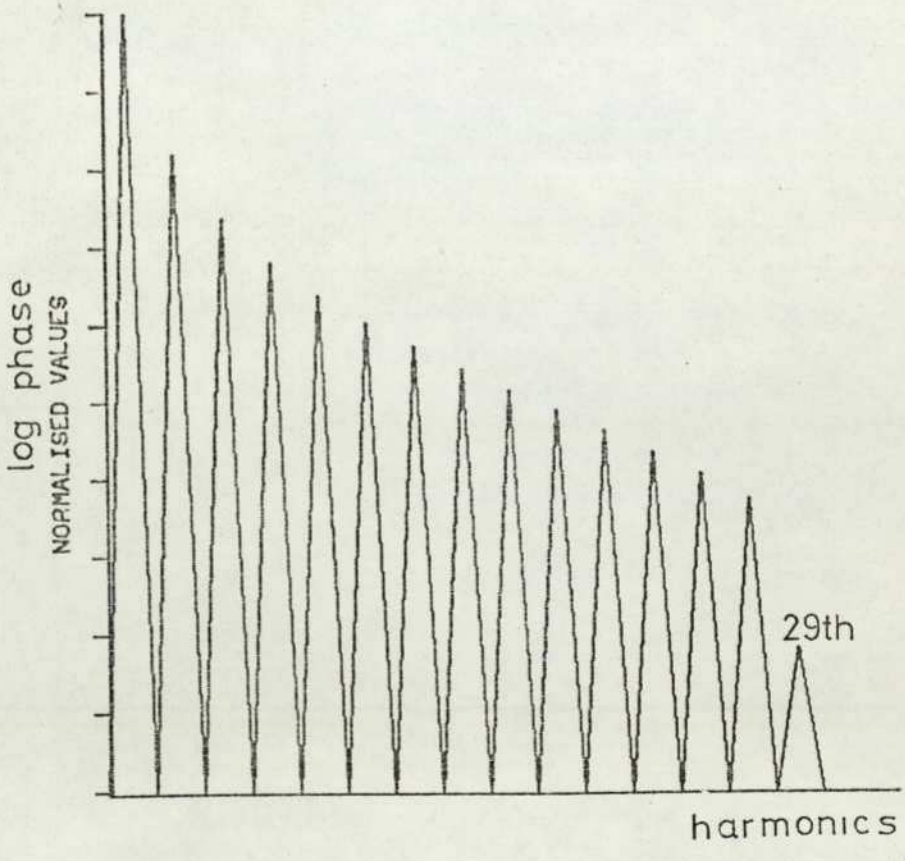


FIG.F1 PHASE PROFILES AND HARMONICS



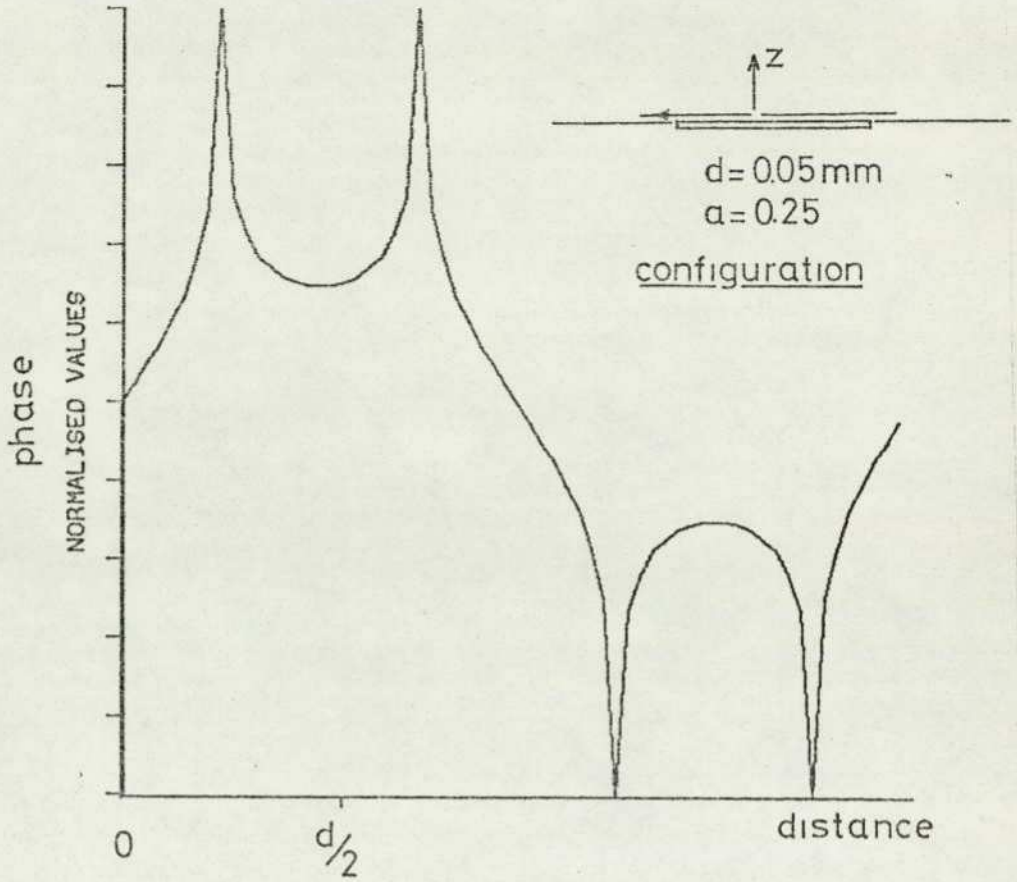
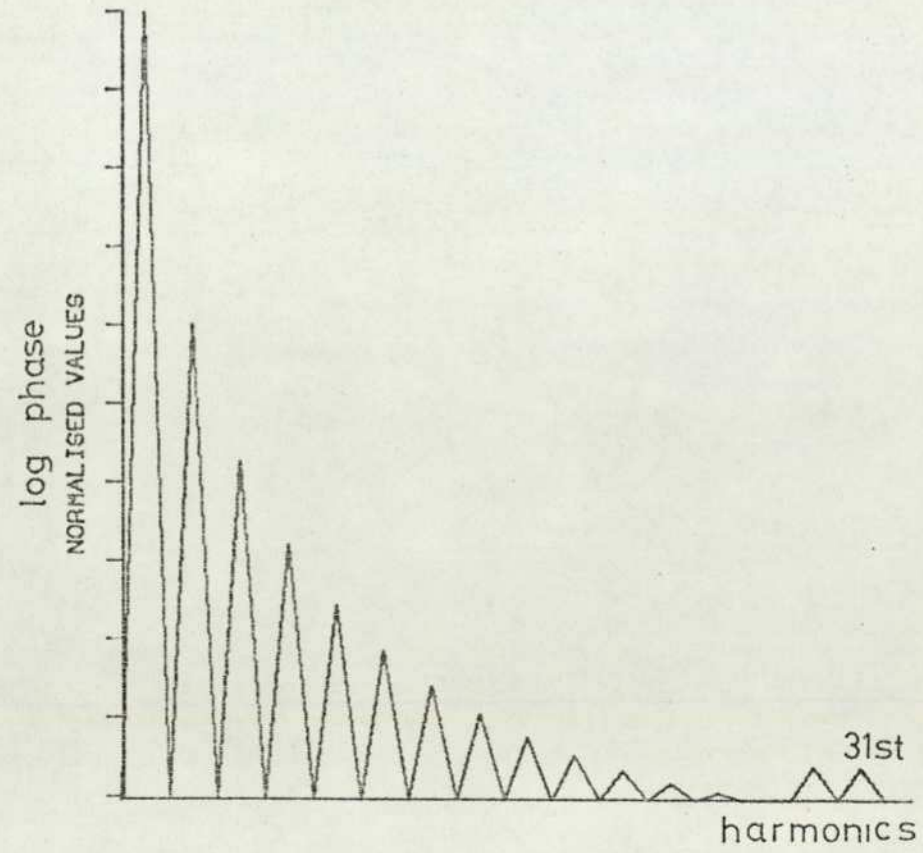


FIG. F2 PHASE PROFILES AND HARMONICS



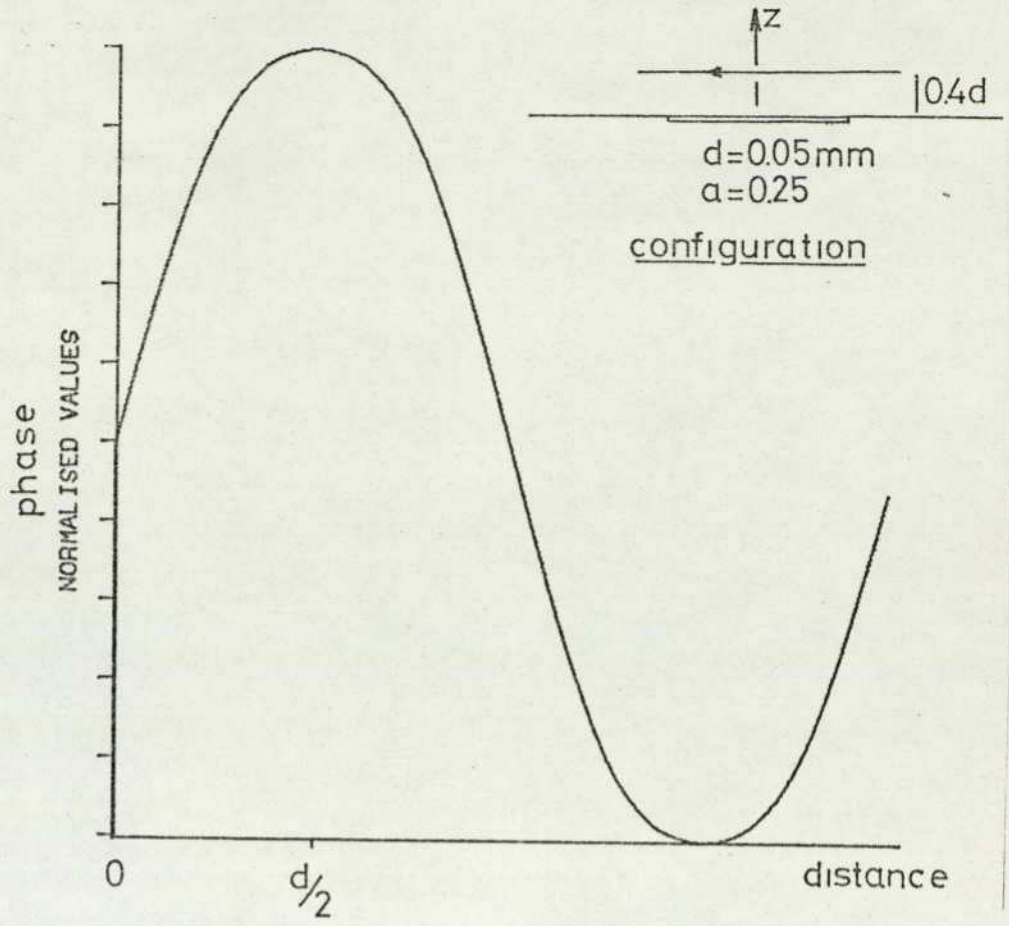
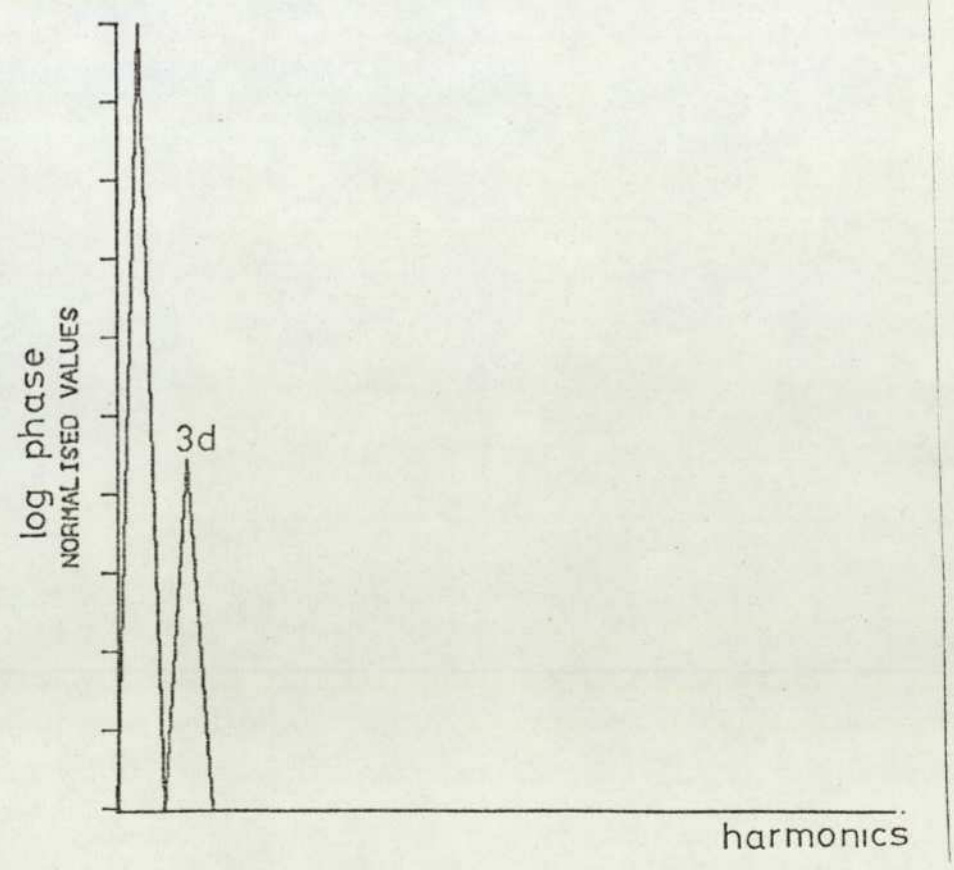


FIG.F3 PHASE PROFILES AND HARMONICS



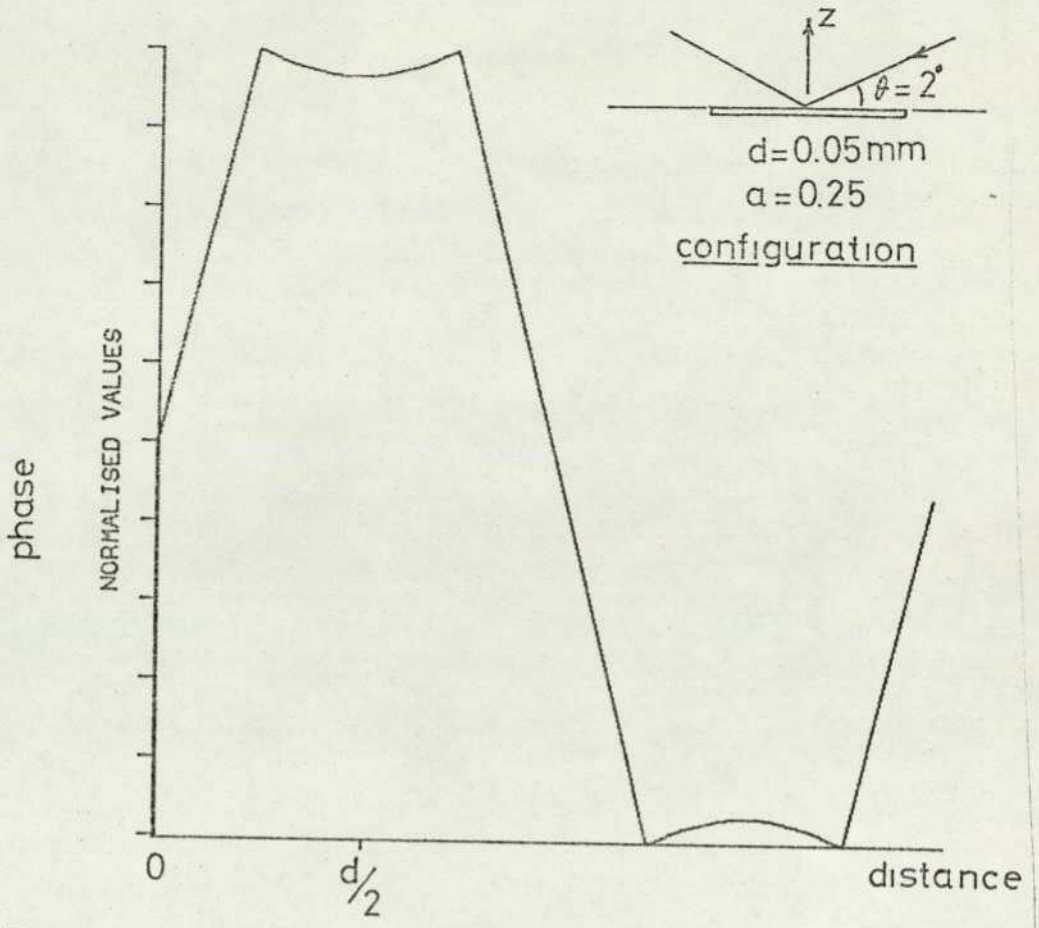
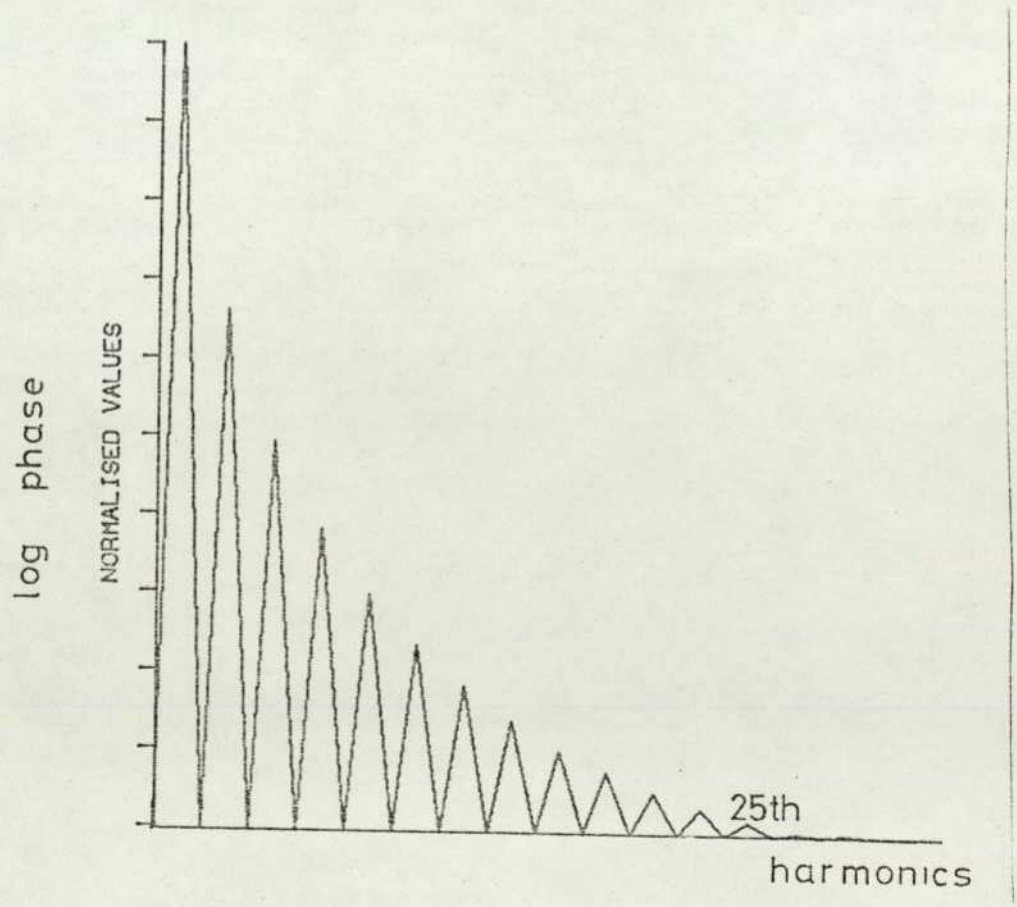


FIG.F4 PHASE PROFILE AND HARMONICS



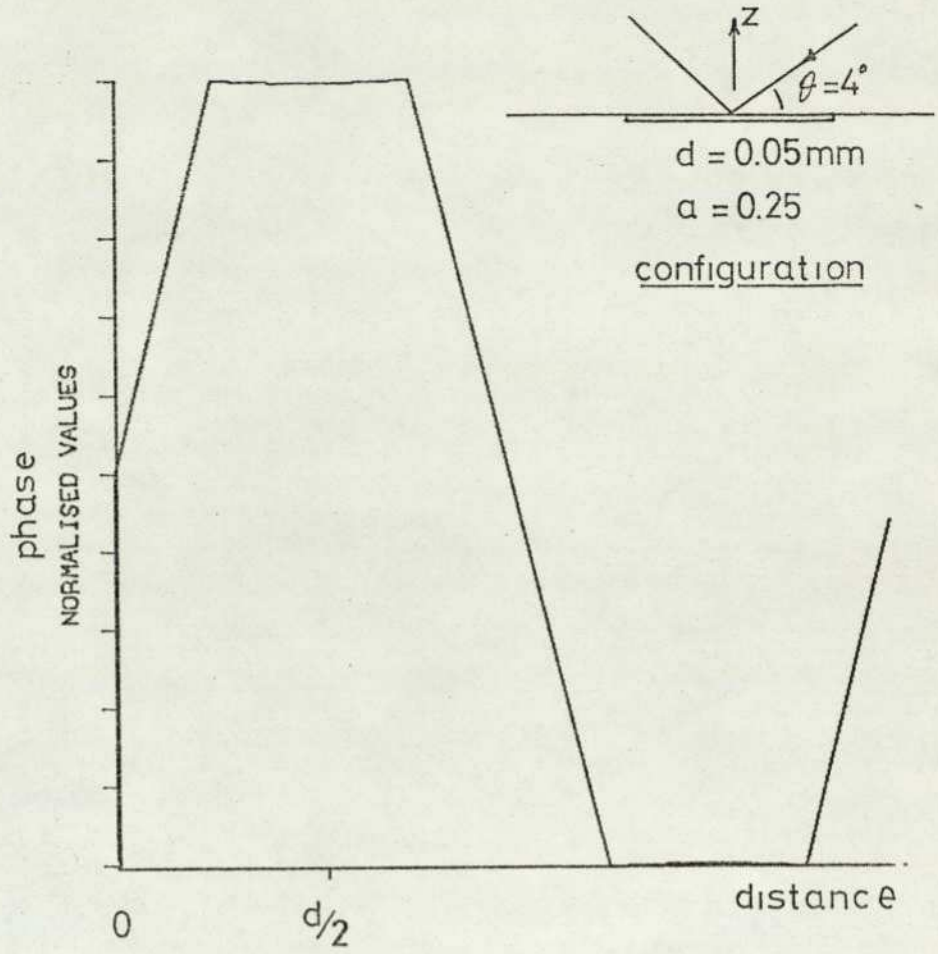
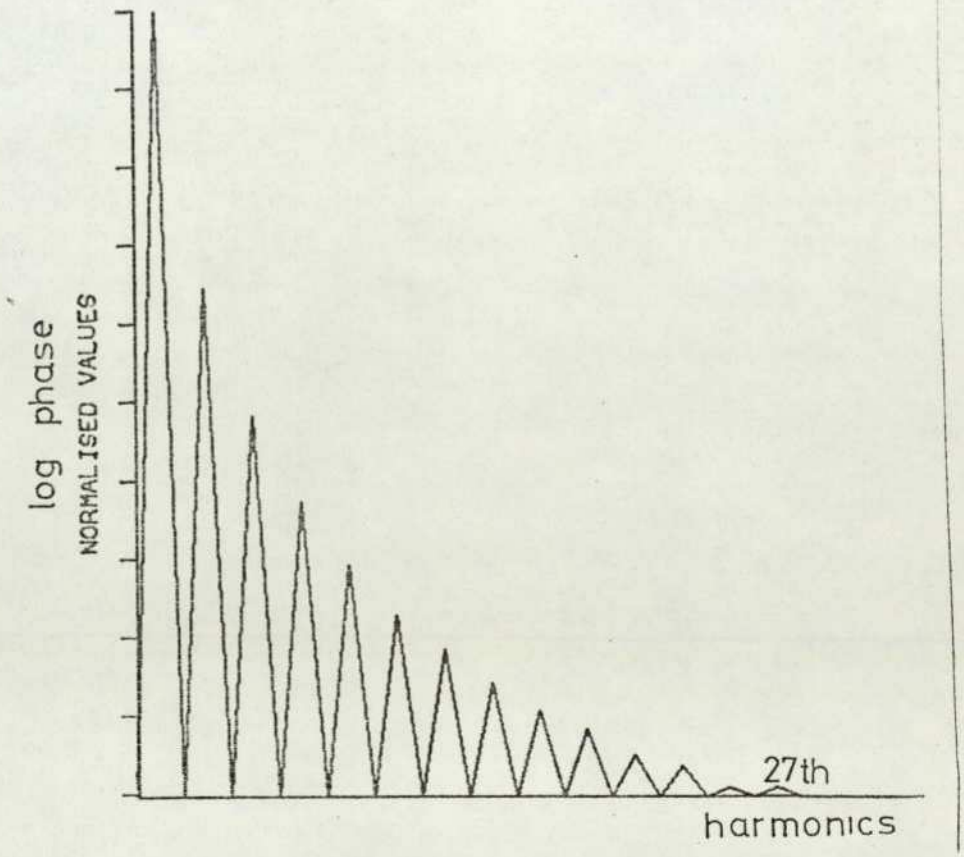


FIG.F5 PHASE PROFILES AND HARMONICS



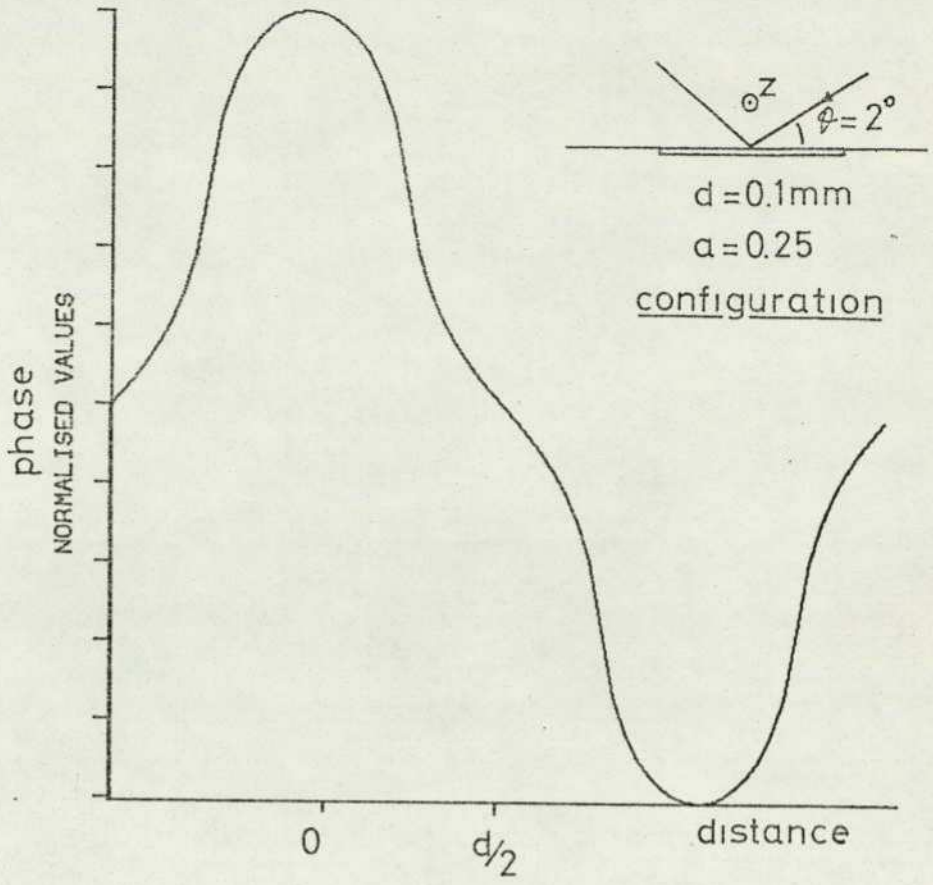
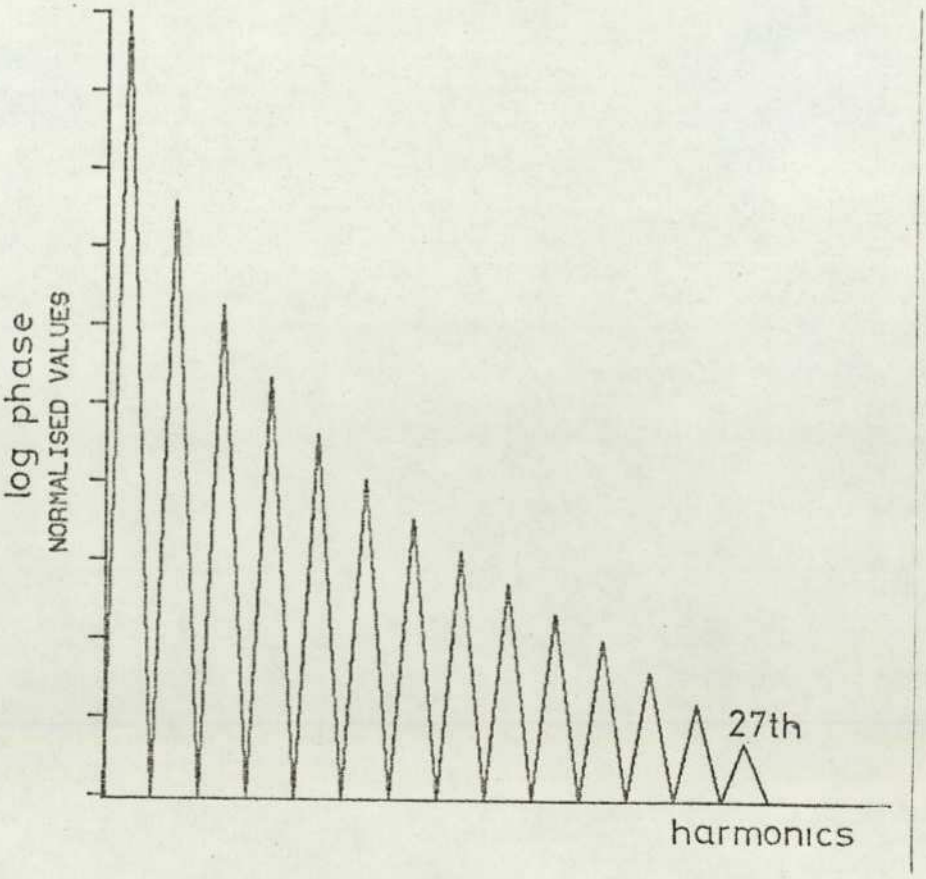


FIG. F6 PHASE PROFILES AND HARMONICS



in Fig. F3 , for the practical realisation of a normal orientation thin film device with a beam at a finite depth within the crystal. An insignificant 3d harmonic is indicated.

Fig. F4 and Fig. F5 compare practical TIR configurations in a normal field situation for two incidence angles (ϑ=2° & ϑ=4°). The qualitative difference is seen to be minimal. Fig. F 6 shows, for contrast, the transverse field case for ϑ=2° where there is a significant difference in harmonic content, compared in the other orientation. It can be seen that, as incidence (ϑ) increases, so the phase profiles tend to become smoother and more rounded, thereby reducing significant harmonic content. Fig. F 8 shows the effect of pitch on phase profile. Fig. F9 may be compared with Fig. F7 and Fig. F5 to illustrate the effect of reducing d from 0.2mm to 0.1mm and to 0.05mm.

Fig. F7 and Fig. F8 show the effect of a practical etch factor reducing the electrode aspect ratio. This parameter appears quite sensitive in affecting device operations as the harmonic content is varied considerably by this change.

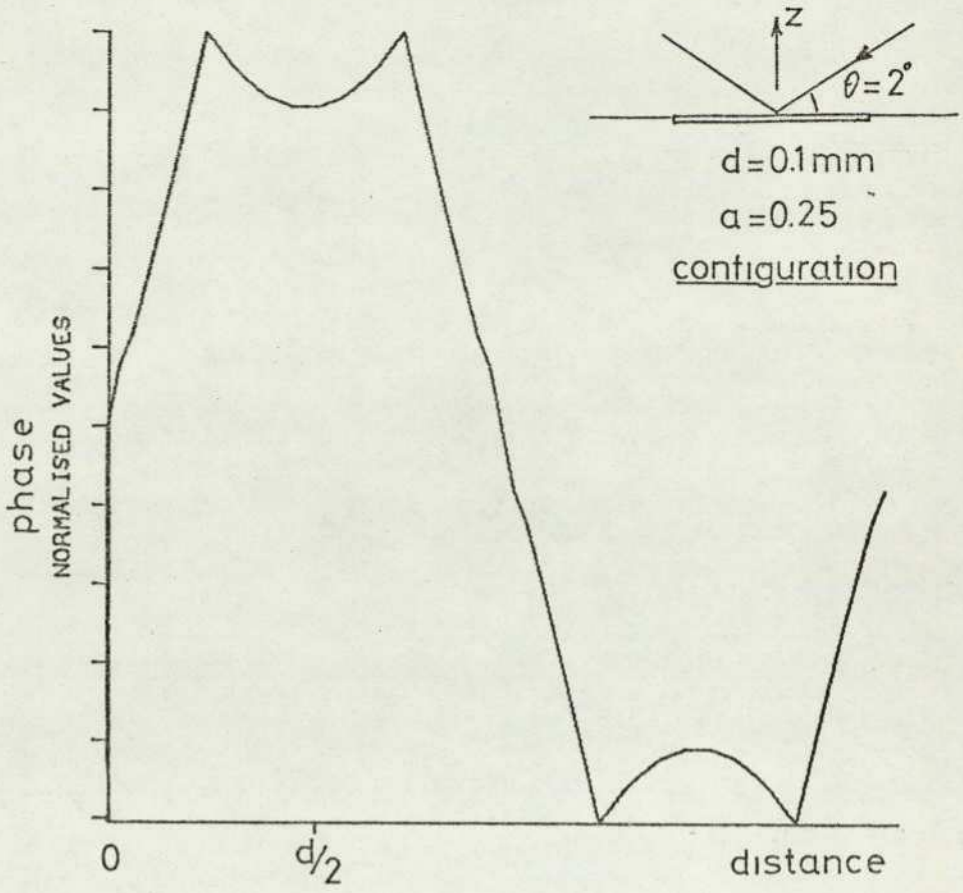
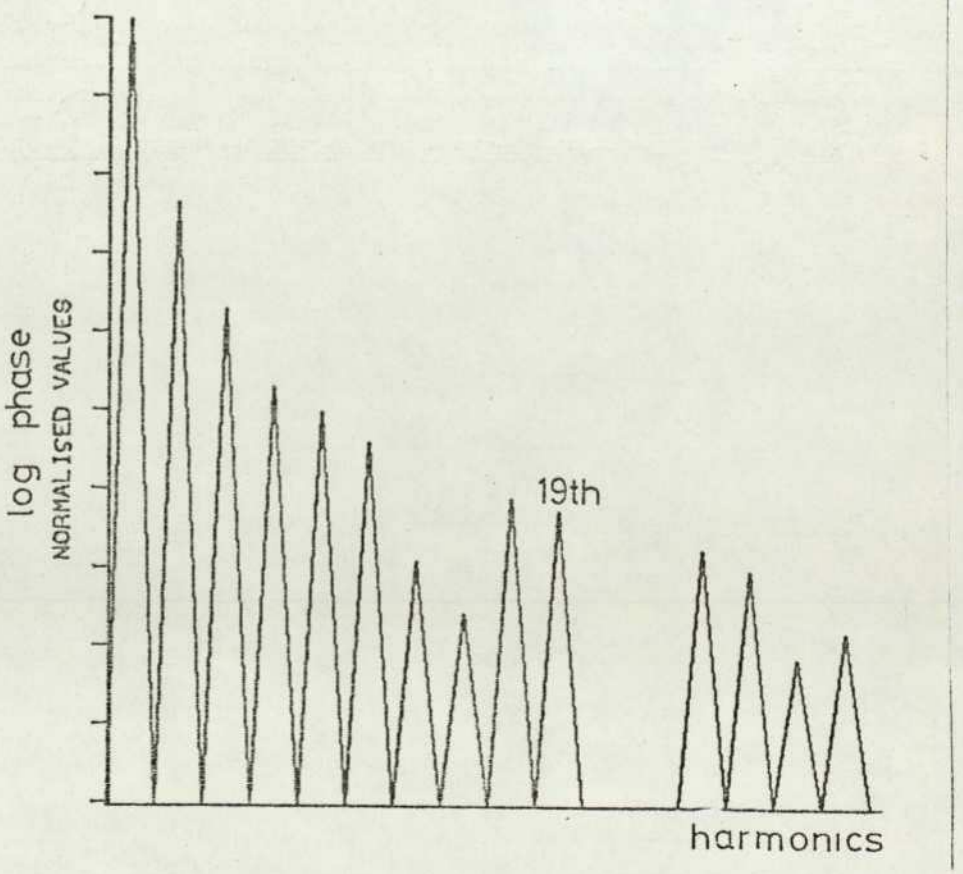


FIG.F7 PHASE PROFILES AND HARMONICS



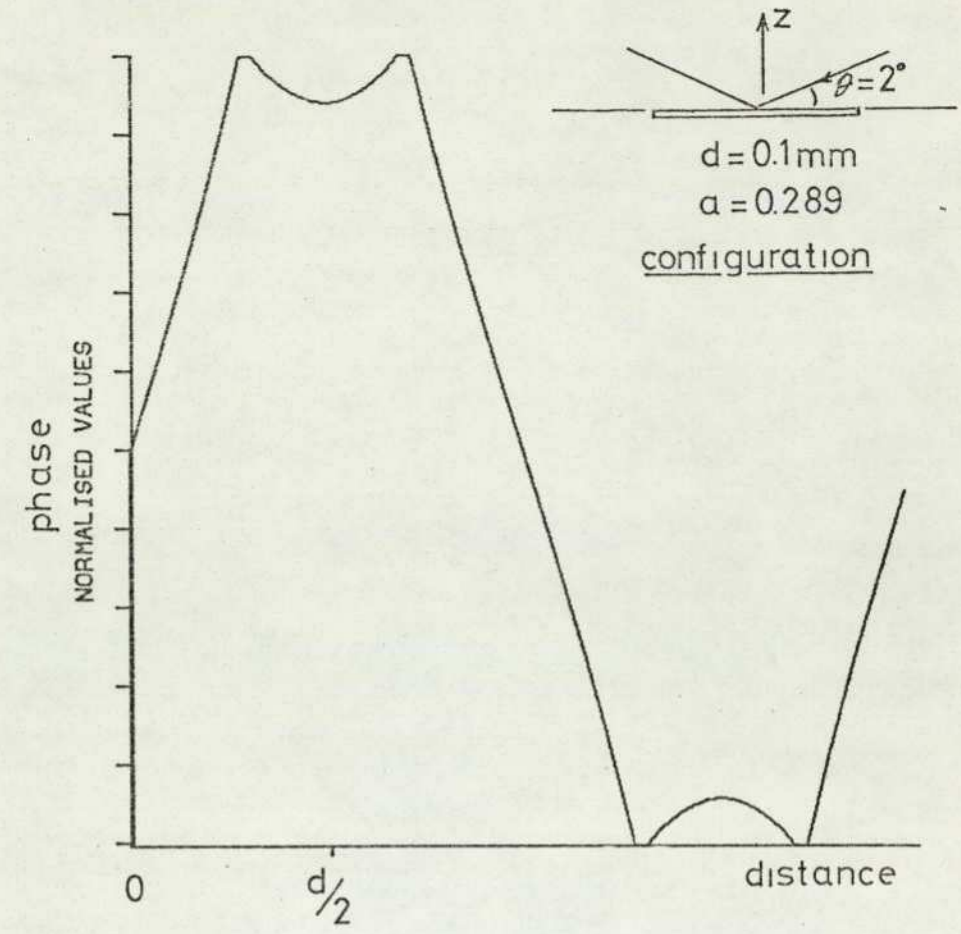
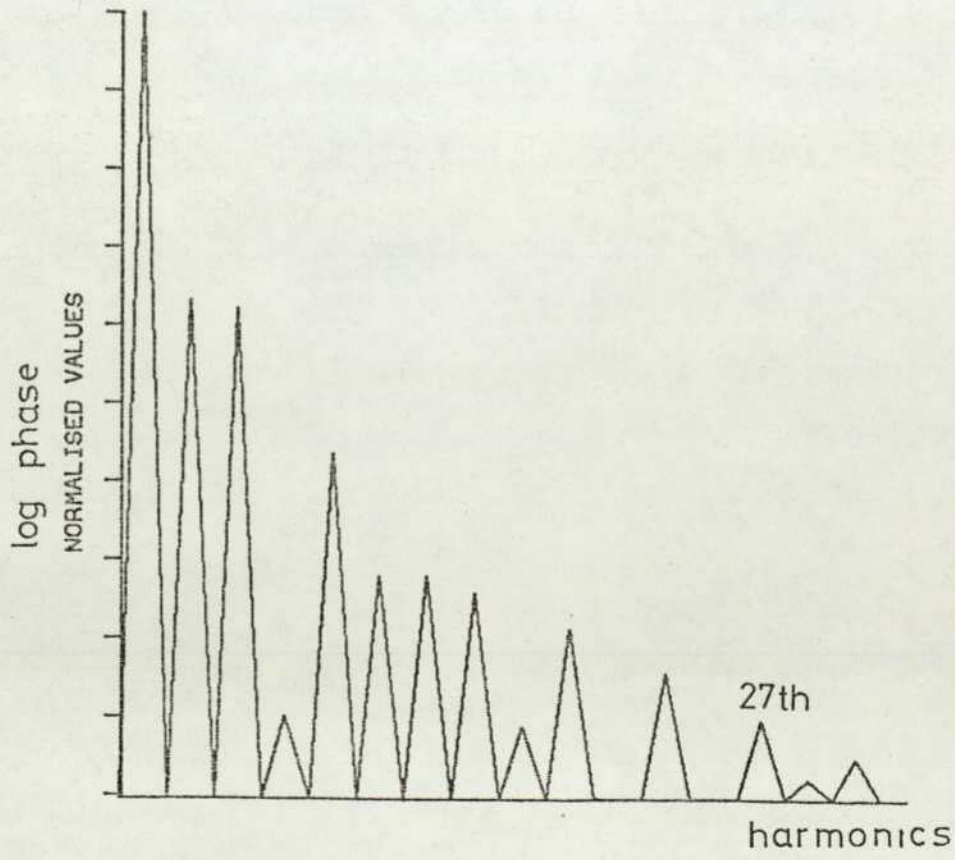


FIG. F8 PHASE PROFILES AND HARMONICS



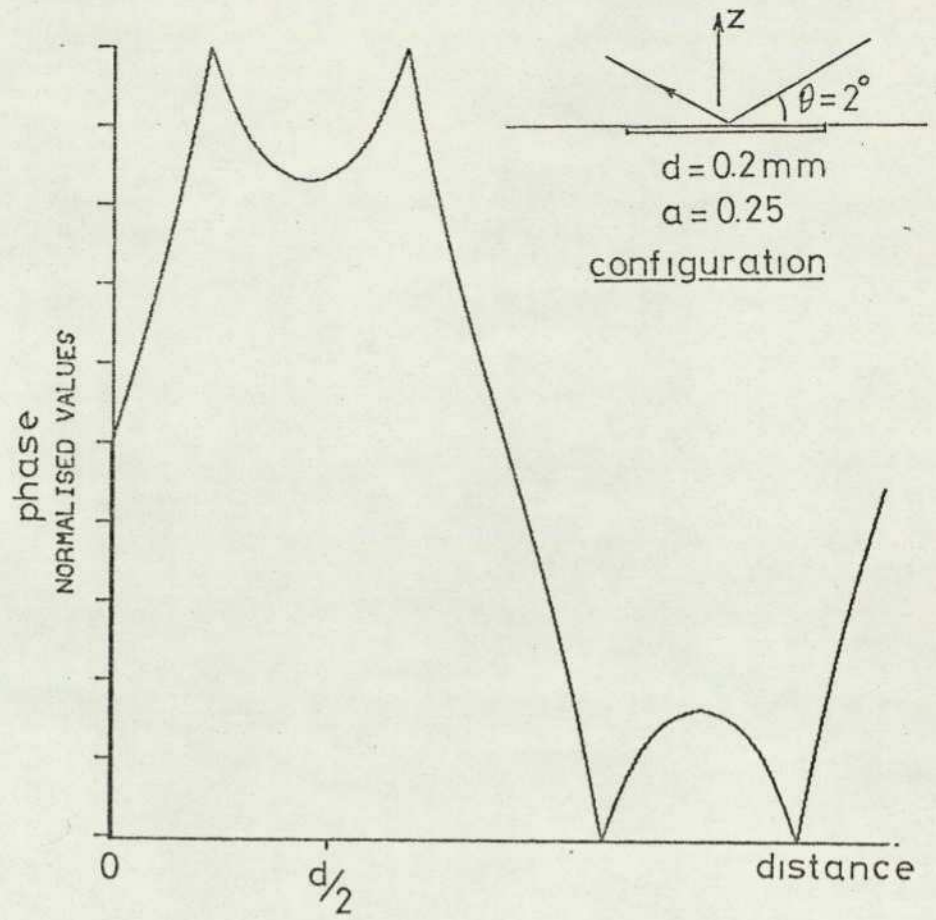
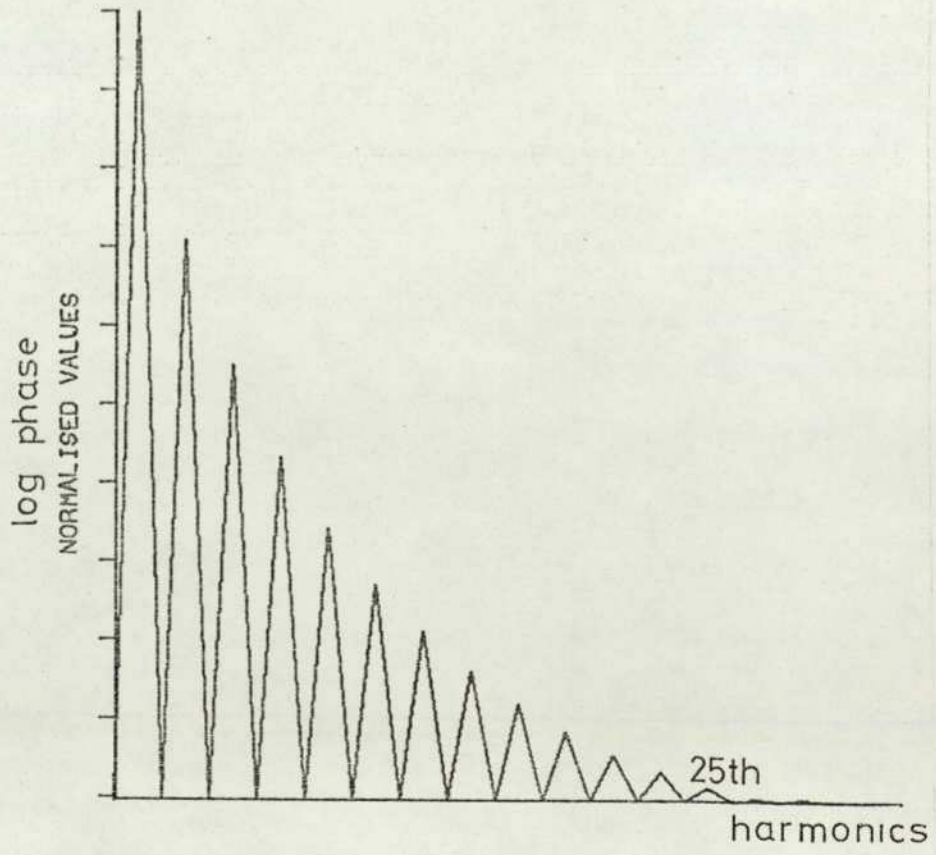


FIG.F9 PHASE PROFILES AND HARMONICS



APPENDIX P1

FIXPAC PROGRAMS

APPENDIX P1

Fixpac illustrative programs for section 2.

SLIT FUNCTION

PF1	$I_o f_1(\emptyset)$	where $f_1(\emptyset) = 1$
PF2	$I_o f_1(\emptyset)$	$f_1(\emptyset) = \cos \emptyset$
PF3	$I_o f_1(\emptyset)$	$f_1(\emptyset) = \frac{1+\cos \emptyset}{2}$

INTERFERENCE FUNCTION

PF4	I_1	by vector sum method
PF5	I_1	for linear amplitude incident profile.

INTERFERENCE FUNCTION - CONTROLLED SOURCES

PF6	I_1	adjacent controlled sources (ABAB)
PF7	I_1	adjacent controlled sources (AABB)
PF8	I_1	adjacent controlled sources (AAABBBAAA)

LENS TRANSFORM DEVICE CALCULATIONS

PF9	phase controlled (slope across whole array).
PF10	phase profiles at a phase near focus.

PF1

```
TEXT1P1E
*PI=
←S109
V16=V20
TEXT1P1E
  *S=
←S109
V3=V20
TEXT1P1E
  *WAVE=
←S109
V5=V20
V8=-90
TEXT1P1E
  *THETA(0)=
←S109
V6=V20*V16,SLF
FIXV20+0
V2=V20
V13=180
FLTV13+0
V20=V6/V13,SLF
←S319
V7=V20
V12=V13
V13=0
V10=V10+15
[8]V10=V8
FLTV10+0
V12=180
FLTV12+0
←3,V2-V8=0
V17=V10*V16,SLF
V20=V17/V12,SLF
←S319
V9=V20-V7,SLF
V10=V9*V16,SLF
V10=V10/V5,SLF
V20=V10*V3,SLF
←S319
V10=V20/V10,SLF
V10=V10/V3,SLF
V14=V10*V10,SLF
←7
[3]V14=1
FLTV14+0
[7]V11=1000
FLTV11+0
V14=V14*V11,SLF
FIXV14+0
V8=V8+1
V15=V8*10.I
V23=20
←S84
←8,V8-91<0
V23=10
V15=15
V14=0
←S84
[9]←S5
2000 0 0 31
←9
END

Z

A
```

PF2

```
TEXT1P1E
*PI=
←S109
V16=V20
TEXT1P1E
  *S=
←S109
V3=V20
TEXT1P1E
  *WAVE=
←S109
V5=V20
V8=-90
TEXT1P1E
  *THETA(0)=
←S109
V6=V20*V16,SLF
FIXV20+0
V2=V20
V13=180
FLTV13+0
V20=V6/V13,SLF
←S319
V7=V20
V12=V13
V13=0
V10=V10+15
[8]V10=V8
FLTV10+0
V12=180
FLTV12+0
←3,V2-V8=0
V17=V10*V16,SLF
V20=V17/V12,SLF
V13=V20
←S319
V9=V20-V7,SLF
V10=V9*V16,SLF
V10=V10/V5,SLF
V20=V10*V3,SLF
←S319
V10=V20/V10,SLF
V10=V10/V3,SLF
V14=V10*V10,SLF
←7
[3]V14=1
FLTV14+0
[7]V11=1000
FLTV11+0
V14=V14*V11,SLF
V20=V13
←S319,1
V10=1
FLTV10+0
V11=V10*V20,SLF
V14=V14*V11,SLF
V10=2
FLTV10+0
V14=V14/V10,SLF
FIXV14+0
V8=V8+1
V15=V8*10.I
V23=20
←S84
←8,V8-91<0
V23=10
V15=15
V14=0
←S84
[9]←S5
2000 0 0 31
←9
END

Z

A
```

PF3

```
TEXT1P1E
*PI=
←S109
V16=V20
TEXT1P1E
  *S=
←S109
V3=V20
TEXT1P1E
  *WAVE=
←S109
V5=V20
V8=-90
TEXT1P1E
  *THETA(0)=
←S109
V6=V20*V16,SLF
FIXV20+0
V2=V20
V13=180
FLTV13+0
V20=V6/V13,SLF
←S319
V7=V20
V12=V13
V13=0
V10=V10+15
[8]V10=V8
FLTV10+0
V12=180
FLTV12+0
←3,V2-V8=0
V17=V10*V16,SLF
V20=V17/V12,SLF
V13=V20
←S319
V9=V20-V7,SLF
V10=V9*V16,SLF
V10=V10/V5,SLF
V20=V10*V3,SLF
←S319
V10=V20/V10,SLF
V10=V10/V3,SLF
V14=V10*V10,SLF
←7
[3]V14=1
FLTV14+0
[7]V11=1000
FLTV11+0
V14=V14*V11,SLF
V20=V13
←S319,1
V10=1
FLTV10+0
V11=V10*V20,SLF
V14=V14*V11,SLF
V10=2
FLTV10+0
V14=V14/V10,SLF
FIXV14+0
V8=V8+1
V15=V8*10.I
V23=20
←S84
←8,V8-91<0
V23=10
V15=15
V14=0
←S84
[9]←S5
2000 0 0 31
←9
END

Z

A
```

PF4

```
V8=V8+1
V15=V8
FLTV15+0
FIXV15+0
V23=20
←S84
V9=900
←8,V8-V9<0
V23=10
V15=0
V14=0
←S84
[9]←S5
200000 0 0 31
←9
END
```

PF5

```
V1=V20
V2=V20
V3=V20
V6=V20
V7=V20
V1=V1
V2=0
V3=10
FLTV3+0
V6=0
FLTV6+0
V10=V10/V15,SLF
V15=0
V12=180
FLTV12+0
V17=V10+V16,SLF
V20=V17/V12,SLF
←S319
V7=V7+V20,SLF
V9=V2*V9,SLF
V5=V9/V5,SLF
V9=V9+V16,SLF
V10=2
FLTV10+0
V9=V9*V10,SLF
V11=1
V12=-V9
V17=V4
FIXV17+0
[4]V12=V12+V9,SLF
V20=V12
V13=1
FLTV13+0
V10=V13/V4,SLF
V13=V10*V11,SLF
FLTV11+0
V13=V13*V11,SLF
FIXV11+0
V10=V10-V13,SLF
←S319,1
V13=V10*V20,SLF
V15=V15+V13,SLF
V20=V12
←S319
V13=V10*V20,SLF
V6=V6+V13,SLF
V11=V11+1
←4,V17-V11>0
V10=V15*V15,SLF
V14=V6*V6,SLF
V14=V14+V10,SLF
V9=1000
FLTV9+0
V14=V14*V9,SLF
FIXV14+0
V8=V8+1
V15=V8
FLTV15+0
FIXV15+0
V23=20
←S84
V9=900
←8,V8-V9<0
V23=10
V15=0
V14=0
←S84
[9]←S5
2000 0 0 31
←9
END
```

```
TEXT1P1E
 *PI=
←S109
V2=V20
TEXT1P1E
*THETA(0)(1)=
←S109
V3=V20
TEXT1P1E
*THETA(0)(2)=
←S109
V4=V20
TEXT1P1E
*D=
←S109
V5=V20
TEXT1P1E
*N=
←S109
V6=V20
TEXT1P1E
*WAVE=
←S109
V11=V20
TEXT1P1E
*DEL=
←S109
V12=V20
V7=-900
V18=0
[8]V20=V3*V2,SLF
V8=180
FLTV8+0
V20=V20/V8,SLF
←S319
V9=V20
V10=10
FLTV10+0
V20=V7
FLTV20+0
V10=V20/V10,SLF
V10=V10*V2,SLF
V20=V10/V8,SLF
←S319
V9=V9+V20,SLF
V10=V20
V20=V4*V2,SLF
V20=V20/V8,SLF
←S319
V10=V10+V20,SLF
V9=V9*V5,SLF
V10=V10*V5,SLF
V9=V9/V11,SLF
V10=V10/V11,SLF
V8=2
FLTV8+0
V9=V9*V8,SLF
V9=V9*V2,SLF
V9=V9*V8,SLF
V13=V12*V8,SLF
V13=V13*V2,SLF
V10=V10*V2,SLF
V10=V10*V8,SLF
V13=V10+V13,SLF
V10=V10*V8,SLF
V8=1
FLTV8+0
V17=V8/V6,SLF
V16=1
V20=V13
←S319,1
V14=V20*V17,SLF
V14=V14+V17,SLF
V20=V13
←S319
V15=V20*V17,SLF
V8=2
FLTV8+0
V6=V6/V8,SLF
FIXV6+0
V6=V6-1
←4,V6=0
[3]FLTV16+0
V20=V16*V9,SLF
  ←S319,1
V8=V20*V17,SLF
V20=V16*V10,SLF
V20=V20+V13,SLF
←S319,1
V20=V20*V17,SLF
V20=V8+V20,SLF
V14=V14+V20,SLF
V20=V16*V9,SLF
←S319
V8=V20*V17,SLF
V20=V16*V10,SLF
V20=V20+V13,SLF
←S319
V20=V20*V17,SLF
V20=V8+V20,SLF
V15=V15+V20,SLF
FIXV16+0
V16=V16+1
←3,V6-V16>0
[4]V6=V6+1
FLTV6+0
V8=2
FLTV8+0
V6=V6*V8,SLF
V17=1000
FLTV17+0
V8=V14*V    LF
V9=V15*V15,  LF
V14=V8+V9,SLF
V14=V14*V17,SLF
FIXV14+0
V15=V7
V7=V7+1
V23=20
←S84
←8,V7-901<0
V23=10
V15=0
V14=0
←S84
[9]←S5
2000 0 0 31
←9
END

Z

A
```

PF 7

```
TEXT1P1E
 *P1=
←S109
V2=V20
TEXT1P1E
*THETA(0)(1)=
←S109
V3=V20
TEXT1P1E
*THETA(0)(2)=
←S109
V4=V20
TEXT1P1E
*D=
←S109
V5=V20
TEXT1P1E
*N=
←S109
V6=V20
TEXT1P1E
*WAVE=
←S109
V11=V20
TEXT1P1E
*DEL=
←S109
V12=V20  ?1
V7=-900
V18=0
[8]V20=V3*V2,SLF
V8=180
FLTV8+0
V30-V20/V8,SLF
←S319
V9=V20
V10=10
FLTV10+0
V20=V7
FLTV20+0
V10=V20/V10,SLF
V10=V10*V2,SLF
V20=V10/V8,SLF
←S319
V9=V9+V20,SLF
V10=V30
V30=V4*V2,SLF
V20=V30/V8,SLF
←S319
V10=V10+V20,SLF
V9=V9*V5,SLF
V10=V10*V5,SLF
V9=V9/V11,SLF
V10=V10/V11,SLF
V8=0
FLTV8+0
V9=V9*V8,SLF
V8=V8*V2,SLF
V12=V12  ?2
V13=V12*V8,SLF
V13=V13*V2,SLF
V10=V10*V2,SLF
V10=V10*V8,SLF
V8=1
FLTV8+0
V17=V8/V6,SLF
V16=0
FIXV8+0
V6=V6-1
V14=0
V15=0
V8=V12
V12=0
[3]FLTV16+0
←3,V12-1=0
V20=V16*V9,SLF
←S319,1
V21=V20*V17,SLF
V20=V15*V8,SLF
←S319
V20=V20*V17,SLF
V20=1  ?4
FLTV20+0
V16=V16+V20,SLF
V20=V16*V9,SLF
←S319,1
V20=V20*V17,SLF
V15=V15+V20,SLF
V15=V15+V21,SLF
V20=V16*V9,SLF
←S319
V20=V20*V17,SLF
V14=V14+V20,SLF
V14=V14+V23,SLF
V20=1
FLTV20+0
V16=V16+V20,SLF
V10=1
←6
[5]V20=V16*V10,SLF
V13=V13  ?3
V20=V20+V13,SLF
←S319,1
V31=V20*V17,SLF
V20=V16*V10,SLF
V20=V20+V13,SLF
←S319
V23=V20*V17,SLF
V20=1
FLTV20+0
V16=V16+V20,SLF
V20=V16*V10,SLF
V20=V20+V13,SLF
←S319,1
V30=V20*V17,SLF
V16=V16+V20,SLF
V15=V15+V21,SLF
V20=V16*V10,SLF
V20=V20+V13,SLF
←S319
V30=V20*V17,SLF
V14=V14+V30,SLF
V14=V14+V23,SLF
V20=1
FLTV20+0
V16=V16+V20,SLF
V12=0
[6]FIXV16+0
←3,V6-V16>0
V12=V8
V6=V6+1
FLTV6+0
V17=1000
FLTV17+0
V8=V14*V14,SLF
V9=V15*V15,SLF
V14=V8+V9,SLF
V14=V14*V17,SLF
FIXV14+0
V15=V7
V7=V7+1
V23=20
←S84
←3,V7-901<0
V20=10
V15=0
V14=0
←S84
[9]←S5
2000 0 0 31
←9
END

Z

A
```

```
TEXT1P1E
 *P I=
←S109
V2=V20
TEXT1P1E
*THETA(0)(1)=
←S109
V3=V20
TEXT1P1E
*THETA(0)(2)=
←S109
V4=V20
TEXT1P1E
*D=
←S109
V5=V20
TEXT1P1E
*N=
←S109
V6=V20
TEXT1P1E
*WAVE=
←S109
V11=V20
TEXT1P1E
*DEL=
←S109
V12=V20
V7=-900
V18=0
[8]V20=V3*V2,SLF
V8=180
FLTV8+0
V20=V20/V8,SLF
←S319
V9=V20
V10=10
FLTV10+0
V20=V7
FLTV20+0
V10=V20/V10,SLF
V10=V10*V2,SLF
V20=V10/V8,SLF
←S319
V9=V9+V20,SLF
V10=V20
V20=V4*V2,SLF
V20=V20/V8,SLF
←S319
V10=V10+V20,SLF
V9=V9*V5,SLF
V10=V10*V5,SLF
V9=V9/V11,SLF
V10=V10/V11,SLF
V8=2
FLTV8+0
V9=V9*V8,SLF
V9=V9*V2,SLF
V13=V12*V9,SLF
V13=V13*V2,SLF
V10=V10*V2,SLF
V10=V10*V8,SLF
V8=1
FLTV8+0
V17=V8/V5,SLF
V16=0
FIXV6+0
V6=V6-1
V14=0
V15=0
V8=V12
V12=0
[3]←12,V6-V16>0
FLTV16+0
←5
[12]FLTV16+0
←5,V12=0
V20=V16*V9,SLF
←S319,1
V21=V20*V17,SLF
V20=V15*V9,SLF
←S319
V23=V20*V17,SLF
V20=1  ?1
FLTV20+0
V15=V15+V20,SLF
V20=V16*V9,SLF
←S319,1
V20=V20*V17,SLF
V15=V15+V20,SLF
V15=V15+V21,SLF
V20=V16*V9,SLF
←S319
V20=V20*V17,SLF
V14=V14+V20,SLF
V14=V14+V23,SLF
V20=1
FLTV20+0
V16=V16+V20,SLF
V12=1
←6
[5]←11,V12-1=0
FIXV16+0
←13,V6-V16>0
FLTV16+0
←5
[13]FLTV16+0
V20=V16*V9,SLF
←S319,1
V21=V20*V17,SLF
V20=V15*V9,SLF
←S319
V23=V20*V17,SLF
V20=1  ?2
FLTV20+0
V16=V16+V20,SLF
V20=V16*V10,SLF
V20=V20+V13,SLF
←S319,1
V20=V20*V17,SLF
V15=V15+V20,SLF
V15=V15+V21,SLF
V20=V16*V10,SLF
V20=V20+V13,SLF
←S319
V20=V20*V17,SLF
V14=V14+V20,SLF
V14=V14+V23,SLF
V12=2
V20=1
FLTV20+0
V16=V16+V20,SLF
←5
[11]←20,V12-2=0
FIXV16+0
←14,V6-V16>0
FLTV16+0
←6
[14]FLTV16+0
V20=V16*V10,SLF
V20=V20+V13,SLF
←S319,1
V21=V20*V17,SLF
V20=V15*V10,SLF
V20=V20+V13,SLF
←S319
V23=V20*V17,SLF
V20=1  ?3
FLTV20+0
V16=V16+V20,SLF
V20=V15*V10,SLF
V20=V20+V13,SLF
←S319,1
V20=V20*V17,SLF
V15=V15+V20,SLF
V15=V15+V21,SLF
V20=V16*V10,SLF
V20=V20+V13,SLF
←S319
V20=V20*V17,SLF
V14=V14+V20,SLF
V14=V14+V23,SLF
V20=1
FLTV20+0
V16=V16+V20,SLF
V12=0
[8]FIXV16+0
←9,V6-V16>0
V12=V8
V6=V6+1
FLTV6+0
V17=1000
FLTV17+0
V8=V14*V14,SLF
V9=V15*V15,SLF
V14=V8+V9,SLF
V14=V14*V17,SLF
FIXV14+0
V15=V7
V7=V7+1
V23=20
←S84
←9,V7-901<0
V23=10
V15=0
V14=0
←S84
[9]←S5
2000 0 0 3
←2
END
```

PF9

```
TEXT1P1E
 *APERTURE=
←S109
V4=V20
TEXT1P1E
 *F=
←S109
V8=V20
TEXT1P1E
 *WAVE=
←S109
V5=V20
TEXT1P1E
 *I=
←S109
V15=V20
V7=-1000
V13=0
TEXT1P1E
 *R=
←S109
V9=V20
V9=V9/V6,SLF
V5=V5/V8,SLF
V8=2
FLTV8+0
V20=V4/V8,SLF
V8=V20*V20,SLF
V20=V6*V5,SLF
V20=V20+V8,SLF
←S308
V4=V20-V6,SLF
V4=V4  ?1
V13=V13  ?2
V2=100
FLTV2+0
V3=100
FLTV3+0
V10=2
FLTV10+0
V9=V9/V10,SLF
V21=-V7
FLTV21+0
V2=V9/V21,SLF
V12=V9*V9,SLF
V2=V2  ?3
V20=V3*V3,SLF
V20=V12+V20,SLF
←S309
V21=V20-V3,SLF
V21=V21  ?4
[7]V10=V9*V9,SLF
V11=V3*V3,SLF
V20=V10+V11,SLF
←S309
V12=V20
V12=V12-V3,SLF
V12=V12/V21,SLF
V21=V21  ?5
V9=V9-V2,SLF
V2=V2  ?6
V12=V12*V4,SLF
V4=V4  ?7
V17=V4-V12,SLF
V17=V17/V5,SLF
V13=V13  ?8
V13=V17-V13,SLF
V13=V13  ?9
V8=2
FLTV8+0
V20=V8*V13,SLF
V20=V20*V16,SLF
V20=V20  ?10
←S319
V14=V20
V17=1000
FLTV17+0
V14=V14  ?11
V14=V14*V17,SLF
V7=V7+1
V16=V7
V23=20
FIXV14+0
←11,V14>0
V14=-V14
[11]V14=V14
←S84
←7,V7-1001<0
V23=10
V15=0
V14=0
←S84
[9]←S5
2000 0 0 31
←9
END

Z

A
```

PF 10

```
TEXT1P1E
 *APERTURE=
←S109
V4=V20
TEXT1P1E
 *F=
←S109
V8=V20
TEXT1P1E
 *WAVE=
←S109
V5=V20
TEXT1P1E
 *I=
←S109
V15=V20
V7=-1000
V13=0
TEXT1P1E
 *R=
←S109
V9=V20
V9=V9/V6,SLF
V5=V5/V8,SLF
V8=2
FLTV8+0
V20=V4/V8,SLF
V8=V20*V20,SLF
V20=V6*V5,SLF
V20=V20+V8,SLF
←S308
V4=V20-V6,SLF
V4=V4  ?1
V13=V13  ?2
V2=100
FLTV2+0
V3=100
FLTV3+0
V10=2
FLTV10+0
V9=V9/V10,SLF
V21=-V7
FLTV21+0
V2=V9/V21,SLF
V12=V9*V9,SLF
V2=V2  ?3
V20=V3*V3,SLF
V20=V12+V20,SLF
←S309
V21=V20-V3,SLF
V21=V21  ?4
[7]V10=V9*V9,SLF
V11=V3*V3,SLF
V20=V10+V11,SLF
←S309
V12=V20
V12=V12-V3,SLF
V12=V12/V21,SLF
V21=V21  ?5
V9=V9-V2,SLF
V2=V2  ?6
V12=V12*V4,SLF
V4=V4  ?7
V17=V4-V12,SLF
V17=V17/V5,SLF
V13=V13  ?8
V13=V17-V13,SLF
V13=V13  ?9
V20=V20  ?10
V14=V13
V17=1000
FLTV17+0
V14=V14  ?11
V14=V14*V17,SLF
V7=V7+1
V16=V7
V23=20
FIXV14+0
←11,V14>0
V14=-V14
[11]V14=V14
[13]←12,V14-1000<0
V14=V14-1000
←13
[12]←S84
←7,V7-1001<0
V23=10
V15=0
V14=0
←S84
[9]←S5
2000 0 0 31
←9
END

Z

A
```

APPENDIX P2

FORTRAN PROGRAMS

APPENDIX P2

Fortran programs to compute various aspects of device performance. Ten program groupings comprising nineteen programs are presented in this appendix.

1. Field Programs

To predict voltage and field distributions due to interdigital electrodes in isotropic and anisotropic media.

Program GRAT - Computes voltages within the material.

Program GRGD - Computes normal and orthogonal components of field.
(over half electrode pitch)

Program FGRA - as GRAT but over part of electrode pitch.

Program FIGD - as GRGD but over part of electrode pitch.

2. Phase Profile Programs

To compute phase profiles with excitation for various device configurations.

Programs GTWV - for normal field operation
TGWV - for normal field with a sub-electrode layer.

Programs GTWI - for transverse field operation.
TGWI - for transverse field operation with a sub electrode layer.

APPENDIX P2 continued

3. Zero-Order Characteristics and Misalignment Sensitivity

To predict modulator performance and gain information about angular aperture and noncollimated light operation.

Program VLTI - gives the zero order characteristic for various device configurations.

Program VDI2 - gives the zero order performance versus misalignment.

4. Electrode/Crystal Gap Effects

To predict the deterioration of sensitivity caused by an electrode sublayer.

Program AGAP - gives details of field variations due to various sub-layers.

5. Slit-Function Estimation Program

An estimate of slit function on an orthogonal propagation basis is made.

Program SLFN - gives points on the slit function at zero order extinction for various configurations.

6. Far-Field Diffraction Pattern and Energy in Orders

To predict position and content of the far field orders for various device configurations.

Program DIFT - gives far field pattern of a given phase profile for various illumination profiles.

Program QSIN - gives energy deflected outside orders versus excitation (for Q-switching considerations).

APPENDIX P2 continued

7. Device Capacitance Calculations:

To assess device capacitance for various materials and electrode combinations.

Program CAPC - predicts value of device capacitance for various configurations.

8. Total Internal Reflection Characteristics

To assess phase change and intensity effect due to incident beam polarisation.

Program ADPR - calculates phase change and intensities for various angles and material combinations.

9. Crystal Orientation and Optimisation

To predict the improvement possible by using a phase-optimised orientation of crystal.

Program PHOP - general uniaxial crystal phase optimisation program (ADP illustrated).

Program LINO - $LiNBO_3$ phase optimisation program.

10. Focussed Array of Five Sources Onto a Grating

To assess performance of the transformed array in Section 3.

Program FARR - gives a far field prediction for the overlapping slit function case.

```
      PROGRAM GRAT(INPUT,OUTPUT,TAPE1=INPUT,TAPE2=OUTPUT)
      DIMENSION PHI(10)

C     INPUT CONSTANTS
05
      PI=4.0*ATAN(1.0)
      DEL=0.002
      LIM=10
      V0=50.0
10    MN=0
      MQ=0
   39 CONTINUE

C          GRATING CONFIGURATIONS
15
      D=0.05
      IF(MN-1) 40,0,41
      D=0.10
      GO TO 40
20 41 D=0.20
   40 CONTINUE
      IF(MQ-1) 0,101,101

C          DIELECTRIC CONSTANTS
25
      E1=45.0
      E3=27.0
      GO TO 102

30
C          ISOTROPIC CASE

  101 E1=1.0
      E3=1.0
35  102 CONTINUE

      E=1.0
      A=0.25
      SD=0.5
40
C   PRELIMINARY CALCULATIONS

      F1=E3/E1
      F2=SQRT(F1)
45    F3=E1*F2
      F4=F2*T
      Q1=(4.0*V0)/PI
      Q2=PI/D
      F5=D/2.0
50    FLIM=LIM
      F5=F5/(FLIM-1.0)

C          OUTPUT BLOCK

55    WRITE (2,18) F5
```

```
      18 FORMAT(6H X(MM),3X,13HZ IN STEPS OF,F8.4,2HMM)
         WRITE (2,103) E1,E3,D
     103 FORMAT(4H E1=,F8.4,5X,3HE3=,F8.4,5X,2HD=,F8.4,2HMM)

60    C   INITIAL VALUES

         M=0
         N=1
         REM=0.0
65       Z=0.0
         X=0.0
      11 CONTINUE

      C          COMPUTE FIELDS BY SERIES SUMMATION
70
         F6=F2*X
         F7=(PI*Z)/D
         QN=N

75    C   EVALUATE AN

         A1=Q1*SIN(QN*PI*A)/(QN*QN*PI)
         AN=A1/A

80    C   EVALUATE PHI(C)

         U=QN*Q2*F6
         IF(U-70.0) 0,16,16
         V=-U
85       PHIC=AN*EXP(V)*SIN(QN*F7)
         GO TO 17
      16 PHIC=AN*SIN(QN*F7)
      17 N=N+2
         IF(ABS(PHIC)-0.02) 12,12,0
90       REM=REM+PHIC
         GO TO 11
      12 M=M+1
         N=1
         PHI(M)=REM
95       REM=0.0
         IF(M-LIM) 0,13,13
         Z=Z+F5
         GO TO 11
         IF(PHI(10)) 0,200,0
100
      C          OUTPUT BLOCK

      13 WRITE(2,15) X,(PHI(K),K=1,M)
      15 FORMAT (1H ,F8.4,5X,10F8.2)
105
      C          STEP INTERVALS

         Z=0.0
         X=X+DEL
110      M=0
```

```
      IF(X-SD) 11,11,0
200   MN=MN+1
      IF(MN-3) 39,0,0
      MN=0
115   MQ=MQ+1
      IF(MQ-2) 39,0,0
      STOP
      END
```

X(MM) Z IN STEPS OF 0.0111MM
E1= 1.0000 E3= 1.0000 D= 0.2000MM

0.0000	0.00	11.12	22.11	33.29	44.29	50.26	49.64	49.97	49.85	49.98
0.0020	0.00	10.78	21.48	32.25	42.32	48.06	48.10	48.75	48.74	48.88
0.0040	0.00	10.45	20.84	31.05	40.48	46.04	46.61	47.53	47.62	47.75
0.0060	0.00	10.15	20.20	29.97	38.77	44.15	45.17	46.23	46.50	46.65
0.0080	0.00	9.86	19.59	28.91	37.17	42.41	43.78	45.02	45.38	45.55
0.0100	0.00	9.54	18.92	27.88	35.67	40.73	42.42	43.82	44.26	44.42
0.0120	0.00	9.24	18.29	26.98	34.26	39.20	41.11	42.63	43.15	43.31
0.0140	0.00	8.95	17.67	25.92	32.93	37.74	39.84	41.46	42.05	42.25
0.0160	0.00	8.65	17.07	24.99	31.67	36.37	38.61	40.30	40.98	41.17
0.0180	0.00	8.34	16.48	24.07	30.48	35.06	37.41	39.15	39.88	40.11
0.0200	0.00	8.07	15.91	23.20	29.35	33.82	36.26	38.04	38.82	39.06
0.0220	0.00	7.80	15.36	22.36	28.27	32.59	35.15	36.95	37.77	38.04
0.0240	0.00	7.53	14.83	21.56	27.25	31.47	34.05	35.89	36.74	37.02
0.0260	0.00	7.26	14.31	20.80	26.28	30.40	32.99	34.87	35.73	36.00
0.0280	0.00	7.02	13.82	20.06	25.35	29.37	31.97	33.85	34.72	35.02
0.0300	0.00	6.78	13.34	19.35	24.46	28.39	30.98	32.85	33.75	34.06
0.0320	0.00	6.55	12.87	18.65	23.61	27.44	30.03	31.88	32.80	33.11
0.0340	0.00	6.33	12.45	18.00	22.79	26.53	29.10	30.94	31.88	32.19
0.0360	0.00	6.11	12.01	17.36	22.01	25.65	28.20	30.04	30.97	31.26
0.0380	0.00	5.92	11.60	16.76	21.24	24.81	27.33	29.14	30.08	30.37
0.0400	0.00	5.72	11.20	16.21	20.53	24.00	26.48	28.25	29.21	29.51
0.0420	0.00	5.52	10.81	15.65	19.84	23.22	25.66	27.40	28.36	28.67
0.0440	0.00	5.33	10.44	15.12	19.18	22.47	24.87	26.58	27.54	27.84
0.0460	0.00	5.15	10.09	14.61	18.54	21.74	24.10	25.78	26.73	27.04
0.0480	0.00	4.97	9.75	14.12	17.91	21.04	23.35	25.01	25.95	26.25
0.0500	0.00	4.81	9.42	13.65	17.32	20.36	22.63	24.25	25.18	25.46
0.0520	0.00	4.64	9.10	13.21	16.75	19.71	21.95	23.52	24.44	24.74
0.0540	0.00	4.49	8.79	12.77	16.21	19.08	21.25	22.81	23.71	24.01
0.0560	0.00	4.34	8.50	12.35	15.68	18.47	20.60	22.12	23.03	23.30
0.0580	0.00	4.21	8.22	11.94	15.17	17.88	19.96	21.45	22.34	22.61
0.0600	0.00	4.07	7.94	11.54	14.68	17.30	19.34	20.80	21.67	21.94

```
      PROGRAM GRGD(INPUT,OUTPUT,TAPE1=INPUT,TAPE2=OUTPUT)
      DIMENSION PHI(10)

C     INPUT CONSTANTS

      L=1
      PI=4.0*ATAN(1.0)
      DEL=0.002
      LIM=10
      V0=50.0
      MN=0
      ML=0
   39 CONTINUE

C           GRATING CONFIGURATIONS

      D=0.05
      A=0.25
      IF(MN-1) 40,100,41
  100 D=0.10
      A=0.25
      GO TO 40
   41 D=0.20
      A=0.25
   40 CONTINUE
      IF(ML-1) 500,26,26

C           DIELECTRIC CONSTANTS

  500 E1=45.0
      E3=27.0
   26 CONTINUE
      E=1.0
      SD=0.1

C     PRELIMINARY CALCULATIONS

      F1=E3/E1
      F2=SQRT(F1)
      F3=E1*F2
      Q1=(4.0*V0)/PI
      Q2=PI/D
      F5=D/2.0
      FLIM=LIM
      F5=F5/(FLIM-1.0)

C           OUTPUT HEADINGS

   24 WRITE (2,18) F5
   18 FORMAT (6H X(MM),3X,13HZ IN STEPS OF,F8.4,2HMM)
      WRITE (2,200) E1,E3,D
  200 FORMAT(4H E1=,F8.4,5X,3HE3=,F8.4,5X,2HD=,F8.4,2HMM)
      WRITE (2,301) A
  301 FORMAT (3H A=,F8.4,2HMM)
      IF(L-1) 101,101,19
```

```
      101 WRITE (2,20)
       20 FORMAT (3H EX)
          GO TO 25
       19 WRITE (2,21)
   60     21 FORMAT (3H EZ)
          25 CONTINUE

      C   INITIAL VALUES

   65     M=0
          N=1
          REM=0.0
          Z=0.0
          X=0.0
   70     11 CONTINUE

      C          COMPUTE FIELDS BY SERIES SUMMATION

          F6=F2*X
   75     F7=(PI*Z)/D
          QN=N

      C   EVALUATE AN

   80     A1=Q1*SIN(QN*PI*A)/(QN*QN*PI)
          AN=A1/A

      C   EVALUATE PHI(C)

   85     U=QN*Q2*F6
          IF(U-70.0) 102,16,16
      102 V=-U
          PHIC=AN*EXP(V)*SIN(QN*F7)
          GO TO 17
   90     16 PHIC=0.0
          17 N=N+2

      C   L CONTROLLED SEGMENT
      C          EX OR EZ SUMMATION
   95
          IF(L-1) 103,103,22
      103 PHIC=PHIC*(-QN)*Q2*F2
          GO TO 23
          22 PHIC=AN*EXP(V)*QN*Q2*COS(QN*F7)
  100     23 CONTINUE
          REM=REM+PHIC
          IF(N-400) 11,12,12
          12 M=M+1
          N=1
  105     PHI(M)=REM
          REM=0.0
          IF(M-LIM) 105,204,204
      105 Z=Z+F5
          GO TO 11
  110     204 IF(L-2) 201,202,202
```

```
      201 MI=10
          GO TO 203
      202 MI=1
      203 IF(PHI(MI)) 13,106,13
115
C           OUTPUT BLOCK

       13 WRITE (2,15) X,(PHI(K),K=1,M)
       15 FORMAT (1H ,F8,4,5X,10F10,2)
120
C           STEP INTERVALS

          Z=0,0
          X=X+DEL
125       M=0
          IF(X-SD) 11,11,106
      106 L=L+1
          IF(L-3) 24,107,107
      107 L=1
130       MN=MN+1
          IF(MN-3) 39,108,108
      108 MN=0
          ML=ML+1
          IF(ML-1) 300,300,109
135
C           ISOTROPIC CASES

      300 E1=1,0
          E3=1,0
140       GO TO 39
      109 STOP
          END
```

```
X(MM)   Z IN STEPS OF   ,0028MM
E1= 45,0000     E3= 27,0000     D=   ,0500MM
A=   ,2500MM
EX
  0,0000          0,00   -489,80  -1032,63  -1728,09  -2992,31  -3166,36  -2254,91  -1927,34  -1781,37  -1738,49
  ,0020           0,00   -486,99  -1020,34  -1676,74  -2804,64  -2775,18  -2196,56  -1904,90  -1766,77  -1725,40
  ,0040           0,00   -465,93   -964,29  -1529,73  -2125,16  -2294,28  -2041,94  -1834,78  -1722,47  -1687,41
  ,0060           0,00   -434,99   -886,71  -1358,27  -1779,20  -1944,43  -1858,21  -1734,64  -1654,63  -1628,08
  ,0080           0,00   -398,56   -801,06  -1195,16  -1521,49  -1681,50  -1678,74  -1619,13  -1570,00  -1552,32
  ,0100           0,00   -360,45   -716,43  -1058,58  -1320,01  -1473,70  -1514,44  -1498,80  -1475,13  -1465,38
  ,0120           0,00   -323,32   -637,62   -925,42  -1156,80  -1303,32  -1366,97  -1379,98  -1375,42  -1372,85
  ,0140           0,00   -288,71   -566,53   -817,73  -1021,22  -1159,95  -1235,15  -1266,04  -1274,90  -1276,27
  ,0160           0,00   -257,30   -503,47   -724,97   -908,51  -1037,05  -1117,16  -1158,64  -1176,36  -1181,24
  ,0180           0,00   -229,25   -448,01   -644,77   -808,09   -930,26  -1011,29  -1058,45  -1081,64  -1088,46
  ,0200           0,00   -204,43   -399,36   -575,11   -722,76   -836,55   -916,83   -965,63   -991,84   -999,93
  ,0220           0,00   -182,55   -356,70   -514,28   -648,14   -753,70   -830,13   -880,02   -907,56   -915,29
  ,0240           0,00   -163,27   -319,23   -460,92   -582,47   -680,04   -752,55   -801,35   -829,06   -837,99
  ,0260           0,00   -146,29   -286,23   -413,91   -524,35   -614,27   -682,37   -729,22   -756,34   -765,18
  ,0280           0,00   -131,29   -257,08   -372,30   -472,69   -555,34   -618,85   -663,23   -689,27   -697,83
  ,0300           0,00   -118,01   -231,26   -335,35   -426,61   -502,41   -561,31   -602,94   -627,62   -635,77
  ,0320           0,00   -106,22   -208,30   -302,43   -385,38   -454,77   -509,15   -547,94   -571,09   -578,78
  ,0340           0,00    -95,72   -187,84   -273,02   -348,40   -411,83   -461,87   -497,81   -519,37   -526,55
  ,0360           0,00    -86,35   -169,56   -246,67   -315,17   -373,07   -419,00   -452,15   -472,13   -478,80
  ,0380           0,00    -77,98   -153,18   -223,03   -285,25   -338,05   -380,11   -410,60   -429,03   -435,19
  ,0400           0,00    -70,47   -138,49   -201,77   -258,29   -306,39   -344,64   -372,80   -389,75   -395,42
```

```
      PROGRAM FGRA(INPUT,OUTPUT,TAPE1=INPUT,TAPE2=OUTPUT)
      DIMENSION PHI(10)

C     INPUT CONSTANTS

      PI=4,0*ATAN(1,0)
      DEL=0,0001
      LIM=10
      V0=50,0
      MN=0
      MQ=0
   39 CONTINUE

C          GRATING CONFIGURATIONS

      D=0,05
      IF(MN-1) 40,0,41
      D=0,10
      GO TO 40
   41 D=0,20
   40 CONTINUE
      IF(MQ-1) 0,101,101

C          DIELECTRIC CONSTANTS

      E1=45,0
      E3=27,0
      GO TO 102

C          ISOTROPIC CASE

  101 E1=1,0
      E3=1,0
  102 CONTINUE

      E=1,0
      A=0,25
      SD=0,01

C   PRELIMINARY CALCULATIONS

      F1=E3/E1
      F2=SQRT(F1)
      F3=E1*F2
      F4=F2*T
      Q1=(4,0*V0)/PI
      Q2=PI/D
      F5=D/2,0
      FLIM=LIM
      F5=F5/(5,0*(FLIM-1,0))

C          OUTPUT HEADINGS

      WRITE (2,18) F5
   18 FORMAT(6H X(MM),3X,13HZ IN STEPS OF,F8,4,2HMM)
```

```
      WRITE (2,103) E1,E3,D
  103 FORMAT(4H E1=,F8.4,5X,3HE3=,F8.4,5X,2HD=,F8.4,2HMM)

C     INITIAL VALUES
   60
      M=0
      N=1
      REM=0.0
      Z=F5*20.0
   65 X=0.0
   11 CONTINUE

C           COMPUTE FIELDS BY SERIES SUMMSTION

   70 F6=F2*X
      F7=(PI*Z)/D
      QN=N

C     EVALUATE AN
   75
      A1=Q1*SIN(QN*PI*A)/(QN*QN*PI)
      AN=A1/A

C     EVALUATE PHI(C)
   80
      U=QN*Q2*F6
      IF(U-70.0) 0,16,16
      V=-U
      PHIC=AN*EXP(V)*SIN(QN*F7)
   85 GO TO 17
   16 PHIC=AN*SIN(QN*F7)
   17 N=N+2
      IF(ABS(PHIC)-0.02) 12,12,0
      REM=REM+PHIC
   90 GO TO 11
   12 M=M+1
      N=1
      PHI(M)=REM
      REM=0.0
   95 IF(M-LIM) 0,13,13
      Z=Z+F5
      GO TO 11
      IF(PHI(10)) 0,200,0

  100 C           OUTPUT BLOCK

   13 WRITE(2,15) X,(PHI(K),K=1,M)
   15 FORMAT (1H ,F8.4,5X,10F8.2)

  105
C           LOOP CONSTANTS

      Z=F5*20.0
      X=X+DEL
  110 M=0
```

```
      IF(X-SD) 11,11,0
200   MN=MN+1
      IF(MN-3) 39,0,0
      MN=0
115   MQ=MQ+1
      IF(MQ-2) 39,0,0
      STOP
      END
```

```
      PROGRAM FIGD(INPUT,OUTPUT,TAPE1=INPUT,TAPE2=OUTPUT)
      DIMENSION PHI(10)

C     INPUT CONSTANTS
05
      L=1
      PI=4.0*ATAN(1.0)
      DEL=0.001
      LIM=10
10    V0=50.0
      MN=0
      ML=0
   39 CONTINUE

15  C       GRATING CONFIGURATIONS

      D=0.05
      A=0.311
      IF(MN-1) 40,100,41
20  100 D=0.10
      A=0.289
      GO TO 40
   41 D=0.20
      A=3.0/8.0
25    40 CONTINUE
      IF(ML-1) 500,26,26

C       DIELECTRIC CONSTANTS

30  500 E1=45.0
      E3=2.0
    26 CONTINUE

      E=1.0
35    SD=0.05

C   PRELIMINARY CALCULATIONS

      F1=E3/E1
40    F2=SQRT(F1)
      F3=E1*F2
      Q1=(4.0*V0)/PI
      Q2=PI/D
      F5=D/2.0
45    FLIM=LIM
      F5=F5/(5.0*(FLIM-1.0))

C       OUTPUT HEADINGS

50    24 WRITE (2,18) F5
    18 FORMAT(6H X(MM),3X,13HZ IN STEPS OF,F8.4,2HMM)
      WRITE (2,200) E1,E3,D
  200 FORMAT(4H E1=,F8.4,5X,3HE3=,F8.4,5X,2HD=,F8.4,2HMM)
      WRITE (2,301) A
55  301 FORMAT(3H A=,F8.4,2HMM)
```

```
      IF(L-1) 101,101,19
  101 WRITE (2,20)
   20 FORMAT (3H EX)
      GO TO 25
   19 WRITE (2,21)
   21 FORMAT (3H EZ)
   25 CONTINUE

C   INITIAL VALUES

      M=0
      N=1
      REM=0.0
      Z=F5*25.0
      X=0.0

C           COMPUTE FIELDS BY SERIES SUMMATION

   11 CONTINUE
      F6=F2*X
      F7=(PI*Z)/D
      QN=N

C   EVALUATE AN

      A1=Q1*SIN(QN*PI*A)/(QN*QN*PI)
      AN=A1/A

C   EVALUATE PHI(C)

      U=QN*Q2*F6
      IF(U-70.0) 102,16,16
  102 V=-U
      PHIC=AN*EXP(V)*SIN(QN*F7)
      GO TO 17
   16 PHIC=0.0
   17 N=N+2

C   L CONTROLLED SEGMENT
C         EX OR EZ SUMMATION

      IF(L-1) 103,103,22
  103 PHIC=PHIC*(-QN)*Q2*F2
      GO TO 23
   22 PHIC=AN*EXP(V)*QN*Q2*COS(QN*F7)
   23 CONTINUE
      REM=REM+PHIC
      IF(N-400) 11,12,12
   12 M=M+1
      N=1
      PHI(M)=REM
      REM=0.0
      IF(M-LIM) 105,204,204
  105 Z=Z+F5
```

```
                    GO TO 11
                204 IF(L-2) 201,202,202
                201 MI=10
                    GO TO 203
115             202 MI=1
                203 IF(PHI(MI)) 13,106,13

              C          OUTPUT BLOCK

120              13 WRITE(2,15) X,(PHI(K),K=1,M)
                 15 FORMAT (1H ,F8.4,5X,10F10.2)

                    Z=F5*20.0
                    X=X+DEL
125                 M=0
                    IF(X-SD) 11,11,106
                106 L=L+1
                    IF(L-3) 24,107,107
                107 L=1
130                 MN=MN+1
                    IF(MN-3) 39,108,108
                108 MN=0
                    ML=ML+1
                    IF(ML-1) 300,300,109
135
              C          ISOTROPIC CASES

                300 E1=1.0
                    E3=1.0
140                 GO TO 39
                109 STOP
                    END
```

```
X(MM)   Z IN STEPS OF   .0006MM
E1= 45.0000     E3= 27.0000     D=   .0500MM
A=   .3110MM
EX
  0.0000      -2551.79  -2931.11  -3550.35  -6064.22  -3600.66  -3036.59  -2720.10  -2532.43  -2406.17  -2295.10
   .0010      -1627.76  -1759.25  -1905.23  -2070.20  -2260.73  -2486.31  -2758.07  -3066.07  -3257.55  -3120.29
   .0020      -1594.27  -1716.25  -1848.37  -1992.14  -2148.49  -2315.87  -2485.25  -2630.70  -2707.29  -2688.22
   .0030      -1544.14  -1653.61  -1768.65  -1888.69  -2011.83  -2133.58  -2245.29  -2333.69  -2384.61  -2391.70
   .0040      -1483.26  -1579.87  -1678.59  -1778.06  -1875.87  -1968.16  -2049.50  -2113.54  -2154.85  -2171.28
   .0050      -1416.80  -1501.72  -1586.58  -1669.95  -1749.82  -1823.46  -1887.69  -1939.29  -1975.83  -1996.41
   .0060      -1348.51  -1423.45  -1497.13  -1568.35  -1635.58  -1697.03  -1750.79  -1795.13  -1828.80  -1851.40
   .0070      -1280.82  -1347.49  -1412.31  -1474.34  -1532.51  -1585.61  -1632.47  -1672.09  -1703.78  -1727.34
   .0080      -1215.16  -1275.02  -1332.81  -1387.83  -1439.29  -1486.39  -1528.39  -1564.67  -1594.84  -1618.77
   .0090      -1152.26  -1206.52  -1258.68  -1308.21  -1354.55  -1397.16  -1435.53  -1469.28  -1498.17  -1522.11
   .0100      -1092.47  -1142.08  -1189.65  -1234.80  -1277.11  -1316.20  -1351.73  -1383.45  -1411.19  -1434.91
   .0110      -1035.88  -1081.58  -1125.35  -1166.91  -1205.94  -1242.18  -1275.40  -1305.40  -1332.09  -1355.43
   .0120       -982.44  -1024.80  -1065.37  -1103.92  -1140.23  -1174.09  -1205.34  -1233.84  -1259.53  -1282.38
   .0130       -932.02   -971.50  -1009.32  -1045.30  -1079.28  -1111.10  -1140.63  -1167.79  -1192.52  -1214.79
   .0140       -884.47   -921.42   -956.84   -990.59  -1022.53  -1052.56  -1080.57  -1106.49  -1130.28  -1151.93
```

```
      PROGRAM GTWV(INPUT,OUTPUT,TAPE1=INPUT,TAPE2=OUTPUT)
      DIMENSION GAM(10)
C           ELECTRO-OPTIC COEFFICIENTS
      R13=6.6E-9
      R33=30.8E-9
      R22=3.4E-9
C           REFRACTIVE INDICES
      QNO=2.286
      QNE=2.20
      A=0.25
      WAVL=6.328E-4
      QL=1.0
      PI=4.0*ATAN(1.0)
      AV=0.0
      JD=0
      JT=0
      MQ=0
C           DIELECTRIC CONSTANTS
      E3=27.0
      E1=45.0
      F3=SQRT(E3/E1)
      JE=0
      THET=0.0
      D=0.05
      DEL=D/9.0
      V=0.0
C           HEADINGS FOR OUTPUT
  400 WRITE(2,401) JT,D,A,E1,E3,DEL
  401 FORMAT(7H THETA=,I8,4X,2HD=,F6.4,4X,2HA=,F6.4,4X,3HE1=,F6.3,4X,
     13HE3=,F6.3,4X,7H STEPS ,F6.4,3H MM)
  300 WRITE (2,301)
  301 FORMAT(2X,6H VOLTS,25X,17HWAVELENGTH RETARD,54X,7HAVERAGE)
  402 CONTINUE
C           EVALUATE P AND Q
      DEL=D/9.0
      F3=SQRT(E3/E1)
      F1=1.0/(WAVL*COS(THET))
      CS=COS(THET)*COS(THET)
      SS=SIN(THET)*SIN(THET)
      P=CS*R33+SS*R13
      PL=CS/(QNE*QNE)+SS/(QNO*QNO)
      PW=PL*PL*PL
      PL=SQRT(PW)
```

```
      P=P/PL
      GM1=0.0
      GN1=0.0
      K=1
   60 Z=0.0
      Q=-SS*R22/PL
      GN=1.0
  500 CONTINUE
   65 C      EVALUATE R
      R=4.0*V/(GN*PI)
      R=R*SIN(GN*PI*A)
      R=R/(GN*PI*A)
   70 F2=GN*PI/D
      C    EXP TERMS
      ZQ=-F2*F3
      VW=ZQ*QL*TAN(THET)
      IF(VW+70.0) 516,501,501
   75   516 EX1=-1.0
        GO TO 517
        501 EX1=EXP(VW)-1.0
        517 CONTINUE
      IF(JT) 515,520,515
   80   515 CONTINUE
      SN1=SIN(F2*Z)
      CS1=COS(F2*Z)
      C          E INTEGRAL SUMMATION
   85
      V1=R*EX1*SN1/TAN(THET)
      V2=R*EX1*CS1/(F3*TAN(THET))
      GM1=GM1+V1
      GN1=GN1+V2
   90 GN=GN+2.0
      IF(GN-200.0) 500,500,600
  600 GN=1.0
      GO TO 504
   95 C    THETA=0 SEGMENT
  520 X=0.03
      IF(MQ) 502,907,502
  907 WRITE(2,521) X
  100 521 FORMAT(3H X=,F8.4)
      MQ=1
  502 CONTINUE
      C      EVALUATE R
  105
      R=4.0*V/(GN*PI)
      R=R*SIN(GN*PI*A)
      R=R/(GN*PI*A)
      R=R*EXP(-GN*PI*F3*X/D)
  110 F2=GN*PI/D
```

```
      CS2=COS(F2*Z)
      V3=R*CS2*F2*QL
C           E INTEGRAL SUMMATION
115
      GM1=GM1-V3
      QN=QN+2.0
      IF(QN-200.0) 502,502,518
120   C           EVALUATE RETARDATIONS
  518 GAM(K)=2.0*GM1*R33*QNE*ONE*QNE/WAVL
      GO TO 519
  504 PAM=P*GN1-Q*GM1
125   GAM(K)=F1*PAM
  519 Z=Z+DEL
      QN=1.0
      GM1=0.0
      GN1=0.0
130   AV=AV+ABS(GAM(K))
      K=K+1
      IF(K-10) 500,500,505
  505 AV=AV/10.0
135   C           OUTPUT BLOCK
      WRITE(2,506) V,(GAM(KK),KK=1,10),AV
  506 FORMAT(1X,F8.4,10F9.4,2X,F10.4)
140   K=1
      Z=0.0
      AV=0.0
C           VOLTAGE STEPS
145
      V=V+10.0
      IF(V-100.0) 402,402,507
  507 V=0.0
150   C           LOOP CONSTANTS
      JT=JT+1
      THET=THET+PI/180.0
      MQ=0
155   IF(JT-10) 400,400,508
  508 JT=0
      THET=0.0
      JD=JD+1
160   C           OTHER GRATING CONFIGURATIONS
  510 D=0.10
      DEL=D/9.0
      A=0.25
165   IF(JD-1) 400,400,511
```

```
                511 D=0.2
                    DEL=D/9.0
                    A=0.25
                    IF(JD-2) 400,400,512
170             512 JD=-1
                    JE=JE+1
                    IF(JE-1) 513,513,514

                C         ISOTROPIC CASES
175
                513 E1=1.0
                    E3=1.0
                    D=0.05
                    A=0.25
180                 GO TO 400
                514 STOP
                    END
```

THETA= 0 D= .0500 A= .2500 E1=45.000 E3=27.000 STEPS .0056 MM

VOLTS	WAVELENGTH RETARD										AVERAGE
X= .0300											
0.0000	0.0000	0.0000	0.0000	0.0000	0.0000	0.0000	0.0000	0.0000	0.0000	0.0000	0.0000
10.0000	-.1764	-.1645	-.1313	-.0835	-.0285	.0285	.0835	.1313	.1645	.1764	.1168
20.0000	-.3528	-.3290	-.2627	-.1670	-.0569	.0569	.1670	.2627	.3290	.3528	.2337
30.0000	-.5291	-.4935	-.3940	-.2505	-.0854	.0854	.2505	.3940	.4935	.5291	.3505
40.0000	-.7055	-.6580	-.5254	-.3341	-.1139	.1139	.3341	.5254	.6580	.7055	.4674
50.0000	-.8819	-.8224	-.6567	-.4176	-.1424	.1424	.4176	.6567	.8224	.8819	.5842
60.0000	-1.0583	-.9869	-.7881	-.5011	-.1708	.1708	.5011	.7881	.9869	1.0583	.7010
70.0000	-1.2346	-1.1514	-.9194	-.5846	-.1993	.1993	.5846	.9194	1.1514	1.2346	.8179
80.0000	-1.4110	-1.3159	-1.0507	-.6681	-.2278	.2278	.6681	1.0507	1.3159	1.4110	.9347
90.0000	-1.5874	-1.4804	-1.1821	-.7516	-.2563	.2563	.7516	1.1821	1.4804	1.5874	1.0516
100.0000	-1.7638	-1.6449	-1.3134	-.8351	-.2847	.2847	.8351	1.3134	1.6449	1.7638	1.1684

THETA= 1 D= .0500 A= .2500 E1=45.000 E3=27.000 STEPS .0056 MM

VOLTS	WAVELENGTH RETARD										AVERAGE
0.0000	0.0000	0.0000	0.0000	0.0000	0.0000	0.0000	0.0000	0.0000	0.0000	0.0000	0.0000
10.0000	-.2764	-.2616	-.1977	-.0660	-.0176	.0176	.0659	.1977	.2616	.2764	.1639
20.0000	-.5528	-.5233	-.3955	-.1319	-.0353	.0353	.1319	.3955	.5233	.5528	.3277
30.0000	-.8292	-.7849	-.5932	-.1979	-.0529	.0529	.1978	.5932	.7849	.8292	.4916
40.0000	-1.1055	-1.0466	-.7910	-.2638	-.0706	.0705	.2638	.7909	1.0465	1.1055	.6555
50.0000	-1.3819	-1.3082	-.9887	-.3298	-.0882	.0882	.3297	.9887	1.3082	1.3819	.8194
60.0000	-1.6583	-1.5698	-1.1865	-.3957	-.1059	.1058	.3957	1.1864	1.5698	1.6583	.9832
70.0000	-1.9347	-1.8315	-1.3842	-.4617	-.1235	.1234	.4616	1.3842	1.8315	1.9347	1.1471
80.0000	-2.2111	-2.0931	-1.5820	-.5277	-.1411	.1411	.5276	1.5819	2.0931	2.2111	1.3110
90.0000	-2.4875	-2.3548	-1.7797	-.5936	-.1588	.1587	.5935	1.7796	2.3547	2.4875	1.4748
100.0000	-2.7638	-2.6164	-1.9775	-.6596	-.1764	.1763	.6595	1.9774	2.6164	2.7638	1.6387

THETA= 2 D= .0500 A= .2500 E1=45.000 E3=27.000 STEPS .0056 MM

```
      PROGRAM TGWV(INPUT,OUTPUT,TAPE1=INPUT,TAPE2=OUTPUT)
      DIMENSION GAM(10)
C           ELECTRO-OPTIC COEFFICIENTS
      R13=8,6E-9
      R33=30,8E-9
      R22=3,4E-9
C           REFRACTIVE INDICES
      QNO=2,286
      QNE=2,20
      A=0,25
      WAVL=5,328E-4
      QL=1,0
      PI=4,0*ATAN(1,0)
      JD=0
      SL=0,005
      WRITE(2,12) SL
   12 FORMAT (15H SURFACE LIMIT=,F10,4,2HMM)
      AV=0,0
      JT=0
C           DIELECTRIC CONSTANTS
      E3=27,0
      E1=45,0
      F3=SQRT(E3/E1)
      JE=0
      THET=0,0
      D=0,05
      DEL=D/9,0
      V=0,0
C           HEADINGS FOR OUTPUT
  400 WRITE(2,401) JT,D,A,E1,E3,DEL
  401 FORMAT(7H THETA=,I8,4X,2HD=,F6,4,4X,2HA=,F6,4,4X,3HE1=,F6,3,4X,
     13HE3=,F6,3,4X,7H STEPS ,F6,4,3H MM)
  300 WRITE (2,301)
  301 FORMAT(2X,6H VOLTS,25X,17HWAVELENGTH RETARD,54X,7HAVERAGE)
  402 CONTINUE
C           EVALUATE P AND Q
      DEL=D/9,0
      F3=SQRT(E3/E1)
      F1=1,0/(WAVL*COS(THET))
      CS=COS(THET)*COS(THET)
      SS=SIN(THET)*SIN(THET)
      P=CS*R33+SS*R13
```

```
      PL=CS/(QNE*QNE)+SS/(QNO*QNO)
      PW=PL*PL*PL
      PL=SQRT(PW)
      P=P/PL
60    GM1=0.0
      GN1=0.0
      K=1
      Z=0.0
      Q=-SS*R22/PL
65    QN=1.0
  500 CONTINUE
C      EVALUATE R
70    R=4.0*V/(QN*PI)
      R=R*SIN(QN*PI*A)
      R=R/(QN*PI*A)
      F2=QN*PI/D
C    EXP TERMS
75    ZQ=-F2*F3
      VW=ZQ*(QL*TAN(THET)+SL)
      IF(VW+70.0) 516,501,501
  516 EX1=-EXP(-F2*F3*SL)
      GO TO 517
80    501 EX1=EXP(VW)-EXP(-F2*F3*SL)
      517 CONTINUE
      IF(JT) 515,502,515
  515 CONTINUE
      SN1=SIN(F2*Z)
85    CS1=COS(F2*Z)
C          E INTEGRAL SUMMATION
      V1=R*EX1*SN1/TAN(THET)
90    V2=R*EX1*CS1/(F3*TAN(THET))
      GM1=GM1+V1
      GN1=GN1+V2
      QN=QN+2.0
      IF(QN-100.0) 500,500,600
95    600 QN=1.0
      GO TO 504
C    THETA=0 SEGMENT
100   502 CONTINUE
C      EVALUATE R
      R=4.0*V/(QN*PI)
105   R=R*SIN(QN*PI*A)
      R=R/(QN*PI*A)
      F2=QN*PI/D
      CS2=COS(F2*Z)
      V3=R*CS2*F2*QL
110
```

```
C          E INTEGRAL SUMMATION

           GM1=GM1-V3
           GN=GN+2.0
115        IF(GN-100.0) 502,502,518

C          EVALUATE RETARDATIONS

  518 GAM(K)=2.0*GM1*R33*GNE*GNE*GNE/WAVL
120        GO TO 519
  504 PAM=P*GN1-Q*GM1
      GAM(K)=F1*PAM
  519 Z=Z+DEL
      GN=1.0
125   GM1=0.0
      GN1=0.0
      AV=AV+ABS(GAM(K))
      K=K+1
      IF(K-10) 500,500,505
130 505 AV=AV/10.0

C          OUTPUT BLOCK

      WRITE(2,506) V,(GAM(KK),KK=1,10),AV
135 506 FORMAT(1X,F8.4,10F9.4,2X,F10.4)

      K=1
      Z=0.0
      AV=0.0
140
C          VOLTAGE STEPS

      V=V+10.0
      IF(V-150.0) 402,402,507
145 507 V=0.0
      JT=JT+1
      THET=THET+PI/180.0
      IF(JT-10) 400,400,508
  508 JT=0
150   THET=0.0
      JD=JD+1

C          OTHER GRATING CONFIGURATIONS

155 510 D=0.10
      DEL=D/9.0
      A=0.25
      IF(JD-1) 400,400,511
  511 D=0.2
160   A=0.25
      DEL=D/9.0
      IF(JD-2) 400,400,512
  512 JD=-1
      JE=JE+1
165   IF(JE-1) 513,513,514
```

```
      C          ISOTROPIC CASES
            513 F1=1.0
170               E3=1.0
                  D=0.05
                  A=0.25
                  GO TO 400
            514 STOP
175               END
```

SURFACE LIMIT= .0050MM

THETA= 0 D= .0500 A= .2500 E1=45.000 E3=27.000 STEPS .0056 MM

VOLTS	WAVELENGTH RETARD										AVERAGE
0.0000	0.0000	0.0000	0.0000	0.0000	0.0000	0.0000	0.0000	0.0000	0.0000	0.0000	0.0000
10.0000	-.8367	-.8207	-.8518	-.0041	.0003	-.0003	.0041	.8518	.8207	.8367	.5027
20.0000	-1.6734	-1.6413	-1.7037	-.0081	.0007	-.0007	.0081	1.7037	1.6413	1.6734	1.0054
30.0000	-2.5101	-2.4620	-2.5555	-.0122	.0010	-.0010	.0122	2.5555	2.4620	2.5101	1.5081
40.0000	-3.3468	-3.2827	-3.4074	-.0162	.0013	-.0013	.0162	3.4074	3.2827	3.3468	2.0109
50.0000	-4.1834	-4.1033	-4.2592	-.0203	.0016	-.0016	.0203	4.2592	4.1033	4.1834	2.5136
60.0000	-5.0201	-4.9240	-5.1110	-.0243	.0020	-.0020	.0243	5.1110	4.9240	5.0201	3.0163
70.0000	-5.8568	-5.7447	-5.9629	-.0284	.0023	-.0023	.0284	5.9629	5.7447	5.8568	3.5190
80.0000	-6.6935	-6.5653	-6.8147	-.0324	.0026	-.0026	.0324	6.8147	6.5653	6.6935	4.0217
90.0000	-7.5302	-7.3860	-7.6665	-.0365	.0029	-.0029	.0365	7.6665	7.3860	7.5302	4.5244
100.0000	-8.3669	-8.2067	-8.5184	-.0405	.0033	-.0033	.0405	8.5184	8.2067	8.3669	5.0271
110.0000	-9.2036	-9.0273	-9.3702	-.0446	.0036	-.0036	.0446	9.3702	9.0273	9.2036	5.5299
120.0000	-10.0403	-9.8480	-10.2221	-.0486	.0039	-.0039	.0486	10.2221	9.8480	10.0403	6.0326
130.0000	-10.8769	-10.6687	-11.0739	-.0527	.0042	-.0042	.0527	11.0739	10.6687	10.8769	6.5353
140.0000	-11.7136	-11.4893	-11.9257	-.0567	.0046	-.0046	.0567	11.9257	11.4893	11.7136	7.0380
150.0000	-12.5503	-12.3100	-12.7776	-.0608	.0049	-.0049	.0608	12.7776	12.3100	12.5503	7.5407

THETA= 1 D= .0500 A= .2500 E1=45.000 E3=27.000 STEPS .0056 MM

VOLTS	WAVELENGTH RETARD										AVERAGE
0.0000	0.0000	0.0000	0.0000	0.0000	0.0000	0.0000	0.0000	0.0000	0.0000	0.0000	0.0000
10.0000	-.2128	-.1975	-.1456	-.0731	-.0213	.0213	.0731	.1455	.1975	.2128	.1300
20.0000	-.4257	-.3950	-.2911	-.1461	-.0426	.0426	.1461	.2911	.3950	.4257	.2601
30.0000	-.6385	-.5925	-.4367	-.2192	-.0640	.0639	.2192	.4366	.5925	.6385	.3901
40.0000	-.8513	-.7900	-.5822	-.2922	-.0853	.0852	.2922	.5822	.7900	.8513	.5202
50.0000	-1.0641	-.9875	-.7278	-.3653	-.1066	.1065	.3653	.7277	.9874	1.0641	.6502
60.0000	-1.2770	-1.1850	-.8733	-.4384	-.1279	.1279	.4383	.8733	1.1849	1.2770	.7803
70.0000	-1.4898	-1.3824	-1.0189	-.5114	-.1492	.1492	.5114	1.0188	1.3824	1.4898	.9103
80.0000	-1.7026	-1.5799	-1.1645	-.5845	-.1706	.1705	.5844	1.1644	1.5799	1.7026	1.0404
90.0000	-1.9154	-1.7774	-1.3100	-.6575	-.1919	.1918	.6575	1.3099	1.7774	1.9154	1.1704
100.0000	-2.1283	-1.9749	-1.4556	-.7306	-.2132	.2131	.7305	1.4555	1.9749	2.1283	1.3005
110.0000	-2.3411	-2.1724	-1.6011	-.8037	-.2345	.2344	.8036	1.6010	2.1724	2.3411	1.4305
120.0000	-2.5539	-2.3699	-1.7467	-.8767	-.2558	.2557	.8766	1.7466	2.3699	2.5539	1.5606
130.0000	-2.7667	-2.5674	-1.8922	-.9498	-.2771	.2770	.9497	1.8921	2.5673	2.7667	1.6906
140.0000	-2.9796	-2.7649	-2.0378	-1.0229	-.2985	.2983	1.0227	2.0377	2.7648	2.9796	1.8207
150.0000	-3.1924	-2.9624	-2.1834	-1.0959	-.3198	.3196	1.0958	2.1832	2.9623	3.1924	1.9507

```
      PROGRAM GTW1(INPUT,OUTPUT,TAPE1=INPUT,TAPE2=OUTPUT)
      DIMENSION GAM(10)
C          ELECTRO-OPTIC COEFFICIENTS
      R13=8.6E-9
      R33=30.8E-9
      R22=3.4E-9
C          REFRACTIVE INDICES
      ONO=2.286
      ONE=2.20
      A=0.25
      WAVL=6.328E-4
      QL=1.0
      PI=4.0*ATAN(1.0)
      JD=0
      SL=0.01
      WRITE(2,12) SL
   12 FORMAT (15H SURFACE LIMIT=,F10.4,2HMM)
      AV=0.0
      JT=0
C          DIELECTRIC CONSTANTS
      E3=27.0
      E1=45.0
      F3=SQRT(E3/E1)
      JE=0
      THET=0.0
      D=0.05
      DEL=D/9.0
      V=0.0
C          HEADINGS FOR OUTPUT
  400 WRITE(2,401) JT,D,A,E1,E3,DEL
  401 FORMAT(7H THETA=,I8,4X,2HD=,F6.4,4X,2HA=,F6.4,4X,3HE1=,F6.3,4X,
     13HE3=,F6.3,4X,7H STEPS ,F6.4,3H MM)
  302 WRITE (2,301)
  301 FORMAT(2X,6H VOLTS,25X,17HWAVELENGTH RETARD,54X,7HAVERAGE)
  402 CONTINUE
C          EVALUATE P AND Q
      DEL=D/9.0
      F3=SQRT(E3/E1)
      F1=1.0/(WAVL*COS(THET))
      CS=COS(THET)*COS(THET)
      SS=SIN(THET)*SIN(THET)
      P=CS*R33+SS*R13
```

```
      PL=CS/(ONE*ONE)+SS/(ONO*ONO)
      PW=PL*PL*PL
      PL=SQRT(PW)
      P=P/PL
60    GM1=0.0
      GN1=0.0
      K=1
      Z=0.0
      Q=-SS*R22/PL
65    QN=1.0
  500 CONTINUE

C      EVALUATE R

70    R=4.0*V/(QN*PI)
      R=R*SIN(QN*PI*A)
      R=R/(QN*PI*A)
      F2=QN*PI/D
C    EXP TERMS
75    ZQ=-F2*F3
      VW=ZQ*(QL*TAN(THET)+SL)
      IF(VW+70.0) 516,501,501
  516 EX1=-EXP(-F2*F3*SL)
      GO TO 517
80    501 EX1=EXP(VW)-EXP(-F2*F3*SL)
      517 CONTINUE
      IF(JT) 515,502,515
  515 CONTINUE
      SN1=SIN(F2*Z)
85    CS1=COS(F2*Z)

C          E INTEGRAL SUMMATION

      V1=R*EX1*SN1/TAN(THET)
90    V2=R*EX1*CS1/(F3*TAN(THET))
      GM1=GM1+V1
      GN1=GN1+V2
      QN=QN+2.0
      IF(QN-100.0) 500,500,600
95    600 QN=1.0
      GO TO 504

C    THETA=0 SEGMENT

100   502 CONTINUE

C      EVALUATE R

      R=4.0*V/(QN*PI)
105   R=R*SIN(QN*PI*A)
      R=R/(QN*PI*A)
      F2=QN*PI/D
      CS2=COS(F2*Z)
      V3=R*CS2*F2*QL
110
```

```
C          E INTEGRAL SUMMATION

           GM1=GM1+V3
           QN=QN+2,0
115        IF(QN-100,0) 502,502,518

C          EVALUATE RETARDATIONS

  518 GAM(K)=2,0*GM1*R33*QNE*QNE*QNE/WAVL
120        GO TO 519
  504 PAM=P*GN1-Q*GM1
      GAM(K)=F1*PAM
  519 Z=Z+DEL
      QN=1,0
125   GM1=0,0
      GN1=0,0
      AV=AV+ABS(GAM(K))
      K=K+1
      IF(K-10) 500,500,505
130   505 AV=AV/10,0

C          OUTPUT BLOCK

      WRITE(2,506) V,(GAM(KK),KK=1,10),AV
135   506 FORMAT(1X,F8,4,10F9,4,2X,F10,4)

      K=1
      Z=0,0
      AV=0,0
140

C          VOLTAGE STEPS

      V=V+10,0
      IF(V-150,0) 402,402,507
145   507 V=0,0

C          LOOP CONSTANTS

      JT=JT+1
150   THET=THET+PI/180,0
      IF(JT-10) 400,400,508
  508 JT=0
      THET=0,0
      JD=JD+1
155

C          OTHER GRATING CONFIGURATIONS

  510 D=0,10
      DEL=D/9,0
160   A=0,25
      IF(JD-1) 400,400,511
  511 D=0,2
      A=0,25
      DEL=D/9,0
165   IF(JD-2) 400,400,512
```

```
.RN

                                  D=1.0
                                  E1=45.0
                                  E3=27.0
                                  D=0.05
                                  A=0.25
                                  GO TO 400
                              314 STOP
                                  END
```

ETA= 0 D= ,0500 A= ,2500 E1=45,000 E3=27,000 STEPS ,0056 MM

VOLTS	WAVELENGTH RETARD										AVERAGE
,0000	0,0000	0,0000	0,0000	0,0000	0,0000	0,0000	0,2200	0,0000	0,0000	0,0000	0,0000
,0000	-,8367	-,8207	-,8518	-,0041	,0003	-,0003	,2241	,8518	,8207	,8367	,5027
2,0000	-1,6734	-1,6413	-1,7037	-,0081	,0007	-,0007	,2281	1,7037	1,6413	1,6734	1,0054
3,0000	-2,5101	-2,4620	-2,5555	-,0122	,0010	-,0010	,2122	2,5555	2,4620	2,5101	1,5081
4,0000	-3,3468	-3,2827	-3,4074	-,0162	,0013	-,0013	,2162	3,4074	3,2827	3,3468	2,0109
5,0000	-4,1834	-4,1033	-4,2592	-,0203	,0016	-,0016	,2203	4,2592	4,1033	4,1834	2,5136
6,0000	-5,0201	-4,9240	-5,1110	-,0243	,0020	-,0020	,2243	5,1110	4,9240	5,0201	3,0163
7,0000	-5,8568	-5,7447	-5,9629	-,0284	,0023	-,0023	,2284	5,9629	5,7447	5,8568	3,5190
8,0000	-6,6935	-6,5653	-6,8147	-,0324	,0026	-,0026	,2324	6,8147	6,5653	6,6935	4,0217
9,0000	-7,5302	-7,3860	-7,6665	-,0365	,0029	-,0029	,2365	7,6665	7,3860	7,5302	4,5244
10,0000	-8,3669	-8,2067	-8,5184	-,0405	,0033	-,0033	,2405	8,5184	8,2067	8,3669	5,0271
11,0000	-9,2036	-9,0273	-9,3702	-,0446	,0036	-,0036	,2446	9,3702	9,0273	9,2036	5,5299
12,0000	-10,0403	-9,8480	-10,2221	-,0486	,0039	-,0039	,2486	10,2221	9,8480	10,0403	6,0326
13,0000	-10,8769	-10,6687	-11,0739	-,0527	,0042	-,0042	,2527	11,0739	10,6687	10,8769	6,5353
14,0000	-11,7136	-11,4893	-11,9257	-,0567	,0046	-,0046	,2567	11,9257	11,4893	11,7136	7,0380
15,0000	-12,5503	-12,3100	-12,7776	-,0608	,0049	-,0049	,2608	12,7776	12,3100	12,5503	7,5407

ETA= 1 D= ,0500 A= ,2500 E1=45,000 E3=27,000 STEPS ,0056 MM

VOLTS	WAVELENGTH RETARD										AVERAGE
,0000	0,0000	0,0000	0,0000	0,0000	0,0000	0,0000	0,2220	0,0000	0,0000	0,0000	0,0000
,0000	-,1633	-,1509	-,1146	-,0659	-,0208	,0208	,2659	,1146	,1509	,1633	,1031
,0000	-,3266	-,3018	-,2293	-,1318	-,0416	,0416	,1317	,2293	,3018	,3266	,2062
,0000	-,4899	-,4527	-,3439	-,1976	-,0624	,0623	,1976	,3439	,4527	,4899	,3093
,0000	-,6532	-,6036	-,4586	-,2635	-,0831	,0831	,2635	,4586	,6036	,6532	,4124
,0000	-,8165	-,7545	-,5732	-,3294	-,1039	,1039	,3293	,5732	,7545	,8165	,5155
,0000	-,9798	-,9054	-,6879	-,3953	-,1247	,1247	,3952	,6879	,9054	,9798	,6186
,0000	-1,1431	-1,0563	-,8025	-,4611	-,1455	,1454	,4611	,8025	1,0563	1,1431	,7217
,0000	-1,3064	-1,2072	-,9172	-,5270	-,1663	,1662	,5270	,9171	1,2072	1,3064	,8248
,0000	-1,4697	-1,3581	-1,0318	-,5929	-,1871	,1870	,5928	1,0318	1,3581	1,4697	,9279
,0000	-1,6330	-1,5090	-1,1465	-,6588	-,2078	,2078	,6587	1,1464	1,5090	1,6330	1,0310
,0000	-1,7963	-1,6599	-1,2611	-,7246	-,2286	,2286	,7246	1,2611	1,6599	1,7963	1,1341
,0000	-1,9596	-1,8108	-1,3758	-,7905	-,2494	,2493	,7924	1,3757	1,8107	1,9596	1,2372
,0000	-2,1229	-1,9617	-1,4904	-,8564	-,2702	,2701	,8563	1,4904	1,9616	2,1229	1,3403
,0000	-2,2862	-2,1126	-1,6051	-,9223	-,2910	,2909	,9222	1,6050	2,1125	2,2862	1,4434
,0000	-2,4495	-2,2635	-1,7197	-,9882	-,3118	,3117	,9880	1,7196	2,2634	2,4495	1,5465

ETA= 2 D= ,0500 A= ,2500 E1=45,000 E3=27,000 STEPS ,0056 MM

```
24/05/73 UNIVERSITY OF MINNESOTA 7600 FORTRAN COMPILER SCOPE V2.0    PSR10     05/11/73  09.49.30
      MNF(E=2,T)
0001008       1*       PROGRAM TGW1(INPUT,OUTPUT,TAPE1=INPUT,TAPE2=OUTPUT)
0001428       2*       DIMENSION GAM(10)

                  C          ELECTRO-OPTIC COEFFICIENTS

0001428       3*       R13=8.6E-9
0001548       4*       R33=30.8E-9
0001568       5*       R22=3.4E-9

                  C          REFRACTIVE INDICES

0001578       6*       QNO=2.286
0001618       7*       QNE=2.20

0001628       8*       A=0.25
0001648       9*       WAVL=6.328E-4
0001658      10*       QL=1.0
0001678      11*       PI=4.0*ATAN(1.0)
0001738      12*       AV=0.0
0001748      13*       JD=0
0001758      14*       JT=0
0001768      15*       MQ=0

                  C          DIELECTRIC CONSTANTS

0001778      16*       E3=27.0
0002008      17*       E1=45.0
0002018      18*       F3=SQRT(E3/E1)

0002078      19*       JE=0
0002078      20*       THET=0.0
0002108      21*       D=0.05
0002128      22*       DEL=D/9.0
0002138      23*       V=0.0

                  C          HEADINGS FOR OUTPUT

0002148      24*   400 WRITE(2,401) JT,D,A,E1,E3,DEL
0002338      25*   401 FORMAT(7H THETA=,I8,4X,2HD=,F6.4,4X,2HA=,F6.4,4X,3HE1=,F6.3,4X,
                     13HE3=,F6.3,4X,7H STEPS ,F6.4,3H MM)
0002338      26*   300 WRITE (2,301)
0002428      27*   301 FORMAT(2X,6H VOLTS,25X,17HWAVELENGTH RETARD,54X,7HAVERAGE)

0002428      28*   402 CONTINUE
0002438      29*       DEL=D/9.0
0002448      30*       F3=SQRT(E3/E1)

                  C          EVALUATE P AND Q

0002528      31*       F1=1.0/(WAVL*COS(THET))
0002578      32*       CS=COS(THET)*COS(THET)
0002648      33*       SS=SIN(THET)*SIN(THET)
0002718      34*       P=CS*R33+SS*R13
0002758      35*       PL=CS/(QNE*QNE)+SS/(QNO*QNO)
0003028      36*       PW=PL*PL*PL
0003038      37*       PL=SQRT(PW)
0003078      38*       P=P/PL
0003108      39*       GM1=0.0
0003108      40*       GN1=0.0
```

```
000311B      41*          K=1
000312B      42*          Z=0.0
000313B      43*          Q=-SS*R22/PL
000316B      44*          QN=1.0
000317B      45*      500 CONTINUE

                     C       EVALUATE R

000322B      46*          R=4.0*V/(QN*PI)
000326B      47*          R=R*SIN(QN*PI*A)
SEQ    47* CAUTION - RESULT = R TO LEFT OF = APPEARED TO LEFT OF PREVIOUS =    ********************************
000333B      48*          R=R/(QN*PI*A)
SEQ    48* CAUTION - RESULT = R TO LEFT OF = APPEARED TO LEFT OF PREVIOUS =    ********************************
000336B      49*          F2=QN*PI/D
                     C     EXP TERMS
000340B      50*          ZQ=-F2*F3
000341B      51*          VW=ZQ*QL*TAN(THET)
000350B      52*          IF(VW+70.0) 516,501,501
000352B      53*      516 EX1=-1.0
000354B      54*          GO TO 517
000355B      55*      501 EX1=EXP(VW)-1.0
000363B      56*      517 CONTINUE
000365B      57*          IF(JT) 515,520,515
000366B      58*      515 CONTINUE
000370B      59*          SN1=SIN(F2*Z)
000375B      60*          CS1=COS(F2*Z)

                     C           E INTEGRAL SUMMATION

000402B      61*          V1=R*EX1*SN1/TAN(THET)
000411B      62*          V2=R*EX1*CS1/(F3*TAN(THET))
000421B      63*          GM1=GM1+V1
000423B      64*          GN1=GN1+V2
000425B      65*          QN=QN+2.0
000427B      66*          IF(QN-200.0) 500,500,600
000431B      67*      600 QN=1.0
000434B      68*          GO TO 504

                     C     THETA=0 SEGMENT

000435B      69*      520 X=0.005
000440B      70*          IF(MQ) 502,907,502
000441B      71*      907 WRITE(2,521) X
000452B      72*      521 FORMAT(3H X=,F8.4)
000452B      73*          MQ=1
000452B      74*      502 CONTINUE

                     C       EVALUATE R

000454B      75*          R=4.0*V/(QN*PI)
000460B      76*          R=R*SIN(QN*PI*A)
SEQ    76* CAUTION - RESULT = R TO LEFT OF = APPEARED TO LEFT OF PREVIOUS =    ********************************
000465B      77*          R=R/(QN*PI*A)
SEQ    77* CAUTION - RESULT = R TO LEFT OF = APPEARED TO LEFT OF PREVIOUS =    ********************************
000470B      78*          R=R*EXP(-QN*PI*F3*X/D)
SEQ    78* CAUTION - RESULT = R TO LEFT OF = APPEARED TO LEFT OF PREVIOUS =    ********************************
000477B      79*          F2=QN*PI/D
000502B      80*          CS2=COS(F2*Z)
000507B      81*          V3=R*CS2*F2*QL
```

```
                      C          E INTEGRAL SUMMATION

000511B      82*           GM1=GM1-V3
000513B      83*           QN=QN+2.0
000515B      84*           IF(QN-200.0) 502,502,518

                      C          EVALUATE RETARDATIONS

000517B      85*      518  GAM(K)=2.0*GM1*R33*QNE*QNE*QNE/WAVL
000532B      86*           GO TO 519
000534B      87*      504  PAM=P*GN1-Q*GM1
000540B      88*           GAM(K)=F1*PAM
000546B      89*      519  Z=Z+DEL
000553B      90*           QN=1.0
000554B      91*           GM1=0.0
000554B      92*           GN1=0.0
000555B      93*           AV=AV+ABS(GAM(K))
000564B      94*           K=K+1
000565B      95*           IF(K-10) 500,500,505
000566B      96*      505  AV=AV/10.0

                      C          OUTPUT BLOCK

000571B      97*           WRITE(2,506) V,(GAM(KK),KK=1,10),AV
000614B      98*      506  FORMAT(1X,F8.4,10F9.4,2X,F10.4)

000614B      99*           K=1
000614B     100*           Z=0.0
000615B     101*           AV=0.0

                      C          VOLTAGE STEPS

000615B     102*           V=V+10.0
000620B     103*           IF(V-100.0) 402,402,507
000622B     104*      507  V=0.0

                      C          LOOP CONSTANTS

000624B     105*           JT=JT+1
000626B     106*           THET=THET+PI/180.0
000630B     107*           MQ=0
000631B     108*           IF(JT-10) 400,400,508
000633B     109*      508  JT=0
000635B     110*           THET=0.0
000636B     111*           JD=JD+1

                      C          OTHER GRATING CONFIGURATIONS

000637B     112*      510  D=0.10
000642B     113*           DEL=D/9.0
000643B     114*           A=0.25
000644B     115*           IF(JD-1) 400,400,511
000647B     116*      511  D=0.2
000652B     117*           DEL=D/9.0
000653B     118*           A=0.25
000654B     119*           IF(JD-2) 400,400,512
000657B     120*      512  JD=-1
000661B     121*           JE=JE+1
000663B     122*           IF(JE-1) 513,513,514
```

```
                C         ISOTROPIC CASES
000664B     123*    513 E1=1,0
000667B     124*        E3=1,0
000667B     125*        D=0,05
000670B     126*        A=0,25
000672B     127*        GO TO 400
000674B     128*    514 STOP
000677B     129*        END
```

THETA= 0 D= ,0500 A= ,2500 E1=45,000 E3=27,000 STEPS ,0056 MM

VOLTS	WAVELENGTH RETARD										AVERAGE
X= ,0050											
0	0	0	0	0	0	0	0	0	0	0	0
10,0000	-,6526	-,6203	-,4407	-,1347	-,0299	,0299	,1347	,4407	,6203	,6526	,3757
20,0000	-1,3053	-1,2406	-,8815	-,2694	-,0598	,0598	,2694	,8815	1,2406	1,3053	,7513
30,0000	-1,9579	-1,8609	-1,3222	-,4041	-,0897	,0897	,4041	1,3222	1,8609	1,9579	1,1270
40,0000	-2,6106	-2,4812	-1,7629	-,5389	-,1197	,1197	,5389	1,7629	2,4812	2,6106	1,5026
50,0000	-3,2632	-3,1015	-2,2036	-,6736	-,1496	,1496	,6736	2,2036	3,1015	3,2632	1,8783
60,0000	-3,9159	-3,7218	-2,6444	-,8083	-,1795	,1795	,8083	2,6444	3,7218	3,9159	2,2540
70,0000	-4,5685	-4,3421	-3,0851	-,9430	-,2094	,2094	,9430	3,0851	4,3421	4,5685	2,6296
80,0000	-5,2212	-4,9625	-3,5258	-1,0777	-,2393	,2393	1,0777	3,5258	4,9625	5,2212	3,0053
90,0000	-5,8738	-5,5828	-3,9666	-1,2124	-,2692	,2692	1,2124	3,9666	5,5828	5,8738	3,3810
100,0000	-6,5265	-6,2031	-4,4073	-1,3471	-,2991	,2991	1,3471	4,4073	6,2031	6,5265	3,7566

THETA= 1 D= ,0500 A= ,2500 E1=45,000 E3=27,000 STEPS ,0056 MM

VOLTS	WAVELENGTH RETARD										AVERAGE
0	0	0	0	0	0	0	0	0	0	0	0
10,0000	-,2764	-,2616	-,1977	-,0660	-,0176	,0176	,0659	,1977	,2616	,2764	,1639
20,0000	-,5528	-,5233	-,3955	-,1319	-,0353	,0353	,1319	,3955	,5233	,5528	,3277
30,0000	-,8292	-,7849	-,5932	-,1979	-,0529	,0529	,1978	,5932	,7849	,8292	,4916
40,0000	-1,1055	-1,0466	-,7910	-,2638	-,0706	,0705	,2638	,7909	1,0465	1,1055	,6555
50,0000	-1,3819	-1,3082	-,9887	-,3298	-,0882	,0882	,3297	,9887	1,3082	1,3819	,8194
60,0000	-1,6583	-1,5698	-1,1865	-,3957	-,1059	,1058	,3957	1,1864	1,5698	1,6583	,9832
70,0000	-1,9347	-1,8315	-1,3842	-,4617	-,1235	,1234	,4616	1,3842	1,8315	1,9347	1,1471
80,0000	-2,2111	-2,0931	-1,5820	-,5277	-,1411	,1411	,5276	1,5819	2,0931	2,2111	1,3110
90,0000	-2,4875	-2,3548	-1,7797	-,5936	-,1588	,1587	,5935	1,7796	2,3547	2,4875	1,4748
100,0000	-2,7638	-2,6164	-1,9775	-,6596	-,1764	,1763	,6595	1,9774	2,6164	2,7638	1,6387

```
      PROGRAM VLTI(INPUT,OUTPUT,TAPE1=INPUT,TAPE2=OUTPUT)
      DIMENSION GAM(10),A(9,9),B(9),X(9),AP(10),VX(10)
      DIMENSION RMG(9)
C     HORIZONTAL FIELD VERSION
C FOR EY
C           ELECTRO-OPTIC COEFFICIENTS
      R13=8.6E-9
      R33=30.8E-9
      R22=3.4E-9
      R51=28.0E-9
C           REFRACTIVE INDICES
      QNO=2.232
      QNE=2.151
      AA=0.25
      WAVL=11.5E-4
      XA=0.0
      STP=0.0
      DZ=0.0
      QL=1.0
      PI=4.0*ATAN(1.0)
      JD=0
      JT=0
      MQ=0
C           DIELECTRIC CONSTANTS
      E3=27.0
      E1=45.0
      JE=0
      E3=SQRT(E3/E1)
      THET=0.0
      D=0.05
      NP=36
      DEL=D/9.0
      QQ=1.0
  400 V=0.0
C           HEADINGS FOR OUTPUT
      WRITE(2,802)
  802 FORMAT(/10X,10H**********/)
      IC=0
      WRITE(2,401) JT,D,AA,E1,E3,DEL,V
  401 FORMAT(/7H THETA=,I8,4X,2HD=,F6.4,4X,2HA=,F6.4,4X,3HE1=,F6.3,4X,
     1 3HE3=,F6.3,7H STEPS ,F6.4,3H MM,2X,2HV=,F8.2,1HV)
      WRITE(2,16) NP
   16 FORMAT(19H NUMBER OF FINGERS=,I8)
```

```
                ILL=1
              402 CONTINUE
60          C         EVALUATE P AND Q
                DEL=D/9.0
                F3=SQRT(E3/E1)
                F1=1.0/(COS(THET)*WAVL)
65              CS=COS(THET)*COS(THET)
                SS=SIN(THET)*SIN(THET)
                P=CS*R33+SS*R13
                PL=CS/(QNE*QNE)+SS/(QNO*QNO)
                PW=PL*PL*PL
70              PL=SQRT(PW)
                P=P/PL
                GM1=0.0
                GN1=0.0
                K=1
75              Z=0.0
                Q=-SS*R22/PL
                QN=1.0
              500 CONTINUE
80          C         EVALUATE R
                R=4.0*V/(QN*PI)
                R=R*SIN(QN*PI*AA)/(QN*PI*AA)
                F2=QN*PI/D
85          C   EXP TERM
                ZQ=-F2*F3
                VW=ZQ*QL*TAN(THET)
                IF(VW+70.0) 516,501,501
              516 EX1=-1.0
90              GO TO 517
              501 EX1=EXP(VW)-1.0
              517 CONTINUE
                IF(JT) 515,520,515
              515 CONTINUE
95              SN1=SIN(F2*Z)
                CS1=COS(F2*Z)
            C         E INTEGRAL SUMMATION
100             V1=R*EX1*SN1/TAN(THET)
                V2=R*EX1*CS1/(F3*TAN(THET))
               21 GM1=GM1+V1
                GN1=GN1+V2
                QN=QN+2.0
105             IF(QN-100.0) 500,500,504
            C    THETA=0 SEGMENT
              520 CONTINUE
110             IF(MQ) 222,51,222
```

```
      51 WRITE(2,521) XA
     521 FORMAT(3H X=,F8.4,2HMM)
     222 MQ=1
     502 CONTINUE
115
C        EVALUATE R

         R=4.0*V/(QN*PI)
         R=R*SIN(QN*PI*AA)/(QN*PI*AA)
120      R=R*EXP(-QN*PI*F3*XA/D)
         F2=QN*PI/D
         CS2=COS(F2*Z)
         V3=R*CS2*F2

125   C     E INTEGRAL SUMMATION

      23 GM1=GM1+V3
         QN=QN+2.0
         IF(QN-100.0) 502,502,518
130
C           EVALUATE RETARDATIONS

     518 GAM(K)=GM1*R33*QNE*QNE*QNE*QL/WAVL
         GO TO 519
135  504 PAM=P*GN1+Q*GM1
         IF(ILL.GT.1) PAM=P*GN1-Q*GM1
         GAM(K)=F1*PAM
     519 Z=Z+DEL/2.0
         GM1=0.0
140      GN1=3.0
         QN=1.0
         DZ=Z-DEL/2.0
         K=K+1
         IF(K-10) 500,500,525
145  525 CONTINUE

C           CURVE FIT SEGMENT
C    GAUSS-SIEDEL

150      IF(V.GT.0.0) GO TO 209
         DO 602 MN=1,9
     602 X(MN)=0.0
         GO TO 97
     209 CONTINUE
155      DO 50 I=1,9
         B(I)=GAM(I+1)-GAM(10)
      50 X(I)=0.0
         DO 60 KK=1,9
         DO 60 I=1,9
160      QI=I
         Z=DEL*QI/2.0
      60 A(I,KK)=Z**KK
         N=9
         EPS=0.0
165      MAX=50
```

```
            ITER=1
 98         BIG=0.0
            DO 100 I=1,N
102         SUM=0.0
170         IF(I.EQ.1) GO TO 105
            LAST=I-1
            DO 106 J=1,LAST
106         SUM=SUM+A(I,J)*X(J)
            IF(I.EQ.N) GO TO 103
175     105 INIT=I+1
            DO 107 J=INIT,N
107         SUM=SUM+A(I,J)*X(J)
103         TEMP=(B(I)-SUM)/A(I,I)
            IF(ABS(TEMP-X(I)).GT.BIG) BIG=ABS(TEMP-X(I))
180     100 X(I)=TEMP
201         IF(BIG.LT.EPS) GO TO 97
110         IF(ITER.GE.MAX) GO TO 97
            ITER=ITER+1
            GO TO 98
185      97 CONTINUE
            IF(ILL.GT.1) GO TO 970
            DO 20 II=1,9
 20         RMG(II)=X(II)
            ILL=ILL+1
190         GO TO 402
970         CONTINUE
            ILL=1
807         TH=0.0
            IT=1
195
C           INCREMENTAL VECTOR SUMMATION
C  VECTOR SUM OVER PITCH

 13         Z=-D
200         DDL=D/50.0
            AMX=0.0
            AMY=0.0
            PO=D*SIN(TH)/50.0
            QIL=1.0
205      10 G=0.0
            GM=1.0
            PZ=Z
            IF(Z.LT.(-D/2.0)) GO TO 700
            GO TO 701
210     700 PZ=Z+D
            GO TO 702
701         IF(Z.LT.0.0) GO TO 703
            GO TO 704
703         PZ=-Z
215         DO 18 IL=1,9
 18         G=G+RMG(IL)*(PZ**IL)
            GO TO 19
704         IF(Z.LT.(D/2.0)) GO TO 705
            GO TO 706
220     705 PZ=Z
```

```
      GM=-1.0
      GO TO 702
  705 PZ=D-Z
      GM=-1.0
  702 CONTINUE
      DO 17 IL=1,9
   17 G=G+X(IL)*(PZ**IL)
   19 G=G*GM
      ANG=2.0*PI*((QIL-1.0)*PD/WAVL+G)
      AMX=AMX+COS(ANG)/100.0
      AMY=AMY+SIN(ANG)/100.0
      QIL=QIL+1.0
      Z=Z+DDL
      IF(Z.LT.0) GO TO 10
      FX=(AMX*AMX+AMY*AMY)
      KL=10
      IF(FX.LT.QQ) GO TO 808
      KL=IC
      IC=10
      STP=1.0
      GO TO 810
  808 IC=IC+1
      VX(IC)=V
      AP(IC)=FX
  810 CONTINUE
      IF(IC.LT.10) GO TO 800

C           OUTPUT BLOCK

      WRITE(2,200) (VX(KJ),KJ=1,KL)
  200 FORMAT(//7H VOLTS ,10F10.3)
      WRITE(2,202) (AP(KJ),KJ=1,KL)
  202 FORMAT(7H INTENS,10F10.3)

      IF(STP.EQ.1.0) GO TO 801
      IC=0

C           VOLTAGE STEPS

  800 V=V+10.0
      IF(XA.EQ.0.04) V=V+3.0
      IF(JT.GT.6) V=V+40.0
      QQ=FX
      Z=0.0
      K=1
      GO TO 402
  801 QQ=2.0
      K=1
      V=0.0
      MQ=0
      STP=3.0
      IC=0
      Z=0.0
      XA=XA+0.01
      IF(XA.LT.0.05) GO TO 400
```

```
                      JT=JT+2
                      THET=THET+PI/90.0
                      IF(JT-10) 400,400,508
                  508 JT=0
      280             XA=0.0
                      THET=0.0
                      JD=JD+1

                  C          GRATING CONFIGURATIONS
      285
                  510 D=0.10
                      AA=0.25
                      NP=18
                      IF(JD-1) 400,400,511
      290         511 D=0.2
                      AA=0.25
                      NP=10
                      IF(JD-2) 400,400,512
                  512 JD=0
      295             JE=JE+1
                      IF(JE-1) 513,513,514

                  C          ISOTROPIC CASES

      300         513 E1=1.0
                      E3=1.0
                      D=0.05
                      AA=0.25
                      NP=36
      305             DEL=D/9.0
                      V=0.0
                      GO TO 400
                  514 STOP
                      END
```

****

```
THETA=      0    D= .0500    A= .2500    E1=45.000    E3=27.000 STEPS  .0056 MM  V=    0.00V
NUMBER OF FINGERS=      36
X=  0.0000MM

VOLTS      0.000    10.000    20.000
INTENS     1.000      .265      .067
```

****

```
THETA=      0    D= .0500    A= .2500    E1=45.000    E3=27.000 STEPS  .0056 MM  V=    0.00V
NUMBER OF FINGERS=      36
X=  .0100MM

VOLTS      0.000    10.000    20.000    30.000    40.000
INTENS     1.000      .771      .320      .037      .009
```

****

```
      PROGRAM VDI2(INPUT,OUTPUT,TAPE1=INPUT,TAPE2=OUTPUT)
C     VERTICAL FIELD VERSION
C  DIVERGENCE
      DIMENSION GAM(20),A(9,9),B(9),X(9),AP(10),VX(10),RMG(9),XFG(10)
C        ELCTRO OPTIC COEFFICIENTS
      R13=8.6E-9
      R33=30.8E-9
      R22=3.4E-9
      R51=28.0E-9
C        REFRACTIVE INDICES
      ONO=2.286
      ONE=2.20
      AA=0.25
      WAVL=6.328E-4
      STP=0.0
      QL=1.0
      PI=4.0*ATAN(1.0)
      ALPH=0.0
      JT=3
C        DIELECTRIC CONSTANTS
      E3=27.0
      E1=45.0
      JE=0
      THET=3.1*PI/180.0
      D=0.2
      NP=10
      DEL=D/9.0
      QQ=2.0
  400 V=0.0
C        HEADINGS FOR OUTPUT
      WRITE(2,802)
  802 FORMAT(/10X,10H**********/)
      IC=0
      WRITE(2,401) JT,D,AA,E1,E3,DEL,V
  401 FORMAT(/7H THETA=,I8,4X,2HD=,F6.4,4X,2HA=,F6.4,4X,3HE1=,F6.3,4X,
     13HE3=,F6.3,7H STEPS ,F6.4,3H MM,2X,2HV=,F8.2,1HV)
      WRITE(2,16) NP
   16 FORMAT(19H NUMBER OF FINGERS=,I8)
      ILL=1
      WAL=ALPH*180.0/PI
      WRITE(2,521) WAL
  521 FORMAT(7H ALPHA=,F8.3)
```

```
      402 CONTINUE
C           EVALUATE P AND Q
   60       DFL=D/9,0
            F1=SQRT(E3/E1)
            F3=1,0/(COS(THET)*WAVL)
            CS=COS(THET)*COS(THET)
            SS=SIN(THET)*SIN(THET)
   65       P=CS*R33+SS*R13
            PL=CS/(QNE*QNE)+SS/(QNO*QNO)
            PW=PL*PL*PL
            PL=SQRT(PW)
            P=P/(PL*2,0)
   70       GM1=0,0
            GN1=0,0
            K=1
            Z=0,0
            Q=2,0*SIN(THET)*COS(THET)*R51/PL
   75       QN=1,0
            SUM1=0,0
            SUM2=0,0
            SUM3=0,0
            SUM4=0,0
   80       ADD1=0,0
            ADD2=0,0
            ICN=0
C           EVALUATE R
   85     102 R=4,0*V*SIN(QN*PI*AA)/(QN*QN*PI*PI*AA)
            F2=QN*PI/D
C           EVALUATE RETARDATION AS FUNCTION OF ALPHA
   90
            SUM1=SUM1+R*EXP(-F2*F1*QL*TAN(THET))*(COS(F2*Z)*(F2*TAN(ALPH)*SIN
           1(F2*QL*TAN(ALPH))-F2*F1*TAN(THET)*COS(F2*QL*TAN(ALPH)))-SIN(F2*Z)
           2*(F2*F1*TAN(THET)*SIN(F2*QL*TAN(ALPH))+F2*TAN(ALPH)*COS(F2*QL*TAN(
           3ALPH))))/(F2*(F1*F1*TAN(THET)*TAN(THET)+TAN(ALPH)*TAN(ALPH)))
   95       SUM2=SUM2-R*(F1*TAN(THET)*COS(F2*Z)+TAN(ALPH)*SIN(F2*Z))/(F1*F1*
           1TAN(THET)*TAN(THET)+TAN(ALPH)*TAN(ALPH))
            SUM3=SUM3-R*F1*EXP(-F2*F1*QL*TAN(THET))*(SIN(F2*Z)*(TAN(ALPH)*SIN
           1(F2*QL*TAN(ALPH))-F1*TAN(THET)*COS(F2*QL*TAN(ALPH)))-COS(F2*Z)*(
           2F1*TAN(THET)*SIN(F2*QL*TAN(ALPH))+TAN(ALPH)*COS(F2*QL*TAN(ALPH))))
  100       3/(F1*F1*TAN(THET)*TAN(THET)+TAN(ALPH)*TAN(ALPH))
            SUM4=SUM4+R*F1*(F1*TAN(THET)*SIN(F2*Z)+TAN(ALPH)*COS(F2*Z))/(F1*
           1F1*TAN(THET)*TAN(THET)+TAN(ALPH)*TAN(ALPH))
            QN=QN+2,0
            IF(QN,LT,50,0) GO TO 102
  105       GN1=SUM1+SUM2+ADD1
            GM1=SUM3+SUM4+ADD2
            ICN=ICN+1
            IF(ICN,GT,1) GO TO 504
            ADD1=GN1
  110       ADD2=GM1
```

```
                SUM1=0.0
                SUM2=0.0
                SUM3=0.0
                SUM4=0.0
115             ALPH=-ALPH
                QN=1.0
                GO TO 102
            504 PAM=P*GM1+Q*GN1
                GAM(K)=F3*PAM/2.0
120             PAM2=PAM-2.0*Q*GN1
                XFG(K)=F3*PAM2/2.0
                ICN=0
                ALPH=-ALPH
                ADD1=0.0
125             ADD2=0.0
            519 Z=Z+DEL/2.0
                SUM1=0.0
                SUM2=0.0
                SUM3=0.0
130             SUM4=0.0
                QN=1.0
                K=K+1
                IF(K-10) 102,102,525
            771 DO 773 JZ=1,10
135         773 GAM(JZ)=XFG(JZ)
            525 CONTINUE


140         C          CURVE FIT SEGMENT
            C    GAUSS-SIEDEL

                IF(Y.GT.0.0) GO TO 209
                DO 602 MN=1,9
145         602 X(MN)=0.0
                GO TO 97
            209 CONTINUE
                DO 50 I=1,9
                B(I)=GAM(I+1)-GAM(1)
150          50 X(I)=0.0
                DO 60 KK=1,9
                DO 60 I=1,9
                QI=I
                Z=DEL*QI/2.0
155          60 A(I,KK)=Z**KK
                N=9
                EPS=0.0
                MAX=50
                ITER=1
160          98 BIG=0.0
                DO 100 I=1,N
                SUM=0.0
                IF(I.EQ.1) GO TO 105
                LAST=I-1
165             DO 106 J=1,LAST
```

```
      106 SUM=SUM+A(I,J)*X(J)
          IF(I.EQ.N) GO TO 103
      105 INIT=I+1
          DO 107 J=INIT,N
  170 107 SUM=SUM+A(I,J)*X(J)
      103 TEMP=(B(I)-SUM)/A(I,I)
          IF(ABS(TEMP-X(I)).GT.BIG) BIG=ABS(TEMP-X(I))
      100 X(I)=TEMP
          IF(BIG.LT.EPS) GO TO 97
  175     IF(ITER.GE.MAX) GO TO 97
          ITER=ITER+1
          GO TO 98
       97 CONTINUE
          IF(ILL.GT.1) GO TO 970
  180     DO 20 II=1,9
       20 RMG(II)=X(II)
          ILL=ILL+1
          GO TO 771
      970 CONTINUE
  185     ILL=1
          TH=0.0
          IT=1

C             INCREMENTAL VECTOR SUMMATION
  190
          Z=-D
          DDL=D/50.0
          AMX=0.0
          AMY=0.0
  195     PD=D*SIN(TH)/50.0
          QIL=1.0
       10 G=0.0
          GM=1.0
          PZ=Z
  200     IF(Z.LT.(-D/2.0)) GO TO 700
          GO TO 701
      700 PZ=Z+D
          GO TO 702
      701 IF(Z.LT.0.0) GO TO 703
  205     GO TO 704
      703 PZ=-Z
          DO 18 IL=1,9
       18 G=G+RMG(IL)*(PZ**IL)
          GO TO 19
  210 704 IF(Z.LT.(D/2.0)) GO TO 705
          GO TO 706
      705 PZ=Z
          GM=-1.0
          GO TO 702
  215 706 PZ=D-Z
          GM=-1.0
      702 CONTINUE
          DO 17 IL=1,9
       17 G=G+X(IL)*(PZ**IL)
  220  19 G=G*GM
```

```
                ANG=2.0*PI*((QIL-1.0)*PD/WAVL+G)
                AMX=AMX+COS(ANG)/100.0
                AMY=AMY+SIN(ANG)/100.0
                QIL=QIL+1.0
  225           Z=Z+DDL
                IF(Z.LT.D) GO TO 10
                FX=(AMX*AMX+AMY*AMY)
                KL=10
                IF(FX.LE.QQ) GO TO 808
  230           KL=IC
                IC=10
                STP=1.0
                GO TO 810
              808 IC=IC+1
  235           VX(IC)=V
                AP(IC)=FX
              810 CONTINUE
                IF(IC.LT.10) GO TO 800

  240       C          OUTPUT BLOCK

                WRITE(2,200) (VX(KJ),KJ=1,KL)
              200 FORMAT(/7H VOLTS ,10F10.3)
                WRITE(2,202) (AP(KJ),KJ=1,KL)
  245           202 FORMAT(7H INTENS,10F10.3)

                IF(STP.EQ.1.0) GO TO 801
                IC=0
              800 V=V+5.0
  250           QQ=FX
                IF(ALPH.GT.PI/180.0) V=V+15.0
                IF(QQ.LT.0.05) V=V+3.0
                K=1
                GO TO 402
  255           801 QQ=2.0
                K=1
                V=0.0
                STP=0.0
                IC=0
  260           Z=0.0
                ALPH=ALPH+PI/360.0
                IF(ALPH.GT.PI/36.0) GO TO 512
                GO TO 400
              512 JE=JE+1
  265           ALPH=0.0
                IF(JE-1) 513,513,514

            C          ISOTROPIC CASES

  270         513 E1=1.0
                E3=1.0
                D=2.2
                NP=18
                AA=0.25
  275           DEL=D/9.0
```

```
            V=0.0
            GO TO 400
        514 STOP
            END
```

```
REGISTER ALLOCATION
  1 REGISTERS ASSIGNED OVER THE LOOP BEGINNING AT LINE   148
  1 REGISTERS ASSIGNED OVER THE LOOP BEGINNING AT LINE   165
  1 REGISTERS ASSIGNED OVER THE LOOP BEGINNING AT LINE   169
```

****

THETA= 3 D= .2000 A= .2500 E1=45.000 E3=27.000 STEPS .0222 MM V= 0.00V
NUMBER OF FINGERS= 10
ALPHA= 0.000

VOLTS	0.000	5.000	10.000	15.000	20.000	25.000	30.000	35.000	40.000	45.000
INTENS	1.000	.971	.888	.762	.608	.445	.292	.163	.071	.020

VOLTS	47.000	49.000
INTENS	.010	.007

****

```
      PROGRAM AGAP(INPUT,OUTPUT,TAPE1=INPUT,TAPE2=OUTPUT)
      DIMENSION PH(10),GZ(10),GX(10)
      PI=4.0*ATAN(1.0)
C           READ ELECTRODE DETAILS
   15 READ(1,14) D,A
   14 FORMAT(F10.4,F10.4)
      IF(D.EQ.0.0) STOP
C           OUTPUT HEADINGS
      WRITE(2,16) D,A
   16 FORMAT(////5H ****,5X,2HD=,F10.4,2HMM,5X,2HA=,F10.4)
C           V=100 VOLTS APPLIED
      V=50.0
C           DIELECTRIC CONSTANTS OF XTAL AND GAP MATERIAL
      E=10.0
      EA=1.0
C           INITIAL VALUES
      T=0.0
      DT=0.002
      X=T
      DX=0.002
   70 CONTINUE
      DEL=D/9.0
      K=1
      Z=0.0
  101 QN=1.0
      P=0.0
      EZ=0.0
      EX=0.0
C           LOOPS TO EVALUATE FIELDS IN XTAL AT INTERVALS OF APERTURE
  100 F1=8.0*V*SIN(QN*PI*A)*EXP(QN*PI*T/D)*EA
      F2=QN*PI*QN*PI*A
      FX=QN*PI*T/D
      IF(FX.GT.70.0) GO TO 102
      F3=(E+EA)*EXP(FX)-(E-EA)*EXP(-FX)
      F4=F1*EXP(-QN*PI*X/D)
      P=P+F4*SIN(QN*PI*Z/D)/(F2*F3)
      EZ=EZ+F4*QN*PI*COS(QN*PI*Z/D)/(D*F2*F3)
      EX=EX+F4*(-QN*PI/D)*SIN(QN*PI*Z/D)/(F2*F3)
      QN=QN+2.0
      IF(QN.LE.200.0) GO TO 100
  102 PH(K)=P
      GZ(K)=EZ
      GX(K)=EX
```

```
                    Z=Z+DEL/2.0
                    K=K+1
                    IF(K.LE.10) GO TO 101

60          C           OUTPUT BLOCK

                    XX=X-T
                    WRITE(2,10) XX,T
                 10 FORMAT(7H DEPTH=,F10.4,2HMM,5X,7HAIRGAP=,F10.4,2HMM)
65                  WRITE(2,11) (PH(J),J=1,10)
                 11 FORMAT(7H VOLTS,10F10.4)
                    WRITE(2,12) (GZ(J),J=1,10)
                 12 FORMAT(7H GRAD Z,10F10.4)
                    WRITE(2,13) (GX(J),J=1,10)
70                  13 FORMAT(7H GRAD X,10F10.4)

            C           STEP IN DEPTH IN XTAL AND GAP THICKNESS

                    X=X+DX
75                  IF(X.LE.(T+0.01))GO TO 70
                    T=T+DT
                    X=T
                    IF(T.LE.0.01) GO TO 70
                    T=0.0
80                  GO TO 15
                    END
```

```
****     D=     .2500MM     A=     .2500
DEPTH=    0.0000MM     AIRGAP=    0.0000MM
VOLTS,    0.0000   11.1116   22.2211   33.3355   44.4382   49.9948   50.0013   49.9996   50.0001   50.0000
GRAD Z 3981.9953 4017.7133 3983.1759 4015.1960 3990.3185    7.4566   -8.5902    6.0415   -3.0894    -.0000
GRAD X    0.0000 -644.9022-1329.6984-2271.6180-3797.1605-4032.2509-2934.6269-2486.8479-2302.0721-2244.3094
DEPTH=     .0020MM     AIRGAP=    0.0000MM
VOLTS,    0.0000    9.8451   19.5639   28.9332   37.2790   42.3907   44.2548   45.0523   45.4205   45.5300
GRAD Z 3550.9722 3530.3708 3455.2143 3258.0274 2610.3321 1069.3005  411.6765  193.0293   80.9980    -.0000
GRAD X    0.0000 -622.4253-1300.1959-2116.8866-3163.3716-3384.1223-2785.7639-2438.0807-2267.8509-2216.3696
DEPTH=     .0040MM     AIRGAP=    0.0000MM
VOLTS,    0.0000    8.6396   17.0669   24.9607   31.6993   36.3741   38.9589   40.3062   41.9681   41.1690
GRAD Z 3121.8893 3086.4398 2963.1210 2684.6339 2103.0464 1261.2565  660.6129  341.1067  147.9478     .0000
GRAD X    0.0000 -579.4468-1188.7655-1846.2694-2466.4918-2682.1163-2498.9946-2296.8569-2175.8796-2136.8245
DEPTH=     .0060MM     AIRGAP=    0.0000MM
VOLTS,    0.0000    7.5378   14.8279   21.5506   27.2590   31.5103   34.2674   35.8951   36.7452   37.0093
GRAD Z 2727.6193 2685.1522 2545.0108 2268.0410 1812.1957 1246.5918  763.8842  429.7217  193.5224     .0000
GRAD X    0.0000 -520.7209-1248.3182-1568.4669-2001.8323-2209.3423-2195.7166-2109.8409-2041.6389-2017.4036
DEPTH=     .0080MM     AIRGAP=    0.0000MM
VOLTS,    0.0000    6.5597   12.8735   18.6611   23.6068   27.4532   30.1553   31.8755   32.8174   33.1164
GRAD Z 2375.7793 2332.6736 2196.5027 1951.0859 1593.1842 1173.5477  782.9889  468.4077  217.9495     .0000
GRAD X    0.0000 -457.3272 -907.6102-1328.1231-1666.6322-1863.6030-1922.4482-1909.5066-1883.5474-1872.4593
DEPTH=     .0100MM     AIRGAP=    0.0000MM
VOLTS,    0.0000    5.7066   11.1885   16.2105   20.5407   24.0052   26.5536   28.2539   29.2169   29.5276
GRAD Z 2067.6813 2027.6713 1905.1121 1696.4797 1410.3106 1081.1413  758.3687  472.9353  225.6326     .0000
GRAD X    0.0000 -396.6011 -780.1115-1128.8641-1409.9773-1594.6404-1684.9575-1713.6676-1716.4957-1715.1864
DEPTH=    0.0000MM     AIRGAP=     .0020MM
VOLTS,    0.0000    4.7706    9.4121   13.7678   17.5847   20.3460   22.0189   23.0534   23.6283   23.8133
GRAD Z 1724.8861 1702.3520 1630.4410 1491.7342 1223.4294  762.7239  470.8535  283.4660  134.3444     .0000
GRAD X    0.0000 -315.9202 -638.0626 -973.5689-1320.1393-1459.5745-1393.4843-1343.3897-1315.2386-1306.1552
```

```
PROGRAM     SLFN                                7600 FTN V2,0  CY=63    OPT=2  05/11/73  10,00,34       PAGE      1
                    PROGRAM SLFN(INPUT,OUTPUT,TAPE1=INPUT,TAPE2=OUTPUT)
                    DIMENSION GAM(10),A(9,9),B(9),X(9)
                C       VERTICAL FIELDS
 05
                C   FOR ADDITIVE COMPON T
                C
 10             C          ELECTRO-OPTIC COEFFICIENTS
                    R13=8,6E-9
                    R33=30,8E-9
                    R22=3,4E-9
 15
                C          REFRACTIVE INDICES
                    ONO=2,286
 20                 ONE=2,20

                    AA=0,311
                    WAVL=6,328E-4
                    QL=1,0
 25                 AV=0,0
                    PI=4,0*ATAN(1,0)
                    JT=0
                    JD=0
                    XY=0,0
 30                 MQ=0
                C          DIELECTRIC CONSTANTS
                    E3=27,0
 35                 E1=45,0
                    F3=SQRT(E3/E1)
                    JE=0
                    THET=0,0
                    D=0,05
 40                 DEL=D/9,0
                C          HEADINGS FOR OUTPUT
                  400 READ(1,702) V
 45               702 FORMAT (F6,2)
                      WRITE(2,401) JT,D,AA,E1,E3,DEL,V
                  401 FORMAT(7H THETA=,I8,4X,2HD=,F6,4,4X,2HA=,F6,4,4X,3HE1=,F6,3,4X,
                     13HE3=,F6,3,7H STEPS ,F6,4,3H MM,2X,2HV=,F10,4,1HV)
                  700 WRITE (2,701) V
 50               701 FORMAT(10X,2HV=,F8,2)

                  402 CONTINUE
                      DEL=D/9,0
 55             C          EVALUATE P AND Q
```

```
      F3=SQRT(E3/E1)
      F1=1.0/COS(THET)
      CS=COS(THET)*COS(THET)
60    SS=SIN(THET)*SIN(THET)
      P=CS*R33+SS*R13
      PL=CS/(QNE*QNE)+SS/(QNO*QNO)
      PW=PL*PL*PL
      PL=SQRT(PW)
65    P=P/PL
      GM1=0.0
      GN1=0.0
      K=1
      Z=0.0
70    Q=-SS*R22/PL
      QN=1.0
  500 CONTINUE

C      EVALUATE R
75
      R=4.0*V/(QN*PI)
      R=R*SIN(QN*PI*AA)/(QN*PI*AA)
      F2=QN*PI/D
C   EXP TERM
80    ZQ=-F2*F3
      VW=ZQ*QL*TAN(THET)
      IF(VW+70.0) 516,501,501
  516 EX1=-1.0
      GO TO 517
85    501 EX1=EXP(VW)-1.0
      517 CONTINUE
      IF(JT) 515,520,515
  515 CONTINUE
      SN1=SIN(F2*Z)
90    CS1=COS(F2*Z)

C        E INTEGRAL SUMMATION

      V1=R*EX1*SN1/TAN(THET)
95    V2=R*EX1*CS1/(F3*TAN(THET))
   21 GM1=GM1+V1
      GN1=GN1+V2
      QN=QN+2.0
      IF(QN-100.0) 500,500,600
100   600 QN=1.0
      GO TO 504

C    THETA=0 SEGMENT

105   520 CONTINUE
      IF(MQ) 222,51,222
   51 WRITE(2,521) XY
  521 FORMAT(3H X=,F8.4,2HMM)
  222 MQ=1
110   502 CONTINUE
```

```
C       EVALUATE R

        R=4.0*V/(QN*PI)
        R=R*SIN(QN*PI*AA)/(QN*PI*AA)
        R=R*EXP(-QN*PI*F3*XY/D)
        F2=QN*PI/D
        SN2=SIN(F2*Z)
        V3=R*SN2*F2*F3

C          E INTEGRAL SUMMATION

     23 GM1=GM1+V3
        QN=QN+2.0
        IF(QN-100.0) 502,502,518

C             EVALUATE RETARDATIONS

    518 GAM(K)=GM1*R33*QNE*QNE*QNE
        GO TO 519
    504 PAM=P*GM1-Q*GN1
        GAM(K)=F1*PAM
    519 Z=Z+DEL/2.0
        GM1=0.0
        GN1=0.0
        QN=1.0
        DZ=Z-DEL/2.0
        AV=AV+GAM(K)/(10.0*WAVL)
        K=K+1
        IF(K-10) 500,500,505
    505 AV=AV-GAM(1)/WAVL
        WRITE(2,205)
    205 FORMAT(4X,8H Z RANGE,20X,11HRETARDATION,4X,8HDISTANCE,60X,
       17HAVERAGE)
        WRITE(2,800) DZ,(GAM(KK),KK=1,10),AV
    800 FORMAT(4X,F6.4,2X,10F10.4,2X,F8.4)

C             CURVE FIT SEGMENT
C     GAUSS-SIEDEL

        DO 50 I=1,9
        B(I)=GAM(I+1)-GAM(1)
     50 X(I)=0.0
        DO 60 KK=1,9
        DO 60 I=1,9
        QI=I
        Z=DEL*QI/2.0
     60 A(I,KK)=Z**KK
        N=9
        EPS=0.0
        MAX=50
        ITER=1
     98 BIG=0.0
        DO 100 I=1,N
    102 SUM=0.0
```

```
                      IF(I.EQ.1) GO TO 105
                      LAST=I-1
                      DO 106 J=1,LAST
                  106 SUM=SUM+A(I,J)*X(J)
      170             IF(I.EQ.N) GO TO 103
                  105 INIT=I+1
                      DO 107 J=INIT,N
                  107 SUM=SUM+A(I,J)*X(J)
                  103 TEMP=(B(I)-SUM)/A(I,I)
      175             IF(ABS(TEMP-X(I)).GT.BIG) BIG=ABS(TEMP-X(I))
                  100 X(I)=TEMP
                      S=0.0
                  201 IF(BIG.LT.EPS) GO TO 97
                  110 IF(ITER.GE.MAX) GO TO 97
      180             ITER=ITER+1
                      GO TO 98
                   97 AV=0.0
                      WRITE(2,202)
                  202 FORMAT(/11H POLYNOMIAL,5X,12HCOEFFICIENTS)
      185             WRITE(2,200) X(1),X(2),X(3),X(4),X(5),X(6),X(7),X(8),X(9)
                  200 FORMAT(1X,E10.4,1X,E10.4,1X,E10.4,1X,E10.4,1X,E10.4,1X,E10.4,
                     11X,E10.4,1X,E10.4,1X,E10.4)
                      WRITE(2,204)
                  204 FORMAT(4X,2H Z,9X,9HINTENSITY,5X,5HTHETA)
      190
                C  EVALUATE F'(Z) AND F''(Z)

                      Z=-DZ
                  526 SUM2=0.0
      195             F1Z=0.0
                      F2Z=0.0
                      Z1=Z
                      IF(Z.LT.0.0) Z1=-Z
                      IF(Z.LT.0.0)  GO TO 527
      200             GO TO 528
                  527 CONTINUE
                      DO 529 IK=1,9
                  529 X(IK)=-X(IK)
                  528 CONTINUE
      205             DO 523 JJ=1,9
                      QJ=JJ
                      SUM1=X(JJ)*QJ*(Z1**(JJ-1))
                      F1Z=F1Z+SUM1
                      IF(JJ.EQ.1) GO TO 523
      210             SUM2=X(JJ)*QJ*(QJ-1.0)*(Z1**(JJ-2))
                  523 F2Z=F2Z+SUM2
                      FN=ABS(F2Z)/(1.0+F1Z*F1Z)
                      IF(FN.GT.50.0) GO TO 533
                      QIN=EXP(-FN)
      215             GO TO 534
                  533 QIN=0.0
                  534 CONTINUE
                      IF(F1Z.EQ.0.0) GO TO 525
                      PHA=ATAN(1.0/ABS(F1Z))*180.0/PI
      220             GO TO 524
```

```
                525 PHA=90,0
               C          OUTPUT BLOCK
      225       524 WRITE(2,203) Z,QIN,PHA
                203 FORMAT(1X,F6,4,4X,E12,5,4X,E12,5)

               C          LOOP CONSTANTS
      230
                    IF(Z,LT,0,0) GO TO 531
                    GO TO 532
                531 CONTINUE
                    DO 530 KI=1,9
      235       530 X(KI)=-X(KI)
                532 CONTINUE
                    Z=Z+DEL/2,0
                    IF(Z,LE,DZ) GO TO 526
                    K=1
      240           MQ=0
                    Z=0,0
                    XY=XY+0,02
                    IF(XY,LT,0,05) GO TO 400
                    JT=JT+2
      245           THET=THET+PI/90,0
                    WRITE(2,801)
                801 FORMAT(////10X,10H**********////)
                    IF(JT-10) 400,400,508
                508 JT=0
      250           XY=0,0
                    THET=0,0
                    JD=JD+1

               C          GRATING CONFIGURATIONS
      255
                510 D=0,10
                    AA=0,289
                    IF(JD-1) 400,400,511
                511 D=0,2
      260           AA=3,0/8,0
                    IF(JD-2) 400,400,512
                512 STOP
                    END
```

SUMMARY OF CHANGES MADE BY THE OPTIMIZER
  48 WORDS OF INVARIANT RLIST REMOVED FROM THE LOOP STARTING AT LINE 110

REGISTER ALLOCATION
  1 REGISTERS ASSIGNED OVER THE LOOP BEGINNING AT LINE 151
  1 REGISTERS ASSIGNED OVER THE LOOP BEGINNING AT LINE 168
  1 REGISTERS ASSIGNED OVER THE LOOP BEGINNING AT LINE 172

THETA= 0 D= ,0500 A= ,3110 E1=45,000 E3=27,000 $TEPS ,0056 MM V= 18,3200V

A= 18,32

X= 0,0000MM

Z RANGE	RETARDATION	DISTANCE						AVERAGE
,0250	0,0000	-,0000	-,0001	-,0001	-,0002	-,0003	-,0004	-,0003	-,0002	-,0002	,2921

POLYNOMIAL COEFFICIENTS

-,1169E-01 -,8908E+00 ,1135E+02 ,2017E+05 -,2588E+07 ,4070E+08 ,5530E+10 -,1872E+12 ,7116E+12

Z	INTENSITY	THETA
-,0250	0,	,81075E+02
-,0222	,21722E-07	,86939E+02
-,0194	,17092E-07	,87829E+02
-,0167	,14088E-05	,89431E+02
-,0139	,81125E-01	,88192E+02
-,0111	,57820E-01	,88313E+02
-,0083	,81905E-01	,88789E+02
-,0056	,48928E+00	,89036E+02
-,0028	,48307E+00	,89120E+02
,0000	,16841E+00	,89330E+02
,0028	,48307E+00	,89120E+02
,0056	,48928E+00	,89036E+02
,0083	,81905E-01	,88789E+02
,0111	,57820E-01	,88313E+02
,0139	,81125E-01	,88192E+02
,0167	,14088E-05	,89431E+02
,0194	,17092E-07	,87829E+02
,0222	,21722E-07	,86939E+02
,0250	0,	,81075E+02

```
      PROGRAM DIFT(INPUT,OUTPUT,TAPE1=INPUT,TAPE2=OUTPUT)
      DIMENSION REM(10),OTH(10)
      DIMENSION A(5)
C     FOURIER VERSION
C     ASSUME SINUSOIDAL DISTRIBUTION  AND AGAUSSIAN BEAM
C           CASES INVESTIGATED
C   D=0.1   TH=2   A=0.250  HORIZ TAL FIELDS
C   D=0.1   TH=2   A=0.289       VF
C   D=0.1   TH=2   A=0.250       VF
C        THIS PROGRAM LOOKS AT RESIDUES
C     INITIAL VALUES
      IM=0
   19 PI=4.0*ATAN(1.0)
      WAVL=7.0E-4
      D=0.1
      QN=18.0
C           PHASE RANGE AND INCREMENTS
      PA=PI
      PH=0.0
      IN=0
      QPH=PH*180.0/PI
C           FOURIER COEFFICIENTS
      READ(1,21) (A(K),K=1,5)
   21 FORMAT(5F10.6)
      WRITE(2,22) (A(K),K=1,5)
   22 FORMAT(9H F COEFFS,5F10.4)
      WRITE(2,12) D,QN,QPH
   12 FORMAT(/3H D=,F6.4,2HMM,2X,F8.4,7HFINGERS,2X,3HPH=,F8.4,3HDEG)
   14 EM=0.0
C           FAR FIELD ANGLE
      TH=0.0
      TH=TH*PI/180.0
      PM=0.0
      QM=1.0
      R=QN*50.0
      IC=1
      DD=QN*D/2.0
      QK=2.0*PI/WAVL
      QPH=PH*180.0/PI
C           DIFFRACTION INTEGRAL SUMMATION
```

```
      100 FN1=DD*QK*SIN(TH)/R
          FN2=PI*DD/(D*R)
       10 F1=QM*FN1
          F2=0.0
   60     F3=QM*FN2
          DO 20 N=1,5
          QL=N
       20 F2=F2+PH*A(N)*SIN(QL*F3)
          C=COS(F1+F2)
   65     F1=1.0
C            GAUSSIAN BEAM
          IF(IM.GT.2) F1=EXP(-((4.0*QM*DD/R-QN*D)**2)/(QN*QN*D*D))
   70
          EM=EM+2.0*C*F1
          QM=QM+1.0
          IF(QM.LE.R) GO TO 10
          OTH(IC)=TH*180.0/PI
   75     TH=TH+0.2*PI/180.0
          QM=1.0
          REM(IC)=EM*EM/(4.0*R*R)
          EM=0.0
          IC=IC+1
   80     IF(IC.LE.10) GO TO 100
C            OUTPUT BLOCK
          WRITE(2,11) QPH,OTH(1)
   85    11 FORMAT(7H PHASE=,F10.4,9HTHETA    ,E16.8)
          WRITE(2,13) REM(1)
       13 FORMAT(17X,10H INTENSITY,E16.8)
   90
C            LOOP CONSTANTS
C       SCAN FOR PHI
          PH=PH+PI*0.05
          IF(PH.LE.PA) GO TO 14
   95     WRITE(2,18)
       18 FORMAT(//10H**********//)
          PH=0.0
       17 IF(IM.GT.4) STOP
          IM=IM+1
  100     GO TO 19
          END
```

```
      PROGRAM QSIN(INPUT,OUTPUT,TAPE1=INPUT,TAPE2=OUTPUT)
      DIMENSION QI(11)
      PI=4.0*ATAN(1.0)
      A=0.0
05    DA=PI/90.0
      QN=100.0

C        OUTPUT HEADINGS

10    WRITE(2,10)
   10 FORMAT(3X,6H PHASE,10X,15HENERGY OUTSIDE ,15HORDERS (3D MAX))

   13 SM=0.0

15    C          CALCULATE ENERGY IN FIRST TEN ORDERS
      C          ASSUME SINUSOIDAL PHASE CORRUGATION

      DO 19 KK=1,11
      S=0.0
20    C=0.0
      QJ=KK-1
      DO 11 J=1,100
      R=J
      ANG=A*SIN(2.0*PI*R/QN)+3.6*R*PI*QJ/180.0
25    S=S+SIN(ANG)
   11 C=C+COS(ANG)
   19 QI(KK)=(S*S+C*C)/(QN*QN)
      DO 20 KK=2,11
      SM=SM+2.0*QI(KK)
30    20 QI(KK)=2.0*QI(KK)

C          CALCULATE ENERGY LYING OUTSIDE SUCCESSIVE ORDERS

      SM=SM+QI(1)
35    OP1=SM-QI(1)
      OP2=OP1-QI(2)
      OP3=OP2-QI(3)
      OP4=OP3-QI(4)
      P=A*180.0/PI
40
C    INNER COLUMNS CONTAIN ENERGY IN RESPECTIVE ORDERS
C    ZERO TO FOURTH ORDER ENERGY
C OUTER COLUMNS CONTAIN TOTAL ENERGY OUTSIDE ZERO, FIRST , SECOND
C ORDERS
45
C        OUTPUT BLOCK

      WRITE(2,12) P,QI(1),QI(2),QI(3),QI(4),QI(5)
   12 FORMAT(F10.4,6X,5F12.6)
50    WRITE(2,21) P,SM,OP1,OP2,OP3,OP4
   21 FORMAT(20X,F10.4,6X,5F12.6)

C        LOOPING CONSTANTS

55    A=A+DA
```

```
      IF(A,LT,(10,0*PI)) GO TO 13
      STOP
      END
```

PHASE	ENERGY OUTSIDE ORDERS (3D MAX)						
0,0000	1,000000	,000000	,000000	,000000	,000000		
	0,0000	1,000000	0,000000	-,000000	-,000000	-,000000	
2,0000	,999391	,000609	,000000	,000000	,000000		
	2,0000	1,000000	,000609	,000000	,000000	-,000000	
4,0000	,997565	,002434	,000001	,000000	,000000		
	4,0000	1,000000	,002435	,000001	,000000	,000000	
6,0000	,994528	,005468	,000004	,000000	,000000		
	6,0000	1,000000	,005472	,000004	,000000	,000000	
8,0000	,990288	,009700	,000012	,000000	,000000		
	8,0000	1,000000	,009712	,000012	,000000	,000000	
10,0000	,984856	,015115	,000029	,000000	,000000		
	10,0000	1,000000	,015144	,000029	,000000	,000000	
12,0000	,978247	,021693	,000060	,000000	,000000		
	12,0000	1,000000	,021753	,000060	,000000	,000000	
14,0000	,970480	,029410	,000110	,000000	,000000		
	14,0000	1,000000	,029520	,000110	,000000	,000000	
16,0000	,961575	,038237	,000188	,000000	,000000		
	16,0000	1,000000	,038425	,000188	,000000	,000000	
18,0000	,951557	,048143	,000299	,000001	,000000		
	18,0000	1,000000	,048443	,000300	,000001	,000000	
20,0000	,940453	,059091	,000455	,000002	,000000		
	20,0000	1,000000	,059547	,000456	,000002	,000000	
22,0000	,928293	,071042	,000663	,000003	,000000		
	22,0000	1,000000	,071707	,000666	,000003	,000000	
24,0000	,915110	,083951	,000934	,000005	,000000		
	24,0000	1,000000	,084890	,000939	,000005	,000000	
26,0000	,900940	,097773	,001280	,000007	,000000		
	26,0000	1,000000	,099060	,001288	,000007	,000000	
28,0000	,885820	,112456	,001713	,000011	,000000		
	28,0000	1,000000	,114180	,001724	,000012	,000000	
30,0000	,869792	,127947	,002244	,000017	,000000		
	30,0000	1,000000	,130208	,002261	,000017	,000000	
32,0000	,852899	,144190	,002886	,000025	,000000		
	32,0000	1,000000	,147101	,002912	,000025	,000000	
34,0000	,835184	,161126	,003653	,000036	,000000		
	34,0000	1,000000	,164816	,003690	,000036	,000000	
36,0000	,816697	,178693	,004559	,000051	,000000		
	36,0000	1,000000	,183303	,004610	,000051	,000000	
38,0000	,797484	,196829	,005617	,000070	,000000		
	38,0000	1,000000	,202516	,005687	,000070	,000000	
40,0000	,777597	,215466	,006841	,000095	,000001		
	40,0000	1,000000	,222403	,006937	,000095	,000001	
42,0000	,757089	,234538	,008246	,000126	,000001		
	42,0000	1,000000	,242911	,008373	,000127	,000001	
44,0000	,736012	,253976	,009845	,000165	,000002		
	44,0000	1,000000	,263988	,010012	,000167	,000002	
46,0000	,714421	,273710	,011652	,000214	,000002		
	46,0000	1,000000	,285579	,011869	,000217	,000002	

```
      PROGRAM CAPC(INPUT,OUTPUT,TAPE1=INPUT,TAPE2=OUTPUT)
      E0=8.854E-15
      PI=4.0*ATAN(1.0)
05    C          DIELECTRIC CONSTANTS
      E1=45.0
      E3=27.0
      F1=SQRT(E3*E1)
10    C          DIELECTRIC CONSTANT OF SURROUNDING MATERIAL
      EG=7.5
      C          ELECTRODE LENGTH
15
      QL=1.9
      N=1
      MH=0
  102 DO 200 J=1,3
20    C          FINE,MEDIUM,COARSE GRATING DATA
      IF(J-1) 10,777,10
25    C          COARSE GRATING
  777 A=0.25
      D=0.20
      QN=10.0
30    GO TO 20
   10 IF(J-2) 12,666,12
      C          MEDIUM GRATING DATA
35  666 A=0.25
      D=0.10
      QN=18.0
      GO TO 20
40    C          FINE GRATING DATA
   12 CONTINUE
      A=0.25
      D=0.05
45    QN=36.0
   20 CONTINUE
      C          EVALUATE ONLY FIRST TERM OF FOURIER EXPANSION
50    A1=(SIN(PI*A))**2
      C          CALCULATE CAPACITANCE
      C1=2.0*(QN-1.0)*QL*E0/(PI*PI*PI*A*A)
55    C1=C1*A1
```

```
      CG=C1*EG
      CX=C1*F1

C          OUTPUT BLOCK
60
      WRITE (2,700) EG,E1,E3,QN,D,A
  700 FORMAT(4H/EG=,F6.3,4X,3HE1=,F6.3,4X,3HE3=,F6.3,4X,2HN=,F6.2,4X,
     12HD=,F8.4,4X,2HA=,F8.4)
      WRITE (2,701) CG,CX
65
  701 FORMAT (10H C5GLASS)=,E10.4,5X,8HC(XTAL)=,E10.4,6HFARADS)

  200 CONTINUE
      N=N+1
      IF(N-2) 888,888,101
70
C          OTHER CONFIGURATIONS

  888 E1=45.0
      E3=45.0
75    GO TO 102
  101 IF(N-3) 104,103,104
  103 E1=27.0
      E3=27.0
      GO TO 102
80    104 IF(MM) 105,105,106
  105 MM=MM+1
      E1=84.0
      E3=30.0
      GO TO 102
85    106 STOP
      END
```

```
 EG= 7.500    E1=45.000    E3=27.000    N= 10.00    D=  .2000   A=  .2500
20 C5GLASS)= .5860E-12     C(XTAL)= .2723E-11FARADS
 EG= 7.500    E1=45.000    E3=27.000    N= 18.00    D=  .1000   A=  .2500
22 C5GLASS)= .1107E-11     C(XTAL)= .5144E-11FARADS
 EG= 7.500    E1=45.000    E3=27.000    N= 36.00    D=  .0500   A=  .2500
24 C5GLASS)= .2279E-11     C(XTAL)= .1059E-10FARADS
 EG= 7.500    E1=45.000    E3=45.000    N= 10.00    D=  .2000   A=  .2500
26 C5GLASS)= .5860E-12     C(XTAL)= .2723E-11FARADS
 EG= 7.500    E1=45.000    E3=45.000    N= 18.00    D=  .1000   A=  .2500
28 C5GLASS)= .1107E-11     C(XTAL)= .5144E-11FARADS
 EG= 7.500    E1=45.000    E3=45.000    N= 36.00    D=  .0500   A=  .2500
30 C5GLASS)= .2279E-11     C(XTAL)= .1059E-10FARADS
 EG= 7.500    E1=27.000    E3=27.000    N= 10.00    D=  .2000   A=  .2500
32 C5GLASS)= .5860E-12     C(XTAL)= .2723E-11FARADS
 EG= 7.500    E1=27.000    E3=27.000    N= 18.00    D=  .1000   A=  .2500
34 C5GLASS)= .1107E-11     C(XTAL)= .5144E-11FARADS
 EG= 7.500    E1=27.000    E3=27.000    N= 36.00    D=  .0500   A=  .2500
36 C5GLASS)= .2279E-11     C(XTAL)= .1059E-10FARADS
 EG= 7.500    E1=84.000    E3=30.000    N= 10.00    D=  .2000   A=  .2500
38 C5GLASS)= .5860E-12     C(XTAL)= .2723E-11FARADS
 EG= 7.500    E1=84.000    E3=30.000    N= 18.00    D=  .1000   A=  .2500
40 C5GLASS)= .1107E-11     C(XTAL)= .5144E-11FARADS
 EG= 7.500    E1=84.000    E3=30.000    N= 36.00    D=  .0500   A=  .2500
42 C5GLASS)= .2279E-11     C(XTAL)= .1059E-10FARADS
```

```
      PROGRAM ADPR(INPUT,OUTPUT,TAPE1=INPUT,TAPE2=OUTPUT)

C           CONSTANTS

      QUIN=0.0
      QN=1.48
      J=0
      L=1
      PI=4.0*ATAN(1.0)
C           OUTPUT HEADINGS

      WRITE(2,9)
    9 FORMAT(10H INCIDENCE,4X,4HI(R),5X,4HI(L),4X,6HDEL(R),
     14X,6HDEL(L),4X,4HINCL)
      WRITE (2,16)
   16 FORMAT (4H ADP)

   10 QN1=1.266
      FB=QN/QN1
      BR=FB*SIN(QUIN)
      BQ=BR*BR
      IF(1.0-BQ) 0,11,11
      RIR=1.0
      RIP=1.0
      GO TO 12
   11 CONTINUE

C           CALCULATE REFLECTION CHARACTERISTICS FOR BOTH POLARISATIONS

      FR=FB*COS(QUIN)
      RIR=(FR-SQRT(1.0-BQ))/(FR+SQRT(1.0-BQ))
      RIP=(COS(QUIN)-FB*SQRT(1.0-BQ))/(COS(QUIN)+FB*SQRT(1.0-BQ))
      RIR=RIR**2
      RIP=RIP**2
   12 CONTINUE
      IF(FB*FB*SIN(QUIN)*SIN(QUIN)-1.0) 0,0,17
      DR=0.0
      DL=PI
      IF(COS(QUIN)-FB*SQRT(1.0-FB*FB*SIN(QUIN)*SIN(QUIN))) 0,17,17
      DL=0.0
      GO TO 18
   17 CONTINUE
      IF(J-90) 0,13,13
      TDR=SQRT(ABS(1.0-BQ))/(FB*COS(QUIN))
      TDL=FB*SQRT(ABS(1.0-BQ))/COS(QUIN)
   13 DL=2.0*ATAN(TDL)
      DR=2.0*ATAN(TDR)
   18 IF(ABS(SIN(PI/2.0-QUIN))-1.0/QN) 20,20,0
      QINC=999.9
      GO TO 21
   20 QINC=ASIN(QN*SIN(PI/2.0-QUIN))
      QINC=QINC*180.0/PI
   21 CONTINUE
      DR=DR*180.0/PI
```

```
                DL=DL*180,0/PI

          C          OUTPUT BLOCK

60              WRITE(2,14) J,RIR,RIP,DR,DL,QINC
             14 FORMAT(I6,6X,F10,5,F10,5,F10,5,F10,5,F10,5)

                QUIN=QUIN+PI/180,0

65        C          LOOP CONSTANTS

                J=J+1
                IF(J-90) 10,10,0
                L=L+1
70              J=0
                QUIN=0,0
                QN=2,20
                WRITE (2,15)
             15 FORMAT (16H LITHIUM NIOBATE)
75              IF(L-2) 10,10,0
                STOP
                END
```

```
      PROGRAM PHOP(INPUT,OUTPUT,TAPE1=INPUT,TAPE2=OUTPUT)
C   RUN FOR PHASE MODULATORS
C    MAGNIFIED SCALE

C          OUTPUT HEADINGS

      WRITE(2,210)
  210 FORMAT(6X,5HGAMA1,12X,5HGAMA2,10X,4HDELN,12X,5HDELN1,10X,5HDELN2,
     120X,6HANGLES)

      PI=4,0*ATAN(1,0)

C  CHOOSE AL=PHI,AM=THETA,AN=PSI ACCORDING TO XTAL SYMMETRY
C   START FROM 0,001 AS ANGLES APPEAR AS QUOTIENTS

C          START POINTS

      AL=-5,001
   11 AM=35,001
   12 AN=85,001

   15 PHI=(AL*PI)/180,0
      CETA=(AM*PI)/180,0
      PESI=(AN*PI)/180,0

C  A(I,J) ARE THE DIRECTION COSINES

      A11=COS(PHI)*COS(CETA)*COS(PESI)-SIN(PHI)*SIN(PESI)
      A12=SIN(PHI)*COS(CETA)*COS(PESI)+COS(PHI)*SIN(PESI)
      A13=-(SIN(CETA)*COS(PESI))
      A21=-(COS(PHI)*COS(CETA)*SIN(PESI)+SIN(PHI)*COS(PESI))
      A22=-SIN(PHI)*COS(CETA)*SIN(PESI)+COS(PHI)*COS(PESI)
      A23=SIN(CETA)*SIN(PESI)

C  R(I,J) COEFFICIENT TERMS

      R11=0,0
      R12=0,0
      R13=0,0
      R21=0,0
      R22=0,0
      R23=0,0
      R31=0,0
      R32=0,0
      R33=0,0
      R41=0,245E-10
      R42=0,0
      R43=0,0
      R51=0,0
      R52=0,245E-10
      R53=0,0
      R61=0,0
      R62=0,0
      R63=0,85E-11
```

```
C REFRACTIVE INDEX (UNIAXIAL XTALS ONLY)

      ANN=1,53
60    ANE=1,48

C  KRONECKER DELTA TIMES GYRATION TENSOR

      S11=1,0/(ANN*ANN)
65    S22=S11
      S33=1,0/(ANE*ANE)
      AMMB=A11*A11*S11+A12*A12*S22+A13*A13*S33
      AMMS=A11*A11*(A11*R11+A12*R12+A13*R13)+A12*A12*(A12*R22+A11*R21
     1+A13*R23)+A13*A13*(A13*R33+A12*R32+A11*R31)+2,0*((A11*A12*A13)*(
70   2R41+R52+R63)+A11*A11*(A13*R51+A12*R61)+A12*A12*(A13*R42+A11*R62)
     3+A13*A13*(A12*R43+A11*R53))
      DLTB=A21*A21*S11+A22*A22*S22+A23*A23*S33
      DLTS=A21*A21*(A11*R11+A12*R12+A13*R13)+A22*A22*(A12*R22+A11*R21+
     4A13*R23)+A23*A23*(A13*R33+A12*R32+A11*R31)+2,0*(A11*A23*(A22*R41
75   5+A21*R51)+A12*A23*(A22*R42+A21*R52)+A13*A23*(A22*R43+A21*R53)+
     6A22*(A11*A21*R61+A12*A21*R62+A13*A21*R63))
      ACB=A11*A21*S11+A12*A22*S22+A13*A23*S33
      ACS=A11*A21*(A11*R11+A12*R12+A13*R13)+A12*A22*(A12*R22+A11*R21+
     7A13*R23)+A13*A23*(A13*R33+A12*R32+A11*R31)+A11*((A12*A23+A13*A22
80   8)*R41+(A11*A23+A21*A13)*R51+(A11*A22+A21*A12)*R61)+A12*((A12*
     9A23+A13*A22)*R42+(A11*A23+A13*A21)*R52+(A11*A22+A12*A21)*R62)
     Z+A13*((A12*A23+A13*A22)*R43+(A11*A23+A13*A21)*R53+(A11*A22+A12*A21
     Y)*R63)
      APO=(AMMB+DLTB)/2,0+SQRT((AMMB-DLTB)**2+4,0*ACB**2)/2,0
85    ALO=(AMMB+DLTB)/2,0-SQRT((AMMB-DLTB)**2+4,0*ACB**2)/2,0
      AQO=(AMMS+DLTS)/2,0+(2,0*(AMMB-DLTB)*(AMMS-DLTS)+8,0*ACB*ACS)/(
     A4,0*SQRT((AMMB-DLTB)**2+4,0*ACB**2))
      ARO=(AMMS+DLTS)/2,0-(2,0*(AMMB-DLTB)*(AMMS-DLTS)+8,0*ACB*ACS)/(
     B4,0*SQRT((AMMB-DLTB)**2+4,0*ACB**2))
90
C   WAVL IS LIGHT WAVELENGTH USED

      WAVL=0,6328E-06

95    FUN1=(AQO/SQRT(APO*APO*APO))/2,0
      FUN2=(ARO/SQRT(ALO*ALO*ALO))/2,0

C  DLN IS THE INDUCED BIREFRINGENCE

100   DLN=FUN1-FUN2
      GAMA=(2,0*3,142*DLN)/WAVL
      GAM1=FUN1*2,0*PI/WAVL
      GAM2=FUN2*2,0*PI/WAVL

105   C          MINIMUM LIMIT OF INTEREST
      VAR4=0,414E-03

      IF(ABS(GAM1)-VAR4) 59,60,60

110   C          OUTPUT BLOCK
```

```
                      60 WRITE(2,200) GAM1,GAM2,DLN,FUN1,FUN2,AL,AM,AN
                     200 FORMAT(5E17,8,3F10,2)
     115           C    ANGLE LIMITS SET FROM SYMMETRY
                   C  STEPPING INTERVALS
                      59 PNGL=95,0
     120                 IF(AN-PNGL)30,30,31
                      30 AN=AN+1
                         GO TO 15
                      31 CNGL=45,0
                         IF(AM-CNGL)32,32,77
     125              32 AM=AM+1
                         GO TO 12
                      77 ANGL=5,0
                         IF(AL-ANGL)38,38,37
                      38 AL=AL+1
     130                 GO TO 11
                      37 STOP
                         END
MORE MEMORY WOULD HAVE RESULTED IN BETTER OPTIMIZATION
```

GAMA1	GAMA2	DELN	DELN1	DELN2	ANGLES		
-.41414912E-03	.25119183E-06	-.41735602E-10	-.41710303E-10	.25298345E-13	-2.00	43.00	92.00
-.41426711E-03	.37662931E-06	-.41760118E-10	-.41722186E-10	.37931561E-13	-2.00	43.00	93.00
-.41425891E-03	.50195206E-06	-.41771914E-10	-.41721361E-10	.50553222E-13	-2.00	43.00	94.00
-.41412452E-03	.62712191E-06	-.41770985E-10	-.41707826E-10	.63159485E-13	-2.00	43.00	95.00
-.41417163E-03	.25585456E-06	-.41738338E-10	-.41712570E-10	.25767944E-13	-2.00	44.00	92.00
-.41428252E-03	.38362047E-06	-.41762374E-10	-.41723738E-10	.38635664E-13	-2.00	44.00	93.00
-.41426721E-03	.51126952E-06	-.41773688E-10	-.41722196E-10	.51491614E-13	-2.00	44.00	94.00
-.41412571E-03	.63876283E-06	-.41772278E-10	-.41707946E-10	.64331880E-13	-2.00	44.00	95.00
-.41401245E-03	-.62782990E-07	-.41690215E-10	-.41696538E-10	-.63230788E-14	-1.00	43.00	89.00
-.41429233E-03	.62849020E-10	-.41724732E-10	-.41724726E-10	.63297290E-17	-1.00	43.00	90.00
-.41444601E-03	.62908669E-07	-.41746539E-10	-.41740204E-10	.63357364E-14	-1.00	43.00	91.00
-.41447345E-03	.12573533E-06	-.41755630E-10	-.41742967E-10	.12663213E-13	-1.00	43.00	92.00
-.41437463E-03	.18852368E-06	-.41752002E-10	-.41733015E-10	.18986832E-13	-1.00	43.00	93.00
-.41414959E-03	.25125461E-06	-.41735655E-10	-.41710351E-10	.25304668E-13	-1.00	43.00	94.00
-.41405275E-03	-.63948396E-07	-.41694157E-10	-.41700597E-10	-.64404507E-14	-1.00	44.00	89.00
-.41432909E-03	.64015652E-10	-.41728435E-10	-.41728428E-10	.64472243E-17	-1.00	44.00	90.00
-.41447922E-03	.64076408E-07	-.41750002E-10	-.41743548E-10	.64533432E-14	-1.00	44.00	91.00
-.41450310E-03	.12806928E-06	-.41758852E-10	-.41745953E-10	.12898273E-13	-1.00	44.00	92.00
-.41440071E-03	.19202315E-06	-.41754981E-10	-.41735642E-10	.19339275E-13	-1.00	44.00	93.00
-.41417210E-03	.25591852E-06	-.41738392E-10	-.41712617E-10	.25774385E-13	-1.00	44.00	94.00
-.41400685E-03	.65224629E-07	-.41702543E-10	-.41695974E-10	.65689843E-14	-1.00	45.00	91.00

```
      PROGRAM LINO(INPUT,OUTPUT,TAPE1=INPUT,TAPE2=OUTPUT)

C           CONSIDERING THE TRANSVERSE FIELD CASE
C           ROTATE ABOUT Z THEN ABOUT Y AXES
05          C           LIGHT DOWN Z" AXIS

            PI=4.0*ATAN(1.0)
            IQ=0

10          C           REFRACTIVE INDICES

            QNE=2.20
            QNO=2.286

15          C           ELECTRO-OPTIC COEFFICIENTS

            R13=8.6E-9
            R22=3.4E-9
            R33=30.8E-9
20          R51=28.0E-9

            C           ROTATION RANGE OF INTEREST

            STTH=PI/2.0
25          STPH=PI/2.0
            DPHI1=PI/36.0
            STAP=0.0
            PHI=0.0
            TH=0.0
30
            C           FIELDS APPLIED (VOLTS/MM)
            EX=100.0
            EY=0.0
            EZ=0.0
35
            C           OUTPUT HEADINGS

              9 WRITE(2,10)
             10 FORMAT(5X,3HPHI,5X,5HTHETA,7X,5HDN(X),13X,5HDN(Y),8X,8HROTATION,
40             13X,11HDN(X)-DN(Y))

            C           FIELD TRANSFORMATIONS

            100 FX=COS(TH)*(EX*COS(PHI)+EZ*SIN(PHI))-EY*SIN(TH)
45          FY=EY*COS(TH)+SIN(TH)*(EX*COS(PHI)+EZ*SIN(PHI))
            FZ=EZ*COS(PHI)-EX*SIN(PHI)

            C           CALCULATE INDEX ELLIPSOID SECTION AXES, MAGNITUDE AND
            C           ROTATION
50
            A=-R22*FY+R13*FZ
            B=R22*FY+R13*FZ
            C=R33*FZ
            D=-2.0*R22*FX
55          E=2.0*R51*FY
```

```
      F=2,0*R51*FX
      XN=COS(PHI)*COS(PHI)/(QNO*QNO)+SIN(PHI)*SIN(PHI)/(QNE*QNE)
      YN=1,0/(QNO*QNO)
      XNV=XN+COS(PHI)*COS(PHI)*(A*COS(TH)*COS(TH)+B*SIN(TH)*SIN(TH)+
   60 1D*SIN(TH)*COS(TH))+C*SIN(PHI)*SIN(PHI)-SIN(PHI)*COS(PHI)*(E*SIN(
     2TH)+F*COS(TH))
      YNV=YN+A*SIN(TH)*SIN(TH)+B*COS(TH)*COS(TH)-D*SIN(TH)*COS(TH)
      DNX=SQRT(1,0/XN)-SQRT(1,0/XNV)
      DNY=SQRT(1,0/YN)-SQRT(1,0/YNV)
   65 F1=XNV-YNV
      IF(F1,EQ,0,0) GO TO 20
C          ROTATION TERM
   70 C=COS(PHI)*((B-A)*SIN(2,0*TH)+D*COS(2,0*TH))-SIN(PHI)*(E*COS(TH)
     1-F*SIN(TH))
      ETA=0,5*ATAN(-C/F1)

      GO TO 21
   75 20 ETA=PI/2,0
      21 WETA=ETA*180,0/PI
      WTH=TH*180,0/PI
      WPHI=PHI*180,0/PI
      DIFF=DNX-DNY
   80
C          OUTPUT BLOCK

      WRITE(2,22)WPHI,WTH,DNX,DNY,WETA,DIFF
      22 FORMAT(2F10,4,2E16,7,F10,4,E16,7)
   85
C          LOOPING CONSTANTS

      PHI=PHI+DPHI1
      IF(PHI,LT,STPH) GO TO 100
   90 PHI=STAP
      TH=TH+DPHI1
      IF(TH,GE,STTH) GO TO 8
      GO TO 100
      8 WRITE(2,11)
   95 11 FORMAT(////6H *****)
      IF(IQ,GT,0) STOP
      IQ=1
      STTH=35,0*PI/180,0
      STPH=50,0*PI/180,0
  100 TH=25,0*PI/180,0
      PHI=40,0*PI/180,0
      STAP=PHI
      DPHI1=DPHI1/5,0
      GO TO 9
  105 END
```

PHI	THETA	DN(X)	DN(Y)	ROTATION	DN(X)-DN(Y)
0,0000	0,0000	0,	0,	-45,0000	0,
5,0000	0,0000	-,3346604E-05	-,4477064E-06	,1676	-,2898898E-05
10,0000	0,0000	-,6571022E-05	-,8920057E-06	,0412	-,5679016E-05
15,0000	0,0000	-,9560184E-05	-,1329517E-05	,0178	-,8230667E-05
20,0000	0,0000	-,1221831E-04	-,1756909E-05	,0097	-,1046140E-04
25,0000	0,0000	-,1447326E-04	-,2170931E-05	,0059	-,1230233E-04
30,0000	0,0000	-,1628055E-04	-,2568431E-05	,0038	-,1371212E-04
35,0000	0,0000	-,1762481E-04	-,2946384E-05	,0026	-,1467843E-04
40,0000	0,0000	-,1851870E-04	-,3301913E-05	,0018	-,1521678E-04
45,0000	0,0000	-,1899977E-04	-,3632312E-05	,0013	-,1536746E-04
50,0000	0,0000	-,1912580E-04	-,3935068E-05	,0009	-,1519074E-04
55,0000	0,0000	-,1896904E-04	-,4207875E-05	,0006	-,1476116E-04
60,0000	0,0000	-,1861013E-04	-,4448658E-05	,0004	-,1416147E-04
65,0000	0,0000	-,1813213E-04	-,4655584E-05	,0003	-,1347655E-04

```
      PROGRAM FARR(INPUT,OUTPUT,TAPE1=INPUT,TAPE2=OUTPUT)
      DIMENSION QI(5),QIG(5),PH(5),PHG(5),TH0(5),PD(5)
      WAVL=6.328E-4
      PI=4.0*ATAN(1.0)
05
C           INPUT DATA
C           SOURCE INTENSITIES
10    QI(1)=1.0
      QI(2)=1.0
      QI(3)=1.0
      QI(4)=1.0
      QI(5)=1.0
15
C           SOURCE PHASES
      PH(1)=0.0
      PH(2)=0.0
20    PH(3)=0.0
      PH(4)=0.0
      PH(5)=0.0
C           SYSTEM DIMENSIONS
25
      D=2.0/30.0
      S=99.0
      E=1.0/60.0
      F=100.0
30    A=4.9
C           NUMBER OF SOURCES
      N=5
35
      L=0
    9 CONTINUE
C           OUTPUT BLOCK (INPUT DATA)
40
      WRITE (2,10)
   10 FORMAT (13H INPUT PHASES)
      WRITE (2,11) (PH(K),K=1,5)
   11 FORMAT (5F12.4)
45    WRITE (2,12)
   12 FORMAT (18H INPUT INTENSITIES)
      WRITE (2,13) (QI(K),K=1,5)
   13 FORMAT (5F12.5)
50    C           CALCULATE PATH DIFFERENCES
      PD(3)=0.0
      PD(2)=S*(1.0/COS(ATAN((A/F)/2.0))-1.0)
      PD(4)=PD(2)
55    PD(1)=S*(1.0/COS(ATAN(A/F))-1.0)
```

```
      PD(5)=PD(1)
      WRITE (2,31)
   31 FORMAT (17H PATH DIFFERENCES)
      WRITE (2,32) (PD(K),K=1,5)
60    32 FORMAT (5F12.4)

      M=1
   14 CONTINUE
      QM=M
65
C          CALCULATE GRATING INCIDENCE ANGLES

      TH0(M)=ATAN((A-(QM-1.0)*A/2.0)/F)

70    C          CALCULATE PHASES AT GRATING

      PHG(M)=360.0*(PD(M)/WAVL-AINT(PD(M)/WAVL))+PH(M)
      IF(ABS(PHG(M))-360.0) 30,30,0
      PIT=PHG(M)*360.0/ABS(PHG(M))
75    PHG(M)=PHG(M)-PIT
   30 M=M+1
      IF(M-N) 14,14,0
      WRITE (2,33)
   33 FORMAT (18H GRATING INCIDENCE)
80    WRITE (2,29) (TH0(K),K=1,5)
   29 FORMAT (5F12.5)
      WRITE (2,15)
   15 FORMAT (15H GRATING PHASES)
      WRITE (2,16) (PHG(K),K=1,5)
85    16 FORMAT (5F12.4)


C          GRATING ILLUMINATION DETAILS

90    THET=-PI/18.0
      DELT=PI/1800.0
      J=-100
      PLOP=PI*E/WAVL
      GAMA=0.0
95    WRITE (2,17)
   17 FORMAT (4X,6H THETA,8X,9HINTENSITY,17X,18HGRATING AMPLITUDES)

   18 CONTINUE
      X=0.0
100   Y=0.0

C          AMPLITUDE VECTOR SUMMATION

      DO 20 K=1,5
105   QK=K
      IF(L-1) 27,0,0
      QIG(K)=0.20
      GO TO 19
   27 CONTINUE
110   SLAP=SIN(THET)-SIN(TH0(K))
```

```
      BANG=PLOP*SLAP
      IF(BANG) 28,0,28
      QIG(K)=SQRT(QI(K))
      GO TO 19
  115 28 QIG(K)=SQRT(QI(K))*SIN(BANG)/BANG
   19 CONTINUE
      GAMA=2.0*PI*D*(QK-1.0)*SIN(THET)/WAVL+PHG(K)*PI/180.0
      IF(L-1) 23,0,0
      GL=GAMA*180.0/PI
  120 XX=GL/360.0
      PQ=ABS(XX)
      IF(PQ-1.0) 34,0,0
      XY=AINT(PQ)
      XY=XY*XX/PQ
  125 XX=XY
      GAMA=GAMA-2.0*PI*XX
   34 CONTINUE
   23 CONTINUE

  130 C          OUTPUT FAR FIELD PATTERN DATA

      X=X+QIG(K)*COS(GAMA)
   20 Y=Y+QIG(K)*SIN(GAMA)
      OUT=X*X+Y*Y
  135 QJ=J
      QJ=QJ/10.0
      WRITE(2,21) QJ,OUT,(QIG(MM),MM=1,5)
   21 FORMAT (F8.4,5X,F12.5,5F12.4)

  140 C          LOOP CONSTANTS

      THET=THET+DELT
      J=J+1
      IF(J-100) 18,18,0
  145 L=L+1
      IF(L-2) 9,0,0
      STOP
      END
```

REFERENCES

References - These are classified into seven sections:

1. Deflectors and Modulators - Techniques and devices.

2. Thin Film Diffraction Devices.

3. Discrete Component Diffraction Devices.

4. Electro-Optic Material Considerations.

5. Applications.

6. Construction Processes and Aspects.

7. Optical and Analytical Considerations.

DEFLECTORS AND MODULATORS - TECHNIQUES AND DEVICES.

ADLER, R., "Interaction between light and sound". IEEE Spectrum p.42. (May 1967)

BEASLEY, J.D., "Electro-optical Modulator". US. 3625,592 (Dec. 1971)

BEISER, "Generalised gradient deflector and consequences of scan of convergent light". J. Opt. Amer., 57 p.923 (1967)

BEISER, "Spot distortion during gradient deflection of focused laser beams". J.Q.E. (1967) Q.E.3. p.261

BOER, K.W., "Franz-Keldysh Effect for appreciable deflection of light beams". Short Notes. Phys. Stat. vol.8, pK179, (1965).

BOER, K.W., "Scanning of light beams using Franz-Keldysh Effect". Phys. Stat. Solidi. 9 p.K35, (1965)

BOIVIN, "Electro-Magnetic field in the neighbourhood of the focus of a coherent beam". Phys. Rev. 138 p.1561, (1965)

BROWN, D.E., "Interferometric Laser Beam Scanner". App. Opt. 7, p.2422, (1968)

BUCK, "Optical Beam Deflector". App. Phys. Lett. 8, p.198, (1966)

BURNS, "On the possibility of using conical refraction phenomena for laser beam steering". App.Opt., 3, p.1505, (1964)

CALUCCI, E. Y., "Solid State Light Valve Study". Rome Air Development Centre. SID Proc. 64

CHEN, F.S., GEUSIC, J.E., KURTZ, S.K., SKINNER, J.G., WEMPLE, S., (BELL, T.L.), "Light Modulation and Beam Deflection with KTN crystals". J.App.Phys. vol.37, no.1., p.388, (Jan. 1966)

CHEN, F.S., "The use of perovskite para-electrics in beam deflection light modulators". Proc. IEEE, 52, p.1258, (1964)

CLAYSON, C., "Low Voltage light amplitude modulation". Elect. Lett., vol.2, (Apr. 1966)

COHEN, "Electro-optic gratings (KTN) for light beam modulation and deflection". App. Phys. Lett., 5, p.181, (1964)

COOPER, R.W., PAGE,J.L., "Magneto-Optic Light Modulators". IERE Conf. Sotun 1969, ReEE vol.39, no.6, (1970)

DAKSS, M.L., POWELL, "A Fast Digitalised Scan Laser". IEE JQE, vol.QE.4, no.10, (Oct. 1968)

DUGAN, A.F. et al., "KTN Concentration Gradient light beam deflector". App. Opt. vol.7, no.3, p.556, (March 1968)

Electro-Optical Systems design, p.7, (Dec. 1971) "New Laser Scanning Technique".

ENDERLEIN, "Diffraction of light by a grating caused by the Faraday or Kerr effect in the Electro-Magnetic field of a laser beam". Phys. Stat. Solid., 9, p.K117, (1965)

FOWLER, V.J., SCHLATER, J., "A Survey of Laser Beam Deflection Techniques". App. Opt., vol.5, no.10, p.1675, (Oct. 1966)

GRAF, P., "Modulators and Deflectors". Alta Freq., vol.41, no.10, p.726-43, (Oct. 1972)

GRANT, D.G., MEYER, R.A. & QUALKINBUSH, D.N., "An Optical Phased Array Beam Steering Technique". Proc. of Tech. Prog., Electro-optic Systems Design Conference - 1971 East. New York 1971

GOLDSTEIN, "Crystal Light Modulator providing both aperture and intensity control". US 3679289 (1972)

GORDON, "Electro-optic diffraction grating for light beam modulation and diffraction". JOE, IEEE, vol. QE 1, p.191-8, (Aug. 1965)

GYUNASHYAN, K.S. et al., "A cavity light modulator with a KDP crystal for an electro-optical range-finder". Izv. VUZ Radioelekron (USSR), vol.16, no.7, p.92-4 (July 1973). English translation in: Radio Electron and Commun. Syst. (USA).

HAAS, W. & JOHANNES, R., "Light Beam Scanning using conical refraction and optical activity". App. Opt., vol.5. no.6, p.1088, (June 1966)

HABEGGER, M.A., HARRIS, T.J. & LIPP, J., "TIR Light Deflector". App. Opt., vol.5, no.9, (1966)

HAERTLING, G.H. & McCAMPBELL, C.B.,Jnr., "Ferroelectric Electro-optical Devices". Filed Dec.1.1971., Ser. no.203,701.

HAMMER, J.M., "Optical Modulation System". US patent , no.3,628,177 (Dec. 1971)

HOLT, D., "Laser Beam Deflection Techniques". Optics Technology, (Feb. 1970)

HULME, K.F., "Electro-optic Devices". 3.630,597 (Filed 13 Jan. 1970)

ITTU, M., DABU, R. & NICOLAU, I.F., "KDP (potassium dihydrogen phosphate) electro-optic light modulator". Rev. Roum. Phys. (1973). 18(6), 781-3 (Eng)

JOYNES, G.M.S., CLARK, M.A.G. & DAVIS, Q.V., "Temperature independent low voltage wide bandwidth optical modulators". Electron. Lett., vol.8, no.11, pp.289-90, (1972)

KALIBJAN, "Laser Deflection-modulation in a CdS prism". Proc. IEEE 53, p.1666-7, (1965)

KAMINOW, I.P. & TURNER, E.H., "Electro-optic light modulators". Proc. IEEE, vol.54, no.10, pp.1374-90, (Oct. 1966)

KIEFER, J.E. et al., "Performance Characteristics of an Electro-optic light beam deflector". IEEE Conf. on Laser Eng. and Appl. (1967)

KLAUR, C.N., "Electro-optic phase modulator". US patent no.3,667,829, (June 1972)

KORPEL, et al., "An Ultrasonic Light Deflection System". IEE JQE, p.60, (April 1965)

KORPEL, A., "Phased Array type scanning laser beam". Proc. IEEE, 53, p.1666-7, (1965)

KULCKE, W. et al., "Digital Light Deflectors". App. Optics, vol.5, no.10, p.1657, (Oct. 1966)

LEE, M.E., "Lasers and their Applications to TV Systems". IEEE trans. on Broadcasting, vol.BC-13, no.1, (Jan. 1967)

LEHOVEC, K., "Arrays of Electro-Optical Elements and Associated Electric Circuitry". Patent no.3,631,251, (Feb.26, 1970)

LEY, J.M., "Light Modulators and their applications". Phys. Bull. (GB), vol.24, p.441-3, (july 1973)

LIPNICK, et al., "Nonmechanical Scanning of Light in 1 or 2 dimensions". IEEE JQE Correspondence p.321, (1965)

LIV, "Optical beam deflection by pulsed temp. gradients in bulk GaAs". Proc. IEEE, 53, p.522, (1965)

LOTSPEICH, J.E., "Characteristics of Fabry-Perot Electro-optic Modulators with internal loss". App. Opt. vol.12, no.6, pp1109-10, (June 1973)

MEYER, R.A., "Optical Beam Steering using a multichannel Lithium Tantalate Crystal". App. Opt., vol.11, no.3, p.613-6, (March 1972)

MIKAELYAN, et al., "Investigation of a system for beam deflection by means of $LiNBO_3$ crystals". Sov. J. of QE, vol.1, no.1, p.87-90, (July-Aug. 1971)

MYERS, "Scanning with Lasers". International Science & Technology p.40, (May 1967)

NANAMATSU, S. et al., "Strontium niobate electro-optic modulator". US. 3,747,022 (17 July 1973)

SCHEDEWIE , et al., "Digital Electro-optic light beam deflection used for spectral wavelenth modulation". App. Opt. vol.11, no.4, p.957-8, (Apr. 1972)

SKINNER, "Optimal Electro-optic deflection Scheme". App. Opt. vol.7, no.6, (June 1968)

TAYLOR, G.W., "Liguid Evaporation Light Deflector". App. Opt. vol.11, no.3, p.586, (March 1972)

TISCHER, "Gas lens type deflector structure for light beams". Proc. IEEE, 55, p.83, (1967)

VOROBLEV, K.I. et al., "Electro-optical light modulator based on a barium titanate single crystal". Izv. VUZ Fiz (USSR) no.7, p.35-8 (1973). English translation in: Sov. Phys. J., (USA) - received Aug. 1973

ZELDORICH, "The impossibility of rayscanning with the aid of internal conical refraction phenomenon (+ author's reply)". App. Opt. 4, p.1671, (1965)

THIN FILM DIFFRACTION DEVICES

BARRINGER, B.W., "The electro-optic diffraction modulator". Rank Research Laboratories Report (Jan. 1973)

DE BARROS, "High-speed electro-optic diffraction modulator for baseband operation". Proc. IEE, vol.119, no.7, (July 1972)

DE BARROS, et al., "Nanosecond Baseband Optical Diffraction Modulator". Elect. Lett. vol.7, no.10, p.267 (May 1971)

GFELLER, F.R.,& PITT, C.W., "Colinear Acousto-optic Deflection in Thin Films". Elect. Lett. vol.8, no.22, (nov. (1972)

GIA RUSSO, D.P., HARRIS, J.H., "Electro-optic modulation in a Thin Film Waveguide". App. Opt., vol.10, no.12, p.2786-8, (Dec. 1971)

GIA RUSSO, D.P. & KUMAR, C.S., "Sputtered Ferro-electric Thin-Film Electro-Optic Modulator". App. Phys. Lett. (USA), vol.23, no.5, p.229-31 (Sep. 1973)

HAMMER, J.M., "Digital Electro-optic Grating Deflector and Modulator". App. Phys. Lett., vol.118, no.4, (Feb. 1971)

HAMMER, J.M., CHANNIN, D.J. & DUFFY,M.T., "Fast Electro-optic Waveguide Deflector Modulator". Appl. Phys. Lett., vol 23, no.4, p.176-7 (Aug. 1973)

MARON, W.E., "Waveguide Electro-Optic Modulation in 11-V1 Compounds". J. Appl. Phys., (USA), vol.44, no.8, p.3703-7, (Aug. 1973)

POLKY, J.N. et al., "Interdigital Electro-Optical Modulator". App. Phys. Lett., vol.21, no.7, p.307-9 (Oct. 1972)

SHAH, M.L., "Fast Acoustic Diffraction-Type Optical Waveguide Modulator". App. Phus. Lett., vol.23, no.10, p.556-8 (Nov.1973).

WRIGHT, S. & WILSON, M.G.F., "New form of Electro-optic Deflector". Elect. Lett., vol.9, no.819, p.169-70 (May 1973)

St. LEDGER, et al., "Laser Beam Modulation using Grating Diffraction Effects". Elect. Lett., 4, p.99-100 (1968)

DISCRETE COMPONENT DIFFRACTION DEVICES

GORDON, E.I. & COHEN, M.G., "Electro-Optic Diffraction Grating for Light Beam Modulation and Diffraction". IEEE J. Quantum Electronics, vol. QE 1, no.5, p.191-8 (Aug. 1965)

MOTOKI, T., "Low Voltage Optical Modulators using Electro-Optically induced Phase Gratings". App. Opt., vol.12, no.71, p.1472-6, (July 1973)

NINOMIYA, Y., "Ultrahigh Resolving Electro-Optic Prism Light Deflectors". IEEE JQE, vol. QE 9, no.8, p.791-5 (1973)

NISHIWAKI, A. & MIKAMI,T., "Characteristics of a Total-Reflection-Type Light Modulator with Interdigital Electrodes". Chubu Kogyo Daigaku Kiyo (1972), 8, 51-5 (Japan)

NISHIWAKI, A. et al., "DC Characteristics of the period Skin-Field - Electro-Optic Light Modulator" IEEE JQE, 9(6), 559-63 (June 1973)

ELECTRO-OPTIC MATERIALS CONSIDERATIONS

ASHKIN, A. et al.,"Optically Induced Refractive Index Inhomogeneities in $LiNBO_3$ and $LiTaO_3$". App. Phys. Lett., 9, 72 (1966)

BELYAEV, et al., "Dielectric Constant of Crystals having an Electro-Optic Effect". Soviet Phys. - Solid State, vol.6, no.8, p.2007-8 (Feb. 1965)

BERGMAN, G., "The Electrical Conductivity of $LiNBO_3$". Solid State Comm., vol.6, p.77-9 (1968)

BOLING, N.L. et al., "Laser Induced Surface Damage". Appl. Opt. vol. 12, no.4, p.650-60 (April 1973)

CHEN, F.S., "A Laser Induced Inhomogeneity of Refractive Indices in KTN". J. APP. Phys., vol.38, p. 3418-20 (1967)

CHRISTMAS, T.M. & WILDEY, C.G., "Pulse Measurement of in KDP". Electron. Lett. vol.6, no.6, p.152-3 (March 1970)

CRISP, M.D., "Laser Induced Damage of T.I.R. Surfaces". Opt. Commun. vol.6, no.2, p.213-4 (Oct. 1972)

DOUGHTY, D.C. & LEY, J.M., "Electro-Optic Relaxation Effect in ZnS". Elect. Lett. vol.6, no.5, p. 141-2 (March 1970)

FEYGEL, V.I., "The Shuttering Contrast of Electro-Optic Light Modulators employing Class 42 Crystals". Sov. J. Technol. (USA), vol.39, no.10, p.594-5 (Oct. 1972)

FREISER, M.J., "A Survey of Magneto-Optic Effects". IEEE trans. on magnetics, vol. Mag-4, no.2, (June 1968)

HOLDEN, M.V. & WARNER, J., "Temperature Dependence of the Refractive Indices of pure $LiNBO_3$". Phys. Lett. vol.22, no.3, p.243-5 (Aug. 1966)

HOOKABE, K. & MATUSO, Y., "Novel type of Cut for KDP Crystals for low-voltage Light Modulation". Elect. Lett., vol.6, no.17, p.350-1 (Aug. 1970)

HULME, K.F., "Oblique Cut Longitudinal Electro-Optic Modulators". IEEE JQE, vol. QE 7, no.6 (June 1971)

IVANOV, I.V. et al., "Absolute Stabilization of the Temperature of Electro-Optical Crystals". Zh . Tekh. Fiz. 1973, 43(7), 1547-50 (Russ)

JONA, & SHIRANE, "Ferroelectric Crystals". Intern. Series of Monographs on Solid State Phus. 537.226.33:537.548 Jon (1962)

KALYMNIOS, D., "Optimisation of Electro-Optic Crystal Modulators". Elect. Lett., vol.6, no.25, p.804-5 (Dec. 1970)

KRUEGER, U. et al., "Electro-Optic materials for Digital Light Beam Deflectors". Proc. IEEE (1973), 61(7), 992- 1007 (Enng.)

LENZO, et al., "Electro-Optic coefficients in Single Domain Ferroelectric $LiNBO_3$". J. Opt. Soc. Amer. 56, 633 (1966)

LIBRECHT, F.M., "Optimum Cut for a $LiNBO_3$ Transverse Light Modulator". JQE July 1971 p.374.

MALDONADO, J.R. et al., "Ferroelectric Ceramic Light Gates Operated in a Voltage Controlled Mode". IEEE trans. on E.D. vol. ED. 17, no.2, p.148 (Feb. 1970)

MARPLE, D.T.F., "Refractive Index ZnSe, ZnTe and CdTe". J. Appl. Phys., vol.35, no.3, pt.1, p.539-42 (March 1964)

MILEK, J.T. & NEUBERGER, M., "Handbook of Electronic Materials:- 'Linear Electro-Optic Modular Materials' ". IFI/Plenum (1972)

MURPHY, "Conduction in Single Crystals of ADP". J. Appl. Phys. 35, p.2609-14 (Sept. 1964)

NASSAN, et al., "Ferroelectric $LiNBO_3$ pt. 1....5". J. Phys. Chem. Solids, vol.27, p.983, 988 (1966)

NINOMIYA, Y., "Deterioration of the Extinction ratio of Light Modulators due to light - absorption Heating". Electron. and Commun. Jap. (USA), vol.55, no.9, p.90-7 (Sept. 1972)

NINOMIYA, Y., "Optimization of Crystal Cut for Light Modulators and Deflectors". NHK Gijutsu Kenkyu, 25(2), 81-91 (Japan) (1973)

PATTENDEN, "A Study of the Influence of Electrode Configuration on the Electric Field Distribution in an Electro-Optic Modulator comprising a uniaxial crystal". PhD. Thesis (TCU) (1971)

PHILLIPS, R.A., "Temperature variation of Index of Refr. of ADP". J. Opt. Soc., vol.56, no.5, (May 1966)

RASHIDI, K., "Pulse Response of O Z Cut ADP Modulators". Elect. Lett., vol.7, no.4, p.114-5 (Feb. 1971)

STEVENSON, J.L. et al., "Improvements in or relating to Electro-Optic Apparatus". Patent spec. 1,331,228 (1969)

THATCHER, P.D. et al., "Ferroelectric Electro-Optic Ceramics with Reduced Scattering". IEEE trans. on ED, vol. ED 16, no.6, p.515 (June 1969)

VEDAM, K. & DAVIS, T.A., "Piezo- and Thermo-optic Behavior of $LiNBO_3$". Appl. Phys. Lett., vol.12, no.4, p.138-40 (Feb. 1968)

VOLKOVA, E.N. & VELICHKO, I.A., "Electro-Optical Properties of Potassium Dihydrogen Phosphate Crystals having different degrees of Diffraction". Sov. Phys. -Crystallogr. (USA), vol.18, no.2, p.409-10 (March-April 1973)

VORONOV, V.V., et al., "Electric and Electro-Optical Properties of Stoichiometric Barium Strontium Niobate Single Crystals". Fiz. Treid. Tela (Leningrad) 1973, 15(7), 2198-200 (Russ)

WILLIAMS, R., "Electric Field Induced Light Absorption in CdS". Phys. Review, vol.117, no.6, p.1487 (March 1960)

ZOOK, et al., "Temp. Dependence and Model of the Electro-Optic Effect on $LiNBO_3$". Appl. Phys. Lett., 11 159, (1967)

ZVEREV, et al., "Laser Radiation Induced Damage to the surface of $LiNBO_3$ and Tantalate Single Crystals". Soviet JQE, vol.2, no.2, p.167-9 (Sept./Oct. 1972)

APPLICATIONS

AAGARD, et al., "Advanced Optical Storage Technigues for Computers". Appl. Opt. vol.11, no.10, p.2133-9 (Oct. 1972)

BAKER, C.E. et al., "A Multicolour Laser Digital Data Display System". 7th SID (1966)

BAKER, C.E. (T.I), "Laser Display Technology". IEEE Spect. (Dec. 1968)

BAKER, C.E. et al., "The Laser Display - a large-screen, real time, display technique". 4th SID Symposium (1965)

BEASLEY, J.D. "Electro-Optic Laser Scanner for TV projection display". Appl. Opt. vol. 10, no.8, (Aug. 1971)

BLACKMER, L.L. et al., "Application of Phase Modulation to Digital Data Recording by means of Superimposed Diffraction Gratings". Appl. Opt. vol.10, no.5, (May 1971)

CHEN, "Introduction to Optical Communications". Proc. IEEE, 58, p.1440-57, (1970)

CHRISTMAS, T. et al., "Precise PTM Control of Ruby Laser". Elect. Lett., vol.6, no.22.

DARNE, F.R. et al., "Advances in Techniques for Large Dynamic Display Devices". 4th. SID Symposium (1964)

FOWLER, V.J. et al., "A Photochromic Laser Display". Proc. IEEE (March 1967)

LASSER, M.E., "Lasers and their Applications to TV Systems". IEEE trans. on Broadcasting. vol. BC - 13, no.1 (Jan 1967)

CONSTRUCTION PROCESSES AND ASPECTS

BEESLEY, et al., "Sensitivity of Resist-Coated Silicon Slices to Argon Laser Wavelengths". Elect. Lett. vol.5, no.12, (June 1969)

BEESLEY, H.J., et al., "The Use of Photoresist as a Holographic Recording Medium". App. Opt. vol.9, no.12, (Dec. 1970)

BEILBY, G.T., "Surface Flow in Crystalline Solids under Mechanical Disturbance". Roy. Soc. Proc. vol.72, p.218 25, (May 1973)

HAMMOND, V.J., "The Case for 1m Beam Etching" Elect. Eng. News. (Oct. 1971)

LEY, J.M. et al., "The Preparation of Electro-Optic Crystals for use in Laser Modulation". Research Memorandum T.C.U. (March 1971)

'NATURE'...."POLISHING OF MATERIALS" Sept. 1926, Feb. 1927, Jan.1 1927, Jan.29 1927, Mar.19 1927.

TWYMAN, F. "Prism and Lens Making" Hilger (1952)

OPTICAL AND ANALYTICAL CONSIDERATIONS

BINNS, & LAWRENSON., "Analysis and Computation of Electric & Magnetic Field Problems". Pergamon, (1963)

BLOOM, A.L., "Gas Lasers". Wiley. (1968)

BOIVIN, "Electo-Magnetic Field in the Neighbouhood of the Focus of a Coherent Beam". Phys. Rec. 138, p.1561 (1965)

CARLIN, "The Minimum Spot Size for a Focused Laser and the Uncertainty Relation". Proc. IEEE 52, p.1371, (1964)

City University Laser Voc. School, "Lasers and their Applications". (Sept. 1971)

DITCHBURN, G., "Light". pub. Blackie. 535 DIT, (1963)

FRANCON, M., "Diffraction, Coherence in Optics" Pergamon. 535. 42 FRA

GELLES, "Corrected Laser Beam Expander". App. Opt. 7, p.375, (1968)

GORDON, E.I., "A Review of Acousto-Optical Deflection and Modulation Devices". Proc. IEEE vol.54, no.10, (Oct. 1966)

Handbuch der Phyik. 530.031 FLO.

HARVEY, A.F., "Coherent Light". 621.366 HAR.

IEE Colloquium Digest. "Thin Film Optical Waveguides". Organised by prof. groups. (1973/7)

KLEIN, "Optics". 535. KLE. Wiley. (1970)

KOGELNIK, H. & T.C.I., "Laser Beams and Resonators". App. Opt. vol.5, no.10, p.1550 (Oct. 1966)

KRAUS, J.D., "Antennas". Mc.Graw Hil. 1950. p.548, 621.396.67. KRA.

LAVB, L.J., "Resolution in Light Deflectors". Laser Focus p.36, (Aug. 1971)

LEE, T.C. et al., "Cascade Operation of Light Beam Deflectors by Fly's Eye Lenses" App. Opt. vol.10, no.8, p.1965 (Aug. 1971)

LEWIS, "Scan angle multiplication by Dielectric Interface". Proc. IEEE 53, p.742 (1965)

LONGHURST. R.S., "Geometrical & Physical Optics". Longmans.

MACALARA, "2 Lenses to Collimate Red Light". App. Opt. 4, p.1652 (1965)

MARSHALL, "Crystal Optics" Cooke. (1953)

NYE, "Physical Properties of Crystals". Oxford Press. 537.548 (1965)

PALMER, E.W. et al., "Diffraction Gratings". Contemp. Phys. vol.9, no.3, p.257-76 (1968)

RAMAN, & NATH., "The Diffraction of Light by Sound Waves of High Frequency". Pt. 2., Proc. Ind. Acad. Sci. 1935 (A), 2, p.413. Also part 1, p.406-12.

ROSS, D., "Lasers, Light Amplifiers and Oscillators". 621.375.826 ROS (1969)

SHULMAN, A.R., "Optical Data Processing". 535.8 SHU (1970)

SHURCLIFF, W.A. et al., "Polarised Light". Van Nostrand, 535.5 SHU (1964)

SKOLNIK, M. "Radar Handbook". McGraw Hill (1970)

SKINNER, "Comment on Light Beam Deflectors" App. Opt. 3, p.1504 (1964)

SMITH, H.I. et al., "A High Yield Photolithographic Technique for Surface Wave Devices". J. Electrochem. Soc., vol.118, no.5, p.821-25 (May 1971)

STROKE, G.W., "Holographic Filter". Phys. Lett. vol.33A, p.3 (1970)

STROKE, G.W., "Holographic Furier-Transform Image De-blurring Method" Phys. Lett. vol.25A, p.89,)1967)

STROKE, G.W., "Sharpening Images by Holography". New Scientist p.671 23rd. Sept. 1971.

THOMPSON, "Algebra of Matrices". Helger. 512.943 TUO.

VON HIPPEL, "Dielectrics and Waves". Wilby. (1954)

WAITE, et al., "Spreading of Laser Beams due to Diffraction". Proc. IEEE, 52, p.624 (1964)

WEBB, R.H., "Elementary Wave Optics". Academic Press 535.3

WOOD, E.A., "Crystal & Light". Van Nostrand. 537.548.535.WOO

ZOOK, et al., "Geometrical Interpretation of Gaussian Beam Optics". Appl. Opt. vol.11, no.10, p.2140-5 (Oct.1972)

ZERNIKE, F. & MIDWINTER, J.E., "Applied Nonlinear Optics". Wiley.

PUBLISHED PAPERS

Table 1 INTERVALLEY COUPLING CONSTANTS AND PHONON TEMPERATURES ($\hbar\omega/k$) IN INDIUM PHOSPHIDE

Phonon branch	Coupling constant		Phonon temperature
	screened	unscreened	
	eV/cm	eV/cm	K
LO+TO	3.0×10^8	5.9×10^8	405
LA+TA	3.0×10^8	8.3×10^8	103

calculated magnitude of the maximum negative differential mobility is about 1000 $cm^2/V\,s$.

(*c*) At high field strengths, the drift velocity is found to depend significantly on the screening of the pseudopotential. For example, at 75 kV/cm, we find drift velocities of about 9×10^6 cm/s and 6×10^6 cm/s for screened and unscreened pseudopotentials, respectively, these values corresponding to peak/valley ratios of 2·7 and 4·1. Dipole-domain measurements have given drift velocities of 7×10^6 cm/s and 9×10^6 cm/s in this field range.[3, 14]

(*d*) Although the *X* valleys were included in the calculations, both the screened and unscreened coupling constants were found to be too large for any appreciable population of these valleys to occur up to the highest field strengths investigated. Thus, at 75 kV/cm for a screened pseudopotential, we find that 6% of the electrons occupy the *X* valleys, and that these contribute only 3% to the average velocity. For an unscreened pseudopotential, less than 1% of the electrons are transferred to the *X* valleys.

The conclusion to be drawn from the above discussion is that the theoretical intervalley coupling constants predict, either for a screened or unscreened interaction, a high enough intervalley scattering rate for only the Γ and *L* valleys to be involved in the high-field transport properties of InP. Consequently, the electron-transfer mechanism is very similar to that believed to occur in GaAs, although we predict a smaller negative-differential mobility and higher peak/valley ratio in InP. The detailed form of the calculated velocity/field curve is consistent with the available experimental data, although these data unfortunately show a significant variation at the present time. Further details of the calculations described here, together with the dependence of the drift velocity on the effective mass and anisotropy in the *L* valleys, are described elsewhere.[18]

Acknowledgment: This letter is published by permission of the Director of the UK Royal Radar Establishment.

W. FAWCETT
D. C. HERBERT

Royal Radar Establishment
St. Andrews Road, Great Malvern, Worcs. WR14 3PS, England

11th June 1973

References

1 HILSUM, C., and REES, H. D.: 'Three-level oscillator: a new form of transferred-electron device', *Electron. Lett.*, 1970, 6, pp. 277–278
2 HILSUM, C., and REES, H. D.: 'Three-level transferred-electron effects in InP', *ibid.*, 1971, 7, pp. 437–438
3 BOERS, P. M.: 'Measurements on the velocity/field characteristic of indium phosphide', *ibid.*, 1971, 7, pp. 625–626
4 'T LAM, H., and ACKET, G. A.: 'Comparison of the microwave velocity/field characteristics of *n*-type InP and *n*-type GaAs', *ibid.*, 1971, 7, pp. 722–723
5 GLOVER, G. H.: 'Microwave measurement of the velocity-field characteristic of *n*-type InP', *Appl. Phys. Lett.*, 1972, 20, pp. 224–225
6 NIELSEN, L. D.: 'Microwave measurement of electron drift velocity in indium phosphide for electric fields up to 50 kV/cm', *Phys. Lett.*, 1972, 38A, pp. 221–222
7 HAMMAR, C., and VINTER, B.: 'Calculations of the velocity-field characteristic of *n*-InP', *Solid State Commun.*, 1972, 11, pp. 751–754
8 FAWCETT, W., HILSUM, C., and REES, H. D.: 'Optimum semiconductor for microwave devices', *Electron. Lett.*, 1969, 5, pp. 313–314
9 JAMES, L. W., VAN DYKE, J. P., HERMAN, F., and CHANG, D. M.: 'Band structure and high field transport properties of InP', *Phys. Rev.*, 1970, B1, pp. 399–404
10 HERBERT, D. C., FAWCETT, W., LETTINGTON, A. H., and JONES, D.: 'Electron–phonon interaction and intervalley scattering in semiconductors'. Proceedings of the international conference on the physics of semiconductors, Warsaw, 1972, 2, pp. 1221–1226
11 HERBERT, D. C.: 'Electron–phonon interaction and intervalley scattering in semiconductors', *J. Phys. C.*, 1973 (to be published)
12 ALFREY, G. F., and BORCHERDS, P. H.: 'Phonon frequencies from the Raman spectrum of indium phosphide', *ibid.*, 1972, 5, pp. 275–278
13 FAWCETT, W., BOARDMAN, A. D., and SWAIN, S.: 'Monto Carlo determination of electron transport properties in gallium arsenide', *J. Phys. Chem. Solids*, 1970, 31, pp. 1963–1990
14 PREW, B. A.: 'Determination of the velocity/field characteristic for *n*-type indium phosphide from dipole-domain measurements', *Electron. Lett.*, 1972, 8, pp. 592–594
15 BOERS, P. M.: 'Measurements on dipole domains in indium phosphide', *Phys. Lett.*, 1971, 34A, pp. 329–330
16 PREW, B. A.: 'High-field-current instabilities in InP', *Electron. Lett.*, 1971, 7, pp. 584–585
17 KAUL, R., GRUBIN, H. L., LADD, G. O., and BERAK, J. M.: 'Electrical characteristics of bulk *n*-InP oscillators', *IEEE Trans.*, 1972, ED-19, pp. 988–990
18 FAWCETT, W., and HERBERT, D. C.: 'High-field transport in gallium arsenide and indium phosphide' (to be published)

TOTAL-INTERNAL-REFLECTION ELECTRO-OPTIC DIFFRACTION DEFLECTOR/MODULATOR

Indexing terms: Electro-optical effects, Optical modulation, Modulators

An electro-optic diffraction modulator/deflector using tota internal reflection and no external optics is described. The zero-order extinction voltage decreases, and the interorder angle increases, with decreasing interdigitated electrode pitch. With $LiNbO_3$, all the zero-order energy is deflected by less than 60 V. The active-material volume is low, approximately 0·5 mm^3. Further optimisation is possible.

Electro-optic diffraction deflector/modulators have been reported with zero-order extinction voltages of 25 V,[1, 3, 4] 800 V with 74% extinction[2] or as giving 3·2% modulation with 30 V.[5] Being thin-film devices, their use as discrete components requires prisms or cylindrical lenses, and their performance is degraded by incident beams of finite thickness.[2]

If light energies are to be high, lenses may cause an undesirable increase of power density in the device. When the electrode pitch is reduced, the fringing-field penetration into the material is less, so that increased interorder angle is achieved at the cost of the sensitivity and the extinction ratio.[2]

To minimise these difficulties, devices have been constructed, initially in $LiNbO_3$, with a 2-dimensional entry aperture, intended for use as discrete optical components. Interdigitated electrodes are deposited on, or placed in intimate contact with, a polished surface of the material, and the beam is totally internally reflected from the surface containing the electrodes. The configuration and performance are shown in Fig. 1A.

In this arrangement, r_{33}, r_{13} and r_{22} of $LiNbO_3$ are used, and the electrode-field fringing into the electro-optic material causes phase corrugations to appear in the wavefront (Fig. 1B).

Their shape depends on which of the two orientations considered is used. In all these cases, the incident light was polarised parallel to the *z* axis, as this offered the greater sensitivity.

The induced refractive-index changes in $LiNbO_3$ are:

(*a*) for O*q* parallel to O*z* (light along the *x* axis),

$$\Delta n = \frac{E_z(r_{33}\cos^2\theta + r_{13}\sin^2\theta) - E_y r_{22}\sin^2\theta}{2(n_e^{-2}\cos^2\theta + n_0^{-2}\sin^2\theta)^{3/2}} \quad (1)$$

(*b*) for O*p* parallel to O*z* or O*q* parallel to O*z* $\theta = 0°$,

$$\Delta n = \frac{E_z r_{33} n_e^3}{2} \quad (2)$$

where E_z and E_y are the fringing-field components in the *x* and *y* directions, and E_x is assumed to be zero. The index ellipse rotation is negligible in both cases.

The field components due to the electrodes are:

(*a*) normal to the electrodes:

$$E_1 = -\sum_{n=1,3,5,\ldots} \frac{4V\sin(n\pi a)}{dn\pi a}\left(\sqrt{\frac{e_3}{e_1}}\right) \times \exp\left\{\frac{-n\pi q}{d}\left(\sqrt{\frac{e_3}{e_1}}\right)\right\}\sin\left(\frac{n\pi p}{d}\right) \quad (3)$$

(*b*) parallel to the electrodes:

$$E_2 = \sum_{n=1,3,5,\ldots} \frac{4V \sin(n\pi a)}{dn\pi a} \times \exp\left\{\frac{-n\pi q}{d}\left(\sqrt{\frac{e_3}{e_1}}\right)\right\} \cos\left(\frac{n\pi p}{d}\right) \quad (4)$$

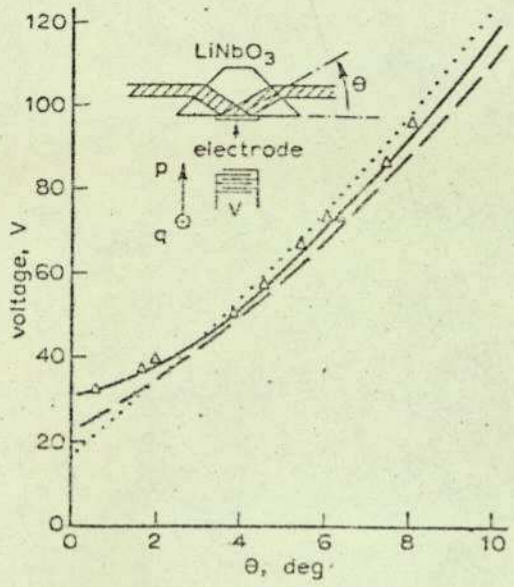


Fig. 1A *Zero-order extinction voltage against inclination angle*
Δ measured for $d = 0{\cdot}1$ mm, Op parallel to Oy, Oq parallel to Oz
Predicted performance:
..... Op parallel to Oz, Oq parallel to Oy
– – – – Op parallel to Oy, Oq parallel to Oz
——— Op parallel to Oy, Oq parallel to Oz, compensated for electrode-finger-width reduction due to etch factor

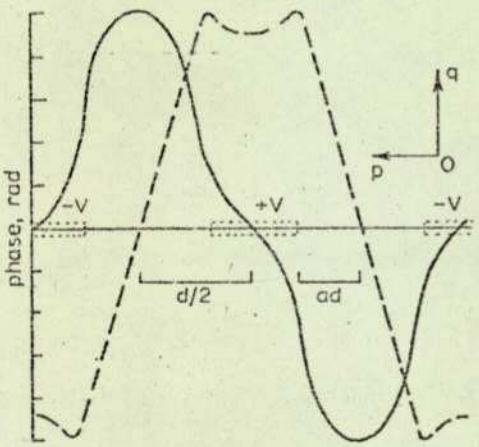


Fig. 1B *Emergent-beam phase profiles for two typical crystal orientations*
$d = 0{\cdot}1$ mm, $\theta = 2°$
——— Op parallel to Oz
– – – – Oq parallel to Oz
..... electrode positions

where e_1 and e_3 are the permittivities of the material. The retardation Γ is given by

$$\Gamma = \frac{4\pi}{\lambda} \int_0^{l \tan\theta/2} \frac{\Delta n\, dq}{\sin\theta} \text{ radians} \quad . \quad . \quad . \quad . \quad . \quad (5)$$

where l is the electrode length. For Oq parallel to Oz, $E_1 = E_z$ and $E_2 = E_y$; and for Op parallel to Oz, $E_1 = E_y$ and $E_2 = E_z$.

From eqns. 3 and 4, the anisotropy causes the Op-parallel-to-Oz orientation to be preferred for alternating voltages, while the Oq-parallel-to-Oz orientation is preferred for direct-voltage use.

The far-field pattern obtained when voltage is applied is of the Raman and Nath type,[6] differing only because of the greater wavefront complexity. If the waveshape is expressed in Fourier form, the far-field intensity may be expressed[4] from antenna theory as

$$I = \frac{1}{R^2}\left[\sum_{m=1}^{R} f(p) \cos\left\{\frac{mnd\pi}{R\lambda} \sin\phi + \sum_{c=0}^{Q-1} \hat{\Gamma} F_c \sin\left(\frac{mn\pi(c-1)}{2R}\right)\right\}\right]^2 \quad (6)$$

where ϕ is the deflection angle, $f(p)$ is the incident amplitude profile, $F_{c=0,1,\ldots,Q-1}$ are the Fourier coefficients, n = number of electrode fingers and $\hat{\Gamma}$ = peak value of retardation.

Alternatively, the intensity can be expressed directly by an incremental interference summation over the device aperture. Both approaches were in good agreement with experimental measurements of the intensity against the voltage for the first four orders of diffraction.

A typical device (Oq parallel to Oz and $d = 0{\cdot}1$ mm) gave an interorder angle of $6{\cdot}9 \times 10^{-3}$ rad at 0·6328 μm and a capacitance of 1·74 pF/mm^2 of electrode area. The predicted and measured performances are shown against the inclination (Fig. 1A) and against the electrode pitch (Fig. 2). The angular resolution of the orders is proportional to the number of electrode pitches across the device aperture.

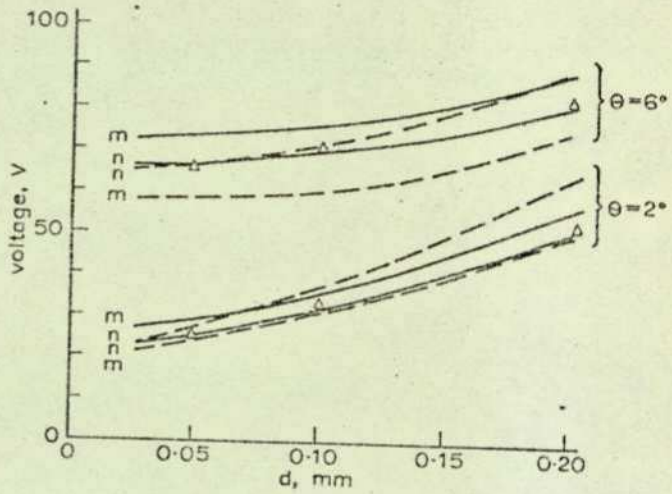


Fig. 2 *Electrode pitch against zero-order extinction voltage for $a = 0{\cdot}25$*
m denotes Op parallel to Oz, *n* denotes Oq parallel to Oz orientations
Δ measured for Oq parallel to Oz orientation at direct voltage and corrected for etch-factor variation of a
——— direct voltage
– – – – alternating voltage

The technique appears to be very promising for small material samples, large apertures or high powers, and for long wavelengths. Further materials, electroding systems and novel applications are under test.

Acknowledgments: The author is indebted to the British Post Office for photoreduction facilities and to the UK Science Research Council for financial support.

M. T. V. SCIBOR-RYLSKI

Optoelectronics Group
Department of Electrical & Electronic Engineering
City University
St. John Street, London ECIV P4B, England

15th June 1973

References

1 ST. LEDGER, J. F., and ASH, E. A.: 'Laser-beam modulation using grating diffraction effects', *Electron. Lett.*, 1968, 4, pp. 99–100
2 HAMMER, J. M.: 'Digital electro-optic grating deflector and modulator', *Appl. Phys. Lett.*, 1971, 18, pp. 147–149
3 DE BARROS, M. A. R. P., and WILSON, M. G. F.: 'Nanosecond baseband optical diffraction modulator', *Electron. Lett.*, 1971, 7, pp. 267–269
4 DE BARROS, M. A. R. P., and WILSON, M. G. F.: 'High-speed electro-optic diffraction modulator for baseband operation', *Proc. IEE*, 1972, 119, pp. 807–814
5 POLKY, J. N., and HARRIS, J. H.: 'Interdigital electro-optic thin-film detector', *Appl. Phys. Lett.*, 1972, 21, pp. 307–309
6 RAMAN, C. V., and NATH, N. S. N.: 'The diffraction of light by sound waves of high frequency—Pt. I', *Proc. Indian Acad. Sci. A*, 1935, 2, pp. 413–420

FURTHER COMMENTS ON T.I.R. DEFLECTOR/MODULATOR PERFORMANCE

Indexing terms: Electro-optical devices, Modulators, Optical modulation

T.I.R. modulator/deflector far-field order intensities are shown to agree with prediction for $LiNBO_3$ *xy*-cut devices, and a 'blazing' effect, controlled by crystal orientation, is suggested. Zero-order extinction ratios were between 40 : 1 and 140 : 1, and seemed optical-finish limited. Misalignment of an 0·1 mm pitch interdigitated electrode device by ±5° halved the device sensitivity, indicating the possibility of use with uncollimated light. White-light (incoherent) operation and optimisation prospects are reported.

Authors have recently reported[1, 2] deflector/modulators that use a field-induced electro-optic diffraction effect in the t.i.r. (total-internal-reflection) region and offer a 2-dimensional aperture. This letter presents performance details allowing further comparison with orthodox compensated low-voltage modulators.

Zero-order extinction voltages have been shown[1] to depend on t.i.r. incidence angle θ and the deposited interdigitated electrode pitch d, and to lie in the region of 60 V for $LiNBO_3$ *xy*-cut devices. The far-field pattern is of the Raman and Nath type, and is most easily found by an incremental vector summation of the wavefront amplitude. So far, field amplitudes for each pitch can be expressed in the orthogonal forms

$$A_x = \lim_{m\to\infty} \sum_{n=1}^{m} \frac{A}{m} \cos\gamma \quad . \quad . \quad . \quad . \quad . \quad . \quad . \quad . \quad (1)$$

and

$$A_y = \lim_{m\to\infty} \sum_{n=1}^{m} \frac{A}{m} \sin\gamma \quad . \quad . \quad . \quad . \quad . \quad . \quad (2)$$

where

$$\gamma = (n-1)\left\{\frac{2\pi d}{m\lambda}\sin\phi + \Gamma\left(\frac{nd}{m}\right)\right\} \quad . \quad . \quad . \quad . \quad (3)$$

A is the amplitude per pitch, ϕ is the far-field deflection angle and $\Gamma(p)$ is the computed phase profile across the device. A similar summation can then be executed for each electrode pitch of the aperture to provide the final intensity pattern. By an intensity weighting of $A[A = A_{(p)}]$, an intensity profile can be accommodated. By this means, or by using a Fourier expression in classical diffraction theory,[1] the voltage intensity far-field characteristic can be predicted. Fig. 1A shows good

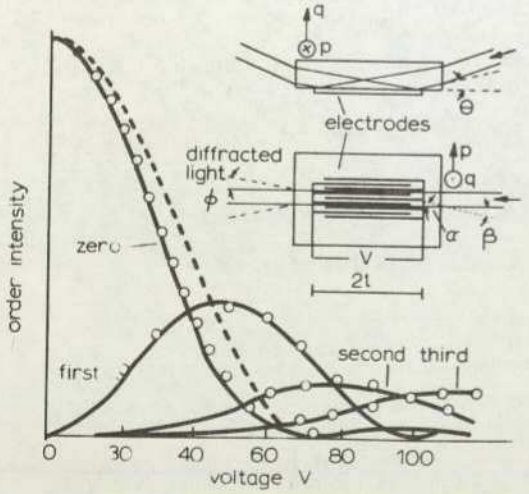


Fig. 1A *Order intensity characteristics of d = 0·1 mm device*
For *z*||*q*, θ = 3·5° at 6328 Å
——— measured
○ predicted
– – – – cosine-squared extinction curve

agreement between predicted and measured performance. A cosine-squared curve, characteristic of birefringent electro-optic modulators, is shown for comparison. It is of interest to note that, at maximum, the first orders contain approximately 11% more energy for the *p*||*z* orientation than they do for *q*||*z* (*z* is the optic axis). Peak intensity in the first order is approximately 15 and 26% more than predicted for the unblazed sinusoidal-phase corrugation case, respectively.

A typical far-field pattern is shown in Fig. 1B for a *p*||*z* orientation device. A 2 mm × 2 mm electrode of 0·1 mm pitch was used, and a cylindrical lens (f = 750 mm) placed in the incident beam provided a square aperture, and is the cause of the aspect ratio of the orders.

As this pattern contains information about the applied device voltage in a parallel word form, it may offer promise, in conjunction with a detector array, as the basis of a very fast open-loop analogue-to-code conversion process. This 'encoding' process has been shown to operate in the nanosecond region;[3] it is insensitive to temperature variation because a phase-modulation technique is used, and is virtually independent of temperature if temperature-independent electro-optic coefficients are used; e.g. r_{22} in $LiNBO_3$.

The electrodes are vacuum-deposited copper on chromium, and offer good adhesion properties. Various film thicknesses were deposited, typical values being approximately 1 and 10 μm for chromium and copper, respectively. As can be seen from Fig. 1B, the reflection phase-change difference between total internal reflection from the crystal/air interface and the reflection from the metal film is negligible in practice.

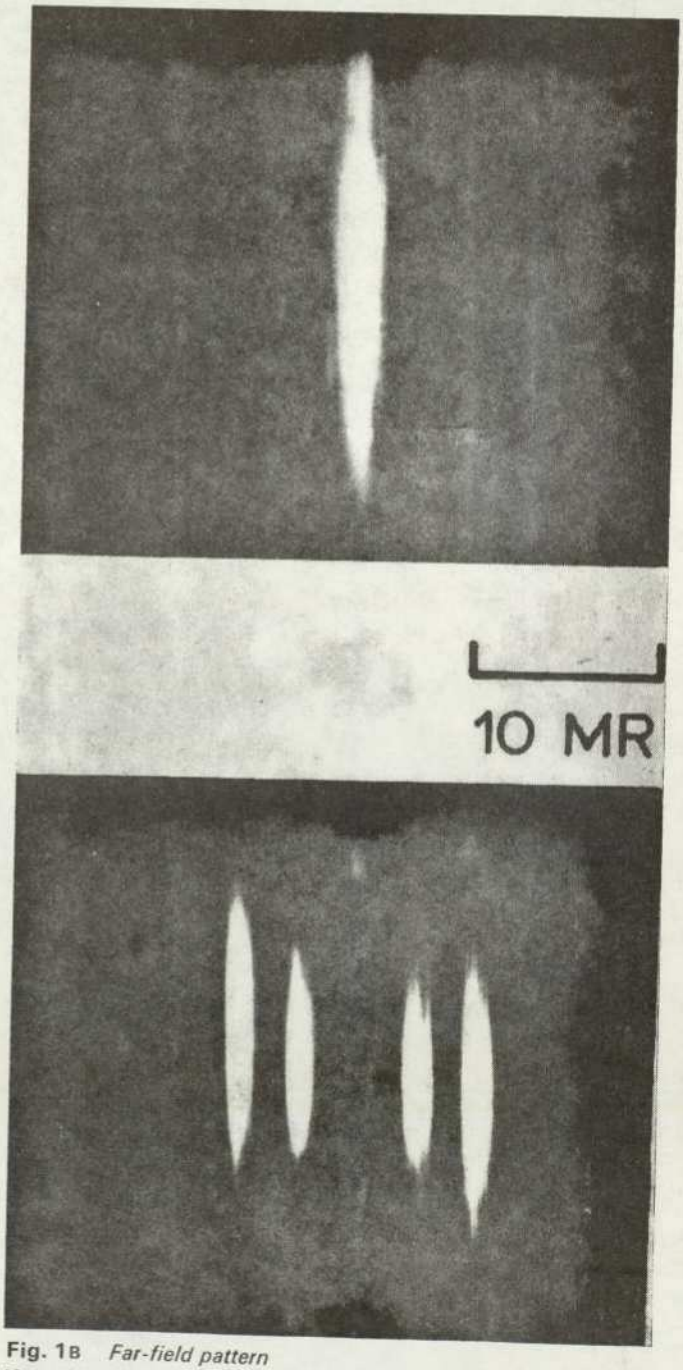


Fig. 1B *Far-field pattern*
Upper: V = 0 V
Lower: V = 60 V

This is in agreement with the predicted values of the reflection phase change (approximately 1° for chromium and $\theta = 6°$). Because of their periodicity, such phase changes will only affect even orders. For operation with uncollimated light, or to indicate alignment sensitivity, a knowledge of the variation of performance with misalignment angle α and β in the plane of deflection is important. Considering the two simple orientation possibilities[1] of $p\|z$ and $q\|z$, as in Fig. 1A, the relevant axis of the index ellipsoid is unaffected by α in the former case, and is only a weak function of it in the latter. So, for small α, the refractive-index change is

$$\Delta n = PE_{(p)} + QE_{(q)} \qquad \text{for } p\|z \quad . \quad . \quad . \quad . \quad . \quad (4)$$

or

$$PE_{(q)} + QE_{(p)} \qquad \text{for } q\|z \quad . \quad . \quad . \quad . \quad . \quad . \quad (5)$$

when the incident light is polarised parallel to z axis, where

$$P = \frac{r_{33}\cos^2\theta + r_{13}\sin^2\theta}{2\left(\dfrac{\cos^2\theta}{n_e^2} + \dfrac{\sin^2\theta}{n_0^2}\right)^{3/2}} \quad . \quad . \quad . \quad . \quad . \quad . \quad (6)$$

and

$$Q = -\frac{r_{22}\sin^2\theta}{2\left(\dfrac{\cos^2\theta}{n_e^2} + \dfrac{\sin^2\theta}{n_0^2}\right)^{3/2}} \quad . \quad . \quad . \quad . \quad . \quad (7)$$

For the zy orientation (y axis transverse to the electrodes),

$$Q = \frac{r_{51}\sin\theta\cos\theta}{2\left(\dfrac{\cos^2\theta}{n_e^2} + \dfrac{\sin^2\theta}{n_0^2}\right)^{3/2}} \quad . \quad . \quad . \quad . \quad . \quad . \quad (8)$$

for the zx orientation (x axis transverse to the electrodes), where n_0 and n_e are the crystal refractive indices and r_{13}, r_{22}, r_{51} and r_{33} are the nonzero electro-optic coefficients of $LiNBO_3$, and $E_{(p)}$ and $E_{(q)}$ are the orthogonal fields

$$E_{(q)} = \sum_{n=1,\,3,\,5} R\frac{n\pi}{d}\exp\left(\frac{-n\pi}{d}\,l\tan\theta\right)\cos\frac{n\pi}{d}(p + l\tan\alpha) \quad . \quad . \quad (9)$$

and

$$E_{(p)} = \sum_{n=1,\,3,\,5} -R\frac{n\pi}{d}\sqrt{(e_3/e_1)}\exp\left(\frac{-n\pi}{d}\,l\tan\theta\right) \times \sin\frac{n\pi}{d}(p - l\tan\alpha) \quad (10)$$

where

$$R = \frac{4V}{n\pi}\frac{\sin n\pi a}{n\pi a} \quad . \quad . \quad . \quad . \quad . \quad . \quad . \quad . \quad . \quad . \quad (11)$$

and e_1 and e_3 are the relative permittivities, V is the applied voltage, a is the metallisation factor, $2l$ is the device length, and the wavefront phase profile is obtained by adding the prereflection and postreflection effects as follows:

$$\Gamma(p) = \frac{2\pi}{\lambda}\int_0^l \{\Delta n_{(\alpha)} + \Delta n_{(-\alpha)}\}\,dl \quad . \quad . \quad . \quad . \quad . \quad (12)$$

and, by an incremental vector summation of the amplitudes, a zero-order extinction voltage can be predicted (Fig. 2).

The extinction ratio for a sinusoidal phase perturbation can be infinite, but will contain a residue if the emergent corrugation contains further harmonics. In the devices investigated, this residue was calculated to be insignificant ($< 10^{-5}$ of the zero-order intensity), and the measured extinction ratios on various devices of 40:1 to 140:1 for zero order and better than 40:1 for first order were considered the result of surface-finish quality and not fully indicative of achievable performance.

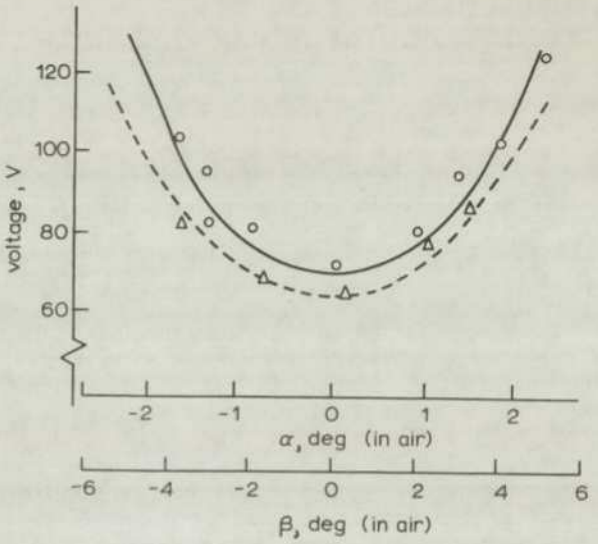


Fig. 2 *Zero-order extinction voltage against misalignment angle*

——— predicted ○ measured for $p\|z$
– – – – predicted △ measured for $q\|z$

These devices were tested with incoherent light (tungsten source), and could be used as modulators or rather chromatic filters as the extinction voltages and interorder angles vary with the incident wavelength. Extinction, or order maximum voltages, and the sine of the interorder angles vary linearly with wavelength in the material. This modulation/deflection principle conveniently reaches into the infrared, with the prospects of high interorder angles.

Operation has also been achieved with ADP 45° y-cut, using this principle, but with a less-efficient matched-contact electrode process. It is to be noted that both orthogonal components of the electrode field contribute to the phase retardation in general, and, by a judicious choice of orientation in a given material, control of the phase profile, and hence a blazing effect, may be achieved. Optimisation in $LiNBO_3$ is promising, as a 21% improvement in sensitivity on the values reported[1] is to be expected from the 30°, 0° and 47° cuts; for ADP, the 45°, 37° and 0° cuts offer a 13% improvement on the 45° y cut. This principle also seems promising with quadratic electro-optic-effect materials, e.g. KTN, where the sine of the interorder angles is doubled and the sensitivity may be greatly enhanced.

Acknowledgment: The author wishes to thank the UK SRC for the support for this project.

M. T. V. SCIBOR-RYLSKI

Optoelectronics Group
Department of Electrical & Electronic Engineering
City University
St. John Street, London EC1V P4B, England

10th December 1973

References

1 SCIBOR-RYLSKI, M. T. V.: 'Total-internal-reflection electro-optic diffraction deflection/modulator', *Electron. Lett.*, 1973, **9**, pp. 309–310
2 NISHIWAKI, A., MIZUNO, T., and HATTORI, S.: 'The d.c. characteristics of periodic skin-field electro-optic light modulators', *IEEE J. Quant. Electron.*, 1973, **QE–9**, pp. 559–563
3 DEBARROS, M. A. R. P., and WILSON, M. G. F.: 'High-speed electro-optic diffraction modulator for baseband operation', *Proc. IEE*, 1972, **119**, (7), pp. 807–914
4 LIBRECHT, F. M., and FRANCOIS, G. E.: 'Optimum cut for a $LiNBO_3$ transverse light modulator', *IEEE J. Quant. Electron.*, 1971, **QE–7**, pp. 374–376
5 KALYMNIOS, D.: 'Optimisation of electro-optic crystal modulators', *Electron. Lett.*, 1970, **6**, pp. 804–805

A TIR electro-optic diffraction Q-switch

D. Kalymnios

Department of Applied Physics,
University of Hull, Hull, HU6 7RX

and

M.T.V. Scibor Rylski

Rank Xerox Development Laboratories,
Church Street, Welwyn, Herts.

The Q-switching action of a novel electro-optic modulator is described. The device employs an inter-digital electrode structure deposited on one face of a $LiNbO_3$ crystal. The application of a relatively low voltage to the electrodes induces a refractive index grating which diffracts a total internally reflected light beam. The zero-order extinction ratio of the device is high and inter-order diffraction angles of 2 - 6 milliradians can readily be achieved. The device has a low capacitance (20-60pf) and has a risetime in the nano-second region.

The DC and pulsed characteristics of a $LiNBO_3$ TIR modulator/deflector will be reported. The crystal dimensions were 19 x 6 x 3·5mm with electrode pitch of 0·2mm and electrode area 18 x $3mm^2$. At 0.63μ the zero-order extinction ratio was 60:1 at 90V. When the modulator was used to Q-switch a Nd^{3+}/YAG laser, operated in TEM_{oo} mode, a single 60nsecs, 5mJ pulse was produced. The driving pulse had an amplitude of 100V and a risetime of 40nsecs. The performance of this novel device will be compared with that of more conventional Q-switches.

A TIR ELECTRO-OPTIC DIFFRACTION Q-SWITCH

D KALYMNIOS

Department of Applied Physics
University of Hull, Hull, HU6 7RX

and

M T V SCIBOR-RYLSKI

Rank Xerox Development Laboratory
Welwyn Hall, Church Street
Welwyn AL6 9LU, Herts

A TIR ELECTRO-OPTIC DIFFRACTION Q-SWITCH

INTRODUCTION

Devices most widely used in Q-switching applications are electro-optic (Pockels cells) or acousto-optic. Pockels cells operate at relatively high voltages, (2-8 kV), and acousto-optic modulators require 30-50 Watts of continuous or pulsed RF drive. A novel Q-switch that operates with less than 100 volts will be described. The device utilises the modulating characteristics of a recently developed electro-optic total internal reflection (TIR) deflector/modulator. The modulator employs an interdigital electrode structure deposited on one face of a lithium-niobate ($LiNbO_3$) crystal. The application of a relatively low voltage to the electrodes, induces a refractive index grating which diffracts a total internally reflected light beam. Inter-order diffraction angles of 2-6 milliradians can readily be achieved. The zero-order extinction ratio of the device is high and can be obtained using less than 100V. The capacitance of the device is low, less than 60 pF, and the risetime is in the nanosecond region. When the modulator was used to Q-switch a Nd^{3+}/YAG laser, operated in TEM_{oo} mode, a single 60 nsecs, 5mJ pulse was produced. The driving pulse had an amplitude of 100V and a risetime of 40 nsecs. The performance of this novel Q-switch will be compared with that of the more conventional type.

TIR MODULATORS - PRINCIPLES OF OPERATION

The general characteristics of TIR devices are briefly described. The total internal reflection modulator/deflector operates by diffraction and can best be compared to the Debye-Sears acousto-optic deflector/modulator. In TIR devices the periodic material perturbation is generated electro-optically by a fringing electric field produced by an interdigitated electrode structure which is deposited on one surface of the electro-optic crystal. A total internally reflected beam from the crystal-electrode

2/...

A TIR ELECTRO-OPTIC DIFFRACTION Q-SWITCH

TIR MODULATORS - PRINCIPLES OF OPERATION continued

interface is diffracted into different orders and the far-field pattern is of the Raman-Nath type (6). The device makes use of all electro-optically affected material, and can be used without lenses or analysers.

A simple realisation of this device uses lithium-niobate as the electro-optic material and for two non-optimum crystal orientations one makes use of the largest electro-optic coefficient, r_{33}. The two orientations that could be used would be for the z-axis to be either transverse to the electrodes or normal to the electrode plane, Fig. 1a. In the former case (Op $\|$ z) the induced refractive index change in the z-direction takes the form (1).

$$\Delta n = \frac{E_z r_{33} n_e^3}{2}$$

while the refractive index change along z in the latter case (Oq $\|$ z), includes contributions from other field components, and is given by

$$\Delta n = \frac{E_z(r_{33}\cos^2\theta + r_{13}\sin^2\theta) - E_y r_{22}\sin^2\theta + E_x r_{51}\sin\theta\cos\theta}{2(n_e^{-2}\cos^2\theta + n_o^{-2}\sin^2\theta)^{3/2}}$$

where θ is the TIR angle of incidence, Fig. 1a. In general either E_x or E_y will be zero depending whether the electrode fingers lie along the x or y axis.

The electric field components inside the crystal can be expressed as (1)

$$E_\perp = -\sum_{n=1,3,5,} A_n V e^{B_n q} \sin C_n p \qquad \text{normal to the electrodes.}$$

and

$$E_\| = \sum_{n=1,3,5,} A_n V e^{B_n q} \cos C_n p \qquad \text{transverse to the electrodes.}$$

3/...

A TIR ELECTRO-OPTIC DIFFRACTION Q-SWITCH

TIR MODULATORS - PRINCIPLES OF OPERATION continued

Where A, B are material constants, C is a function of electrode pitch, and p, q are axes directions parallel and normal to the electrodes respectively. The phase retardation produced by the device is given by

$$\Gamma = \frac{4\pi}{\lambda} \int_0^{\frac{l \tan\theta}{2}} \frac{\Delta n \, dq}{\sin\theta} \qquad \text{radians}$$

Computed phase profiles for the two cases considered are given in Fig. 1b. The far-field pattern can be predicted from classical diffraction theory or computed by incremental summation of amplitudes. For Raman-Nath type characteristics a sinusoidal perturbation is assumed; as seen from Fig. 1b however the phase perturbation in the crystal is not strictly sinusoidal and this has the effect of slightly displacing the non-zero order maxima. The order intensity characteristics for a TIR device is shown in Fig. 2, which also shows for comparison the $\cos^2$ intensity characteristic of an orthodox electro-optic modulator. A densitometer trace of the far field light pattern of the device is shown in Fig. 3.

As all the active area of the crystal is exploited by the beam, it is possible to use an increasingly fine electrode pitch, in order to reduce the zero-order extinction voltage, Fig. 4. This figure also illustrates differences between AC and DC operation in $LiNbO_3$ TIR devices (1). Decreasing the effective electrode area by increasing the angle of incidence θ, leads to an increase in operating voltages, Fig. 5. The result of degrading the electrode mark space ratio (as achieved in practice by etch factor effects) is also shown in Fig. 5. The capacitance of TIR devices can be calculated from the energy stored in the fringing field and for $LiNbO_3$ this is ~ 0.17pF per millimetre of electrode length per unit pitch. Therefore devices of considerable electrode area and of low capacitance (less than 80 pF) can be constructed and be used for high frequency applications.

4/...

A TIR ELECTRO-OPTIC DIFFRACTION Q-SWITCH

A $LiNbO_3$ TIR DEVICE AS Q-SWITCH (FIG.6)

A $LiNbO_3$ TIR modulator of dimensions 19 x 6x3.5 mm has been used to investigate the potential uses of TIR devices in Q-switching applications. The interdigital electrodes, copper on chromium, were deposited on a polished surface of the crystal and lie in the xy plane with the electrode fingers parallel to the x-axis. The electrode pitch was 0.2 mm and the electrode area was approximately (18 x 3)mm^2. The measured capacitance of the device was 53pF and this is in reasonable agreement with the calculated value of 46 pF.

The DC transmission characteristics of the device were determined at 0.63μ using a He-Ne laser. The laser beam was polarised in the zx plane, and the angle of incidence θ, was 5-6°. The transmitted beam was projected on to a screen, placed at a suitable distance from the device. By increasing the applied voltage to the crystal, the zero-order beam was correspondingly diffracted into higher orders. Total extinction of the zero-order occurred at 90V, Fig. 6a, and the extinction ratio was 60:1. It is interesting to note that with no voltage applied to the crystal there is a very small fraction of light, less than 1%, that is diffracted mainly into the first order. This represents an inherent loss of the device probably due to a charge effect and cannot be attributed to small net phase differences arising from reflections at the crystal-air and crystal-electrode interfaces because of the pattern pitch (2). The inter-order diffraction angle at 0.63μ was approximately 2 milliradians and this is sufficient to inhibit lasing action when the device is used inside most laser cavities. Fig. 6b is the far-field pattern when incident light is polarised at 45° to zx plane, and shows that for light polarised transverse to the electrode plane (i.e. normal to the z axis) operation is not so effective, with only 30% of the zero-order intensity being diffracted at 90V. The device therefore is normally operated with light polarised in the most sensitive direction.